

1 **Development of a multi-disciplinary**
2 **toolkit to study time cells in the**
3 **hippocampus**
4

5 A Thesis
6

7 Submitted to the
8

9 Tata Institute of Fundamental Research,
10 Mumbai

11 for the degree of Doctor of Philosophy
12 in (subject)

13 by

14 Kambadur Gundu Ananthamurthy

15
16
17 Tata Institute of Fundamental Research
18 Mumbai

19 [May, 2023]
20 [Final Version Submitted in Month, Year]

21

DECLARATION

22

23 This thesis is a presentation of my original research work.
24 Wherever contributions of others are involved, every effort is
25 made to indicate this clearly, with due reference to the
26 literature, and acknowledgment of collaborative research
27 and discussions.

28

29 The work was done under the guidance of Professor Upinder
30 S. Bhalla, at the Tata Institute of Fundamental Research,
31 Mumbai.

32

33

34 **[candidate's name and signature]**

35

36 In my capacity as supervisor of the candidate's thesis, I
37 certify that the above statements are true to the best of my
38 knowledge.

39

40

41 **[guide's name and signature]**

42 Date:

43 Acknowledgments

44

45 Projects like the ones described in this thesis cannot be accomplished
46 without good, strong leadership. I thank Upi for the opportunity to learn
47 and grow in his lab, and his patience to see me through tough
48 moments.

49 I thank Shona and Mukund for advice and help over the past decade.

50 I thank my seniors Mehrab, Ashesh, Partha, and Subha. I hope I can
51 make them proud, someday.

52 I thank my colleagues Sahil, Dilawar, Oliver, and Aditya for helping me
53 whenever I asked.

54 I thank Sriram, Manoj, Krishna, and Amit for everything I learnt in CIFF.

55 I thank Mohini, Mugdha, Sebastien, Arnab, and Terence, for being my
56 friends for as long as they could.

57 I thank Supriya, Harini, Anupratap, Sohail, and Prabahan, my well-
58 wishers from Shona lab.

59 I thank KS Krishnan for being my Godfather. His absence cannot be
60 filled with anything else.

61 I thank Sanjay, Axel, Panic, Vatsala, Uma, Madan, and Jitu, for always
62 bringing a breath of inspiration to my life and my work.

63 I thank Dr. Shane Heiney for showing me the way with trace eye-blink
64 conditioning, and Dr. Daniel Dombeck for the chronic hippocampus
65 preparation.

66 I'm indebted to the Animal Care and Resource Center (ACRC), the
67 Central Imaging and Flow Facility (CIFF), Dorababu & the Electronics
68 Workshop, Devakumar & the Mechanical Workshop, for anything and
69 everything I have been able to make or create.

70 I thank Swarna and Nikhila for teaching me Tennis. I also thank the
71 Football group, the Badminton group, the Music group, the Theater
72 group, and the Improv group, for always giving me a chance to
73 explore.

74 I thank Neha Panwar for being there in the end.

75 "Very little" is what I'd have achieved without my parents. I hope to be
76 a good person and live up to the values they have taught me.

77 I thank the canteen, the sports facility and gym, hospitality,

78 instrumentation, and admin, for helping me with everything else.

79

for Archana && Buiju,

Index of Tables

Table 1: Summary table of behaviour protocols attempted and essential results.....	104
Table 2: Recipe for ready-to-use cortex buffer. The buffer is typically prepared and stored in aliquots to be used each week. The correct pH range of the buffer was often a crucial factor ensuring the success of the hippocampal preparation.	113

Table of Figures

Figure 1: A schematic representation of the Trisynaptic Pathway as observed with coronal slices along the longitudinal axis of the hippocampus. Image adapted from the webpage for the Neural Circuits and Memory Lab, University of Wisconsin (Milwaukee) [https://sites.lsa.umich.edu/diba-lab/neural-circuits-of-the-hippocampus/].....	25
Figure 2: Water delivery calibration to reward the animal consistently with the same volume of water.....	68
Figure 3: Optoisolator circuit to amplify +5V DC input to +12V DC output.....	71
Figure 4: Lick detector circuit based on a MOSFET design. Whenever the animal performed a lick, a +5V DC Output would be read out.....	72
Figure 5: Typical trial structure with the various phases. Each trial was followed by a randomized Inter-Trial Interval (ITI).....	75
Figure 6: Performance evaluation for two example mice trained to Protocol 1.1 and 1.2. Percentage of total licks in the various trial phases (Pre-Tone, Tone, CT, and ITI), across all sessions of training (coloured bar plots) for A) Mouse 3, and B) Mouse 4.....	76
Figure 7: Performance evaluation for two example mice trained to Protocol 2. Percentage of total licks in the various trial phases (Pre-Tone, Tone, CT, and ITI), across all sessions of training (coloured bar plots), for (A) Mouse S1, and (B) Mouse S2.....	73
Figure 8: Schematic representation of the experimental setup for a simple detection task where the animal must perform a	

lick upon correctly detecting the presence of the conditioned stimulus (CS; from a range of modalities).....	82
Figure 9: Typical trial structure with the various phases and lick dependent relationships.....	83
Figure 10: (A) Performance traces for all the animals individually shown in dashed grey lines. Mean + SEM in black. (B) Mean Performance (%) and Mean Go Tone Lick Percentage (%) with Session for the Go/No-Go Task, plotted in black and green, respectively.....	87
Figure 11: The number of licks in the pre-tone (blue), no-go tone (red), and go tone (green) phases, in a representative animal, in a session with maximum Performance (%).	88
Figure 12: Schematic representation to showcase the two main subtypes of Classical Conditioning (Eye-Blink Conditioning, for our experiments) based on the relative timing and presentation of the CS and US.....	90
Figure 13: Trial by trial (left), and trial-averaged running speed (right) for two example animals, (A) M2 Session 12, and (B) M5 Session 12.....	93
Figure 14: Schematic representation of (A) the behaviour rig with 2-Photon imaging, to train head-fixed mice on a Trace Eye-Blink Conditioning (TEC) task, and (B) relative time intervals between the CS and US.....	95
Figure 15: A picture of a head-fixed mouse clamped on the behaviour rig, with key components: 1) Red LED Illumination, 2) Blue LED CS, 3) Air-puff port directed to the left eye, and 4) Height-adjustable Treadmill.....	96
Figure 16: Steps from behaviour video frame to Fraction of Eye-Closed (FEC) analysis.....	97
Figure 17: Conditioned Responses (CRs) are small amplitude eye-blinks triggered by the CS, and develop with multiple training sessions, while Unconditioned Responses are large eye-blinks to the US, typically consistent across sessions. (A,B) Trial-by-trial FEC traces for (A) M11 Session 2, and (B) Session 4. (C,D) Trial-averaged FEC traces for (C) Session 2 and (D) Session 4, with paired (red) and probe (green) trials.	99
Figure 18: Performance in terms of the percentage of Hit Trials to total trials across sessions, including an ISI switch from 250 ms to 350 ms.....	100
Figure 19: Conditioned Responses (CRs) are preserved for previously learnt ISIs, and switching the ISI to longer intervals results in Complex (multi-CR) eye-blink responses.	

(A,B) Trial-by-trial FEC scores for (A) 250 ms ISI (left) and (B) 500 ms ISI. (C,D) Trial-averaged FEC traces for (C) 250 ms ISI (left) and (D) 500 ms ISI (right), with paired (red) and probe (green) trials.....	101
Figure 20: Conditioned Response (CR) onset timing is maintained across ISI switches. Representative examples from a short ISI switch from (A) 250 ms to (B) 350 ms (right).	102
Figure 21: Bar plots for Conditioned Response (CR) onset across multiple sessions of training after ISI switch from 250 ms to 350 ms, irrespective of how strongly the animals learnt the task. (A) red, strong learner, and (B) blue, weak learner.	102
Figure 22: Representative example of mice trained to 550 ms ISI (Session 6) and 750 ms (Session 4). (A,B), Trial-by-trial FEC responses for (A) 550ms ISI, and (B) 750ms ISI. (C,D) Trial-averaged FEC responses for (C) 550 ms ISI, and (D) 750 ms ISI, with paired (red) and probe trials (green).....	103
Figure 23: (A) A schematic of the rodent brain, showcasing the two hippocampi, one in each hemisphere. The hippocampi lie ~1 mm (mice) below the cortical surface. (B) The hippocampal preparation allows optical access to the deep lying hippocampal CA1 cells, relative to the skull/cortex. The CA1 cell bodies arrange in a laminar fashion, as a tight cell body layer that can be visualized by fluorescence (using either OGB-1 or GCaMP).....	111
Figure 24: Schematic representation for stereotaxic viral injection.....	116
Figure 25: (A) Representative Two-Photon Calcium Image of a plane of Hippocampal CA1 cells, bolus loaded with Oregon Green Bapta-1 (OGB-1), at an instant in time. Example cells marked out post-hoc as pink, green, blue and red. Scale bar 20 μ m. (B) Representative dF/F (%) traces for the calcium activity recorded in a single 10s video for example cells pink, green, blue, and red. Scale bar (1 sec; 10% dF/F).....	118
Figure 26: Tissue Degradation over time. Representative Two-Photon Calcium images of a snapshot in time of the Hippocampal CA1 cell body layer on (A) Day 1 after the surgery and (B) Day 3, after the surgery. Scale bar 30 μ m.	120
Figure 27: Chronic calcium imaging of the same Hippocampal CA1 cells over weeks. Representative 2-Photon images from (A) Day 20, and (B) Day 21, after surgery.	

Landmarks have been marked and were used to confirm frame registration and identify cells. Scale bar 100 μ m.....	121
Figure 28: (A) Representative Two-Photon Calcium Image of a plane of Hippocampal CA1 cells expressing GCaMP6f at an instant in time. Example cells marked out post-hoc in pink, blue, and green, with no-cell background in red. Scale bar 20 μ m. (B) Representative dF/F (%) traces for the calcium activity recorded in a single 10s video for example cells in pink, blue, and green, with no-cell background in red. Scale bar (2 sec; 10% dF/F).....	122
Figure 29: (A) Correlation Coefficients for cell pairs from an example two-photon recording. (B) Meta-K Means clustering with cell pairs using the heuristic that within group pairs would be more similar than between group pairs. In this example, the cells were clustered into two groups, I (red) and II (yellow). (C) Two-Photon image of the field of view of cells; same as Figure 25A. (D) Spatial organization of correlated cell pair groups during spontaneous activity (Modi et al... 2014).....	131
Figure 30: (A) Trial-averaged (25 trials) calcium activity from ~100 CA1 cells in trials where a 5000 Hz tone was presented (red bar). (B) Trial-averaged (18 trials) calcium activity from the same cells in trials where a 5 LPM air-puff to the ipsilateral whiskers was presented (red bar).....	132
Figure 31: (A) Correlation Coefficients for cell pairs from post whisker-puff stimulation periods. (B) Meta-K Means clustering with cell pairs using the heuristic that within group pairs would be more similar than between group pairs. In this example, the cells were clustered into three groups I (red), II (orange), and III (yellow). (D) No clear spatial organization of correlated cell pair groups post whisker stimulation.....	133
Figure 32: (A) Correlation Coefficients for cell pairs from a trial-shuffle control dataset (B) Meta-K Means clustering revealed that there were no cell pair groups identified.....	134
Figure 33: Example Time Cells visualized as event raster plots (A, B, C), along with the trial-summed activity profiles (D, E, F) suggesting ~50% hit trials, for cells 29 and 72 from Session 1 (session type 5) with mouse M26, and slightly lower reliability (~25% hit trials) from cell 105.....	139
Figure 34: Example Other Cells visualized as event raster plots (A, B, C), along with the trial-summed activity profiles	

(D, E, F) for cells 10, 25, and 120 from Session 1 (session type 5) with mouse M26.....	140
Figure 35: Event Time Histograms or tuning curves for Identified Time-Locked Cells with trial-summed peaks in session 4 of training (session type 5) with mouse M26. (A) Unsorted list of Time cells. (B) Peak-sorted list of the same cells. Here, 1 bin = 3 frames = ~210 ms (sampling rate 14.5 Hz without binning; ~5 Hz with binning). As per the (legacy) session type 5 protocol, the CS (50 ms Blue LED flash) was presented in frame bin 39, followed by a stimulus-free trace interval during frame bins 40 and 41, and then the US (50 ms airpuff to ipsilateral eye) was presented in frame bin 42... .	141
Figure 36: Temporal Information (bits) vs Sorted time cell number from the analytically identified Time Cells in Session 4 (session type 5) with mouse M26. No clear trend was observed.....	142
Figure 37: More time cells observed to attain tuning as training sessions. Event Time Histograms of the identified set of time cells between A) Sessions 1 and (B) Session 2, with mouse M26 (session type 5).....	143
Figure 38: Sorted Time Cells form Sequences that develop with learning. Trial-Averaged calcium activity traces for all recorded cells across A) Session 1, B) Session 2, and C) Session 4, with mouse M26 (sessiontype 5). Time 0 ms was aligned to the CS. The CS + Trace + US interval lasted from 0-600 ms, here.....	144
Figure 39: Same/similar tuning across session 1 and session 2 for this example time cell. Blue Event Time Histograms represent the tuning curve for the cell for session 1 (date: 20180508) and Red represent the same but for session 2 (date: 20180509). Pearson's correlation coefficient between the two session pairs was 0.7011.....	145
Figure 40: Three example chronically tracked cell pairs with tuning peaks arriving earlier with training sessions (rows). Blue Event Time Histograms represent the tuning curve for any cell for session 1 (date: 20180508) and Red represent the same but for session 2 (date: 20180509). Pearson's correlation coefficient between the session pairs was 0.6.348, 0.5872 and 0.7027 for A) cell pair 1, B) cell pair 2, and C) cell pair3, respectively.....	146
Figure 41: Example chronically tracked cell pair with de-tuning between session 1 and 4. Blue Event Time Histograms represent the tuning curve for the example cell for session 1	

(date: 20180508) and Red represent the same but for session 4 (date: 20180514). Pearson's correlation coefficient between the two curves was -0.0606.....	147
Figure 42: Comparing chronically tracked time cells across sessions for all matched cell pairs by (A) Correlation Analysis, and (B) Timing of peaks.....	148

Table of Contents

DECLARATION.....	2
Acknowledgments.....	3
Abstract.....	14
Chapter 1 – Introduction.....	16
Projects and overall goals.....	16
Neural systems and behaviour.....	17
Engrams associated with Learning and Memory.....	18
Dynamics in the neural code for engrams.....	20
Theories on the function of the hippocampus.....	23
Space and time in the hippocampus.....	25
“Single-cell, multi-trial” vs. “multi-cell, single-trial” approaches in Neuroscience.....	31
Single-Unit Electrophysiology vs 2-Photon Calcium Imaging to study the Hippocampus.....	36
Calcium imaging by 2-Photon Microscopy.....	37
Automated ROI detection for large-scale Calcium Imaging datasets.....	41
A brief introduction to associative learning.....	42
Short Summaries of the 3 projects.....	44
Project I - How do sensory representations transform with learning?.....	44
Project II - How does the timing of cellular activity adjust to behavioural task variables?.....	45
Project III - What is the best way to detect and score time-tuned cellular activity?.....	47
Code Availability.....	49
Bibliography.....	49
Chapter 2 – Behaviour.....	64
Towards understanding brain activity in a reproducible context.....	64
Operant conditioning [Project I].....	65
Required features.....	66
Water delivery and calibration.....	67
Opto-islator circuit for solenoid control.....	68

Lick detection circuit.....	71
Controlling task details and protocol information.....	72
Head-bar implant, Animal Handling, and Water deprivation.....	74
PROTOCOL 1.1: Stimulus Detection Task.....	74
PROTOCOL 1.2: Stimulus Detection Task with aversive punishment.....	75
Results - Protocol 1.1 and 1.2.....	77
Protocol 2: Stimulus Detection task with timeout box.....	77
Results - Protocol 2.....	79
Protocol 3: Delayed Non-Match to Sample (DNMS).....	80
Results - Protocol 3.....	81
Protocol 4: Go/No-Go Task.....	81
Results - Protocol 4.....	83
Trace Eye-Blink Conditioning [Project II].....	89
Tracking eye-blink responses.....	91
Treadmill and tracking running speed.....	92
Behaviour rig and protocol control - Software.....	93
Analysis - TEC.....	96
Results - TEC.....	98
Bibliography.....	104
Chapter 3 - Imaging.....	107
Physiology in the hippocampus.....	108
Methodology - Acute and chronic imaging [Projects I & II]	110
Preparation of Cortex Buffer.....	112
Oregon Green Bapta-1 injections for acute imaging.....	114
GCaMP and chronic imaging.....	115
Results - Imaging.....	117
2-Photon calcium imaging of hippocampal CA1, <i>in vivo</i>	117
Acute Imaging of OGB-1 loaded hippocampal CA1, <i>in vivo</i>	117
Chronic imaging of hippocampal CA1 using GCaMP.....	119
Spontaneous activity during non-stimulus periods.....	122
Spatial organization of activity correlated cells during spontaneous activity.....	123
Stimulus evoked responses.....	131
Spatial organization of activity correlated cells post whisker-puff stimulation.....	132
Chronic imaging now possible for weeks with the same mouse.....	134
Preliminary analysis to identify time cells.....	135

Tuning, re-tuning, and de-tuning of time cells across sessions.....	142
Bibliography.....	149
Chapter 4 - Analysis.....	155
Chapter 5 - Discussion.....	162
The study of hippocampal CA1 sequences.....	162
Mapping sequences to abstract variables.....	164
Does the brain create or predict?.....	166
Bibliography.....	167
All Bibliography.....	171

81 **Abstract**

82

83 The mammalian Hippocampus is considered important for the
84 formation of several kinds of memory, one of which is the association
85 between stimuli occurring separately in time. Several studies have
86 shown that small populations of Hippocampal CA1 cells fire in time-
87 locked sequences, "bridging" the time gap in temporal tasks (B. Kraus
88 et al., 2013; MacDonald et al., 2011, 2013; Pastalkova et al., 2008),
89 including a single-session version of Trace Eye-Blink Conditioning or
90 TEC (Modi et al., 2014). Such cells are commonly termed time cells
91 (Eichenbaum, 2017; MacDonald et al., 2011).

92 The main goal of the Thesis was to be able to study time cells under a
93 variety of behavioural tasks and conditions and elucidate several
94 physiological properties. We standardised a multi-day Trace Eye-Blink
95 Conditioning (TEC) protocol to train head-fixed C57Bl6 mice (Siegel et
96 al., 2015). TEC involves an association between a previously neutral
97 Conditioned Stimulus (CS) with an eye-blink inducing Unconditioned
98 Stimulus (US), across an intervening, stimulus-free, Trace Interval. We
99 were able to observe stable, adaptive learning with our protocol. We
100 also standardized an *in vivo* imaging preparation to record calcium
101 activity from Hippocampal CA1 cells, adapted from previously
102 published methods (Dombeck et al., 2010; Modi et al., 2014). We used
103 a custom-built two photon laser-scanning microscope and performed
104 galvo-scans through the imaging window, during TEC. The behaviour
105 and Imaging was conducted simultaneously to record calcium activity
106 as the animal learnt the task. Chronic Calcium Imaging allowed us to
107 track and record the activity of the same cells, confirmed

108 morphologically. We could then identify time cells across sessions, and
109 look for adaptations in tuning curves, along multiple sessions.
110 Furthermore, numerous approaches have been developed to analyse
111 time cells and neuronal activity sequences, but it is not clear if their
112 classifications match, nor how sensitive they are to various sources of
113 data variability. We provide two main contributions to address this: A
114 resource of synthetic 2P Calcium activity data, and a survey of several
115 methods for analyzing time cell data using our synthetic data as
116 ground truth. The synthetic dataset and its generation code are useful
117 for profiling future methods, testing analysis tool-chains, and as input
118 to computational and experimental models of sequence detection. We
119 characterized strengths and weaknesses of several time-cell analysis
120 methods. Finally, we benchmark how computational requirements
121 scale with large datasets typical of recent recording technologies.

122 Chapter 1 – Introduction

123

124 The vertebrate Central Nervous System (CNS), consisting primarily of
125 the central ganglia (brain) and the spinal cord, samples and receives
126 information from the external world offering top-down control over the
127 activity of all parts of the body. Functions like exploration, food
128 acquisition, and danger aversion, all involve complex coordination
129 between,
130 ● the Sensory Systems (that integrate information from the
131 environment),
132 ● the Memory Systems (that integrate sensory information with
133 prior experience), and
134 ● the Motor Systems (that integrate motor plans and execute
135 movement).

136

137 Projects and overall goals

138

139 The overall focus of the work and experiments described in this Thesis
140 was to study Memory Systems, specifically, in terms of,

141

142 **Project I:** How do sensory representations transform with
143 learning?

144

145 **Project II:** How does the timing of cellular activity adjust to
146 behavioural task variables?
147
148 **Project III:** What is the best way to detect and score time-tuned
149 cellular activity?
150
151 Narrowing down, we as a lab were interested in the mammalian
152 hippocampus, a brain structure which is important for consolidating
153 information (from Sensory and other Memory Systems) to enable
154 certain kinds of short-term memory and the translation of short-term
155 memory to long-term.
156

157 **Neural systems and behaviour**
158
159 Ramón y Cajal, one of the pioneers of neuroscience around 1900,
160 utilized Camillo Golgi's staining method to conclusively describe
161 neurons in the brain as independent functional units connected to each
162 other in intricate networks made up of many nodes ($\sim 10^6 - 10^9$). These
163 neurons have since been described not just anatomically, but also on
164 the basis of genetics, development, and neurophysiology.
165
166 In the sub-discipline of Learning and Memory an often studied neuron
167 type is the pyramidal neuron, an example of which is the hippocampal
168 CA1 pyramidal neuron. This thesis describes a toolkit of techniques
169 ranging in a wide, multi-disciplinary scope, assembled with
170 standardized hardware and software routines studying animal
171 behaviour, network neurophysiology, and statistical analyses.

172 The aim of the toolkit was to provide the experimental ability to study
173 the hippocampal CA1 pyramidal neuron network, under strictly
174 controlled behavioural contexts designed to train experimental mice on
175 temporal or episodic memory tasks. Specifically, these tasks such as
176 Trace Eye-Blink Conditioning (TEC) have previously been described to
177 elicit hippocampal CA1 sequences (B. J. Kraus et al., 2015;
178 MacDonald et al., 2011, 2013; Mau et al., 2018; Modi et al., 2014;
179 Pastalkova et al., 2008). This spatiotemporal network activity sequence
180 is dynamic and built from individual hippocampal CA1 pyramidal
181 neurons showcasing time tuned activity through spiking. These cells
182 are called time cells (Eichenbaum, 2017; MacDonald et al., 2011).
183

184 **Engrams associated with Learning and
185 Memory**

186
187 The term "engram" (coined by Richard Semon) refers to the physical
188 substrate of memory in the organism, used for storing and recalling
189 memories (Josselyn & Tonegawa, 2020). Donald Hebb's theory of
190 Hebbian Plasticity (Hebb, 1949) postulated that memory formation was
191 correlated to modulations in synaptic strength and connectivity. The
192 theory critically emphasized that the pair of neurons connected through
193 the synapse undergoing plasticity to strengthen efficacy, required the
194 spiking activity of both neurons. In subsequent decades, research into
195 the idea led to the theory of spike-timing-dependent plasticity
196 (Caporale & Dan, 2008), a mechanism of synaptic plasticity based on
197 the relative timing of activity of the neurons. It is still a matter of debate
198 whether the biophysical manifestation of the engram is the synapse,

199 the activity of the neurons, biophysical or chemical processes, but it is
200 likely that the engram is distributed across several computational
201 scales in the brain.

202

203 Eric Kandel's experiments with the Aplysia sensory neurons studied gill
204 withdrawal - an aversive but stable, adaptive behaviour (Carew et al.,
205 1971). The reliability of this learned response allowed the experiments
206 to include crucial electrophysiological and neurochemical circuit
207 dissections that ultimately lead to the discovery of the entire neural
208 circuit orchestrating the task, even to the level of cellular signaling.
209 This led to decades of research focused on the plasticity of synapses
210 across nervous systems in the animal kingdom.

211

212 Research exploring causal relationships between the physical or
213 functional integrity of various brain regions and overt behaviour has
214 been crucial to mapping many brain regions to specific functions and
215 motor responses. Technological advancements in molecular
216 neuroscience led to the development of a number of fluorescent
217 sensors, conditional tagging, activators and inhibitors that allowed
218 cellular resolution tracing of the engram (Luo et al., 2018).

219

220 Experiments by Sheena Josselyn, Alcino Silva, and colleagues led to
221 the discovery that the intrinsic excitability of a pyramidal neuron in any
222 network positively biased the probability of recruitment to the engram
223 (Han et al., 2009; Rogerson et al., 2014; Yiu et al., 2014; Y. Zhou et
224 al., 2009), *viz.*, the tagged set of cells were active when memory was
225 learnt and recalled. The engram seemed to be described in terms of
226 the cellular sub-population involved but the experiment could only
227 identify the same over a relatively longer window of time (~mins.). This

228 could lead to only a static list of cells which may even have included
229 False Positives (Type I error). Importantly, any dynamics in the
230 spatiotemporal patterns of activity of the pyramidal neurons were not
231 amenable to study at shorter timescales (~ms.). On the other hand,
232 physiological recordings could describe these dynamics at short
233 timescales, but were rarely translated to chronic measurements of the
234 activity of the same cells across days and sessions, given technical
235 limitations at the time.
236

237 **Dynamics in the neural code for engrams**

238
239 We first discuss some important results that help motivate the study of
240 physiological recordings in the context of engrams, *i.e.*, the dynamical
241 nature of the neural code (~ms to s). In later sections we will describe
242 these dynamics in more detail.
243
244 Place cells and their role in spatial navigation have been studied in
245 great detail through decades of research ever since they were first
246 described by John O'Keefe (O'Keefe & Dostrovsky, 1971). We did not
247 explicitly study place cells in this thesis but some key discoveries in
248 literature require mention, with the goal to build a case for a theory of
249 CA1 ensemble sequences (Modi et al., 2014). Briefly, place cells are
250 pyramidal neurons that showcased a higher than baseline probability
251 of firing action potentials whenever animals navigating spatial
252 environments visited specific locations. The tuning curves or firing
253 fields for these cells often map to the real spatial trajectory of the
254 animal and is thought to be an assimilation of both brain external

255 stimuli such as visual cues, as well as brain internal variables such as
256 motivation, goal orientation, memory, and experience (Ferbinteanu et
257 al., 2011; Ferbinteanu & Shapiro, 2003; Foster, 2017; Frank et al.,
258 2000; Wood et al., 2000).

259

260 As the animal enters these landmark locations in any spatial context,
261 these place cells showcase Phase Precession, firing earlier in phase to
262 cycles of Theta a network rhythm clocked at ~4-10 Hz, as the animal's
263 position changes relative to the landmark. These navigation mapped
264 place cell sequences are called Theta Sequences (Foster & Wilson,
265 2007), typically mapped to a few active neurons at a time.

266

267 In very specific contexts, these place cells express activity sequences
268 synchronized to Sharp Wave Ripples, a different network activity
269 phenomenon clocked at ~10-30 Hz, often not tied to the animal's
270 location, called Replay Sequences (Csicsvari et al., 2007; Foster &
271 Wilson, 2006). These sequences have been described to play out
272 typically in reverse temporal order to models of place cell sequences
273 describing known trajectories in space.

274

275 There is variability in the firing of place cells in any spatial context, and
276 studies have mapped specific sequences to very specific trajectory
277 goals (going towards or away from locations) with modulation by both
278 egocentric and allocentric orientations cues (Davidson et al., 2009;
279 Ferbinteanu et al., 2011; Ferbinteanu & Shapiro, 2003; Frank et al.,
280 2000; Wood et al., 2000) and movement speed based estimates of
281 distance (Kropff et al., 2015).

282

283 Place cell and time cell sequences have many similarities and
284 differences in descriptive neurophysiology, but may emerge from the
285 same memory organization principles (Buzsáki & Llinás, 2017). It is
286 argued that there is significance to the exact phrasing of the CA1
287 sequence in any given context. Furthermore, a very interesting feature
288 observed is Time-stamping, *viz.*, time dependent overlap of ensemble
289 responses to different contexts and behavioural parameters (Cai et al.,
290 2016; Mau et al., 2018).

291

292 Trace Eye-Blink Conditioning is a behavioural context which has been
293 shown to feature CA1 time cell activity sequences. Transient increases
294 in CA1 excitability post acquisition of the task were described up to 4-5
295 days (Moyer et al., 1990) and could be important to the forging of the
296 task specific spatiotemporal sequences during learning. Moreover,
297 Trace Eye-Blink Conditioning in mice has been previously observed to
298 elicit CA1 activity sequences even in a single session of training (Modi
299 et al., 2014).

300

301 Internally driven as opposed to externally driven network models of
302 activity sequences have been proposed as the mechanism driving
303 hippocampal CA1 sequences (Buzsáki & Llinás, 2017; Eichenbaum,
304 2017). The CA1 neurons participating in any sequence may represent
305 physiologically mappable attractors in temporally specific contexts.

306

307 **Theories on the function of the**
308 **hippocampus**

309

310 Four main ideas of hippocampal function studied over the past few
311 decades are,

312 A) Response Inhibition - Studied mostly in the 1960's, this
313 perspective described the Hippocampus as important to the
314 ability of animals to inhibit their impulses and natural, habitual,
315 or dominant behavioral responses to stimuli, in order to select
316 more appropriate responses. This perspective was justified by
317 two observations with regard to animals with hippocampal
318 damage - 1) these animals tended to be hyperactive, and 2)
319 were unable to withhold previously learnt responses. British
320 psychologist Jeffrey Alan Gray developed this perspective to
321 link hippocampal activity with anxiety (McNaughton & Gray,
322 2000).

323

324 B) Episodic Memory – This perspective was popularized by the
325 psychological studies on Patient H. M. (Henry Molaison), who
326 had been suffering from epileptic seizures and had to undergo
327 extensive hippocampectomy (surgical destruction of the
328 hippocampi), as treatment. American neurosurgeon William
329 Beecher Scoville and British-Canadian neuropsychologist
330 Brenda Milner were pioneers of this study and were able to
331 describe severe anterograde and partial retrograde amnesia in
332 the patient post surgery (Scoville & Milner, 1957). Since the late
333 2000's, the discovery and description of time cells (B. Kraus et

334 al., 2013; B. J. Kraus et al., 2015; MacDonald et al., 2011, 2013;
335 Modi et al., 2014; Pastalkova et al., 2008), has reinvigorated this
336 perspective.

337

338 C) Spatial Cognition - Originally popularized by the remarkable
339 work of American-British neuroscientist John O'Keefe and
340 American psychologist Lynn Nadel, the link between
341 hippocampal function and spatial navigation was solidified with
342 the discovery and subsequent descriptions of place cells (Morris
343 et al., 1982; O'Keefe & Dostrovsky, 1971; O'Keefe & Recce,
344 1993). This perspective is the most popular amongst the known
345 and studied functions of the Hippocampus and has been the
346 subject of a large body of work. Indeed, the Nobel Prize in
347 Physiology or Medicine 2014 was awarded to John O'Keefe,
348 May-Britt Moser, and Edvard I. Moser, for "The Brain's
349 Navigational Place and Grid Cell System".

350

351 D) Contextual Mapping – An emerging consensus in the field is
352 that the hippocampus actually builds contextual maps of the
353 environment or perceived events, with expansions to the neural
354 activity code along any relevant dimension of stimuli. Stimuli or
355 events cuing any modality, e.g., spatial, temporal, frequency,
356 etc., may be assimilated, along with more brain internal
357 variables such as (but not limited to) motivation, expected
358 reward status, prior experience in related tasks, and goal-
359 orientation (task specific). This allows the hippocampus to make
360 predictive models that bind new information streams to
361 collectively update predictions (M. R. Cohen & Kohn, 2011;
362 Eichenbaum, 2017; Miller et al., 2023; O'Keefe & Nadel, 1978).

363

364 **Space and time in the hippocampus**

365

366 Damage to the hippocampal system has been shown to cause the
367 impairment of long-term memory or amnesia, in human patients,
368 rodents, and non-human primates. Interestingly, such damage to the
369 Hippocampus seems to have no observable effect on the capacity for
370 acquisition and expression of skilled performance. These two results
371 suggest the role of the Hippocampus in certain kinds of memory, but
372 not all.

373

374 Anatomically, the hippocampal system receives input from, and in turn,
375 projects to the neocortical brain regions that serve as the site to
376 process higher order categories and modalities of information. It is thus
377 suggested that the Hippocampus holds a privileged position in the
378 brain, receiving the outcomes of the computation of the brain's various
379 modules, and relating to them. A large majority of the cortical
380 information is sent to the Hippocampus via the Entorhinal Cortex (EC).
381 This information is processed in roughly three stereotactically and
382 molecularly separable layers of cells in the following order: EC
383 → Dentate Gyrus → CA3 → CA1. This pathway from the EC to the CA1
384 has three separate synaptic connections (across the layers) and is also
385 known as the Trisynaptic Pathway (Figure 1). The output of the CA1 is
386 then sent to other cortical areas.

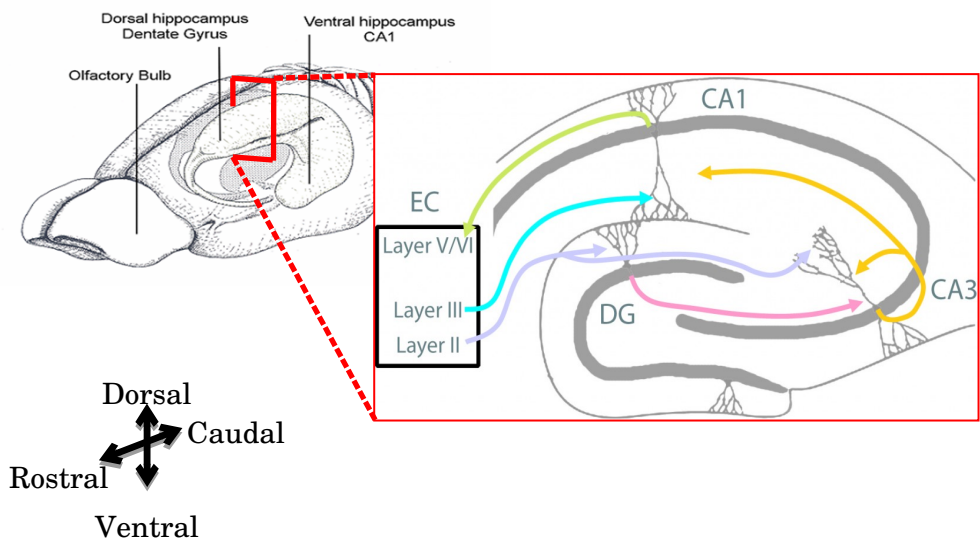


Figure 1: A schematic representation of the Trisynaptic Pathway as observed with coronal slices along the longitudinal axis of the hippocampus. Image adapted from the webpage for the Neural Circuits and Memory Lab, University of Wisconsin (Milwaukee) [<https://sites.lsa.umich.edu/diba-lab/neural-circuits-of-the-hippocampus/>])

388 One of the most significant discoveries in the hippocampal system and
389 surrounding brain structures was the role played in spatial cognition.
390 An enormous corpus of research has conclusively described,
391 • head-direction cells: with tuning curves tied to the direction that
392 experimental animals were oriented to. These cells respond to
393 egocentric vestibular cues as well as allocentric sensory cues
394 (Ranck, 1973; Taube et al., 1990), in the dorsal presubiculum,
395 retrosplenial cortex, entorhinal cortex, thalamus, and striatum,
396 among others.
397 • grid cells: with multi-modal tuning curves at regular spatial
398 positions as a lattice, across the environment being navigated.
399 These cells assimilate information about location, distance, and
400 direction, and are typically found in the entorhinal cortex (Fyhn
401 et al., 2004; Hafting et al., 2005).
402 • boundary vector cells: with tuning curves to the edges of the
403 environment being navigated. These cells are typically found in
404 the subiculum, pre- and para-subiculum, and entorhinal cortex
405 (Bjerknes et al., 2014; Lever et al., 2009; O'Keefe & Burgess,
406 1996; Savelli et al., 2008; Solstad et al., 2008).
407 • speed cells: with modulated firing rates based on the actual
408 running or movement speed of the animals. These cells are
409 typically found in the entorhinal cortex (Kropff et al., 2015).
410 • place cells: with tuning curves to specific locations in the
411 environment (O'Keefe & Dostrovsky, 1971; O'Keefe & Recce,
412 1993). These cells may be found in several hippocampal sub-
413 layers but often studied in the CA1.
414
415 The activity of neurons in the hippocampus of awake, behaving
416 animals is modulated by significant stimuli or objects in the

417 environment as well as relationships between temporally discontiguous
418 but relevant, paired stimuli. With the discovery of place cells, it was
419 clear that the CA1 of animals navigating a spatial environment,
420 showcased location specific firing fields. With the discovery of time
421 cells, it was noted that the CA1 of animals could elicit spatiotemporal
422 sequences of activity whenever the animal was required to make a link
423 between stimuli or events, even with a stimulus-free period in between.
424 Together, these results provided an important physiological parallel
425 between the spatial learning and episode learning deficit seen with
426 damage to the Hippocampus. Curiously, both place cells and time
427 cells, as well as the sequences built up with them were non-
428 topographically mapped, *i.e.*, they may be located anywhere in the
429 hippocampus, with no obvious spatial order (Dombeck et al., 2010;
430 Modi et al., 2014), in contrast to results from the cortex (Dombeck et
431 al., 2009; Ozden et al., 2008).

432

433 In an experiment published in 2008, Eva Pastalkova and colleagues
434 from Gyorgy Buzsaki's lab had rats navigate a figure 8 maze, with the
435 animal being rewarded with water, in between trials, if they managed to
436 alternate between the left and right arms (Pastalkova et al., 2008). As
437 an added nuance in the task, just before launching into the left or right
438 arms, the animal had to spend a fixed amount of time running a
439 treadmill, held in place. This would allow self-motion cues, but with the
440 absence of any other external stimuli. Impressively, single-units
441 recorded from the hippocampal CA1 cells revealed strong correlation
442 with the time spent on the treadmill, despite the absence of external
443 cues, and that different cells tuned to different time points, forming a
444 spatiotemporal sequence of activation (Pastalkova et al., 2008). In a
445 different experiment published in 2011, Christopher J. MacDonald and

446 colleagues from Howard Eichenbaum's lab had rats had to go around
447 a maze and perform a olfactory task (MacDonald et al., 2011). The
448 animals were first presented with an odour, then made to wait for a
449 delay period in a cordoned off section of the maze, before being
450 allowed to either dig for a reward or continue on the maze, depending
451 on the odour presented. As trials progressed, Hippocampal CA1 cells
452 were recorded (single-units) and found to not only be modulated by the
453 decision to be taken, but also to the amount of time spent in the delay
454 period. Experimentally, the delay period could be elongated or
455 shortened, each having an effect on remapping of the tuning fields of
456 the various CA1 cells, but to different extents (MacDonald et al., 2011).

457

458 In 2013, the Eichenbaum group published their findings with head-fixed
459 rats (no movement in space) performing a Delayed Match-To Sample
460 (DMS) task with pairs of odours, where again time tuned activity could
461 be observed with a sequence of Hippocampal CA1 cell activations, that
462 depended on the identity of the first odour (MacDonald et al., 2013). In
463 2014, Mehrab Modi, Ashesh Dhawale, and Upinder Bhalla published
464 their results with head-fixed mice learning and performing a Trace Eye-
465 Blink Conditioning (TEC), wherein it was observed that Hippocampal
466 CA1 cell activity sequences emerged in close relation to the acquisition
467 of behavioural performance, thus cementing the idea that sub-
468 populations of Hippocampal CA1 cells could bridge temporal gaps
469 between relevant, paired stimuli, and that they did so with the activity
470 of time-tuned cells (Modi et al., 2014).

471

472 Finally, it was important to study if these apparently time-tuned cells
473 were tuned to the actual duration of time in a delay period, or whether
474 it was more important for these cells to track the distance run. In an

475 experiment published in 2013, Benjamin Kraus and colleagues from
476 Howard Eichenbaum's lab again had their rats navigate a figure 8
477 maze, but with a motorized treadmill in the central arm, to
478 experimentally regulate the running speed. With this setup, the study
479 was successful at delineating that both time spent running and
480 distance run were important features, and that different cells could tune
481 to either of the features (B. Kraus et al., 2013). Whenever hippocampal
482 CA1 cells showcased time-tuned activity (as opposed to
483 space/location-tuned activity), such cells were dubbed "Time Cells"
484 (Eichenbaum, 2017; MacDonald et al., 2011).

485

486 Other interesting physiological parallels between the CA1 place cells
487 and time cells are,

- 488 1. Phase Precession: In relation to theta oscillations (6-10 Hz)
489 measured as local field potentials (LFP), individual cells tended
490 to fire action potentials at progressively earlier phases with each
491 successive cycle, described first for place cells (O'Keefe &
492 Recce, 1993), and then also for time cells (Pastalkova et al.,
493 2008).
- 494 2. Temporal Compression: Sequences of place or time cells could
495 be elicited at significantly shorter time scales, with fidelity in the
496 participating cells (Dragoi & Buzsáki, 2006; Foster, 2017).
497 Indeed, with regard to the typically studied regime of ~100-200
498 ms or behaviour time scales, the same sequence may be
499 elicited at ~10 ms as short segments during Sharp Wave
500 Ripples (Dragoi et al., 1999; V. Itskov et al., 2008; Jadhav et al.,
501 2012; O'Keefe & Recce, 1993; Valero et al., 2015) or even as
502 the whole sequences during Replay (Csicsvari et al., 2007; Diba
503 & Buzsáki, 2007; Foster, 2017; Foster & Wilson, 2006; Gupta et

504 al., 2010; Pfeiffer & Foster, 2013, 2015)(Foster, 2017; Foster &
505 Wilson, 2006; Gupta et al., 2010; Pfeiffer & Foster, 2013) or
506 Pre-play (Dragoi & Tonegawa, 2011, 2013).

507 3. Remapping: Systematic changes in the experimental paradigm,
508 such as those to the size of the experimental arena or in the
509 time interval between stimuli or events, would result in
510 systematic changes in the firing fields of place (Muller & Kubie,
511 1989) and time cells (MacDonald et al., 2011).

512 4. Variable Firing Fields: The width of the firing fields for a set of
513 place or time cells, respectively, may be variable. However, an
514 important distinction here is that there is as yet no clearly
515 identified predictor of the widths for place cells to spatial
516 directions, while time cells tuned to later time points in the inter-
517 stimulus or delay periods usually exhibit a widening of firing
518 fields (B. J. Kraus et al., 2015; MacDonald et al., 2011, 2013;
519 Mau et al., 2018; Pastalkova et al., 2008). The significance of
520 firing field density and widths is as yet an open line of inquiry.

521

522 Single-units recorded from the medial entorhinal cortex (MEC) as well
523 as the hippocampal CA1 that were found tuned to specific frequency
524 “landmarks” during frequency sweeps self-initiated by rats (Aronov et
525 al., 2017), suggesting that the CA1 could tune to variables other than
526 space and time. This added even more weight to “Contextual Mapping”
527 as an important function of the hippocampus.

528 **“Single-cell, multi-trial” vs. “multi-cell,
529 single-trial” approaches in Neuroscience**

530

531 A dominant, early perspective in neurophysiology had been to record
532 activity from a single cell, over many trials, under a variety of
533 conditions (bath applications in slice physiology, different physiological
534 conditions like stress and genetic background, etc.). For more than one
535 recorded cell, the process would be repeated, till the dataset was
536 complete.

537

538 An intermediate perspective was to record from multiple cells
539 simultaneously, yet treat each cell independently for analysis towards
540 correlation and mechanism studies, across many repeats of
541 experimental conditions or trials (same as above).

542

543 An important and more modern perspective is to record from multiple
544 cells simultaneously, and use this network or population activity to
545 decode single-trial characteristics (position, time, stimulus presence,
546 etc.) using very powerful numerical and mathematical algorithms
547 involving (but not limited to) Bayesian Decoding and Information
548 Theory. The essential idea is that the neuronal code of the brain is not
549 defined just by the activity of single neurons since they may only
550 encode very specific fractions of the experience, but rather that the
551 population encodes the full experience, using a number of distributed
552 and redundant strategies.

553 • Bayesian Decoding: Using the activity of multiple,
554 simultaneously recorded neurons to develop a likelihood
555 estimate of the evidence (firing rate combinations) to the
556 experimental parameter (spatial position, relative time, etc.)
557 and combine this with the experimentally determined prior
558 (probability), to obtain estimates of the conditional or

559 posterior probability of a parameter value, given evidence.
560 Bayes' Rule describes
561
$$P(A|B) = P(B|A).P(A)/P(B)$$

562 ... where,
563 A: Parameter value (position, time, etc.)
564 B: Evidence (cellular firing rate)
565 $P(A)$: Prior Probability (experimentally defined)
566 $P(B)$: Probability of evidence (Firing Rate)
567 $P(A|B)$: Posterior probability of parameter value given
568 evidence
569 $P(B|A)$: Likelihood estimate of evidence given parameter
570 value (based on recordings)
571 This methodology has been used to not only successfully
572 predict specific time points in a trial from population activity, but
573 has also been used to observe that the population activity from
574 a session of recording is able to predict time points in trials
575 conducted on subsequent sessions of recording, up unto 3-4
576 sessions (Mau et al., 2018).
577 • Information Theory: Using recorded cellular activity to
578 estimate how much information this activity carries about
579 experimental parameters (position, time, stimuli, etc.). Three
580 essential metrics have been used,
581 1. Information per activity spike (I_{spike}), in bits/spike
582 2. Information per unit time (I_{sec}), in bits/sec
583 3. Mutual Information (MI) between evidence and
584 parameter value, in bits
585 William Skaggs, Bruce McNaughton and colleagues published a
586 series of experiments working out the value of Information Theory
587 based approaches to deciphering the hippocampal code, reviewed

588 previously (Skaggs et al., 1996). This idea was later adapted strongly
589 by the field but focus throughout, remained on place cells.

590

591 An interesting study published in 2018 even used synthetic test
592 datasets to go to the extent of estimating place cell detection algorithm
593 performance on the basis of I_{spike} , I_{sec} and MI (Souza et al., 2018). They
594 found,

- 595 1. MI could outperform the other two in a variety of scenarios.
- 596 2. I_{spike} and I_{sec} may still be useful in identifying unique
597 subpopulations of place cells.
- 598 3. Important algorithmic adjustments could be made to the
599 calculations of I_{spike} and I_{sec} , to equalize performance between
600 them and MI.

601 There was clear nuance in the population code that required such a
602 perspective during analysis. Eichenbaum and colleagues popularized
603 the use of such metrics in the context of time cells (Mau et al., 2018),
604 yet a systematic approach to identifying the best algorithms for time
605 cells was requisite.

606

607 Correlation analysis between pairs of recorded cells is one of the most
608 important analytical directions taken by neurophysiologists
609 understanding brain function, and has been reviewed previously (M. R.
610 Cohen & Kohn, 2011). However, such analysis can be subject to False
611 Positives, without appropriate significance studies. Specifically, it is
612 important to look at whether the activity profile or tuning curves for cells
613 (in relation to task variables) is significant above chance or other
614 clearly defined cutoffs, using a large number of randomized surrogates
615 of the recorded activity, generated by adding random timing shifts or
616 bootstraps. Multiple pairwise correlations may not be sufficient to

617 identify synchronous sequential activity in the network, without looking
618 at higher orders of correlation across recorded cells. Ultimately, such
619 studies benefit from simultaneous high-yield recordings, updated
620 analytical procedures utilizing surrogate data for significance analysis,
621 examining repetitions across trials (or trial-to-trial variability), and even
622 the use of multiple analytical strategies, as reviewed previously
623 (Foster, 2017; Grün, 2009).

624

625 Synfire chains (Abeles, 1982, 1991, 2009; Abeles et al., 2004) as
626 sequential neuronal activity patterns or motifs have been described in
627 cortical slices *in vitro* (Reyes, 2003), as well as *in vivo* (Ikegaya et al.,
628 2004). The 2004 study described these sequences as songs (Ikegaya
629 et al., 2004) that can incorporate new information as extensions of the
630 motifs by combining multiple synfire chains (Bienenstock, 1995).

631 However, an important consideration is that the original theoretical
632 ideas behind synfire chains assumed feed-forward connections
633 between layers of neurons, with recognition by subsequent neurons
634 looking only at waves of synchrony, rather than specific individual
635 neuronal identities (Abeles, 2004). Another important perspective is
636 that these cortical sequences could be artifacts elicited just by chance,
637 given the nature of membrane voltage fluctuations (McLelland &
638 Paulsen, 2007; Mokeichev et al., 2007). There is thus some speculation
639 over the significance of “cortical songs”, *in vivo*.

640

641 A major step forward with “multi-cell, single-trial” approaches is the
642 benefit of resolving how each cell and inter-cell interactions contribute
643 to stimulus representation, behavioural task variables, and other brain-
644 intrinsic computation. Technological advances in large-scale
645 neurophysiology recordings such as the increased density of tetrode

646 drives, neuropixels, optical sectioning and microscopy, resonant
647 scanning, etc., have enabled the discovery of well coordinated
648 sequences of cellular activity such as Sharp Wave Ripples (SWRs),
649 Replay, and behavioural timescale spatio-temporal sequences, *in vivo*,
650 among others. This is primarily due to a radical improvement in an
651 experimenter's ability to simultaneously record from multiple cells
652 (Foster, 2017), going from yields of ~10 cells to even ~10⁴ cells, per
653 animal.

654

655 **Single-Unit Electrophysiology vs 2-Photon** 656 **Calcium Imaging to study the Hippocampus**

657

658 The most well characterized and studied function of the hippocampus
659 and surrounding tissue (Entorhinal Cortex, Parasubiculum, etc.) was
660 the role these tissue systems played in Spatial Navigation and Coding.
661 Single-Unit Electrophysiology was paramount to being able to isolate
662 the activity from individual cells, and eventually was used to discover
663 and describe properties of place cells (O'Keefe & Dostrovsky, 1971),
664 grid cells (Fyhn et al., 2004; Hafting et al., 2005), head-direction cells
665 (Taube et al., 1990), along with numerous other important
666 physiological discoveries, as detailed previously. However, even with
667 advances in the density of tetrode recordings, the yield of recorded
668 cells from any given animal was often limited to <50 cells. It was only
669 with the invention of Neuropixels (Jun et al., 2017) that this yield could
670 be expanded to ~1000 cells. We had opted to utilize calcium imaging
671 by 2-Photon Microscopy (Denk et al., 1990; Stosiek et al., 2003). This
672 methodology, allowed us to record ~100-150 cells per session with our

673 mice, albeit with significant cost to the recording frame rate on account
674 of the limitations of the technique. We discuss details of our technique
675 along with challenges and preliminary results, in Chapter 3 –
676 “Imaging”.

677

678 The hippocampi (one in each hemisphere) of the mouse brain lie ~1
679 mm below the most superficial layers of cortex (just inside the
680 cranium), a barrier typically too wide for typical 1-photon fluorescence
681 imaging systems (Confocal, Spinning Disk, etc.). This poses a very
682 difficult challenge for imaging preparations since there are hardware
683 and other technical limits to how long the working distance of
684 microscope objectives can be made. The use of 2-photon microscopy
685 combined with combinations of cortical excavations (to aid physical
686 access), microendoscopes, as well as prisms to guide emitted
687 fluorescence, have all been used to achieve deep brain imaging based
688 recordings at cellular resolution, in rodents (Andermann et al., 2013;
689 Attardo et al., 2015; Barreto et al., 2009; Barreto & Schnitzer, 2012;
690 Dombeck et al., 2010; Heys et al., 2014; Murray & Levene, 2012;
691 Velasco & Levene, 2014; Ziv et al., 2013).

692

693 All imaging preparation standardizations described in this thesis invoke
694 2-Photon calcium imaging of hippocampal CA1 cells at cellular
695 resolution (1 pix = ~1 μ m), following cortical excavations just above the
696 left hippocampus (Dombeck et al., 2010).

697 **Calcium imaging by 2-Photon Microscopy**

698

699 Typically, as cells become activated and elicit action potentials, there is
700 often a large concomitant influx of Ca^{2+} ions through voltage gated
701 calcium channels all around the perisomatic membrane, amongst other
702 cellular compartments. Several organic dyes have been developed that
703 reversibly bind Ca^{2+} ions in the cytosol and either become fluorescent
704 or emit greater fluorescence (often with a red shift) when in this Ca^{2+} -
705 bound state (Paredes et al., 2008). Additionally tremendous advances
706 in molecular biology has seen the deployment of Genetically Encoded
707 Calcium Indicators (GECIs) that may be exogenously incorporated into
708 the genome of target cells. These GECIs serve the same function as
709 organic calcium dyes, but may easily be replenished in the cytosol
710 given the cell's natural machinery for transcription and translation, and
711 whose Fluorescence properties can be engineered for brightness,
712 responsivity, Ca^{2+} binding K_d , and fluorescence emission wavelengths.
713 The number of cells that may be recorded by fluorescence is often only
714 limited to either the spread of the organic dye or the imaging
715 magnification settings, allowing for yields of 100-1000 cells.

716
717 With any Imaging based neurophysiology, there is always a trade-off
718 between yield (number of cells recorded simultaneously) and temporal
719 resolution. Increasing the yield by recording over a larger area of tissue
720 requires many more pixels per imaging frame, resulting in a loss of
721 temporal resolution (frame rate). On the other hand, increasing the
722 frame rate necessitates capturing fewer pixels per frame, decreasing
723 yield. There is even a limitation of simply zooming out, since stable
724 fluorescence intensity fluctuations can only be identified when each
725 cell is defined at least by a certain number of pixels, to allow proper
726 isolation.

727

728 Specifically with calcium imaging, the signal to be recorded
729 corresponds to Ca^{2+} flux in the cytoplasm as measured by the change
730 in emitted fluorescence of reporters such as GCaMP, with a $\tau_{\text{rise}} = 10-$
731 100 ms and $\tau_{\text{fall}} = 100\text{-}300$ ms (Chen et al., 2013). This signal is one or
732 two orders of magnitude slower than the action potential ($\sim 2\text{-}5$ ms).
733 However, this may not necessarily be a limitation since a dominant
734 idea in the field is to simply consider rate coding, or time-averaged
735 spiking activity (Abeles, 2004), bringing down the effective temporal
736 resolution of the electrical record.

737

738 Genetically Encoded Voltage Indicators (GEVIs) that fluoresce with
739 higher emission during membrane voltage dynamics have also been
740 developed. However, their localization onto the membrane of the cell,
741 instead of the cytoplasm, diminishes the total emitted photon flux per
742 unit time, and requires longer bin times to achieve reasonable signal-
743 to-noise, as reviewed previously (Mollinedo-Gajate et al., 2021). This
744 unfortunately brings down the frame rate even more than what can be
745 achieved with GECIs. We avoided GEVIs in the projects described in
746 this thesis.

747

748 A major advancement in Fluorescence Imaging was the invention of
749 Confocal and Multiphoton (typically 2-Photon) Microscopes, which
750 allowed for unprecedented recording signal-to-noise by optical
751 sectioning. 2-Photon Imaging itself was an important development for
752 the neurophysiology of tissue greater than 300 μm in thickness, typical
753 of rodent brain tissue, because it avoids wasteful excitation of imaging
754 planes that are not in focus (out-of-plane). The 2-Photon effect
755 requires two photons of longer wavelength (lower energy per photon),
756 to near instantaneously excite a fluorophore. The photon flux is highest

757 at the focal plane (with an N-squared dependence) of the microscope
758 so only the section of the tissue corresponding to the focal place is
759 allowed to achieve fluorescence. Additionally, longer wavelengths of
760 excitation light can more easily penetrate deeper layers of tissue, due
761 to comparatively lower scattering or Rayleigh effect (Denk et al., 1990;
762 Helmchen & Denk, 2005).

763

764 The hippocampus (specifically the hippocampal CA1) was the main
765 brain structure of interest for all our physiology experiments, and lies
766 under about 1 mm of cortical tissue for mice. This is a depth that is
767 difficult to image even with 2-Photon Microscopy. The typical
768 methodology employed in such cases is to perform a cortical
769 excavation just above the Hippocampus filling the crevice with optically
770 clearer agarose or silicone elastomer. Even so, the hippocampal CA1
771 cell body layer (*Stratum Pyramidale*) still lies about 150-300 μm below
772 the external capsule and corpus callosum fibers (left intact for chronic
773 imaging). Accordingly, we combined cortical excavation with 2-Photon
774 microscopy, using a long working distance objective with a wide field of
775 view, imaging cytosolic Ca^{2+} activity with the help of either an organic
776 dye (OGB-1; acute imaging) or a GECI (GCaMP6f; chronic imaging).

777

778 An important perspective that has motivated the use of Imaging based
779 physiology recordings (as opposed to Electrophysiological methods)
780 other than potential yield, is that imaging provides anatomical
781 confirmation of any particular recorded cell, and this in turn allows for,
782 A) Unambiguous isolation of the same cell across multiple imaging
783 sessions (across days and weeks). Single-Units are ultimately
784 only algorithmically resolved and this can be done only for cells
785 that are active and are represented in multiple spatially

786 separated electrodes. However, very recently, Ashesh Dhawale
787 and colleagues from Bence Olveczky's lab have devised a
788 solution to track the movement of electrodes in tissue over time
789 and use this information to ensure chronic recording of the
790 same units (Dhawale et al., 2017). This technique was not
791 available at the time when experiments for this thesis were
792 started.

793 B) Unambiguous detection of the lack of activity in an otherwise
794 recorded cell. Since the cell can be anatomically identified
795 independent of activity, it is possible to observe the absence of
796 Ca^{2+} activity. Automated cell ROI detection (Francis et al., 2012;
797 Maruyama et al., 2014; Mukamel et al., 2009; Pachitariu et al.,
798 2017; Pnevmatikakis et al., 2016) simplifies the pre-processing
799 step of cell isolation even over large batch sizes. These
800 procedures inherently require the use of the calcium activity
801 profiles of recorded cells, viz., inactive cells (though
802 anatomically visible), may not be isolated.

803 **Automated ROI detection for large-scale**
804 **Calcium Imaging datasets**

805
806 A number of automated ROI detection algorithms have been cited in
807 literature that require minimal user intervention, perform relatively fast
808 identification for a large number of identified sources (putative cells).
809 Some popular algorithms include PCA/ICA (Mukamel et al., 2009),
810 Suite2p (Pachitariu et al., 2017), and Non-Negative Matrix
811 Factorization (NNMF)(Pnevmatikakis et al., 2016), which all have been
812 developed to the extent where comparable or oftentimes much better

813 ROI detection is achieved than as compared to the more tedious hand-
814 drawn ROIs which scales very poorly with orders of cells recorded.
815 We have strictly followed Suite2p (Pachitariu et al., 2017) for all
816 physiological ROI (cell sources) described in this thesis.
817

818 **A brief introduction to associative learning**

819
820 The ability to physiologically record cells is insufficient without placing
821 the experimental animals in precisely defined, stable behavioural
822 contexts. Only in this way can neural activity be checked for
823 correlations or mapping to distinct changes in external behaviour
824 variables and the decisions that the animal makes, accordingly.
825 Combining behaviour and recording was considered an important
826 guiding principle in all our experiments.
827
828 Prior to the early 20th century, Structuralism was a dominant
829 perspective in Psychology, insisting on introspection - the observation
830 and report of one's own mind and thoughts. Experiments and
831 discoveries by Ivan Pavlov at the Military Medical Academy in
832 Petrograd (St. Petersburg), eventually led to a dramatic shift in
833 perspective, with the birth of Classical Conditioning, a type of
834 associative learning. Following the very same methodology advocated
835 by Francis Bacon (early 17th century), quantitative data from carefully
836 conducted animal experiments were recorded, with the idea to narrow
837 down on a small number of hypotheses that could explain experimental
838 observations.
839

840 Ivan Pavlov provided essential demonstrations of anticipation and
841 made tremendous progress in understanding the circumstances on
842 which anticipation depends, and this is why Classical Conditioning is
843 also often referred to as Pavlovian Conditioning. Following Pavlov's
844 studies (Pavlov, 1927), it was proposed that Classical Conditioning
845 was a prototypical example of Association. While it does have caveats
846 such as covert learning when observable behaviour may be blocked
847 (Dickinson et al., 1983; Krupa & Thompson, 2003), Associative
848 learning is rich with a variety of animals and association tasks that
849 have been crucial to study memory and learning over the past century.

850

851 Typically, animals require no prior training to elicit a behavioural or
852 motor movement to biologically potent stimulus (appetitive or aversive),
853 called an Unconditioned Stimulus (US). Examples include food, water,
854 electrical shock, temperature shock, etc.. Without pairing with a US, a
855 neutral stimulus elicits no observable response from an animal, and
856 such a stimulus is called a Conditioned Stimulus (CS). Examples
857 include simple auditory tones, flashes of light, among others.

858

859 Classical Conditioning is both the behavioural procedure as well as the
860 learning process that results from the pairing of a previously neutral
861 stimulus (CS) with a biologically potent stimulus (US). Repeated
862 pairing allows animals to make implicit associations between the CS
863 and US, and essentially anticipate the occurrence of the US, once the
864 CS is observed. Animals report this forecasting feat by producing the
865 same response that they would to a US, albeit often a milder version.
866 Typical protocols for Classical Conditioning, follow the regime of
867 Forward pairing, *viz.*, - the CS is presented before the US, and this

868 temporal structure will be followed unanimously across all behaviour
869 experiments described in this thesis.
870
871 The standardization of the behavioural task, physiological recording
872 (imaging) preparation, as well as the custom analysis routines to look
873 for various physiological features are described in this thesis.
874 Combining these multi-disciplinary approaches allowed us to develop a
875 toolkit to study time cells in the hippocampus, under strict behavioural
876 contexts. It is important to note, however, that spatiotemporal
877 sequences of activity as measured by calcium imaging based
878 simultaneous recordings of a large number of cells, are not limited to
879 the hippocampus, being studied even in the visual cortex (Pachitariu et
880 al., 2017; Poort et al., 2015), somatosensory cortex (Petersen, 2019),
881 entorhinal cortex (Heys et al., 2014), and even in the cerebellum
882 (Giovannucci et al., 2017). Essentially, the analytical methods
883 developed can easily be adapted to other neuronal network recordings
884 where time-tuning may be applicable.
885

886 **Short Summaries of the 3 projects**

887 **Project I - How do sensory representations transform**

888 **with learning?**

889 Sensory Systems Neuroscience is a very popular field spanning
890 studies looking at numerous brain regions and sub-regions in the
891 cortex and hippocampus, *in vivo* (R. A. Andersen et al., 1993; Fassihi
892 et al., 2017; Khan et al., 2010; Meeks et al., 2010; Petersen, 2019;
893 Poort et al., 2015; Voelcker et al., 2022), among several others. Many

894 if not most of these studies describe neural activity in animals with
895 expert levels of behavioural learning and performance to the presented
896 stimuli. Lacunae still remain as to mechanisms deployed during active
897 or online learning especially in the early stages of behavioural training.
898

899 We deployed our experiments with the intention to study how Calcium
900 Imaging by 2-Photon could reveal finer population level details of
901 network activity as the animals were tested on the learning of an
902 operant conditioning or lick behaviour task. We were able to,

- 903 1. Prototype OGB-1 based calcium imaging *in vivo*, from head-
904 fixed mice in a manner suited to combined behaviour and
905 recording experiments, and
- 906 2. Study preliminary data from animals that correlation based
907 functional activity clusters of recorded CA1 cells have spatial
908 organization during bouts of spontaneous activity.

909

910 However, we were not satisfied with the level and rate of learning in
911 our test animals eventually leading to a search for more stable
912 behaviour paradigms in mice. Additionally, the use of OGB-1 as the
913 Calcium Indicator also had to be abandoned since this fundamentally
914 disallowed multi-day tracking of the same cells. We discuss our
915 prototyping efforts and preliminary data for this project in detail, in the
916 first few sections each of Chapters 2 (“Behaviour”) and 3 (“Imaging”).

917

918 **Project II - How does the timing of cellular activity adjust
919 to behavioural task variables?**

920

921 Research on the cerebellum has made substantial progress in the
922 elucidation of network mechanisms correlating well with external
923 stimulus timing based variables, as animals learn Trace Eye-Blink
924 Conditioning and Delay Conditioning (Kalmbach, Davis, et al., 2010;
925 Kalmbach, Ohyama, et al., 2010; Medina et al., 2000; Ohyama et al.,
926 2003; Siegel & Mauk, 2013). The predominant studies on time cells in
927 the hippocampus have focused on the context of appetitive reinforcing
928 stimuli (Eichenbaum, 2004, 2017; B. Kraus et al., 2013; B. J. Kraus et
929 al., 2015; MacDonald et al., 2011, 2013; Mau et al., 2018; Pastalkova
930 et al., 2008). Time cells in the behavioural context of Trace Eye-Blink
931 conditioning, an aversive learning paradigm, have been explored (Modi
932 et al., 2014), but details such as correlations with rates of behavioural
933 learning, tuning adaptability, and long-term stability (~weeks) of the
934 time sequences are yet to be studied.

935

936 We prototyped a GCaMP6f based *in vivo* Hippocampal preparation
937 that allowed for chronic, longitudinal recordings of hippocampal CA1,
938 by 2-Photon Calcium Imaging (Dombeck et al., 2010) that could be
939 combined with a stable and adaptable learning protocols of Trace Eye-
940 Blink Conditioning (Siegel et al., 2015).

941 From our preliminary set of recordings we were able to,

- 942 1. Detect time cells in our population recordings,
- 943 2. Observe signs of expansion of the time cell sub-population over
944 early stages of learning, and
- 945 3. Observe shifts in the timing of peak for known, chronically
946 tracked time cells, typically moving away from the US and
947 towards the CS.

948

949 Technical difficulties prevented us from expanding our experimental
950 recording datasets to the point where these results could be looked at
951 more critically and the results may be sufficient for publication. We
952 discuss our prototyping efforts and preliminary data for this project in
953 detail, in the last few sections each of Chapters 2 (“Behaviour”) and 3
954 (“Imaging”).

955

956 **Project III - What is the best way to detect and score
957 time-tuned cellular activity?**

958

959 Given that we had collected a reasonable sample of multi-day tracked
960 cells while head-fixed mice were being trained to a Trace Eye-Blink
961 Conditioning (TEC) task, we wished to move forward to identifying time
962 cells in the most reliable way, with the aim to drawing quality
963 conclusions from the physiology recordings.

964

965 The paper entitled “Synthetic Data Resource and Benchmarks for Time
966 Cell Analysis and Detection Algorithms” (Ananthamurthy & Bhalla,
967 2023) was a consolidation of our progress to analyse physiology data
968 from real and synthetic cells expressed as calcium activity trials and
969 sessions.

970

971 Here, we used a computational approach and developed categorically
972 labelled, user definable, large scale synthetic datasets, as a test bed to
973 compare and benchmark the predictions made by popular time cell
974 detection algorithms. We were able to test the sensitivity of these
975 computational algorithms across a wide array of experimental

976 recording parameters, and could ultimately conclude the best
977 operational regimes for each of them. All of the code base for this
978 project is freely available online
979 (<https://github.com/bhallalab/TimeCellAnalysis>) and is intended to be a
980 resource to researchers.

981

982 The paper is attached as Chapter 4 (“Analysis”).

983 **Code Availability**

984

985 All our code for Synthetic Data generation and time cell Analysis is
986 available at <https://www.github.com/bhallalab/TimeCellAnalysis>.

987

988 All our code for conducting Trace Eye-Blink Conditioning (TEC)
989 behaviour is available at
<https://www.github.com/ananthamurthy/eyeBlinkBehaviour>.

991

992 Analysis scripts for evaluating TEC performance are available at
993 <https://github.com/ananthamurthy/MATLAB/tree/master/TECAnalysis>.

994 **Bibliography**

995

996 Abeles, M. (1982). *Local Cortical Circuits: An Electrophysiological*
997 *Study*. Springer-Verlag. <https://books.google.co.in/books?id=s25lwEACAAJ>

999 Abeles, M. (1991). *Corticonics: Neural Circuits of the Cerebral Cortex*.
1000 Cambridge University Press. <https://doi.org/DOI:10.1017/CBO9780511574566>

1002 Abeles, M. (2004). Time Is Precious. *Science*, 304(5670), 523–524.
1003 <https://doi.org/10.1126/science.1097725>

1004 Abeles, M. (2009). *Synfire Chains* (L. R. B. T.-E. of N. Squire (ed.); pp.
1005 829–832). Academic Press.
1006 <https://doi.org/https://doi.org/10.1016/B978-008045046-9.01437-6>

1007 Abeles, M., Hayon, G., & Lehmann, D. (2004). Modeling
1008 compositionality by dynamic binding of synfire chains. *Journal of*
1009 *Computational Neuroscience*, 17(2), 179–201.
1010 <https://doi.org/10.1023/B:JCNS.0000037682.18051.5f>

- 1011 Ananthamurthy, K. G., & Bhalla, U. S. (2023). Synthetic Data Resource
1012 and Benchmarks for Time Cell Analysis and Detection Algorithms.
1013 *ENeuro*, ENEURO.0007-22.2023.
1014 <https://doi.org/10.1523/ENEURO.0007-22.2023>
- 1015 Andermann, M. L., Gilfoy, N. B., Goldey, G. J., Sachdev, R. N. S.,
1016 Wölfel, M., McCormick, D. A., Reid, R. C., & Levene, M. J. (2013).
1017 Chronic Cellular Imaging of Entire Cortical Columns in Awake
1018 Mice Using Microprisms. *Neuron*, 80(4), 900–913.
1019 <https://doi.org/10.1016/j.neuron.2013.07.052>
- 1020 Andersen, R. A., Snyder, L. H., Li, C.-S., & Stricanne, B. (1993).
1021 Coordinate transformations in the representation of spatial
1022 information. *Current Opinion in Neurobiology*, 3(2), 171–176.
1023 [https://doi.org/https://doi.org/10.1016/0959-4388\(93\)90206-E](https://doi.org/https://doi.org/10.1016/0959-4388(93)90206-E)
- 1024 Aronov, D., Nevers, R., & Tank, D. W. (2017). Mapping of a non-spatial
1025 dimension by the hippocampal-entorhinal circuit. *Nature*,
1026 543(7647), 719–722. <https://doi.org/10.1038/nature21692>
- 1027 Attardo, A., Fitzgerald, J. E., & Schnitzer, M. J. (2015). Impermanence
1028 of dendritic spines in live adult CA1 hippocampus. *Nature*,
1029 523(7562), 592–596. <https://doi.org/10.1038/nature14467>
- 1030 Barreto, R. P. J., Messerschmidt, B., & Schnitzer, M. J. (2009). In vivo
1031 fluorescence imaging with high-resolution microlenses. *Nature
Methods*, 6(7), 511–512. <https://doi.org/10.1038/nmeth.1339>
- 1033 Barreto, R. P. J., & Schnitzer, M. J. (2012). In vivo optical
1034 microendoscopy for imaging cells lying deep within live tissue.
1035 *Cold Spring Harbor Protocols*, 2012(10), 1029–1034.
1036 <https://doi.org/10.1101/pdb.top071464>
- 1037 Bienenstock, E. (1995). A model of neocortex. *Network: Computation
in Neural Systems*, 6(2), 179–224. https://doi.org/10.1088/0954-898X_6_2_004
- 1040 Bjerknes, T. L., Moser, E. I., & Moser, M.-B. (2014). Representation of
1041 Geometric Borders in the Developing Rat. *Neuron*, 82(1), 71–78.
1042 <https://doi.org/10.1016/j.neuron.2014.02.014>

- 1043 Buzsáki, G., & Llinás, R. (2017). Space and time in the brain. *Science*
1044 (New York, N.Y.), 358(6362), 482–485.
1045 <https://doi.org/10.1126/science.aan8869>
- 1046 Cai, D. J., Aharoni, D., Shuman, T., Shobe, J., Biane, J., Song, W.,
1047 Wei, B., Veshkini, M., La-Vu, M., Lou, J., Flores, S. E., Kim, I.,
1048 Sano, Y., Zhou, M., Baumgaertel, K., Lavi, A., Kamata, M.,
1049 Tuszyński, M., Mayford, M., ... Silva, A. J. (2016). A shared neural
1050 ensemble links distinct contextual memories encoded close in
1051 time. *Nature*, 534(7605), 115–118.
1052 <https://doi.org/10.1038/nature17955>
- 1053 Caporale, N., & Dan, Y. (2008). Spike timing-dependent plasticity: a
1054 Hebbian learning rule. *Annual Review of Neuroscience*, 31, 25–
1055 46. <https://doi.org/10.1146/annurev.neuro.31.060407.125639>
- 1056 Carew, T. J., Castellucci, V. F., & Kandel, E. R. (1971). An Analysis of
1057 Dishabituation and Sensitization of The Gill-Withdrawal Reflex In
1058 Aplysia. *International Journal of Neuroscience*, 2(2), 79–98.
1059 <https://doi.org/10.3109/00207457109146995>
- 1060 Chen, T.-W., Wardill, T. J., Sun, Y., Pulver, S. R., Renninger, S. L.,
1061 Baohan, A., Schreiter, E. R., Kerr, R. A., Orger, M. B., Jayaraman,
1062 V., Looger, L. L., Svoboda, K., & Kim, D. S. (2013). Ultrasensitive
1063 fluorescent proteins for imaging neuronal activity. *Nature*,
1064 499(7458), 295–300. <https://doi.org/10.1038/nature12354>
- 1065 Cohen, M. R., & Kohn, A. (2011). Measuring and interpreting neuronal
1066 correlations. *Nature Neuroscience*, 14(7), 811–819.
1067 <https://doi.org/10.1038/nn.2842>
- 1068 Csicsvari, J., O'Neill, J., Allen, K., & Senior, T. (2007). Place-selective
1069 firing contributes to the reverse-order reactivation of CA1
1070 pyramidal cells during sharp waves in open-field exploration. *The*
1071 *European Journal of Neuroscience*, 26(3), 704–716.
1072 <https://doi.org/10.1111/j.1460-9568.2007.05684.x>
- 1073 Davidson, T. J., Kloosterman, F., & Wilson, M. A. (2009). Hippocampal
1074 replay of extended experience. *Neuron*, 63(4), 497–507.
1075 <https://doi.org/10.1016/j.neuron.2009.07.027>

- 1076 Denk, W., Strickler, J. H., & Webb, W. W. (1990). Two-photon laser
1077 scanning fluorescence microscopy. *Science (New York, N.Y.)*,
1078 248(4951), 73–76. <https://doi.org/10.1126/science.2321027>
- 1079 Dhawale, A. K., Poddar, R., Wolff, S. B. E., Normand, V. A.,
1080 Kopelowitz, E., & Ölveczky, B. P. (2017). Automated long-term
1081 recording and analysis of neural activity in behaving animals.
1082 *eLife*, 6, e27702. <https://doi.org/10.7554/eLife.27702>
- 1083 Diba, K., & Buzsáki, G. (2007). Forward and reverse hippocampal
1084 place-cell sequences during ripples. *Nature Neuroscience*, 10(10),
1085 1241–1242. <https://doi.org/10.1038/nn1961>
- 1086 Dickinson, A., Nicholas, D. J., & Mackintosh, N. J. (1983). A re-
1087 examination of one-trial blocking in conditioned suppression. *The
1088 Quarterly Journal of Experimental Psychology B: Comparative
1089 and Physiological Psychology*, 35, 67–79.
1090 <https://doi.org/10.1080/14640748308400914>
- 1091 Dombeck, D. A., Graziano, M. S., & Tank, D. W. (2009). Functional
1092 clustering of neurons in motor cortex determined by cellular
1093 resolution imaging in awake behaving mice. *The Journal of
1094 Neuroscience : The Official Journal of the Society for
1095 Neuroscience*, 29(44), 13751–13760.
1096 <https://doi.org/10.1523/JNEUROSCI.2985-09.2009>
- 1097 Dombeck, D. A., Harvey, C. D., Tian, L., Looger, L. L., & Tank, D. W.
1098 (2010). Functional imaging of hippocampal place cells at cellular
1099 resolution during virtual navigation. *Nature Neuroscience*, 13(11),
1100 1433–1440. <https://doi.org/10.1038/nn.2648>
- 1101 Dragoi, G., & Buzsáki, G. (2006). Temporal encoding of place
1102 sequences by hippocampal cell assemblies. *Neuron*, 50(1), 145–
1103 157. <https://doi.org/10.1016/j.neuron.2006.02.023>
- 1104 Dragoi, G., Carpi, D., Recce, M., Csicsvari, J., & Buzsáki, G. (1999).
1105 Interactions between hippocampus and medial septum during
1106 sharp waves and theta oscillation in the behaving rat. *The Journal
1107 of Neuroscience : The Official Journal of the Society for*

- 1108 *Neuroscience*, 19(14), 6191–6199.
1109 <http://www.ncbi.nlm.nih.gov/pubmed/10407055>
- 1110 Dragoi, G., & Tonegawa, S. (2011). Preplay of future place cell
1111 sequences by hippocampal cellular assemblies. *Nature*,
1112 469(7330), 397–401. <https://doi.org/10.1038/nature09633>
- 1113 Dragoi, G., & Tonegawa, S. (2013). Distinct preplay of multiple novel
1114 spatial experiences in the rat. *Proceedings of the National
1115 Academy of Sciences of the United States of America*, 110(22),
1116 9100–9105. <https://doi.org/10.1073/pnas.1306031110>
- 1117 Eichenbaum, H. (2004). Hippocampus: Cognitive processes and
1118 neural representations that underlie declarative memory. *Neuron*,
1119 44(1), 109–120. <https://doi.org/10.1016/j.neuron.2004.08.028>
- 1120 Eichenbaum, H. (2017). On the Integration of Space, Time, and
1121 Memory. *Neuron*, 95(5), 1007–1018.
1122 <https://doi.org/10.1016/j.neuron.2017.06.036>
- 1123 Fassihi, A., Akrami, A., Pulecchi, F., Schönfelder, V., & Diamond, M. E.
1124 (2017). Transformation of Perception from Sensory to Motor
1125 Cortex. *Current Biology : CB*, 27(11), 1585-1596.e6.
1126 <https://doi.org/10.1016/j.cub.2017.05.011>
- 1127 Ferbinteanu, J., & Shapiro, M. L. (2003). Prospective and retrospective
1128 memory coding in the hippocampus. *Neuron*, 40(6), 1227–1239.
1129 [https://doi.org/10.1016/s0896-6273\(03\)00752-9](https://doi.org/10.1016/s0896-6273(03)00752-9)
- 1130 Ferbinteanu, J., Shirvalkar, P., & Shapiro, M. L. (2011). Memory
1131 Modulates Journey-Dependent Coding in the Rat Hippocampus.
1132 *The Journal of Neuroscience*, 31(25), 9135 LP – 9146.
1133 <https://doi.org/10.1523/JNEUROSCI.1241-11.2011>
- 1134 Foster, D. J. (2017). Replay Comes of Age. *Annual Review of
1135 Neuroscience*, 40, 581–602. <https://doi.org/10.1146/annurev-neuro-072116-031538>
- 1137 Foster, D. J., & Wilson, M. A. (2006). Reverse replay of behavioural
1138 sequences in hippocampal place cells during the awake state.
1139 *Nature*, 440(7084), 680–683. <https://doi.org/10.1038/nature04587>

- 1140 Foster, D. J., & Wilson, M. A. (2007). Hippocampal theta sequences.
1141 *Hippocampus*, 17(11), 1093–1099.
1142 <https://doi.org/10.1002/hipo.20345>
- 1143 Francis, M., Qian, X., Charbel, C., Ledoux, J., Parker, J. C., & Taylor,
1144 M. S. (2012). Automated region of interest analysis of dynamic
1145 Ca²⁺ signals in image sequences. *American Journal of*
1146 *Physiology. Cell Physiology*, 303(3), C236-43.
1147 <https://doi.org/10.1152/ajpcell.00016.2012>
- 1148 Frank, L. M., Brown, E. N., & Wilson, M. (2000). Trajectory encoding in
1149 the hippocampus and entorhinal cortex. *Neuron*, 27(1), 169–178.
1150 [https://doi.org/10.1016/s0896-6273\(00\)00018-0](https://doi.org/10.1016/s0896-6273(00)00018-0)
- 1151 Fyhn, M., Molden, S., Witter, M. P., Moser, E. I., & Moser, M.-B.
1152 (2004). Spatial representation in the entorhinal cortex. *Science*
1153 (*New York, N.Y.*), 305(5688), 1258–1264.
1154 <https://doi.org/10.1126/science.1099901>
- 1155 Giovannucci, A., Badura, A., Deverett, B., Najafi, F., Pereira, T. D.,
1156 Gao, Z., Ozden, I., Kloth, A. D., Pnevmatikakis, E., Paninski, L.,
1157 De Zeeuw, C. I., Medina, J. F., & Wang, S. S.-H. (2017).
1158 Cerebellar granule cells acquire a widespread predictive feedback
1159 signal during motor learning. *Nature Neuroscience*, 20(5), 727–
1160 734. <https://doi.org/10.1038/nn.4531>
- 1161 Grün, S. (2009). Data-Driven Significance Estimation for Precise Spike
1162 Correlation. *Journal of Neurophysiology*, 101(3), 1126–1140.
1163 <https://doi.org/10.1152/jn.00093.2008>
- 1164 Gupta, A. S., van der Meer, M. A. A., Touretzky, D. S., & Redish, A. D.
1165 (2010). Hippocampal Replay Is Not a Simple Function of
1166 Experience. *Neuron*, 65(5), 695–705.
1167 <https://doi.org/https://doi.org/10.1016/j.neuron.2010.01.034>
- 1168 Hafting, T., Fyhn, M., Molden, S., Moser, M.-B., & Moser, E. I. (2005).
1169 Microstructure of a spatial map in the entorhinal cortex. *Nature*,
1170 436(7052), 801–806. <https://doi.org/10.1038/nature03721>
- 1171 Han, J.-H., Kushner, S. A., Yiu, A. P., Hsiang, H.-L. L., Buch, T.,
1172 Waisman, A., Bontempi, B., Neve, R. L., Frankland, P. W., &

- 1173 Josselyn, S. A. (2009). Selective erasure of a fear memory.
1174 *Science (New York, N.Y.)*, 323(5920), 1492–1496.
1175 <https://doi.org/10.1126/science.1164139>
- 1176 Hebb, D. O. (1949). The organization of behavior; a
1177 neuropsychological theory. In *The organization of behavior; a*
1178 *neuropsychological theory*. Wiley.
- 1179 Helmchen, F., & Denk, W. (2005). *Deep tissue two-photon microscopy*.
1180 2(12), 9. <https://doi.org/10.1038/nmeth818>
- 1181 Heys, J. G., Rangarajan, K. V., & Dombeck, D. A. (2014). The
1182 Functional Micro-organization of Grid Cells Revealed by Cellular-
1183 Resolution Imaging. *Neuron*, 84(5), 1079–1090.
1184 <https://doi.org/10.1016/j.neuron.2014.10.048>
- 1185 Ikegaya, Y., Aaron, G., Cossart, R., Aronov, D., Lampl, I., Ferster, D.,
1186 & Yuste, R. (2004). Synfire chains and cortical songs: temporal
1187 modules of cortical activity. *Science (New York, N.Y.)*, 304(5670),
1188 559–564. <https://doi.org/10.1126/science.1093173>
- 1189 Itskov, V., Pastalkova, E., Mizuseki, K., Buzsaki, G., & Harris, K. D.
1190 (2008). Theta-mediated dynamics of spatial information in
1191 hippocampus. *The Journal of Neuroscience : The Official Journal*
1192 *of the Society for Neuroscience*, 28(23), 5959–5964.
1193 <https://doi.org/10.1523/JNEUROSCI.5262-07.2008>
- 1194 Jadhav, S. P., Kemere, C., German, P. W., & Frank, L. M. (2012).
1195 Awake hippocampal sharp-wave ripples support spatial memory.
1196 *Science (New York, N.Y.)*, 336(6087), 1454–1458.
1197 <https://doi.org/10.1126/science.1217230>
- 1198 Josselyn, S. A., & Tonegawa, S. (2020). Memory engrams: Recalling
1199 the past and imagining the future. *Science (New York, N.Y.)*,
1200 367(6473). <https://doi.org/10.1126/science.aaw4325>
- 1201 Jun, J. J., Steinmetz, N. A., Siegle, J. H., Denman, D. J., Bauza, M.,
1202 Barbarits, B., Lee, A. K., Anastassiou, C. A., Andrei, A., Aydin, Ç.,
1203 Barbic, M., Blanche, T. J., Bonin, V., Couto, J., Dutta, B., Gratiy,
1204 S. L., Gutnisky, D. A., Häusser, M., Karsh, B., ... Harris, T. D.
1205 (2017). Fully integrated silicon probes for high-density recording of

- 1206 neural activity. *Nature*, 551(7679), 232–236.
1207 <https://doi.org/10.1038/nature24636>
- 1208 Kalmbach, B. E., Davis, T., Ohyama, T., Riusech, F., Nores, W. L., &
1209 Mauk, M. D. (2010). Cerebellar Cortex Contributions to the
1210 Expression and Timing of Conditioned Eyelid Responses. *Journal
1211 of Neurophysiology*, 103(4), 2039–2049.
1212 <https://doi.org/10.1152/jn.00033.2010>
- 1213 Kalmbach, B. E., Ohyama, T., & Mauk, M. D. (2010). Temporal
1214 Patterns of Inputs to Cerebellum Necessary and Sufficient for
1215 Trace Eyelid Conditioning. *Journal of Neurophysiology*, 104(2),
1216 627–640. <https://doi.org/10.1152/jn.00169.2010>
- 1217 Khan, A. G., Parthasarathy, K., & Bhalla, U. S. (2010). Odor
1218 representations in the mammalian olfactory bulb. *Wiley
1219 Interdisciplinary Reviews. Systems Biology and Medicine*, 2(5),
1220 603–611. <https://doi.org/10.1002/wsbm.85>
- 1221 Kraus, B. J., Brandon, M. P., Robinson, R. J., Connerney, M. A.,
1222 Hasselmo, M. E., & Eichenbaum, H. (2015). During Running in
1223 Place, Grid Cells Integrate Elapsed Time and Distance Run.
1224 *Neuron*, 88(3), 578–589.
1225 <https://doi.org/10.1016/j.neuron.2015.09.031>
- 1226 Kraus, B., Robinson, R., White, J., Eichenbaum, H., & Hasselmo, M.
1227 (2013). Hippocampal “Time Cells”: Time versus Path Integration.
1228 *Neuron*, 78(6), 1090–1101.
1229 <https://doi.org/10.1016/j.neuron.2013.04.015>
- 1230 Kropff, E., Carmichael, J. E., Moser, M.-B., & Moser, E. I. (2015).
1231 Speed cells in the medial entorhinal cortex. *Nature*, 523(7561),
1232 419–424. <https://doi.org/10.1038/nature14622>
- 1233 Krupa, D., & Thompson, R. (2003). Inhibiting the Expression of a
1234 Classically Conditioned Behavior Prevents Its Extinction. *The
1235 Journal of Neuroscience : The Official Journal of the Society for
1236 Neuroscience*, 23, 10577–10584.
1237 <https://doi.org/10.1523/JNEUROSCI.23-33-10577.2003>

- 1238 Lever, C., Burton, S., Jeewajee, A., O'Keefe, J., & Burgess, N.
1239 (2009). Boundary Vector Cells in the Subiculum of the
1240 Hippocampal Formation. *The Journal of Neuroscience*, 29(31),
1241 9771 LP – 9777. <https://doi.org/10.1523/JNEUROSCI.1319-09.2009>
- 1243 Luo, L., Callaway, E. M., & Svoboda, K. (2018). Genetic Dissection of
1244 Neural Circuits: A Decade of Progress. *Neuron*, 98(2), 256–281.
1245 <https://doi.org/https://doi.org/10.1016/j.neuron.2018.03.040>
- 1246 MacDonald, C. J., Carrow, S., Place, R., & Eichenbaum, H. (2013).
1247 Distinct hippocampal time cell sequences represent odor
1248 memories in immobilized rats. *The Journal of Neuroscience : The
1249 Official Journal of the Society for Neuroscience*, 33(36), 14607–
1250 14616. <https://doi.org/10.1523/JNEUROSCI.1537-13.2013>
- 1251 MacDonald, C. J., Lepage, K. Q., Eden, U. T., & Eichenbaum, H.
1252 (2011). Hippocampal “time cells” bridge the gap in memory for
1253 discontiguous events. *Neuron*, 71(4), 737–749.
1254 <https://doi.org/10.1016/j.neuron.2011.07.012>
- 1255 Maruyama, R., Maeda, K., Moroda, H., Kato, I., Inoue, M., Miyakawa,
1256 H., & Aonishi, T. (2014). Detecting cells using non-negative matrix
1257 factorization on calcium imaging data. *Neural Networks : The
1258 Official Journal of the International Neural Network Society*, 55,
1259 11–19. <https://doi.org/10.1016/j.neunet.2014.03.007>
- 1260 Mau, W., Sullivan, D. W., Kinsky, N. R., Hasselmo, M. E., Howard, M.
1261 W., & Eichenbaum, H. (2018). The Same Hippocampal CA1
1262 Population Simultaneously Codes Temporal Information over
1263 Multiple Timescales. *Current Biology*, 28(10), 1499-1508.e4.
1264 <https://doi.org/10.1016/j.cub.2018.03.051>
- 1265 McLelland, D., & Paulsen, O. (2007). Cortical Songs Revisited: A
1266 Lesson in Statistics. *Neuron*, 53(3), 319–321.
1267 <https://doi.org/https://doi.org/10.1016/j.neuron.2007.01.020>
- 1268 McNaughton, N., & Gray, J. A. (2000). Anxiolytic action on the
1269 behavioural inhibition system implies multiple types of arousal

- 1270 contribute to anxiety. *Journal of Affective Disorders*, 61(3), 161–
1271 176. [https://doi.org/10.1016/s0165-0327\(00\)00344-x](https://doi.org/10.1016/s0165-0327(00)00344-x)
- 1272 Medina, J. F., Garcia, K. S., Nores, W. L., Taylor, N. M., & Mauk, M. D.
1273 (2000). Timing mechanisms in the cerebellum: testing predictions
1274 of a large-scale computer simulation. *The Journal of
1275 Neuroscience : The Official Journal of the Society for
1276 Neuroscience*, 20(14), 5516–5525.
1277 <https://doi.org/10.1523/JNEUROSCI.20-14-05516.2000>
- 1278 Meeks, J. P., Arnson, H. A., & Holy, T. E. (2010). Representation and
1279 transformation of sensory information in the mouse accessory
1280 olfactory system. *Nature Neuroscience*, 13(6), 723–730.
1281 <https://doi.org/10.1038/nn.2546>
- 1282 Miller, A. M. P., Jacob, A. D., Ramsaran, A. I., De Snoo, M. L.,
1283 Josselyn, S. A., & Frankland, P. W. (2023). Emergence of a
1284 predictive model in the hippocampus. *Neuron*.
1285 <https://doi.org/10.1016/j.neuron.2023.03.011>
- 1286 Modi, M. N., Dhawale, A. K., & Bhalla, U. S. (2014). CA1 cell activity
1287 sequences emerge after reorganization of network correlation
1288 structure during associative learning. *eLife*, 3, e01982–e01982.
1289 <https://doi.org/10.7554/eLife.01982>
- 1290 Mokeichev, A., Okun, M., Barak, O., Katz, Y., Ben-Shahar, O., &
1291 Lampl, I. (2007). Stochastic Emergence of Repeating Cortical
1292 Motifs in Spontaneous Membrane Potential Fluctuations In Vivo.
1293 *Neuron*, 53, 413–425.
1294 <https://doi.org/10.1016/j.neuron.2007.01.017>
- 1295 Mollinedo-Gajate, I., Song, C., & Knöpfel, T. (2021). Genetically
1296 Encoded Voltage Indicators. *Advances in Experimental Medicine
1297 and Biology*, 1293, 209–224. https://doi.org/10.1007/978-981-15-8763-4_12
- 1299 Morris, R. G. M., Garrud, P., Rawlins, J. N. P., & O'Keefe, J. (1982).
1300 Place navigation impaired in rats with hippocampal lesions.
1301 *Nature*, 297(5868), 681–683. <https://doi.org/10.1038/297681a0>

- 1302 Moyer, J. R., Deyo, R. A., & Disterhoft, J. F. (1990). Hippocampectomy
1303 disrupts trace eye-blink conditioning in rabbits. *Behavioral*
1304 *Neuroscience*, 104(2)(Apr 1990), 243–252.
1305 <https://doi.org/10.1037/0735-7044.104.2.243>
- 1306 Mukamel, E. A., Nimmerjahn, A., & Schnitzer, M. J. (2009). Automated
1307 analysis of cellular signals from large-scale calcium imaging data.
1308 *Neuron*, 63(6), 747–760.
1309 <https://doi.org/10.1016/j.neuron.2009.08.009>
- 1310 Muller, R. U., & Kubie, J. L. (1989). The firing of hippocampal place
1311 cells predicts the future position of freely moving rats. *The*
1312 *Journal of Neuroscience : The Official Journal of the Society for*
1313 *Neuroscience*, 9(12), 4101–4110.
1314 <https://doi.org/10.1523/JNEUROSCI.09-12-04101.1989>
- 1315 Murray, T. A., & Levene, M. J. (2012). Singlet gradient index lens for
1316 deep in vivo multiphoton microscopy. *Journal of Biomedical*
1317 *Optics*, 17(2), 021106. <https://doi.org/10.1117/1.JBO.17.2.021106>
- 1318 O'Keefe, J., & Burgess, N. (1996). Geometric determinants of the
1319 place fields of hippocampal neurons. *Nature*, 381(6581), 425–428.
1320 <https://doi.org/10.1038/381425a0>
- 1321 O'Keefe, J., & Dostrovsky, J. (1971). The hippocampus as a spatial
1322 map. Preliminary evidence from unit activity in the freely-moving
1323 rat. *Brain Research*, 34(1), 171–175. [https://doi.org/10.1016/0006-8993\(71\)90358-1](https://doi.org/10.1016/0006-8993(71)90358-1)
- 1325 O'Keefe, J., & Nadel, L. (1978). The Hippocampus as a Cognitive Map.
1326 In *Philosophical Studies* (Vol. 27).
1327 <https://doi.org/10.5840/philstudies19802725>
- 1328 O'Keefe, J., & Recce, M. L. (1993). Phase relationship between
1329 hippocampal place units and the EEG theta rhythm.
1330 *Hippocampus*, 3(3), 317–330.
1331 <https://doi.org/10.1002/hipo.450030307>
- 1332 Ohyama, T., Nores, W. L., Murphy, M., & Mauk, M. D. (2003). What
1333 the cerebellum computes. *Trends in Neurosciences*, 26(4), 222–
1334 227. [https://doi.org/10.1016/S0166-2236\(03\)00054-7](https://doi.org/10.1016/S0166-2236(03)00054-7)

- 1335 Ozden, I., Lee, H. M., Sullivan, M. R., & Wang, S. S.-H. (2008).
1336 Identification and Clustering of Event Patterns From In Vivo
1337 Multiphoton Optical Recordings of Neuronal Ensembles. *Journal*
1338 *of Neurophysiology*, 100(1), 495–503.
1339 <https://doi.org/10.1152/jn.01310.2007>
- 1340 Pachitariu, M., Stringer, C., Dipoppa, M., Schröder, S., Rossi, L. F.,
1341 Dalgleish, H., Carandini, M., & Harris, K. D. (2017). Suite2p:
1342 beyond 10,000 neurons with standard two-photon microscopy.
1343 *BioRxiv*, 61507. <https://doi.org/10.1101/061507>
- 1344 Paredes, R. M., Etzler, J. C., Watts, L. T., Zheng, W., & Lechleiter, J.
1345 D. (2008). Chemical calcium indicators. *Methods (San Diego,*
1346 *Calif.)*, 46(3), 143–151.
1347 <https://doi.org/10.1016/j.ymeth.2008.09.025>
- 1348 Pastalkova, E., Itskov, V., Amarasingham, A., & Buzsaki, G. (2008).
1349 Internally Generated Cell Assembly Sequences in the Rat
1350 Hippocampus. *Science*, 321(5894), 1322–1327.
1351 <https://doi.org/10.1126/science.1159775>
- 1352 Pavlov, I. P. (1927). Conditioned reflexes: an investigation of the
1353 physiological activity of the cerebral cortex. In *Conditioned*
1354 *reflexes: an investigation of the physiological activity of the*
1355 *cerebral cortex*. Oxford Univ. Press.
- 1356 Petersen, C. C. H. (2019). Sensorimotor processing in the rodent
1357 barrel cortex. *Nature Reviews. Neuroscience*, 20(9), 533–546.
1358 <https://doi.org/10.1038/s41583-019-0200-y>
- 1359 Pfeiffer, B. E., & Foster, D. J. (2013). Hippocampal place-cell
1360 sequences depict future paths to remembered goals. *Nature*,
1361 497(7447), 74–79. <https://doi.org/10.1038/nature12112>
- 1362 Pfeiffer, B. E., & Foster, D. J. (2015). Autoassociative dynamics in the
1363 generation of sequences of hippocampal place cells. *Science*,
1364 349(6244), 180–183. <https://doi.org/10.1126/science.aaa9633>
- 1365 Pnevmatikakis, E. A., Soudry, D., Gao, Y., Machado, T. A., Merel, J.,
1366 Pfau, D., Reardon, T., Mu, Y., Lacefield, C., Yang, W., Ahrens, M.,
1367 Bruno, R., Jessell, T. M., Peterka, D. S., Yuste, R., & Paninski, L.

- 1368 (2016). Simultaneous Denoising, Deconvolution, and Demixing of
1369 Calcium Imaging Data. *Neuron*, 89(2), 285–299.
1370 <https://doi.org/https://doi.org/10.1016/j.neuron.2015.11.037>
- 1371 Poort, J., Khan, A. G., Pachitariu, M., Nemri, A., Orsolic, I., Krupic, J.,
1372 Bauza, M., Sahani, M., Keller, G. B., Mrsic-Flogel, T. D., & Hofer,
1373 S. B. (2015). Learning Enhances Sensory and Multiple Non-
1374 sensory Representations in Primary Visual Cortex. *Neuron*, 86(6),
1375 1478–1490. <https://doi.org/10.1016/j.neuron.2015.05.037>
- 1376 Ranck, J. B. (1973). Studies on single neurons in dorsal hippocampal
1377 formation and septum in unrestrained rats: Part I. Behavioral
1378 correlates and firing repertoires. *Experimental Neurology*, 41(2),
1379 462–531. [https://doi.org/https://doi.org/10.1016/0014-4886\(73\)90290-2](https://doi.org/https://doi.org/10.1016/0014-4886(73)90290-2)
- 1380 Reyes, A. D. (2003). Synchrony-dependent propagation of firing rate in
1381 iteratively constructed networks in vitro. *Nature Neuroscience*,
1382 6(6), 593–599. <https://doi.org/10.1038/nn1056>
- 1383 Rogerson, T., Cai, D. J., Frank, A., Sano, Y., Shobe, J., Lopez-Aranda,
1384 M. F., & Silva, A. J. (2014). Synaptic tagging during memory
1385 allocation. *Nature Reviews Neuroscience*, 15(3), 157–169.
1386 <https://doi.org/10.1038/nrn3667>
- 1387 Savelli, F., Yoganarasimha, D., & Knierim, J. J. (2008). Influence of
1388 boundary removal on the spatial representations of the medial
1389 entorhinal cortex. *Hippocampus*, 18(12), 1270–1282.
1390 <https://doi.org/10.1002/hipo.20511>
- 1391 Scoville, W. B., & Milner, B. (1957). Loss of recent memory after
1392 bilateral hippocampal lesions. In *Journal of Neurology, Neurosurgery & Psychiatry* (Vol. 20, pp. 11–21). BMJ Publishing
1393 Group. <https://doi.org/10.1136/jnnp.20.1.11>
- 1394 Siegel, J. J., & Mauk, M. D. (2013). Persistent Activity in Prefrontal
1395 Cortex during Trace Eyelid Conditioning: Dissociating Responses
1396 That Reflect Cerebellar Output from Those That Do Not. *The Journal of Neuroscience*, 33(38), 15272 LP – 15284.
1397 <https://doi.org/10.1523/JNEUROSCI.1238-13.2013>

- 1401 Siegel, J. J., Taylor, W., Gray, R., Kalmbach, B., Zemelman, B. V.,
1402 Desai, N. S., Johnston, D., & Chitwood, R. A. (2015). Trace
1403 Eyeblink Conditioning in Mice Is Dependent upon the Dorsal
1404 Medial Prefrontal Cortex, Cerebellum, and Amygdala: Behavioral
1405 Characterization and Functional Circuitry. *ENeuro*, 2(4),
1406 ENEURO.0051-14.2015. <https://doi.org/10.1523/ENEURO.0051-14.2015>
- 1408 Skaggs, W., McNaughton, B., Gothard, K., & Markus, E. (1996). An
1409 Information-Theoretic Approach to Deciphering the Hippocampal
1410 Code. *Neural Inf. Process Syst.*, 5.
- 1411 Solstad, T., Boccara, C. N., Kropff, E., Moser, M.-B., & Moser, E. I.
1412 (2008). Representation of Geometric Borders in the Entorhinal
1413 Cortex. *Science*, 322(5909), 1865–1868.
1414 <https://doi.org/10.1126/science.1166466>
- 1415 Souza, B. C., Pavão, R., Belchior, H., & Tort, A. B. L. (2018). On
1416 Information Metrics for Spatial Coding. *Neuroscience*, 375, 62–73.
1417 <https://doi.org/10.1016/j.neuroscience.2018.01.066>
- 1418 Stosiek, C., Garaschuk, O., Holthoff, K., & Konnerth, A. (2003). In vivo
1419 two-photon calcium imaging of neuronal networks. *Proceedings of
1420 the National Academy of Sciences of the United States of
1421 America*, 100(12), 7319–7324.
1422 <https://doi.org/10.1073/pnas.1232232100>
- 1423 Taube, J. S., Muller, R. U., & Ranck, J. B. J. (1990). Head-direction
1424 cells recorded from the postsubiculum in freely moving rats. I.
1425 Description and quantitative analysis. *The Journal of
1426 Neuroscience : The Official Journal of the Society for
1427 Neuroscience*, 10(2), 420–435.
1428 <https://doi.org/10.1523/JNEUROSCI.10-02-00420.1990>
- 1429 Valero, M., Cid, E., Averkin, R. G., Aguilar, J., Sanchez-Aguilera, A.,
1430 Viney, T. J., Gomez-Dominguez, D., Bellistri, E., & de la Prida, L.
1431 M. (2015). Determinants of different deep and superficial CA1
1432 pyramidal cell dynamics during sharp-wave ripples. *Nature
1433 Neuroscience*. <https://doi.org/10.1038/nn.4074>

- 1434 Velasco, M. G. M., & Levene, M. J. (2014). In vivo two-photon
1435 microscopy of the hippocampus using glass plugs. *Biomedical
1436 Optics Express*, 5(6), 1700–1708.
1437 <https://doi.org/10.1364/BOE.5.001700>
- 1438 Voelcker, B., Pancholi, R., & Peron, S. (2022). Transformation of
1439 primary sensory cortical representations from layer 4 to layer 2.
1440 *Nature Communications*, 13(1), 5484.
1441 <https://doi.org/10.1038/s41467-022-33249-1>
- 1442 Wood, E. R., Dudchenko, P. A., Robitsek, R. J., & Eichenbaum, H.
1443 (2000). Hippocampal Neurons Encode Information about Different
1444 Types of Memory Episodes Occurring in the Same Location.
1445 *Neuron*, 27(3), 623–633.
1446 [https://doi.org/https://doi.org/10.1016/S0896-6273\(00\)00071-4](https://doi.org/https://doi.org/10.1016/S0896-6273(00)00071-4)
- 1447 Yiu, A. P., Mercaldo, V., Yan, C., Richards, B., Rashid, A. J., Hsiang,
1448 H.-L. L., Pressey, J., Mahadevan, V., Tran, M. M., Kushner, S. A.,
1449 Woodin, M. A., Frankland, P. W., & Josselyn, S. A. (2014).
1450 Neurons are recruited to a memory trace based on relative
1451 neuronal excitability immediately before training. *Neuron*, 83(3),
1452 722–735. <https://doi.org/10.1016/j.neuron.2014.07.017>
- 1453 Zhou, Y., Won, J., Karlsson, M. G., Zhou, M., Rogerson, T., Balaji, J.,
1454 Neve, R., Poirazi, P., & Silva, A. J. (2009). CREB regulates
1455 excitability and the allocation of memory to subsets of neurons in
1456 the amygdala. *Nature Neuroscience*, 12(11), 1438–1443.
1457 <https://doi.org/10.1038/nn.2405>
- 1458 Ziv, Y., Burns, L. D., Cocker, E. D., Hamel, E. O., Ghosh, K. K., Kitch,
1459 L. J., El Gamal, A., & Schnitzer, M. J. (2013). Long-term dynamics
1460 of CA1 hippocampal place codes. *Nature Neuroscience*, 16(3),
1461 264–266. <https://doi.org/10.1038/nn.3329>

1462 **Chapter 2 – Behaviour**

1463

1464 **Towards understanding brain activity in a
1465 reproducible context**

1466

1467 Our understanding of memory and learning depends upon the type of
1468 learning that is studied (Schreurs, 1989). Two important categories of
1469 memory and learning experiments are,

- 1470 1. Non-associative (Habituation and Sensitization), and
- 1471 2. Associative learning (Classical and Operant Conditioning).

1472

1473 Non-associative learning paradigms provide information about how an
1474 organism responds to repeated presentations of a single stimulus
1475 (Brown, 1998). However, it was of interest to us to study how animals
1476 responded to a number of events and stimuli being associated, and
1477 how the activity of the brain relates to this. Hence, we chose to design
1478 our experiments to incorporate associative learning, which is a
1479 relatively permanent change in behaviour that results from the
1480 temporal conjunction of two or more events or stimuli.

1481

1482 Empirically, reproducible behaviour depends on strong associations
1483 between the events or stimuli being paired, and may often require
1484 many repeated pairings or trials. Additionally, having the animal
1485 engage in the behavioural task and pay attention to the stimuli being

1486 presented, is crucial to look for important correlations between the
1487 experiment conditions (external) and brain activity (internal).

1488

1489 Anaesthetized animals have been previously used to study brain
1490 activity and led to important discoveries, e.g. - visual representation of
1491 moving bars in the visual cortex (Hubel & Wiesel, 1962), habituation in
1492 the Hippocampus (Deshmukh & Bhalla, 2003). However, it was clear
1493 that similar experiments repeated in awake animals did not result in the
1494 same observations. Indeed, animals needed to navigate a known
1495 environment before the discovery of place cells (O'Keefe &
1496 Dostrovsky, 1971), grid cells (Fyhn et al., 2004; Hafting et al., 2005),
1497 and head-direction cells (Ranck, 1973; Taube et al., 1990), among
1498 others, could be made.

1499

1500 The reliability of the overt behavioural responses of the experiment
1501 animals then sets the conditions and parameter list to study physiology
1502 within the confines of reproducible behavioural contexts, and was
1503 considered an important mandate for the standardization of any of the
1504 behavioural tasks described in this chapter. Under the umbrella of
1505 associative learning, we began our experiments with various protocols
1506 related to operant conditioning wherein the reinforcing signal for
1507 learning was a water reward to correctly timed licks. As will be
1508 discussed in the next few sections, we later switched to aversive
1509 conditioning with Trace Eye-Blink Conditioning.

1510 **Operant conditioning [Project I]**

1511

1512 Operant conditioning is both the procedure and a type of associative
1513 learning process through which the strength of a voluntarily performed
1514 behaviour is modified positively (appetitively) by reward (water,
1515 sucrose, food, etc.), or negatively (aversively) by punishment (air-puff
1516 to the eye, electrical shocks, etc.). For example, if the animal responds
1517 to a presented stimulus by performing a lick onto a water spout, then a
1518 water reward would strengthen the behaviour while Lithium Chloride
1519 solution (which is aversive) would weaken it.

1520

1521 We now describe our experiments and results with regard to operant
1522 conditioning, in more detail.

1523

1524 **Required features**

1525

1526 For Project I, the goal was to study how the association of a neutral
1527 stimulus with a water reward modified the neurophysiological activity of
1528 the hippocampal CA1. For this, we required the following.

1529 1. An assortment of different stimuli and modalities (light, tone, etc.)
1530 to be presented to the animal.

1531 2. The animal must withhold any motor movement during the
1532 presentation of the stimuli, to study pure stimulus responses.

1533 3. The animal must perform a lick for a water reward after the end of
1534 the stimulus presentation.

1535 4. The animal must be able to make the association between stimuli
1536 and water reward within 7 days of training (at the time we did not have
1537 the ability to record for multiple days).

1538

1539 The behavioural state of the animal, in terms of anxiety, motivation,
1540 attention, etc., may be variable when a naïve animal is presented with
1541 different stimuli. This may cause a large variability in the activity of
1542 cells, since the animal may not be paying attention to it. Also, if the
1543 animal were rewarded for performing the task it is expected that there
1544 would be motivation to pay attention to the stimuli presented. Finally,
1545 such a task would involve the animal associating the stimuli that it is
1546 trained to with a behavioural task and this would provide an apt context
1547 to study association related changes in stimulus responses.

1548

1549 In this section, we discuss some important protocols that we tried and
1550 tested and a list of the various kinds of behavioural tasks we employed
1551 for head-fixed mice.

1552

1553 For Project I, we tried several variations of operant conditioning
1554 including Stimulus Detection tasks, Delayed Non-Match to Sample
1555 (DNMS), as well as Go/No-Go tasks. Each of these tasks requires
1556 animals to perform licks to the Conditioned Stimuli and for them to be
1557 rewarded (2-3 µL water) or punished based on the task demands and
1558 protocol design.

1559 **Water delivery and calibration**

1560

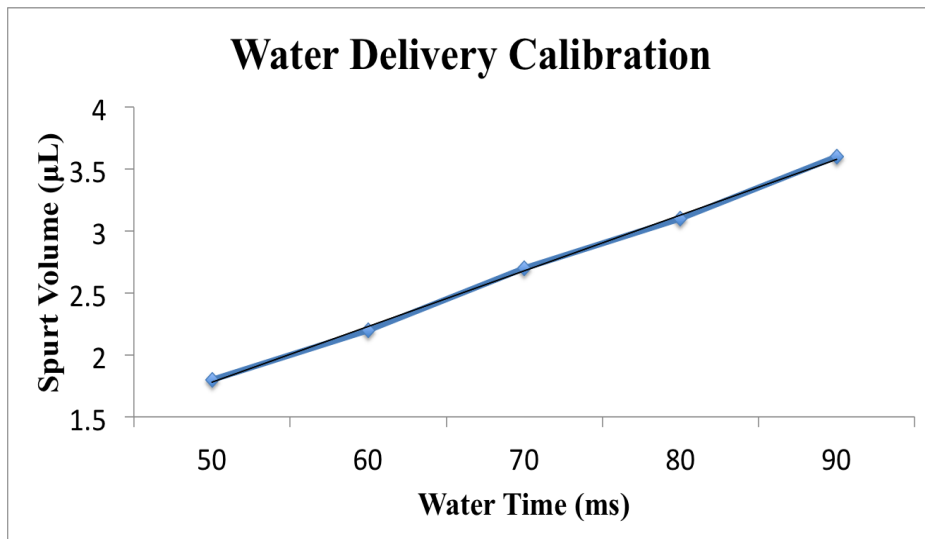


Figure 2: Water delivery calibration to reward the animal consistently with the same volume of water.

1561 The lick port was made from a trimmed and smoothed 16 gauge
 1562 syringe, connected to a water reservoir with small diameter tubing. A
 1563 solenoid valve clamped onto this tubing, gated by a 12V DC signal.
 1564 When this gate was opened, the volume of water could be regulated by
 1565 the duration of the 12V DC signal. We calibrated the duration of gate
 1566 opening to achieve ~2 μ L per pulse or spurt (Jaramillo & Zador, 2014).
 1567 The weight of 100 spouts was measured and then divided by 100 to get
 1568 the weight of 1 spout. 65 ms was found corresponding to 2.5 μ L (this
 1569 value is going to be used for behaviour). In the figure below (Figure 2),
 1570 the measured volumes/weights are plotted as blue filled diamonds,
 1571 error bars are presented as Standard Error and the linear trendline is
 1572 shown in black.

1573 Opto-isolator circuit for solenoid control

1574
 1575 To be able to programmatically control the 12V DC line to the solenoid
 1576 valve, we used the following circuit (Figure 3), which accepted a 5V

1577 digital input from the DAQ (NI USB-6001) interfacing the lab computer
1578 to the behaviour rig.

1579

1580 **Parts list**

1581 1. 470 ohm resistor

1582 2. 15 kohm resistor

1583 3. MCT2e

1584 4. ULN2003

1585 5. Bases (adaptors for MCT2e and ULN2003)

1586 6. +5V and +12V DC inputs from a Power Supply)

1587 7. Source of +5V DC input (DAQ, etc.)

1588 8. Connecting wires

1589 9. Load Resistance (Solenoid, etc.)

1590

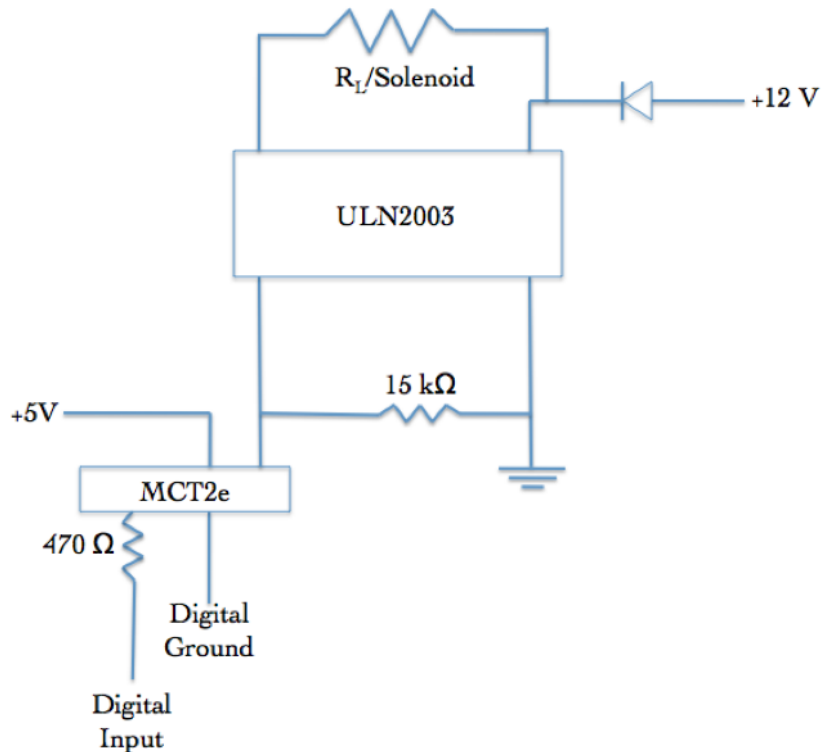


Figure 3: Optoisolator circuit to amplify +5V DC input to +12V DC output.

1592

1593 Lick detection circuit

1594

1595 To be able to monitor the presence or absence of licks to the port, the
 1596 conductive part (metal) of the lick port syringe was connected to a
 1597 MOSFET such that a 5V DC voltage could be read out, whenever the
 1598 animal would make contact with the port. This was designed as a
 1599 readout to Stimulus Detection by the animal. The circuit diagram is
 1600 shown below (Figure 4):

1601

1602 **Parts list**

- 1603 1. +5V Power Supply
- 1604 2. 4.7 kohm resistor
- 1605 3. 22 Mohm resistor
- 1606 4. IN4007 Diode
- 1607 5. NPN Transistor IRF540N (MOSFET)
- 1608

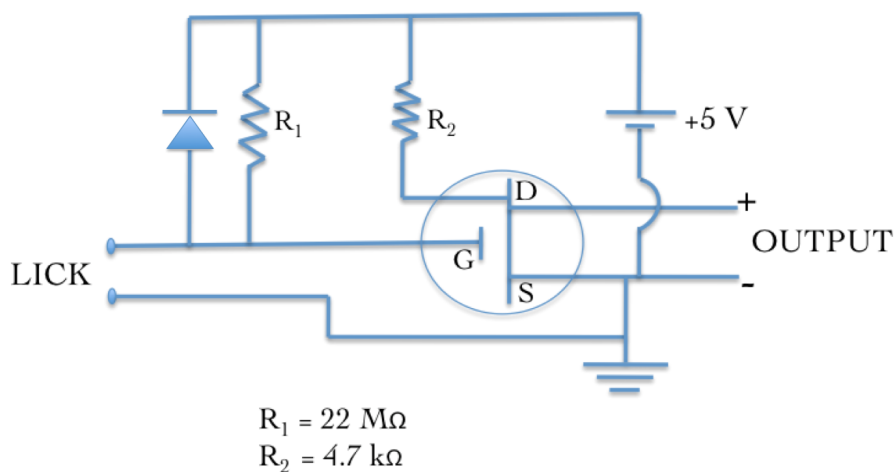


Figure 4: Lick detector circuit based on a MOSFET design. Whenever the animal performed a lick, a +5V DC Output would be read out.

1610 **Controlling task details and protocol information**

1611

- 1612 All protocols were controlled using custom scripts written in NI LabVIEW 8. These scripts were run on a lab desktop which interfaced with the DAQ (NI USB-6001) via USB. The DAQ,
 - 1. Sent the 5V digital input to switch on the solenoid valve
 - 1616 regulating water delivery, and

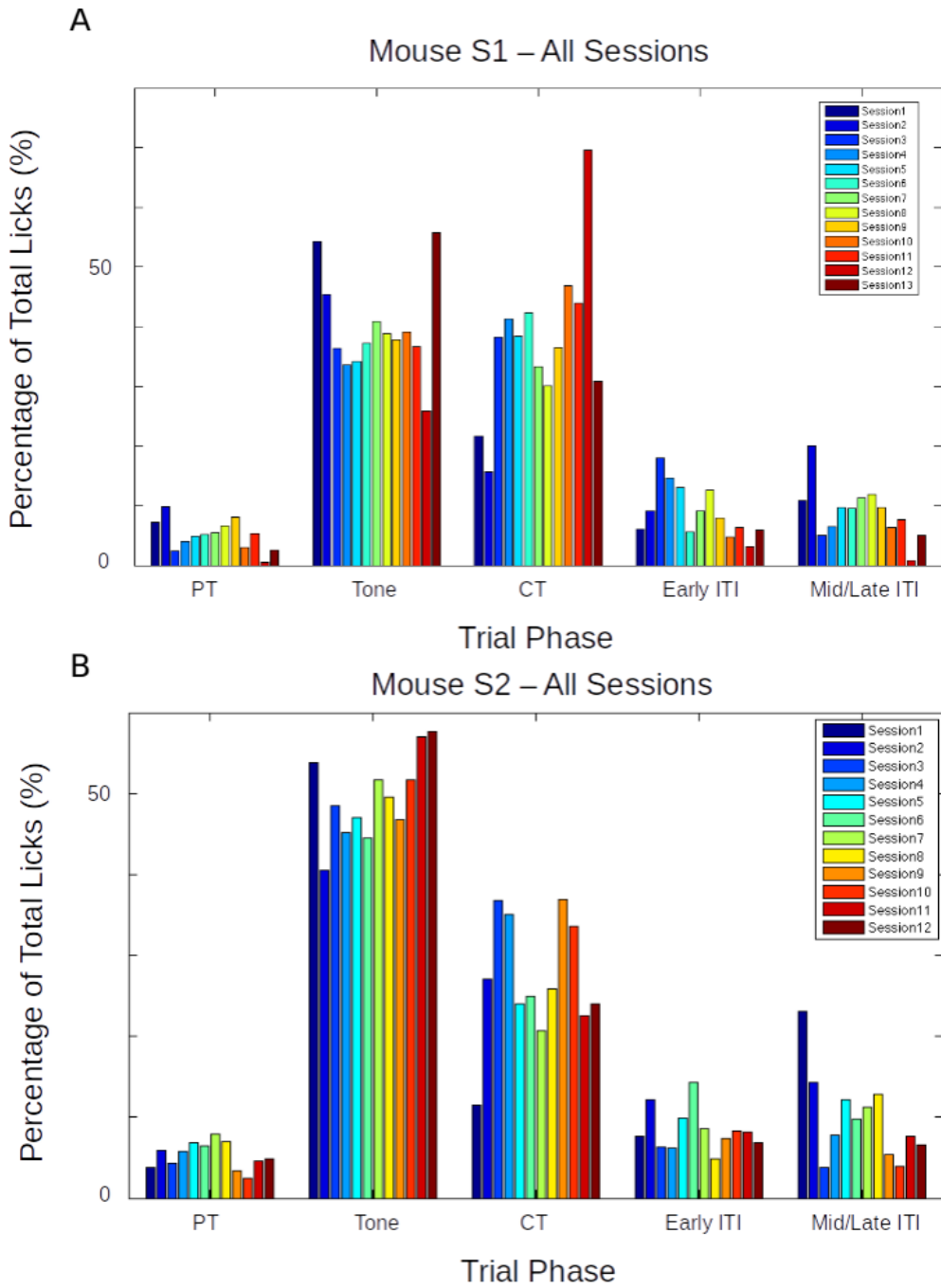


Figure 7: Performance evaluation for two example mice trained to Protocol 2. Percentage of total licks in the various trial phases (Pre-Tone, Tone, CT, and ITI), across all sessions of training (coloured bar plots), for (A) Mouse S1, and (B) Mouse S2.

1618 2. Received the 5V digital output of the lick detection circuit
1619 whenever a lick was produced by the animal.

1620

1621 **Head-bar implant, Animal Handling, and Water
1622 deprivation**

1623

1624 All experiments were planned to be conducted on head-fixed C57Bl/6
1625 mice, with the eventual intention to perform *in vivo* imaging on these
1626 animals. For this, we surgically implanted metal head-bars on the skull
1627 of the animals while they were maintained on 1-2% Isoflurane, above a
1628 heating pad (35°C). Surgeries would last no longer than 30 mins per
1629 animal.

1630

1631 After 1-7 days of recovery after surgery, we handled the animals gently
1632 for 2 days till the animals would appear comfortable with lifting and
1633 gentle collar grabbing. Next, for 3-4 days, we kept the animals head-
1634 clamped. We restricted our animals to ~1ml of water per day, keeping
1635 check that their body weight did not fall to below 80% of the weight on
1636 day 1.

1637

1638 **PROTOCOL 1.1: Stimulus Detection Task**

1639

1640 We first tried the simplest version of the lick task wherein an auditory
1641 tone was followed by a water reward. The animal would have to
1642 withhold licking till the end of the stimulus presentation, and then
1643 perform the lick for the reward (Figure 5).

1644

1645 **Total number of trials:** 600/session; 1 session/day

1646 **Trial phases:**

- 1647 1. Stimulus free pre-tone (PT): 1 s
- 1648 2. Tone: 5 kHz for 1 s
- 1649 3. Critical timeout (CT): 100 ms
- 1650 4. Inter-trial Interval (ITI): randomized between 2 s to 5

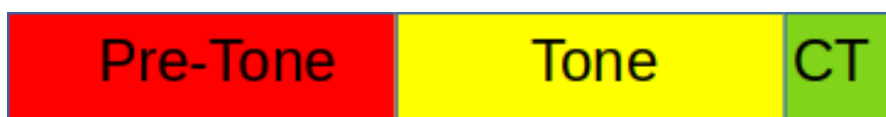


Figure 5: Typical trial structure with the various phases. Each trial was followed by a randomized Inter-Trial Interval (ITI).

1652 Only licks during the critical timeout (CT) phase immediately after the
1653 Tone phase were rewarded while licks in other phases resulted in a
1654 phase restart.

1655

1656 **PROTOCOL 1.2: Stimulus Detection Task with aversive
1657 punishment**

1658

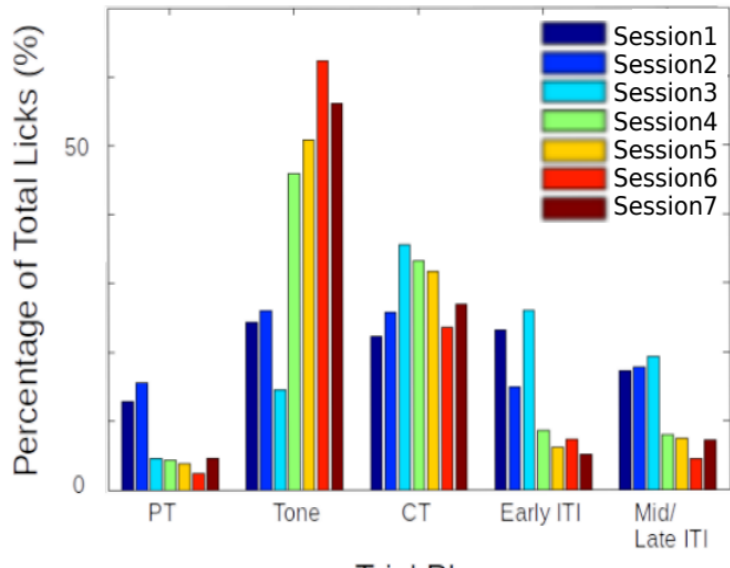
1659 **Total number of trials:** 600/session; 1 session/day

1660

1661 Only licks during the critical timeout (CT) phase immediately after the
1662 Tone phase were rewarded while licks in other phases resulted in an
1663 aversive punishment, *viz.*, 100 ms air-puff to the body of the animal,
1664 before a phase restart. For Mouse 3 we started Protocol 1.2 from
1665 Session 3 while for Mouse 4 we started Protocol 1.2 from Session 2.

A

Mouse 3 – All Sessions

**B**

Mouse 4 – All Sessions

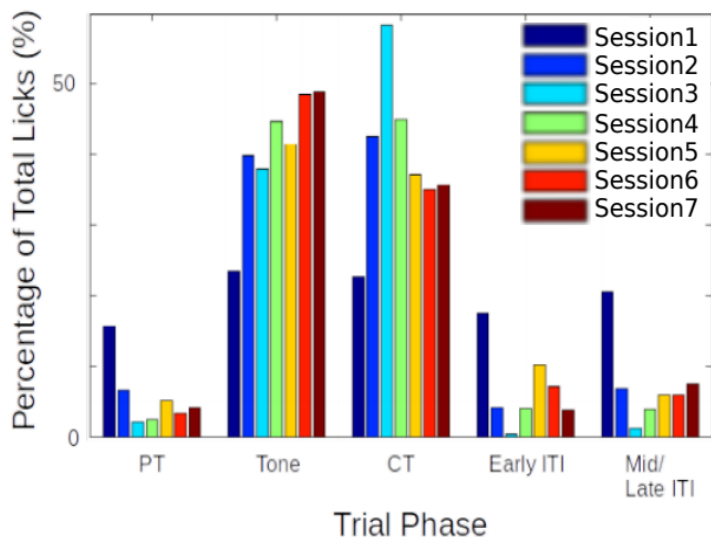


Figure 6: Performance evaluation for two example mice trained to Protocol 1.1 and 1.2. Percentage of total licks in the various trial phases (Pre-Tone, Tone, CT, and ITI), across all sessions of training (coloured bar plots) for A) Mouse 3, and B) Mouse 4

1667 **Results – Protocol 1.1 and 1.2**

1668

1669 The behavioural performance for each of the experiment animals was
1670 evaluated using custom analysis scripts written in MATLAB 2011. Here
1671 are the results from two mice trained based on Protocols 1.1 and 1.2
1672 (Figure 6).

1673 In both the examples shown, animals would typically produce a great
1674 percentage of total licks even during the Tone period. This failure to
1675 withhold licks carried on for 7-14 sessions, and the task was ultimately
1676 unsuccessful.

1677

1678 **Total animals trained:** 2

1679 **Conclusion:** Fail

1680

1681 **Protocol 2: Stimulus Detection task with timeout box**

1682

1683 We also tried the same Stimulus Detection protocol, without an air-puff
1684 punishment, but with incorrect licks punished by a trial abort and a
1685 stimulus-free timeout phase, which the animal could escape from if it
1686 withheld licking. We decided to train the animals in blocks, each with a
1687 specific goal that the animal had to achieve.

1688

1689 **Trial phases:**

1690 1 Stimulus-free pre-tone (PT): 1 s

1691 2 Tone: 5 kHz for a variable duration (based on Block)

1692 3 Critical timeout (CT): 1000 ms

1693 4 Inter-trial Interval (ITI): randomized between 2 s to 5 s

1694

1695 Only licks during the critical timeout (CT) phase immediately after the
1696 Tone phase were rewarded while licks in other phases resulted in a
1697 phase restart.
1698
1699 **Block 1:** Unconditional Water to get the animal to associate the tone
1700 - ~20 trials
1701 - 100 or 200 ms Tone duration
1702 - Unconditional water provided at the end of the tone, irrespective of
1703 lick
1704
1705 **Block 2:** Conditional Water to get the animal to learn that licking
1706 with/after tone is going to be rewarded
1707 - 100 or 200 ms Tone duration
1708 - 1000 ms Reward phase
1709 - Lick during/after tone (Reward phase) = reward
1710 - No lick = no reward
1711 - Lick during pre-tone = no reward/abortion of trial
1712 - Lick during ITI = no reward/abortion of trial
1713 - Animals graduate to the next Block of training only after achieving at
1714 least 70-80% success rates
1715
1716 **Block 3:** Training the animal to learn "when" to lick
1717 - 1000 ms pre-tone, 100 or 200 ms Tone, 1000 ms Reward phase, 3-5
1718 s randomized ITI
1719 - Lick during Reward phase = reward
1720 - Any lick during the pre-tone or the tone, aborts the trial and sends the
1721 program to a Timeout phase (lasting, 2-3 s)
1722 - The timeout phase ends only when there is a 2-3 s (specified) interval
1723 of no licking

1724 - If the timeout phase ends, a new trial begins
1725 - Licks during ITI are also "punished" accordingly
1726 - Animals graduate to the next Block of training only after achieving 70-
1727 80% success rates
1728
1729 **Block 4:** Same as Block 3, but with a gradually increasing tone
1730 duration in steps of 50/100 ms
1731 - The tone duration is gradually increased, the increase being tailored
1732 to the performance of the animal
1733 - It will be attempted to get the animals to learn to wait for 500-700 ms
1734 - Animals graduate to the next Block of the experiment only after
1735 achieving 70-80% success rates

1736

1737 **Results – Protocol 2**

1738
1739 The behavioural performance for each of the experiment animals was
1740 evaluated using custom analysis scripts written in MATLAB. Here are
1741 two representative examples of mice trained based on Protocol 2 –
1742 Block 3 (Figure 7).

1743

1744

1745 Again, as is clear from the examples above, that while the mice
1746 eventually produced a decent percentage of total licks in the critical
1747 timeout (CT) phase to get a water reward, they did not learn to
1748 withhold licks during the Tone phase, even after >10 sessions. The
1749 task was ultimately unsuccessful.

1750

1751 **Total animals trained:** 4

1752 **Conclusion:** Fail

1753

1754 **Protocol 3: Delayed Non-Match to Sample (DNMS)**

1755

1756 Delayed Non-Match to Sample (DNMS) is a task that is ideally suited
1757 to study working memory and recognition (Binder et al., 2009), but we
1758 decided to try it. This task involves trial-by-trial presentation of two
1759 stimuli separated by a stimulus-free delay interval. For any given trial,
1760 If the two pseudorandomly chosen pairs of stimuli were identical, then
1761 licks would not be rewarded. However, if the pair of stimuli were
1762 different, then licks would be rewarded with 2 μ L water.

1763

1764 We tried to incorporate more tones, in the hope that this may improve
1765 the chances of the animals focusing on the task specifics, instead of
1766 producing licks to just any particular stimulus.

1767

1768 **Tones used:** 6000 Hz, 8500 Hz, 10000 Hz, and 11500 Hz

1769 **Trial phases:**

1770 1. Pre-Tone duration (ms): 1000 ms

1771 2. CS 1 duration (ms): 350 ms

1772 3. Delay Interval duration (ms): 250 ms

1773 4. CS 2 duration (ms): 350 ms (unless a correct lick is
1774 elicited)

1775 5. ITI duration (s): randomized from 1 s to 3 s

1776 **Punishment:** Timeout Box (minimum of 3s of no licks to escape)

1777 **Reward:** 2 μ L of water

1778

1779 **Results – Protocol 3**

1780

1781 >70-80% of the trials had to be aborted because the animals would not
1782 withhold licking after the 1st of the pair of tones was presented. This
1783 did not change even after 7 days (sessions) of training.

1784

1785 **Total animals trained:** 6

1786 **Conclusion:** Fail

1787

1788 **Protocol 4: Go/No-Go Task**

1789

1790 In an attempt to simplify the behavioural task, we decided to
1791 reconfigure the DNMS task to a simpler Go/No-Go task. Here, we
1792 would again present the animal with two stimuli, but with the only
1793 condition being that the animal would have to lick after the second
1794 stimulus, and not before. This simplifies the behaviour to a certain
1795 extent, because the animals need only use the first stimulus as a cue
1796 for the second. Failure to perform this task could more easily then be
1797 attributed to a lack of attention in that trial. Only the data from the trials
1798 where the animal succeeds to do the task would be considered for
1799 analysis. Training related changes in actual stimulus representations
1800 would be carefully dissected out. Furthermore, such a task would
1801 control for the behavioural state of the animal and help provide
1802 important datasets.

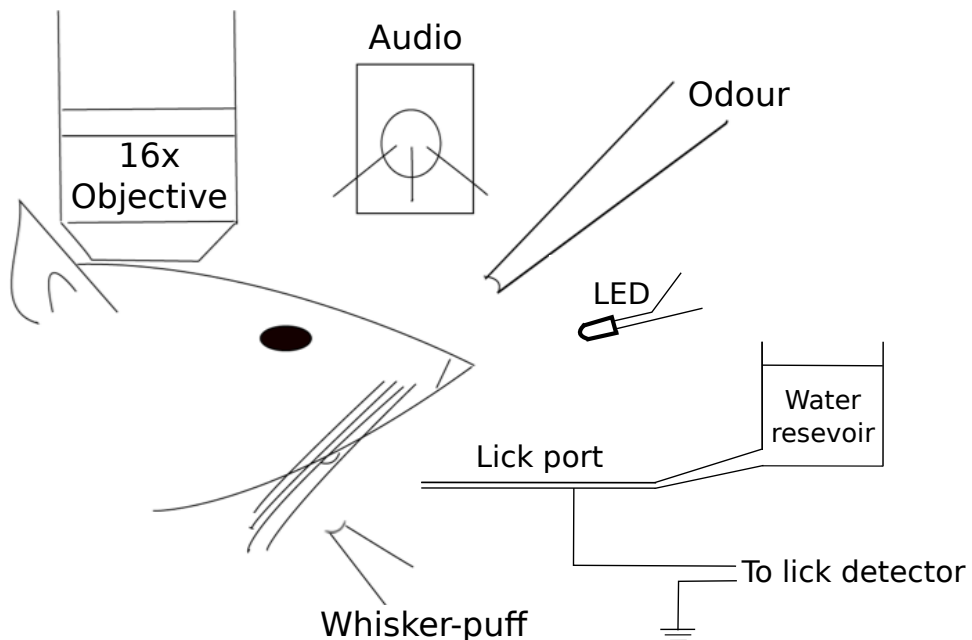


Figure 8: Schematic representation of the experimental setup for a simple detection task where the animal must perform a lick upon correctly detecting the presence of the conditioned stimulus (CS; from a range of modalities).

- 1804 In terms of imaging, we hoped to use the no-go stimulus to record a
 1805 clean stimulus response without the possible contamination of
 1806 movement (licking behaviour), and the go stimulus to verify attention
 1807 (Figure 8).
- 1808 Trials were designed to go through the following phases and have the
 1809 animal graduate to subsequent phases, only after correctly performing
 1810 the behaviour:
- 1811 1. Pre-tone: Stimulus-free period; no lick
 1812 2. No-go tone: 7kHz tone period; no lick
 1813 3. Go tone: 10kHz tone period; lick for reward

1814 If the animal would perform an incorrect lick, the particular phase
1815 currently occurring was restarted. Only licks to the Go tone were
1816 rewarded (Figure 9).

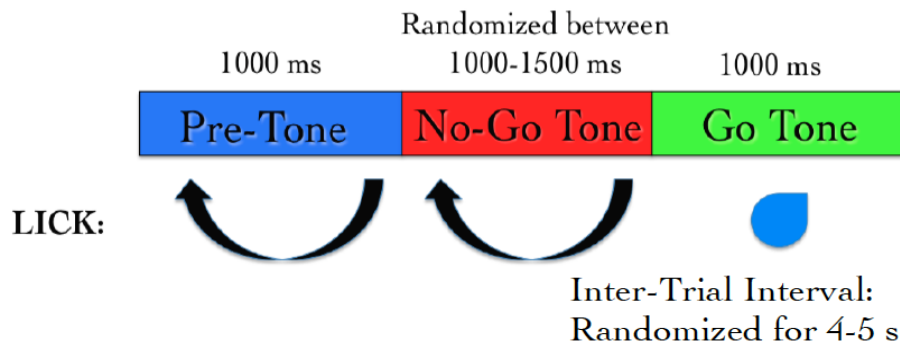


Figure 9: Typical trial structure with the various phases and lick dependent relationships.

1818 Results – Protocol 4

1819
1820 The behavioural performance improves only after ~3-4 sessions of
1821 training (Figure 10A). This is primarily due to an increase in the
1822 percentage of trials with a correct Go tone lick, as shown (Figure 10B).
1823

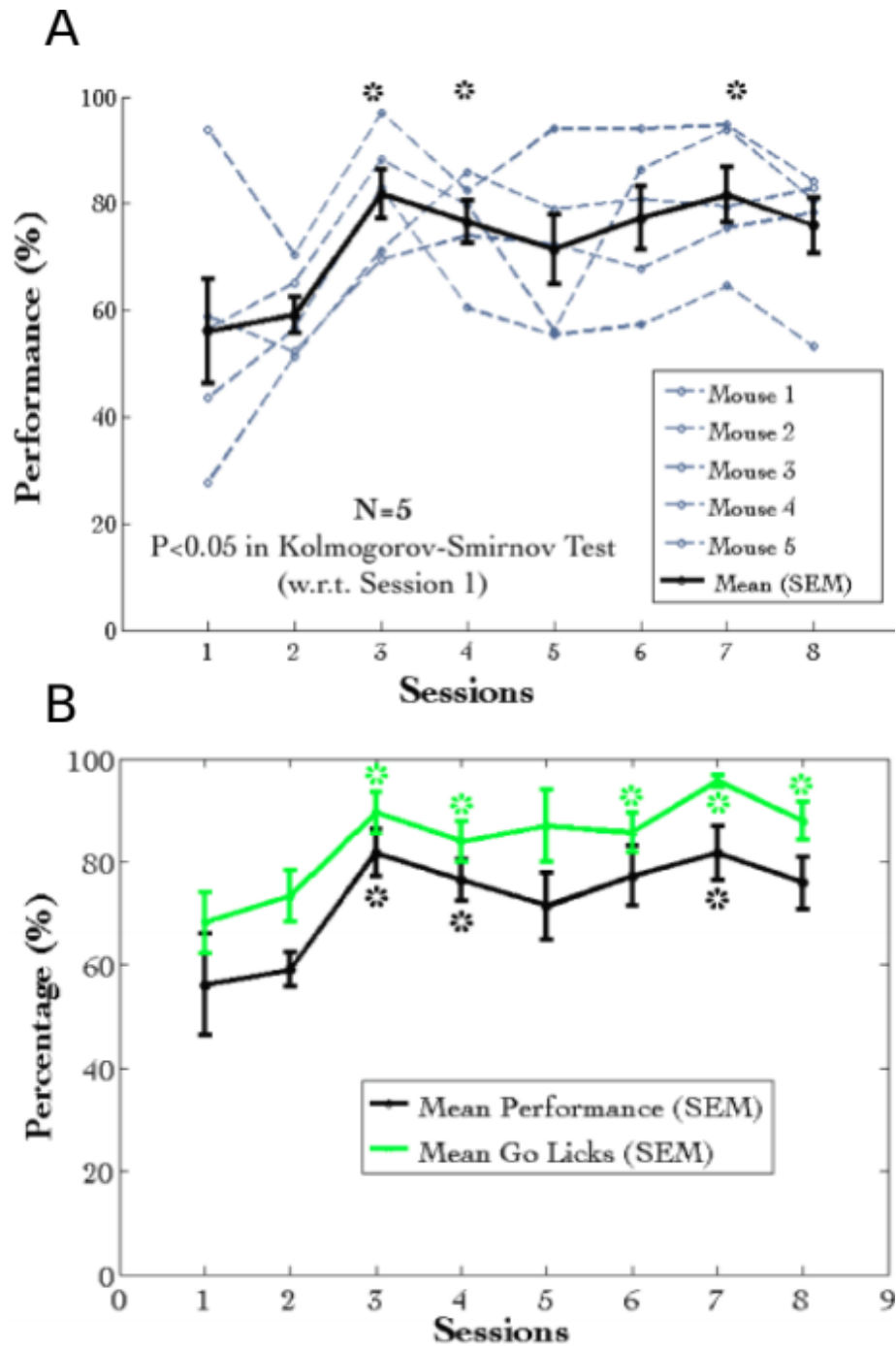


Figure 10: (A) Performance traces for all the animals individually shown in dashed grey lines. Mean + SEM in black. (B) Mean Performance (%) and Mean Go Tone Lick Percentage (%) with Session for the Go/No-Go Task, plotted in black and green, respectively.

1825 A plot of the lick histogram for the various trial phases revealed that
1826 despite reaching the maximum success rate, the animals continued to
1827 lick during the no-go tone phase (incorrect lick) for a long duration of
1828 time (Figure 11). There was no difference in the amounts of time spent
1829 in the pre-tone or no-go tone phases. This suggested that the animals
1830 did not discriminate between the Go and no-go tones. Accordingly, the
1831 current protocol was not being learnt as expected.

1832

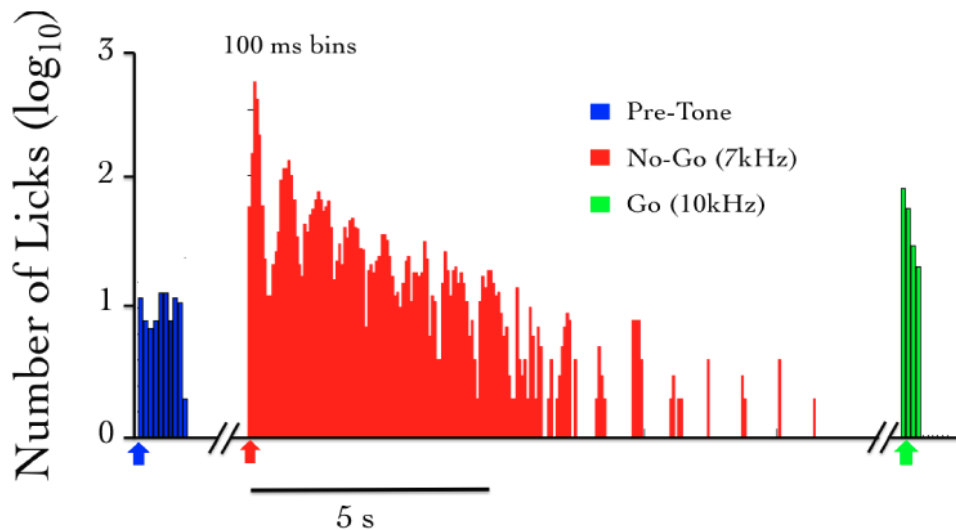


Figure 11: The number of licks in the pre-tone (blue), no-go tone (red), and go tone (green) phases, in a representative animal, in a session with maximum Performance (%).

1834 We were not able to get discriminatory detection. Animals would resort
1835 to performing licks continuously and agnostically to the go and no-go
1836 stimulus. In a study published many years later, it was determined that
1837 discriminatory tasks such as the one described above, could often
1838 require 3-4 weeks of training (Guo et al., 2014), since the animal was
1839 not punished with anything more than a delay or phase restart.

1840

1841 **Total animals trained:** 5

1842 **Conclusion:** Fail

1843

1844 Eventually, we had to abandon these experiments, to switch to an
1845 aversive conditioning task, *viz.*, Trace Eye-Blink Conditioning (TEC).

1846 With the change in the main behavioural task we also changed the
1847 project goals. The TEC task was standardized with the intention to
1848 work on Project II which is to study how animals make complex
1849 associations between different types of stimuli and how they adapt to
1850 changes to the inter-stimulus interval (ISI).

1851

1852 **Trace Eye-Blink Conditioning [Project II]**

1853

1854 Eye-blink Conditioning is a class of Classical Conditioning and requires
1855 the presentation of a neutral stimulus (Conditioned Stimulus, CS) along
1856 with an eye-blink eliciting, mildly aversive stimulus (Unconditioned
1857 Stimulus, US). Depending on whether the CS presentation overlaps
1858 with the US presentation or if the two stimuli are separated by a
1859 stimulus free interval in between (Trace interval), the concomitant
1860 procedure is called Delay Conditioning or Trace Conditioning,
1861 respectively (Figure 12). In either case, precise timing of the CS and
1862 US is mandated.

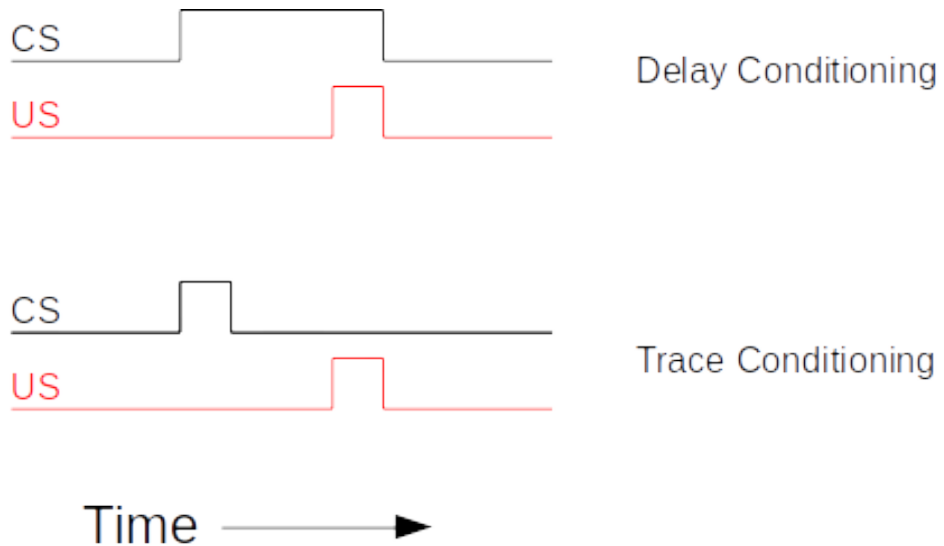


Figure 12: Schematic representation to showcase the two main subtypes of Classical Conditioning (Eye-Blink Conditioning, for our experiments) based on the relative timing and presentation of the CS and US.

1864 The CS is usually an auditory tone or a visual stimulus (e.g.- LED
 1865 Flash), while the US is typically a mild air-puff to the cornea, or a
 1866 gentle electric shock to the eye-lid. Naive animals (rabbits, rodents,
 1867 monkeys, etc.) produce a robust, reflexive eye-blink to the US
 1868 (Unconditioned Response, UR) and ignore the CS, in early trials.
 1869 However, with repeated pairing of CS and US, the animals are able to
 1870 associate the two, and use the CS as a cue to predict the US,
 1871 producing a partial, preemptive eye-blink just before the expected time
 1872 of the US (Conditioned Response, CR). The CR develops in amplitude
 1873 over multiple pairings or training sessions. In well trained animals, the
 1874 CR begins at a time point closer and closer to the CS onset, and
 1875 usually merges with the UR. The animals produce this CR in an
 1876 attempt to avoid the US.
 1877

1878 Traditionally, Trace Eye-Blink Conditioning has been an important
1879 hippocampus-dependent behavioural task, and has been adapted to a
1880 variety of different species, spanning rabbits, rats, and mice.

1881

1882 Damage or inhibition of the hippocampus has been shown to limit task
1883 acquisition without affecting other non-hippocampus dependent tasks
1884 such as Delay Conditioning. In an experiment, Ibotenic Acid was used
1885 in a session dependent fashion, to observe both limitations in first
1886 acquiring the Trace Conditioning task, as well as detriments to
1887 behavioural recall, even after animals learn the task to a high degree of
1888 proficiency, suggesting the pivotal role that the hippocampus plays in
1889 temporal tasks of this nature (Tseng et al., 2004).

1890

1891 A single session of Trace Eye-Blink Conditioning, with strong stimuli
1892 (CS and US), has been previously employed (Modi et al., 2014), but
1893 with only upto 50% of the animals learning the task. Typically animals
1894 require around 3-7 sessions (~200-600 trials) to robustly learn the task.
1895 Accordingly, we designed and standardized a multi-session version of
1896 TEC, to allow more animals to learn and acquire the task, based on
1897 previously published work (Siegel et al., 2015).

1898

1899 **Tracking eye-blink responses**

1900

1901 The most foolproof way to track eye-blink responses (especially with
1902 head-fixed animals) chronically (for multiple sessions across days), is
1903 to use a video camera. We used a Point Grey Chameleon3 1.3 MP
1904 Monochrome USB3.0 camera) for this purpose. It is cost effective and
1905 with proper scaling of the resolution and field of view, can achieve

1906 recording rates of >200 frames per second (FPS). An important criteria
1907 for getting faster frame rates is to have better illumination, so that the
1908 camera may be set to lower exposure settings. We used a set of 5-10
1909 Red colour LEDs as the light source, and these are run using a 12V
1910 DC line, with current limited resistors in series. Additionally, we used
1911 an IR-blocking filter to avoid capturing the 2-Photon excitation light
1912 (910-920 nm) when conduction behaviour and imaging experiments
1913 simultaneously. Finally, to focus the light from the eye of the animal
1914 onto the camera sensor, we used a Tamron M118FM16 lens (1/1.8,
1915 16mm F/1.4).

1916 **Treadmill and tracking running speed**

1917
1918 Allowing the head-fixed animals to run on a treadmill was an important
1919 behaviour rig consideration, as this allows the animals to be more
1920 comfortable and less stressed. We used a 6 inch cylindrical massage
1921 roller with a stainless steel axle running along the length. This axle had
1922 ball bearings on the two ends, to allow for free rotation against clamps.
1923 Additionally, we used linear actuators to be able to adjust the height of
1924 the treadmill relative to the head-fixing clamps.

1925
1926 On one side of the treadmill, we used a printed pattern of black
1927 squares (side length: 1cm) along the circumference. This allowed an
1928 IR LED - Photodetector pair to catch the edges of the black printed
1929 squares. The number of edges detected per unit time, then gave us the
1930 run speed of the animals being trained. We followed previously
1931 published routines and protocols (Siegel et al., 2015) for setting up the
1932 treadmill and run speed tracking (Figure 13).

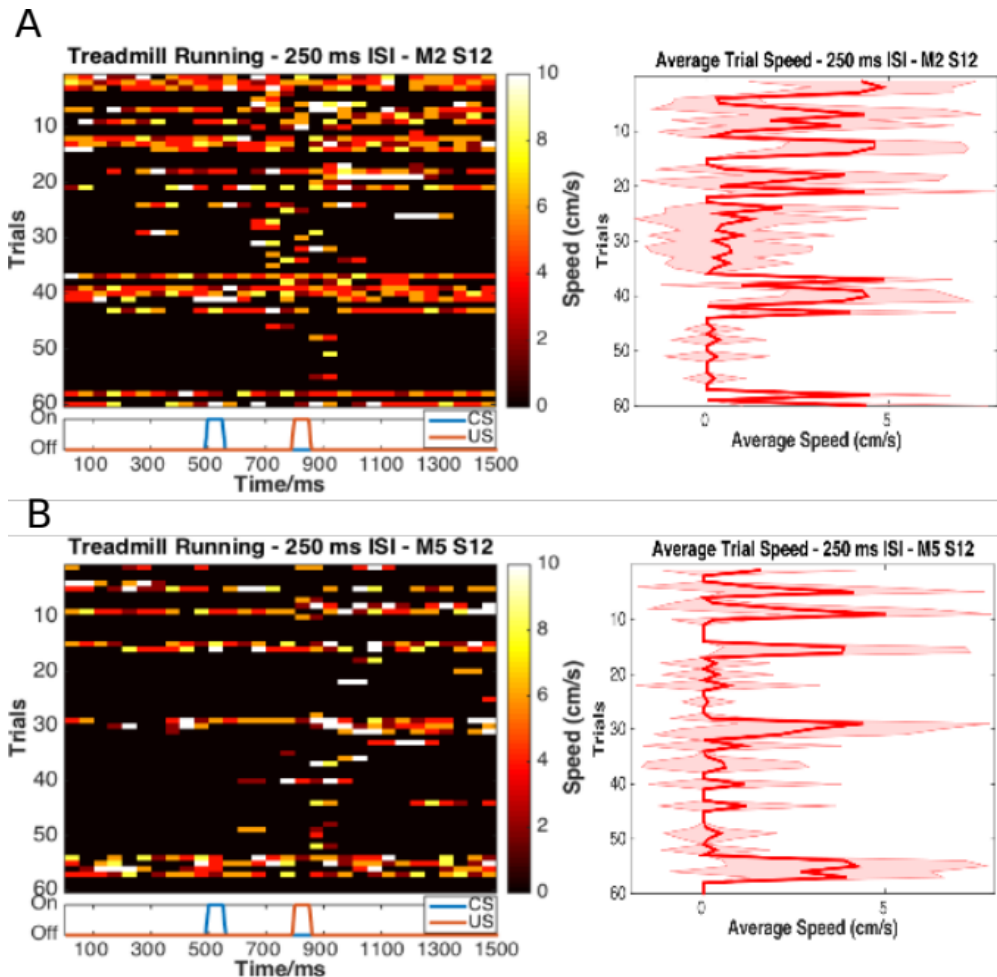


Figure 13: Trial by trial (left), and trial-averaged running speed (right) for two example animals, (A) M2 Session 12, and (B) M5 Session 12.

1934 Behaviour rig and protocol control - Software

1935

1936 For our initial experiments we used the open-source behaviour
 1937 controlling software suite Bonsai (Windows version). Later on, we were
 1938 able to implement our own custom codes that allowed integration of
 1939 the video camera, Arduino for stimulus delivery and treadmill tracking,

1940 and the software side of the protocols. Dilawar S. Rajput was
1941 instrumental in setting up the camera pipeline and integrating it into the
1942 Arduino code. The Camera server was implemented in C++ with
1943 Spinnaker API (Point Grey) and this fetched frames from the camera.
1944 The camera client was written in Python, and this read the frames to
1945 produce a copy to monitor the video feed live, as well as write the
1946 video frames to disk as .tif files.
1947 With this setup, the maximum memory usage was ~1.3 GB RAM, and
1948 the code (available at <https://github.com/BhallaLab/PointGreyCamera>)
1949 had the following dependencies:
1950 • libopencv-dev, python-opencv
1951 • cmake, g++, gnu-make
1952 • libtiff-dev, python-tifffile, python-numpy
1953 • python-gnuplotlib, gnuplot-x11
1954
1955 An important requirement for our behaviour experiment design was to
1956 be able to train the animals systematically under reproducible
1957 conditions, with the aim to have stable behavioural training and animal
1958 performance. We used a blue LED as the Conditioned Stimulus (CS,
1959 50 ms flash) with an air-puff to the eye serving as the Unconditioned
1960 Stimulus (US, 50 ms pulse). We used an Arduino to orchestrate
1961 stimulus delivery and protocol design. All experiments were performed
1962 on head-fixed C57Bl6 mice, since we planned to use a stationary,
1963 custom-built two-microscope to image hippocampal CA1 activity during
1964 task acquisition and recall (Figure 14; Figure 15).

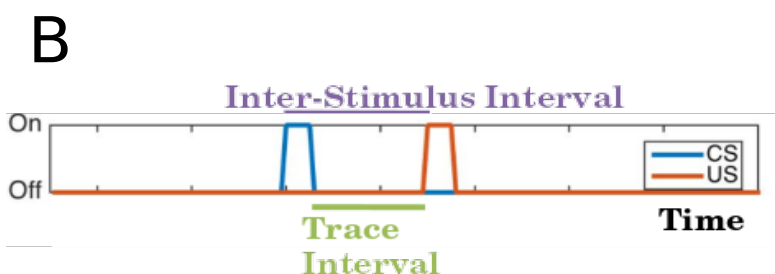
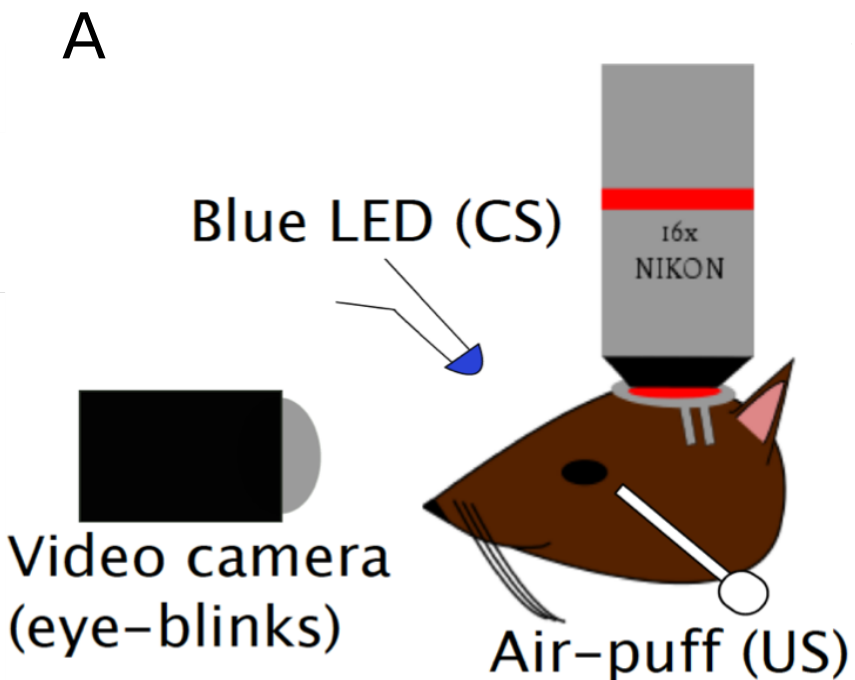


Figure 14: Schematic representation of (A) the behaviour rig with 2-Photon imaging, to train head-fixed mice on a Trace Eye-Blink Conditioning (TEC) task, and (B) relative time intervals between the CS and US.

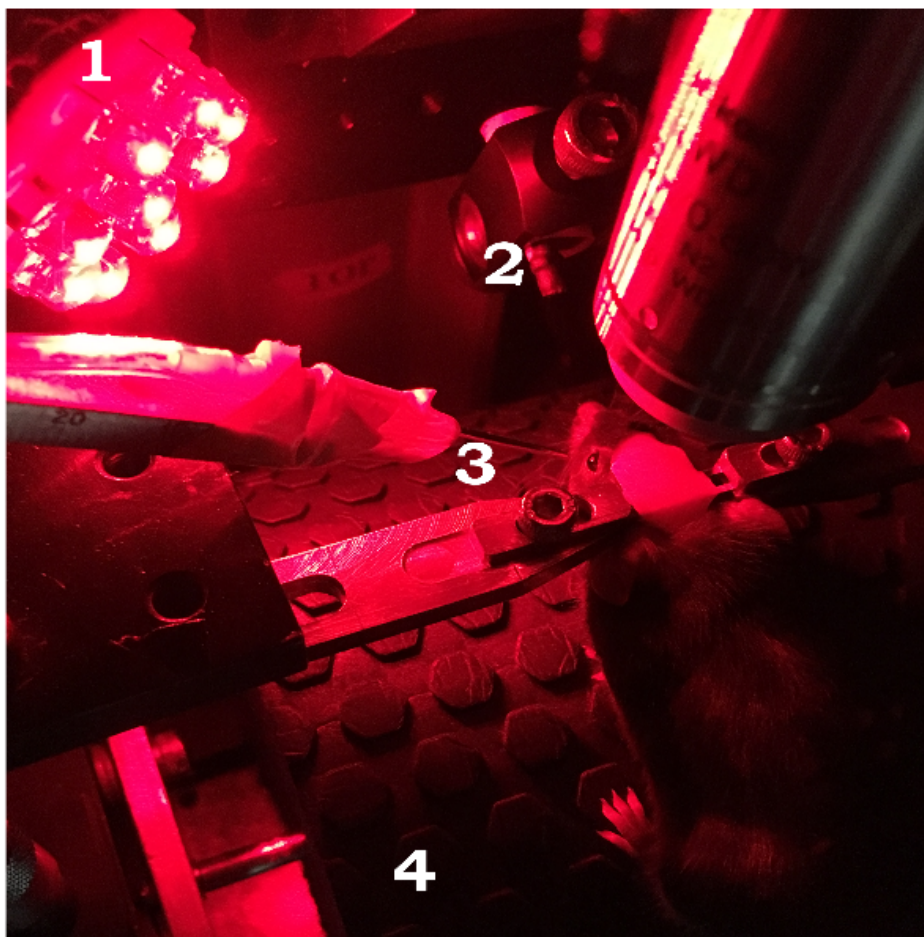


Figure 15: A picture of a head-fixed mouse clamped on the behaviour rig, with key components: 1) Red LED Illumination, 2) Blue LED CS, 3) Air-puff port directed to the left eye, and 4) Height-adjustable Treadmill

1967 Analysis - TEC

1968

1969 Once the .tif movies of the eye of the animal being trained were saved,
1970 they were analyzed by a custom script written in MATLAB, wherein for
1971 every frame we (Figure 16),

- 1972 1. Adjust contrast (optional)
- 1973 2. Apply a median filter (optional)
- 1974 3. Crop out the pixels defining the eye and surrounding
- 1975 (identical number of pixels for all trials and animals)
- 1976 4. Binarize the image of the eye to get black pixels defining the
- 1977 visible (opened) portion of the eye
- 1978 5. Count the relative proportion of open vs closed eye pixels in
- 1979 the cropped image, and
- 1980 6. Assign each frame with a Fraction of Eye Closure (FEC)
- 1981 score.
- 1982

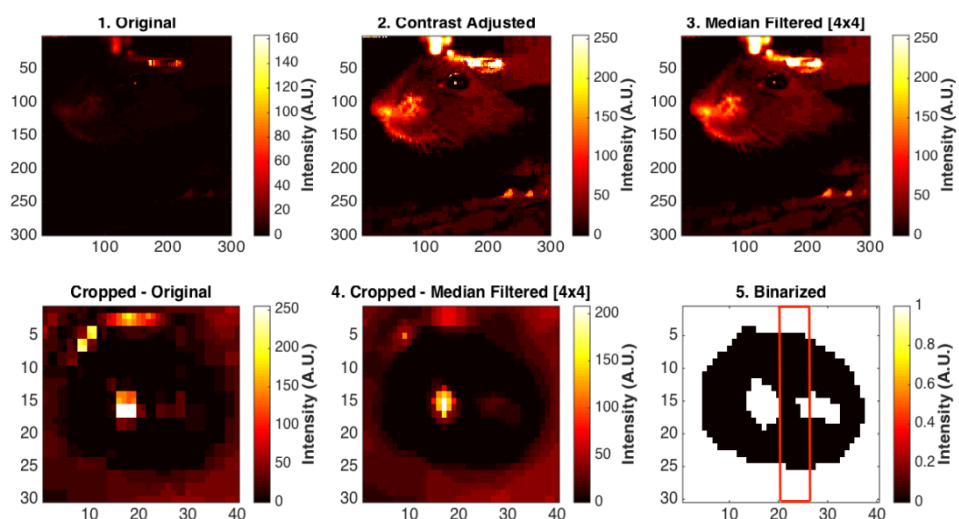


Figure 16: Steps from behaviour video frame to Fraction of Eye-Closed (FEC) analysis

- 1984 The FEC score then allowed us to analyse each trial's worth of frames
- 1985 for eye-blanks. There are many features of the eye-blink that could be
- 1986 used to gauge the overall performance of the animal in terms of both
- 1987 the Conditioned Response (CR) as well as the Unconditioned
- 1988 Response (UR), but for our experiments, we chose to use Eye-Blink

1989 Amplitude (Siegel et al., 2015). Additionally, we studied whether the
1990 animals could produce CRs in the absence of the US, by
1991 pseudorandomly selecting 10% trials to skip the US (Probe Trials).

1992

1993 **Results - TEC**

1994

- 1995 1. Animals showcase task acquisition by performing Conditioned
1996 Responses (CRs), observed as pre-emptive blinks timed to
1997 avoid the aversive US. The kinetics of the CR (timing,
1998 amplitude, etc.) are dependent on the amount of training, but
1999 are identical across paired and probe trials (Figure 17).

2000

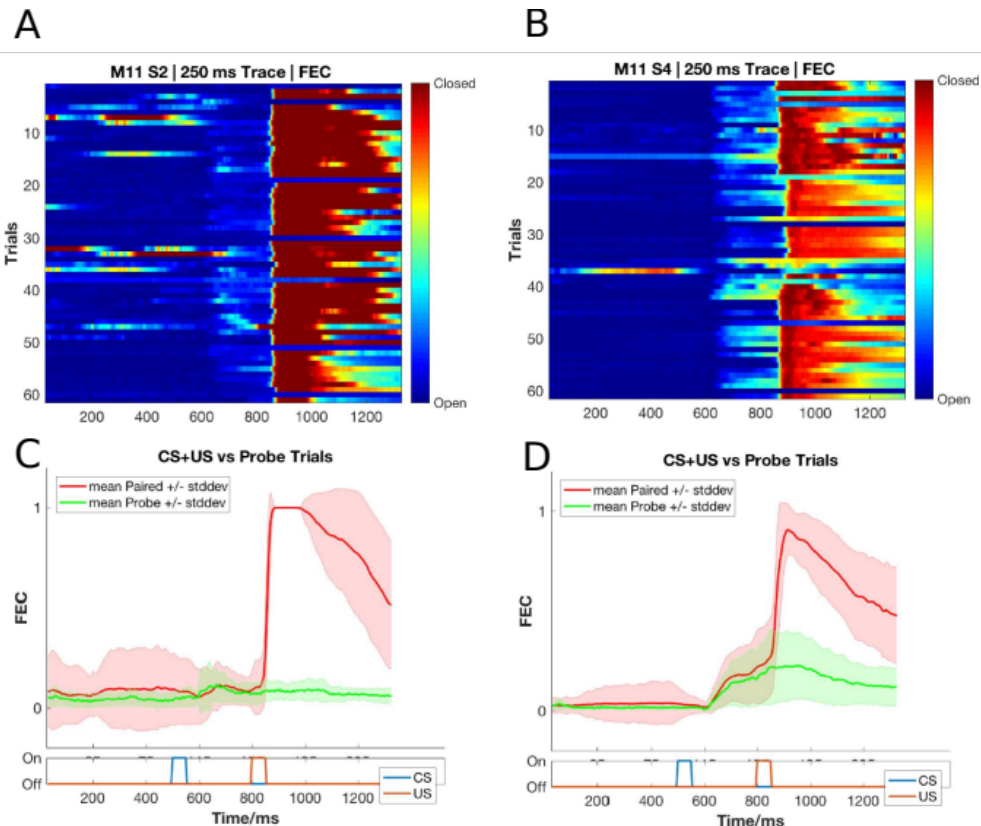


Figure 17: Conditioned Responses (CRs) are small amplitude eye-blinks triggered by the CS, and develop with multiple training sessions, while Unconditioned Responses are large eye-blinks to the US, typically consistent across sessions. (A,B) Trial-by-trial FEC traces for (A) M11 Session 2, and (B) Session 4. (C,D) Trial-averaged FEC traces for (C) Session 2 and (D) Session 4, with paired (red) and probe (green) trials.

- 2002 2. Most animals can pick up the task within 4-7 sessions (1
2003 session/day, 60 trials/session), even if on water deprivation.
2004 Animals can also be subsequently trained to different inter-
2005 stimulus intervals. Using the Conditioned Response (CR)
2006 amplitude, each trial can be binarized to whether a CR was

2007 elicited (Hit Trial) or not (Miss Trial), by thresholding at mean trial FEC + 2*Std. Dev.. Performance for the session is then estimated as the ratio of Hit Trials to Total Trials (Figure 18).
 2008
 2009
 2010

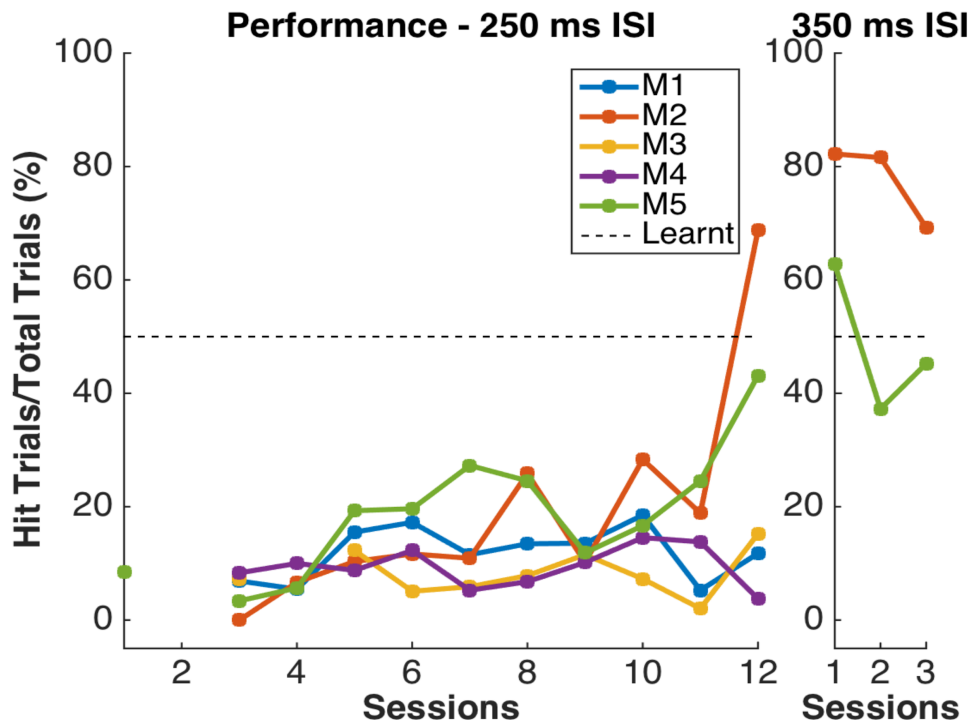


Figure 18: Performance in terms of the percentage of Hit Trials to total trials across sessions, including an ISI switch from 250 ms to 350 ms.

2012 3. Animals that learn multiple ISIs, especially when the second ISI
 2013 is $\geq 2x$ the first ISI, showcase complex eye-blinks without
 2014 extinction of the previously learnt CRs. Once an animal
 2015 showcases the ability to produce Conditioned Responses (CRs)
 2016 to one inter-stimulus interval (ISI), this interval can be
 2017 elongated. In the example shown below we first trained the
 2018 animal to a 250 ms ISI, and then switched to a 500 ms ISI
 2019 (Figure 19).

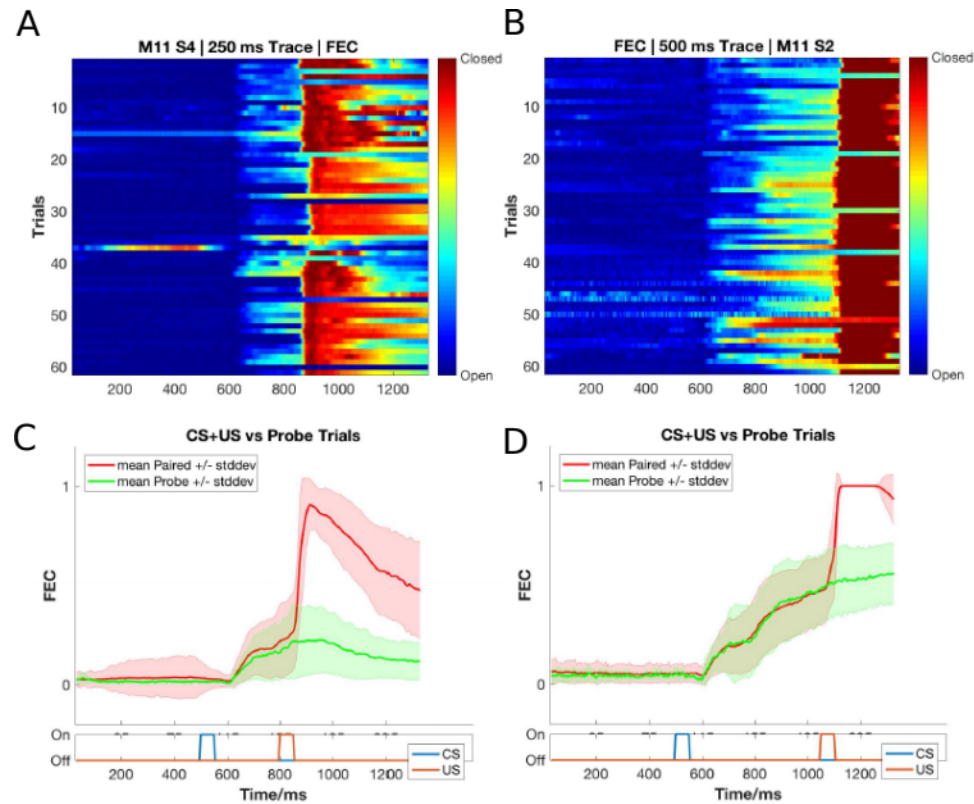


Figure 19: Conditioned Responses (CRs) are preserved for previously learnt ISIs, and switching the ISI to longer intervals results in Complex (multi-CR) eye-blink responses. (A,B) Trial-by-trial FEC scores for (A) 250 ms ISI (left) and (B) 500 ms ISI. (C,D) Trial-averaged FEC traces for (C) 250 ms ISI (left) and (D) 500 ms ISI (right), with paired (red) and probe (green) trials.

- 2021 4. The onset of the Conditioned Response (CR) is not affected by
 2022 the ISI switch, irrespective of how strongly the animals learn the
 2023 task. CRs during paired and probe trials were near identical,
 2024 showcasing that the animal (Figure 20; Figure 21).
 2025
 2026
 2027

2028

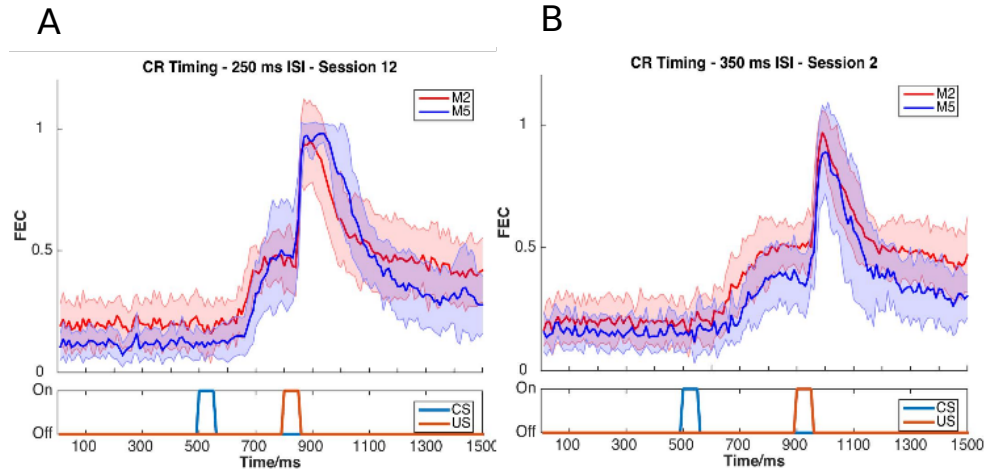


Figure 20: Conditioned Response (CR) onset timing is maintained across ISI switches. Representative examples from a short ISI switch from (A) 250 ms to (B) 350 ms (right).

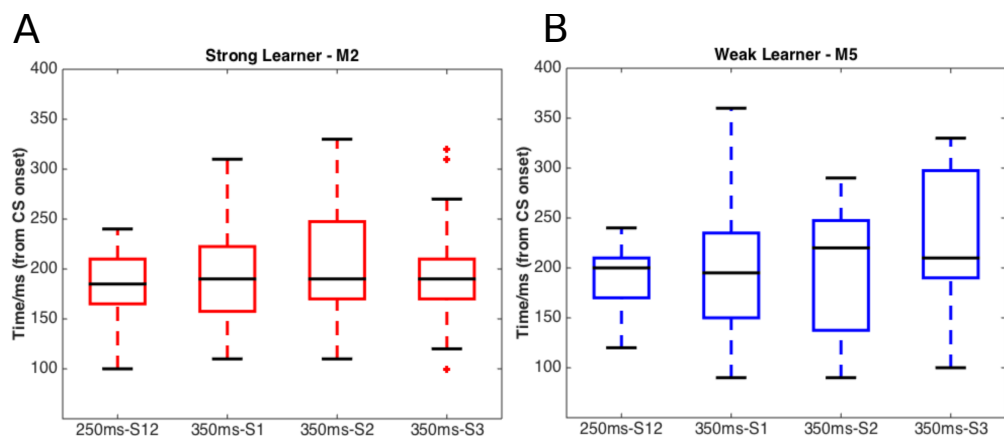


Figure 21: Box plots for Conditioned Response (CR) onset across multiple sessions of training after ISI switch from 250 ms to 350 ms, irrespective of how strongly the animals learnt the task. (A) red, strong learner, and (B) blue, weak learner.

2031 5. Animals can also be trained to very long ISIs from Session 1,
2032 with acquisition taking <10-14 days. Here we tried to train
2033 animals to either a 550 ms ISI or a 750 ms ISI. Note, however,

2034 that unless multiple ISIs are taught to the same animal, the CR
 2035 eye-blink is singular (Figure 22).
 2036

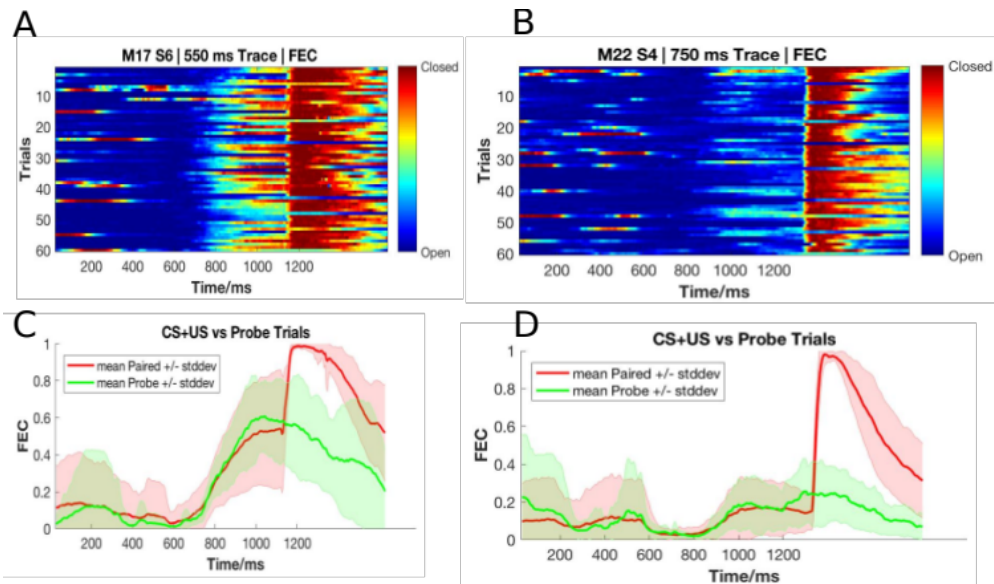


Figure 22: Representative example of mice trained to 550 ms ISI (Session 6) and 750 ms (Session 4). (A,B), Trial-by-trial FEC responses for (A) 550ms ISI, and (B) 750ms ISI. (C,D) Trial-averaged FEC responses for (C) 550 ms ISI, and (D) 750 ms ISI, with paired (red) and probe trials (green).

2038 **Total animals trained:** 18 [Conditioned Responses visible]
 2039 **Conclusion:** Success
 2040
 2041 Ultimately, we were satisfied with the Trace Eye-Blink Conditioning
 2042 paradigm since we could observe stable conditioned responses that
 2043 developed over a reasonably short period of training time (<1 week),
 2044 and adaptable conditioned responses to behaviour parameter
 2045 modulations, in head-fixed mice that could be subjected to
 2046 simultaneous 2-Photon calcium imaging.
 2047

Table 1: Summary table of behaviour protocols attempted and essential results

NAME	PUNISHMENT TYPE	REMARKS
Operant Protocol 1.1 (Stimulus Detection)	No water reward for incorrect licks.	Lack of water reward for incorrect licks not enough for behavioural discrimination at <1 week of training.
Operant Protocol 1.2 (Stimulus Detection)	Air-puff punishment for incorrect licks.	Strong punishment for incorrect licks not enough for behavioural discrimination at <1-2 weeks of training.
Operant Protocol 2 (Stimulus Detection)	Timeout (3s) punishment for incorrect licks.	Alternate or weaker punishment attempted but not enough for behavioural discrimination at <1-2 weeks of training, even with behavioural shaping in blocks of training.
Operant Protocol 3 (DNMS)	Timeout (3s) punishment for incorrect licks.	Alternate punishment attempted but not enough for behavioural discrimination at <1 week of training. No obvious effect of adding delay intervals between stimulus presentations.
Operant Protocol 4 (Go/No-Go) Aversive Protocol (Trace Eye-Blink Conditioning)	Trial phase repeat punishment for incorrect licks. No punishment.	Alternate punishment attempted but not enough for behavioural discrimination at <1 week of training Animals learn the task and produce stable, adaptable conditioned responses (CRs) within 1 week of training.

2048

2049 **Bibliography**

- 2050 Brown, G. D. (1998). Nonassociative learning processes affecting swimming probability in the seashell *Tritonia diomedea*: habituation, sensitization and inhibition. *Behavioural Brain Research*, 95(2), 151–165.
 2051 [https://doi.org/https://doi.org/10.1016/S0166-4328\(98\)00072-2](https://doi.org/https://doi.org/10.1016/S0166-4328(98)00072-2)

- 2055 Deshmukh, S. S., & Bhalla, U. S. (2003). Representation of odor
2056 habituation and timing in the hippocampus. *The Journal of*
2057 *Neuroscience : The Official Journal of the Society for*
2058 *Neuroscience*, 23(5), 1903–1915.
2059 <https://doi.org/10.1523/JNEUROSCI.23-05-01903.2003>
- 2060 Fyhn, M., Molden, S., Witter, M. P., Moser, E. I., & Moser, M.-B.
2061 (2004). Spatial representation in the entorhinal cortex. *Science*
2062 (*New York, N.Y.*), 305(5688), 1258–1264.
2063 <https://doi.org/10.1126/science.1099901>
- 2064 Guo, Z. V, Hires, S. A., Li, N., O'Connor, D. H., Komiyama, T., Ophir,
2065 E., Huber, D., Bonardi, C., Morandell, K., Gutnisky, D., Peron, S.,
2066 Xu, N., Cox, J., & Svoboda, K. (2014). Procedures for Behavioral
2067 Experiments in Head-Fixed Mice. *PLOS ONE*, 9(2), e88678.
2068 <https://doi.org/10.1371/journal.pone.0088678>
- 2069 Hafting, T., Fyhn, M., Molden, S., Moser, M.-B., & Moser, E. I. (2005).
2070 Microstructure of a spatial map in the entorhinal cortex. *Nature*,
2071 436(7052), 801–806. <https://doi.org/10.1038/nature03721>
- 2072 Hubel, D. H., & Wiesel, T. N. (1962). Receptive fields, binocular
2073 interaction and functional architecture in the cat's visual cortex.
2074 *The Journal of Physiology*, 160(1), 106–154.
2075 <https://doi.org/10.1113/jphysiol.1962.sp006837>
- 2076 Jaramillo, S., & Zador, A. M. (2014). Mice and rats achieve similar
2077 levels of performance in an adaptive decision-making task . In
2078 *Frontiers in Systems Neuroscience* (Vol. 8).
2079 <https://www.frontiersin.org/articles/10.3389/fnsys.2014.00173>
- 2080 O'Keefe, J., & Dostrovsky, J. (1971). The hippocampus as a spatial
2081 map. Preliminary evidence from unit activity in the freely-moving
2082 rat. *Brain Research*, 34(1), 171–175. [https://doi.org/10.1016/0006-8993\(71\)90358-1](https://doi.org/10.1016/0006-8993(71)90358-1)
- 2084 Ranck, J. B. (1973). Studies on single neurons in dorsal hippocampal
2085 formation and septum in unrestrained rats: Part I. Behavioral
2086 correlates and firing repertoires. *Experimental Neurology*, 41(2),

- 2087 462–531. <https://doi.org/https://doi.org/10.1016/0014->
2088 4886(73)90290-2
- 2089 Schreurs, B. G. (1989). Classical conditioning of model systems: A
2090 behavioral review. *Psychobiology*, 17(2), 145–155.
2091 <https://doi.org/10.3758/BF03337830>
- 2092 Siegel, J. J., Taylor, W., Gray, R., Kalmbach, B., Zemelman, B. V.,
2093 Desai, N. S., Johnston, D., & Chitwood, R. A. (2015). Trace
2094 Eyeblink Conditioning in Mice Is Dependent upon the Dorsal
2095 Medial Prefrontal Cortex, Cerebellum, and Amygdala: Behavioral
2096 Characterization and Functional Circuitry. *ENeuro*, 2(4),
2097 ENEURO.0051-14.2015. <https://doi.org/10.1523/ENEURO.0051->
2098 14.2015
- 2099 Taube, J. S., Muller, R. U., & Ranck, J. B. J. (1990). Head-direction
2100 cells recorded from the postsubiculum in freely moving rats. I.
2101 Description and quantitative analysis. *The Journal of
2102 Neuroscience : The Official Journal of the Society for
2103 Neuroscience*, 10(2), 420–435.
2104 <https://doi.org/10.1523/JNEUROSCI.10-02-00420.1990>

2105 **Chapter 3 – Imaging**

2106

2107 The mammalian hippocampus is considered important in the formation
2108 of new memories about experienced events (episodic or
2109 autobiographical memory), general declarative memory (memories that
2110 can be explicitly verbalized), spatial memory and navigation, and
2111 associations between stimuli that are distinct in time, among other
2112 functions. To achieve this, the Hippocampus must integrate information
2113 from different areas of the cortex.

2114

2115 Much of the cortical information that enters the Hippocampus (at the
2116 Dentate Gyrus), comes through the Entorhinal Cortex, along the
2117 Perforant Path (Hjorth-Simonsen & Jeune, 1972). The Dentate Gyrus
2118 cell network then relays this information to the CA3 cell network
2119 through Mossy Fibers, which in turn relays the information to CA1
2120 cells, through the Schaffer Collateral Fibers. This is popularly known as
2121 the Trisynaptic Circuit or Pathway (Figure 1 from Chapter 1 -
2122 "Introduction") and there is scope and evidence for computation and
2123 information processing at every step (MacDonald et al., 2011;
2124 McHugh et al., 2007; Modi et al., 2014; Nakashiba et al., 2008; Suh et
2125 al., 2011). Finally, the CA1 cells have their outputs to other brain
2126 regions. It is important to note, however, that regions like the CA1 are
2127 known to have access to information directly from other brain regions,
2128 as well (P. Andersen et al., 2006).

2129

2130 Literature in the field suggests that naïve animals may have some
2131 sensory gating of "Neutral" stimuli at the level of the CA1 (Abe et al.,

2132 2014; Bellistri et al., 2013; Kamondi, 1998). The source of this
2133 inhibition (at least the step before the local interneurons) seems to be
2134 the Medial Septum, through Fimbria-Fornix (Abe et al., 2014). Also,
2135 behavioural relevance allows the CA1 to elicit depolarizations that can
2136 be mapped to brain external stimuli (Dombeck et al., 2010; Harvey et
2137 al., 2009; P. M. Itskov et al., 2011; MacDonald et al., 2011, 2013; Modi
2138 et al., 2014; Pastalkova et al., 2008).

2139

2140 The Hippocampus consists of ventral and dorsal portions both of which
2141 are of similar composition but are parts of different neural circuits
2142 (Moser & Moser, 1998). The dorsal hippocampus performs primarily
2143 cognitive functions and in memory function, while the ventral
2144 hippocampus modulates emotional and affective processes (Fanselow
2145 & Dong, 2010).

2146

2147 **Physiology in the hippocampus**

2148

2149 The Hippocampus is located deep in the medial temporal lobe of
2150 mammals and is defined by several sub-structures, including the
2151 Dentate Gyrus (one site for information input to the hippocampus) and
2152 the Hippocampus Proper constituted by the CA1, CA2, CA3 and CA4
2153 cellular levels.

2154

2155 Using extracellular tungsten microelectrodes in naïve unanesthetized
2156 rabbits serially exposed to multimodal stimuli (Vinogradova, 2001), it
2157 was reported that in the CA1,

2158 1. A major fraction the reactive neurons have unimodal responses
2159 (41-44%)
2160 2. Multimodal neurons are modality-unspecific but have
2161 differentiated responses to stimuli of different modalities and even to
2162 various stimuli within a single modality
2163 3. Many neurons respond by Phasic (evoked responses last for the
2164 duration and as long as the stimulus) and Specific (stimulus-specific
2165 pattern) responses
2166 4. Neurons with inhibitory responses are encountered less
2167 frequently than those with various types of excitatory
2168 5. Habituation (non-responsiveness to repeatedly presented stimuli) is
2169 present though not among all the responsive cells (71-75%) and is
2170 often gradual
2171
2172 Imaging based activity studies have the advantage of being able to
2173 capture many more cells (>100 from the same animal) during
2174 experiments (Dombeck et al., 2010; Pachitariu et al., 2017; Peron et
2175 al., 2015; Poort et al., 2015; Sofroniew et al., 2016) as compared to
2176 typical electrophysiological measurements. Imaging provides an
2177 unambiguous method to identify cells that are not active during a
2178 period of interest. Another advantage is that it provides anatomical
2179 confirmation to help track the same cell over multiple days of
2180 recording, without ambiguity, for longitudinal studies. Finally, imaging
2181 techniques have gained momentum in the study of the hippocampal
2182 CA1 various spatial scales, from cellular resolution somatic studies
2183 (Dombeck et al., 2010; Modi et al., 2014), to dendritic (Mizrahi, 2004;
2184 Sheffield & Dombeck, 2014), axonic boutons terminating on the CA1
2185 interneuron populations (Kaifosh et al., 2013; Lovett-Barron et al.,
2186 2014), as well as spines (Attardo et al., 2015), *in vivo*.

2187
2188 We designed our imaging studies (for this thesis), with the aim to
2189 understand the network and cellular mechanisms of the hippocampal
2190 CA1 that corresponded with behavioral learning induced changes. We
2191 started by looking for CA1 responses to neutral stimuli in naive
2192 animals, *in vivo*. Subsequently, we planned to subject these animals to
2193 behavioural training and study if and how the same cells would
2194 respond.

2195
2196 Depending on the intended duration of the imaging experiments, *viz.*, a
2197 few hours (single session) or a few days and weeks (multiple
2198 sessions), we were able to standardize both an Acute as well as a
2199 Chronic *in vivo* hippocampal preparation. We now discuss the *in vivo*
2200 hippocampal preparation, physiology recordings, and a brief summary
2201 of the results. An important perspective for our experiments was to
2202 study how sensory stimulus responses of hippocampal CA1 develop
2203 with associative learning.

2204

2205 **Methodology – Acute and chronic imaging** 2206 **[Projects I & II]**

2207
2208 The overall experiment deals with optically measuring the activity of
2209 the dorsal CA1 hippocampal neurons when different stimulus
2210 modalities are presented to a male C57BL/6 mouse. The thesis covers
2211 experiments conducted acutely (lasting <10 hours) using OGB-1 as a
2212 calcium sensor), as well as chronically (~7-21 days) using a genetically
2213 encoded calcium indicator, GCaMP6f).

2214

2215 The 2-Photon excitation wavelength for OGB-1 experiments was set to
2216 810 nm (scattering coefficient: $\sim 3 \text{ rad}^2/\text{mm}$) and the same for
2217 GCaMP6f was set to 910 nm (scattering coefficient: $\sim 2 \text{ rad}^2/\text{mm}$) to
2218 image cell bodies (Min et al., 2017) in the CA1, *in vivo*. However,
2219 despite the relatively low scattering of longer wavelengths, the
2220 hippocampus cannot be imaged directly, through the cortex since the
2221 layer of cortex is too thick ($\sim 1\text{-}1.5 \text{ mm}$) to allow proper excitation of the
2222 sample. These infra-red (IR) photons are expected to be scattered
2223 almost completely, well before the imaging depth of the CA1 layer.
2224 These layers of cortex have to accordingly be carefully suctioned out to
2225 allow the microscope objective to have optical access to the exposed
2226 tissue (Figure 23).

2227

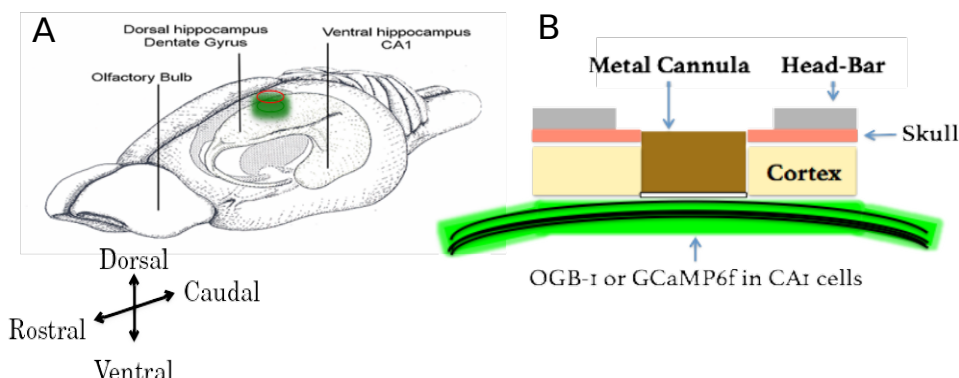


Figure 23: (A) A schematic of the rodent brain, showcasing the two hippocampi, one in each hemisphere. The hippocampi lie $\sim 1 \text{ mm}$ (mice) below the cortical surface. (B) The hippocampal preparation allows optical access to the deep lying hippocampal CA1 cells, relative to the skull/cortex. The CA1 cell bodies arrange in a laminar fashion, as a tight cell body layer that can be visualized by fluorescence (using either OGB-1 or GCaMP).

2229 We first put the animal under anesthesia using a vapor chamber
2230 saturated with 3% isoflurane. Next, the animal was cheek-clamped and
2231 a light state of anesthesia was maintained using 1-2% isoflurane,
2232 provided directly to the nozzle of the animal, keeping track of ~1 Hz
2233 breathing rate and a body temperature of 35-37 °C (with heating pad).
2234 The animal was given a haircut and a circular incision of ~5 cm
2235 circumference was made on the scalp, revealing the skull below. We
2236 then affixed head-bars and skull screws with the help of dental cement,
2237 to be able to clamp the animal post surgery on the 2-Photon
2238 Microscope.

2239

2240 The left, dorsal hippocampus was targeted with a 3-5 mm circular
2241 craniotomy aimed at 1.5 mm left and 2.0 mm behind bregma, tearing
2242 and peeling out the Dura to reveal the cortex. We then carefully
2243 aspirated out the cortex (part of the somatosensory cortex) under
2244 repeated washes of Cortex Buffer (see table 1 for recipe), until the
2245 horizontal CC fibre layer was visible. Finally, we added a drop of low
2246 gelling agarose and a 5 mm coverslip (for acute preps); Kwik-Sil and
2247 inserted a 3 mm metal cannula with a coverslip attached at the bottom
2248 (for chronic preps). We used different sensors depending on the
2249 requirement for the preparation, *viz.*, acute (OGB-1) or chronic imaging
2250 (GCaMP6f). We refer to this series of steps as the hippocampal
2251 preparation.

2252 **Preparation of Cortex Buffer**

2253

2254 We prepared cortex buffer by weighing out the required amount of the
2255 salts, NaCl, KCl, Glucose and HEPES (see table 1 for recipe) and

2256 making up the volume of the solution with Milli Q Water to ~1000 ml.
2257 We then set the pH of the buffer using a calibrated pH meter to 7.35,
2258 using 1M NaOH_(aq).
2259 Then, fill up the volume to 1000 ml and verify the pH (should not have
2260 changed). Filter the contents through a 0.22 um membrane using a
2261 vacuum filtration, and store at 6 °C.
2262

Table 2: Recipe for ready-to-use cortex buffer. The buffer is typically prepared and stored in aliquots to be used each week. The correct pH range of the buffer was often a crucial factor ensuring the success of the hippocampal preparation.

Ingredient	Concentration (mM)	Amount (g or ml) for 1000 ml
NaCl (s)	125	7.31 g
KCl (s)	5	0.373 g
Glucose (s)	10	1.8 g
HEPES (s)	10	2.38 g
CaCl ₂ (aq)	2	1.6 ml of 1.25 M stock solution
MgCl ₂ (aq)	2	1.5 ml of 1.3 M stock

		solution0
2263		

2264 **Oregon Green Bapta-1 injections for acute**

2265 **imaging**

2266

2267 To prepare Oregon Green Bapta-1 (OGB-1) dye for microinjections, we
2268 first dissolve a 50 µg tube of OGB-1 in 5 µl of Pluronic Acid, and vortex
2269 the mix for 5 minutes. Separately, we dilute 20 µl of Phenol Red into
2270 500 µl of cortex buffer, and transfer 45 µl of this solution to the OGB-1
2271 mix. Next, we sonicate the 50 µl solution for 20 mins., followed by
2272 centrifugation at 10000 RPM for 5 seconds. The remaining supernatant
2273 is split into 7 aliquots (7 µl), and stored at -20 C for a maximum of one
2274 week (7 days).

2275

2276 For acute/single-day experiments, we injected OGB-1 using pulled,
2277 dye loaded micropipettes (~2 MΩ resistance, ~2 µm diameter) at a
2278 depth of 100-150 µm (Figure 23) from the topmost layer of exposed
2279 tissue, till a slow but detectable pulse of dye (visualized as a red/pink
2280 solution) may be visible just below the tissue surface. This allows the
2281 dye to be soaked up by the basal dendrites of the CA1 and takes 30-
2282 60 mins for incorporation into the cytoplasm. We typically allow the
2283 animal 1-2 hours of respite before the subsequent imaging session.
2284 High pressure ejection of the dye into the tissue may damage the
2285 neuropil, while very low pressures or clogs in the pipette affect the
2286 spread of the dye across the tissue. We aimed to image ~100 x 100
2287 µm² of the tissue in any particular ROI, and achieved this with 5

2288 minute injections with each micropipette aiming to load the dye at 2-3,
2289 well separated positions spread across the entire exposed dorsal
2290 surface. We estimated that the dye volume was <1000 nl/injection.
2291 After the injection cycle with any micropipette, we left the tissue
2292 undisturbed for at least 5-10 mins before pulling the micropipette out of
2293 the tissue.

2294

2295 Once all the injections were complete, the exposure was sealed using
2296 5% low gelling agarose making sure the temperature was cool enough
2297 to avoid heat-related tissue damage.

2298

2299 OGB-1 is eventually cleared from the cytoplasm but allows for a limited
2300 window for imaging studies (Stosiek et al., 2003). Reopening the
2301 agarose seal and re-injections were never attempted to prevent
2302 unnecessary damage to the underlying tissue. Additionally, the
2303 agarose plug itself was found to be unstable beyond 1-3 days. This
2304 resulted in the imaging possibility being limited to the same day as the
2305 surgery (acute imaging).

2306

2307 **GCaMP and chronic imaging**

2308

2309 For chronic/multi-day experiments, we standardized a stereotaxic viral
2310 injection step, where we inject the gene for GCaMP5 or GCaMP6f into
2311 the dorsal hippocampus at -1.5 mm lateral, 2 mm posterior, and 1.3
2312 mm dorsal from bregma on the skull surface (Figure 24).

2313

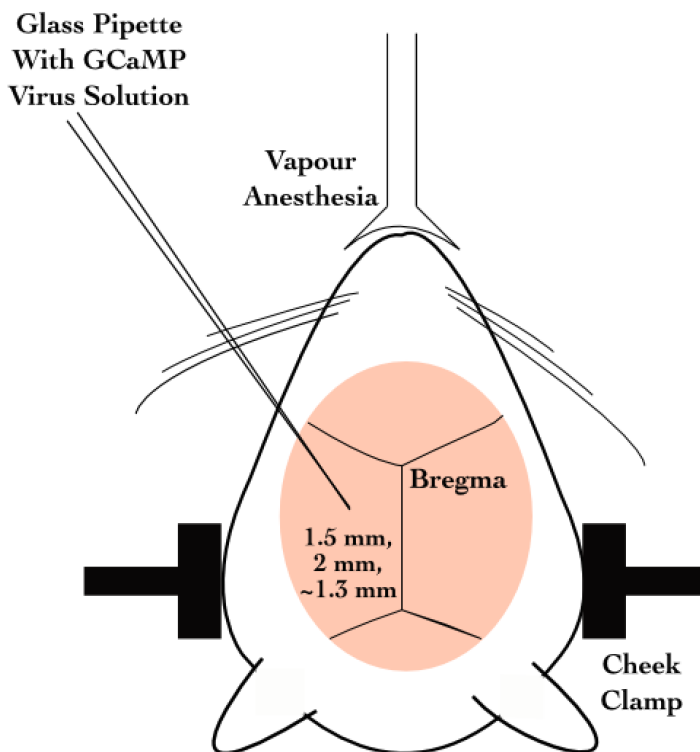


Figure 24: Schematic representation for

2314 stereotaxic viral injection.

2315

2316 Later on, we switched to directly using GCaMP6f transgenic mice
2317 (background: C56BL/6) which express GCaMP6f in the Hippocampus

2318 [Tg(Thy1-

2319 GCaMP6f)GP5.17Dkim JAX stock #025393]. This helped us
2320 circumvent the dye loading or viral injection steps, aiding in the
2321 potential success of the preparations, by way of tissue health and
2322 recording quality.

2323

2324 **Results - Imaging**

2325

2326 **2-Photon calcium imaging of hippocampal CA1, *in vivo***

2327

2328 The CA1 cell body layer is ~200 µm deep, in through the hippocampal
2329 surface. At these depths, scattering of excitation as well as emission
2330 light is significant. However, we are able to image at these depths with
2331 Two-Photon Imaging LASER Scanning Imaging (810 nm for OGB-1
2332 and 910 nm for GCaMP5/GCaMP6f), where a high intensity pulsed
2333 LASER allows for two photons to near instantaneously excite
2334 fluorophores in a thin z-slice plane which is the focal plane of the
2335 Objective. Our LASER, the Coherent Chameleon Ultra II emits ~3 W at
2336 810 nm, and ~2 W at 910 nm. At these depths, there is scattering of
2337 emitted photons. However, since only the focal plane is excited any
2338 and all emitted photons that we capture are part of the signal. We use
2339 a Nikon 16x water immersion, 0.8 NA, 3 mm working distance
2340 Objective (N16XLWD-PF), to get a large field of view.

2341

2342 **Acute Imaging of OGB-1 loaded hippocampal CA1, *in*
2343 *vivo***

2344

2345 We injected OGB-1 dye into brain tissue for our acute imaging
2346 experiments (see Methodology for details). OGB-1 spreads throughout
2347 the cytoplasm and neuropil, and infiltrates the cell nucleus, giving the
2348 cells the appearance of solid circles (cells). The cell body (soma)

2349 ranges from 10-15 μm depending on the orientation of the imaging
2350 layer in 3D tissue space (Figure 25A).

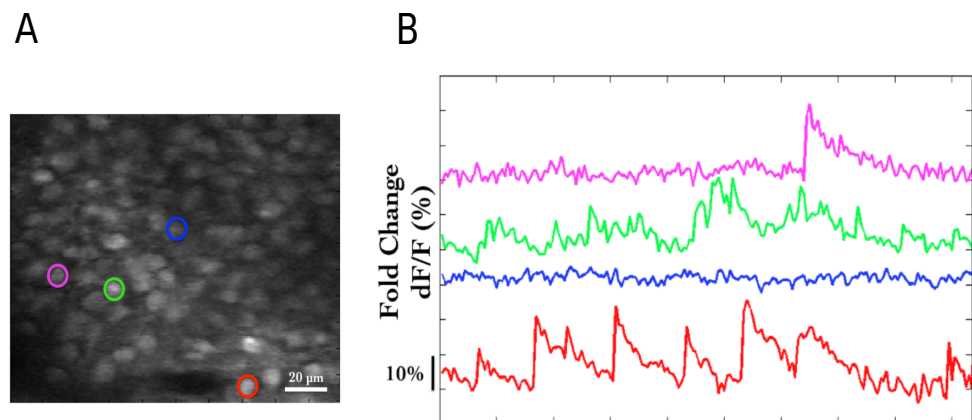


Figure 25: (A) Representative Two-Photon Calcium Image of a plane of Hippocampal CA1 cells, bolus loaded with Oregon Green Bapta-1 (OGB-1), at an instant in time. Example cells marked out post-hoc as pink, green, blue and red. Scale bar 20 μm . (B) Representative dF/F (%) traces for the calcium activity recorded in a single 10s video for example cells pink, green, blue, and red. Scale bar (1 sec; 10% dF/F).

2351 Each cell in the recorded region of interest (ROI), is identified, marked
2352 out (in pixel identity), based on local activity of correlated pixels in the
2353 time series movies. The average intensity of the pixels corresponding
2354 to each cell for each frame in each recording video, is saved as the
2355 raw calcium fluorescence trace. Next, these raw calcium traces are
2356 baseline normalized to equate the baselines for each cell at 0, and
2357 describe the dynamic range of the intensity values as 0 to 1, or 1 to
2358 100%. The corresponding time series of baseline normalized dF/F for
2359 the representative example cells are shown (Figure 25B; Figure 28B).
2360

2361 **Chronic imaging of hippocampal CA1 using GCaMP**

2362

2363 For chronic imaging, tissue health was of paramount concern since it
2364 could easily degrade in time (Figure 26). With practice and
2365 standardization, we were able to get the preparations to survive for 2-4
2366 weeks at very good signal-to-noise. Preparations that resulted in very
2367 poor signal-to-noise were often recorded but have been filtered out of
2368 the data showcased in this thesis. While preparations can sometimes
2369 last even months, typically it is crucial to consider if the ROI for
2370 recording could provide >20 cells, to continue the experiment.

2371 GCaMP is typically designed to be cytosolic and does not typically
2372 cross into the cell nucleus. GCaMP labeled cell bodies appear as
2373 doughnuts in the imaging slice (Figure 26A; Figure 27).

2374

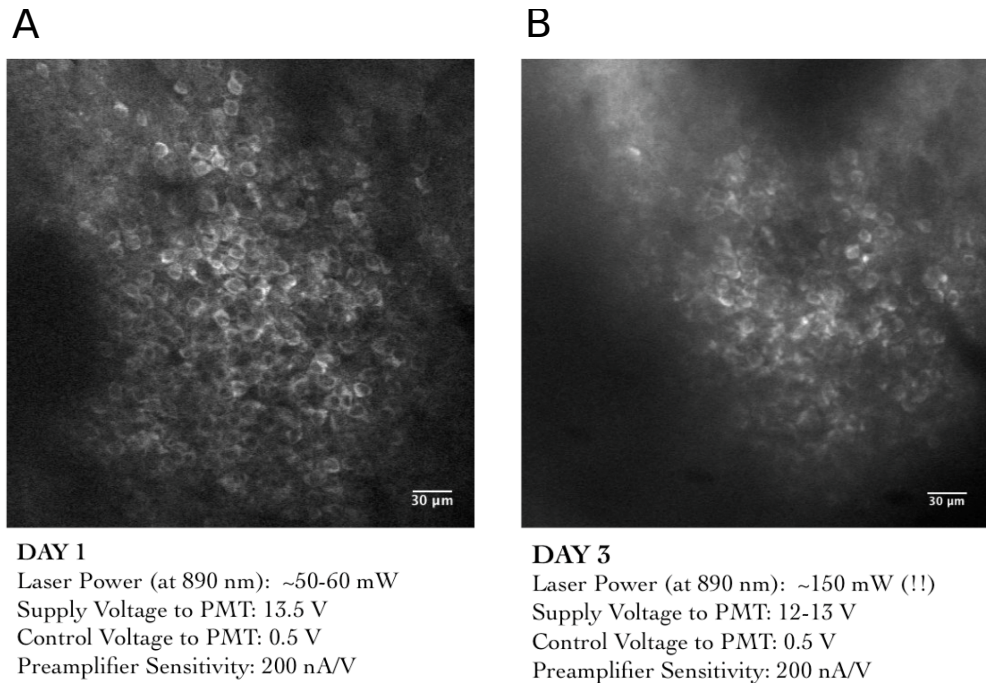


Figure 26: Tissue Degradation over time. Representative Two-Photon Calcium images of a snapshot in time of the Hippocampal CA1 cell body layer on (A) Day 1 after the surgery and (B) Day 3, after the surgery. Scale bar 30 μ m.

2376 Recordings with very good signal-to-noise, where the same chronically
 2377 labeled CA1 cells could be anatomically identified on subsequent days
 2378 even >2-3 weeks post surgery (Figure 27) were eventually acquired,
 2379 and are featured in the data presented in Chapter 4.
 2380

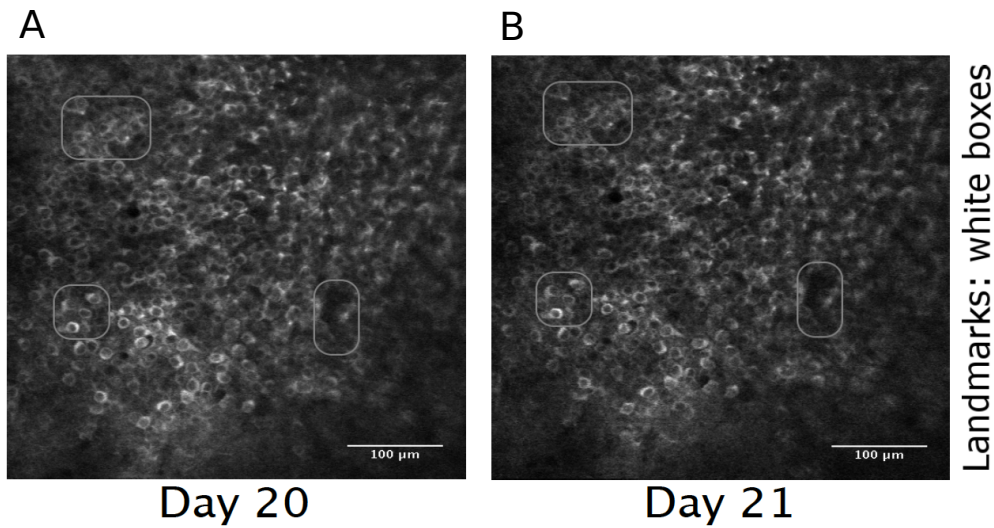


Figure 27: Chronic calcium imaging of the same Hippocampal CA1 cells over weeks. Representative 2-Photon images from (A) Day 20, and (B) Day 21, after surgery. Landmarks have been marked and were used to confirm frame registration and identify cells. Scale bar 100 μm .

2382 The magnification and resolution of the field of view are important
 2383 parameters to consider when balancing magnification for the resolution
 2384 and the maximization of the number of cells being simultaneously
 2385 recorded from (Figure 25A; Figure 28A).

2386

2387 While recording at high frame rates for live imaging, we captured a
 2388 relatively large number of cells (~100) in time-series imaging frames, at
 2389 frame rates of around 10-15 frames per second (FPS). Subsequently,
 2390 we subjected the animal to various stimuli across trials and saved
 2391 these images for analysis.

2392

2393

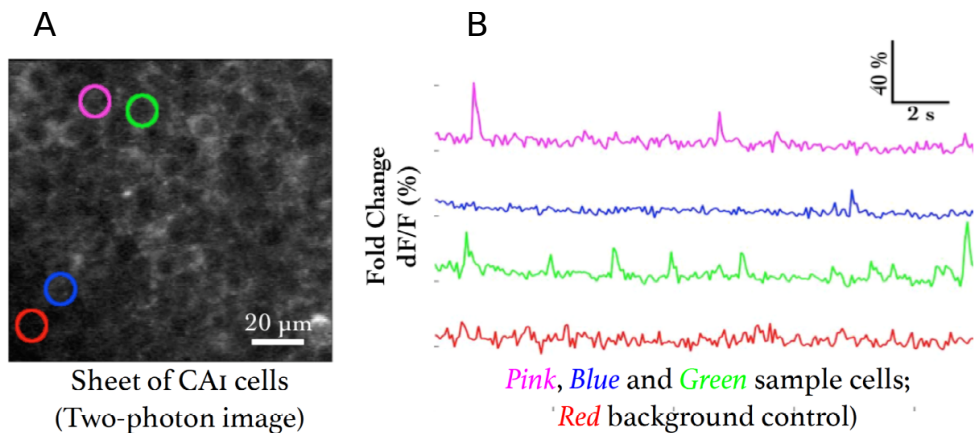


Figure 28: (A) Representative Two-Photon Calcium Image of a plane of Hippocampal CA1 cells expressing GCaMP6f at an instant in time. Example cells marked out post-hoc in pink, blue, and green, with no-cell background in red. Scale bar 20 μ m. (B) Representative $dF/F (\%)$ traces for the calcium activity recorded in a single 10s video for example cells in pink, blue, and green, with no-cell background in red. Scale bar (2 sec; 10% dF/F).

2395 Spontaneous activity during non-stimulus periods

2396

2397 We recorded the calcium activity from a large number of hippocampal
 2398 CA1 cell bodies, while presenting various neutral and conditioning
 2399 stimuli, including fairly large periods of time before and after stimulus
 2400 presentation. Activity of cells, typically observed *in vivo*, in these
 2401 periods is termed spontaneous activity. Cells may showcase variable
 2402 rate (number of calcium events per sec) and timing. Given proper
 2403 signal isolation for identified cells in an ROI, each source or “cell” may
 2404 be considered independent, *i.e.* - there is minimized cross talk between
 2405 the fluorescence emitted by each cell body.

2406

2407 **Spatial organization of activity correlated cells during**
2408 **spontaneous activity**

2409

2410 As part of our Acute Imaging experiments using OGB-1, we studied the
2411 Pearson's Correlation Coefficient for the activity traces across all cell
2412 pairs, during bouts of spontaneous activity, viz., all frames from the
2413 beginning of the trial till the presentation of the stimulus, across all
2414 trials. Cell pairs showcased a range of correlation coefficients (Figure
2415 29) and we were able to cluster cells based on activity using Meta-K
2416 Means (Modi et al., 2014; unpublished data from Dhawale, 2013).

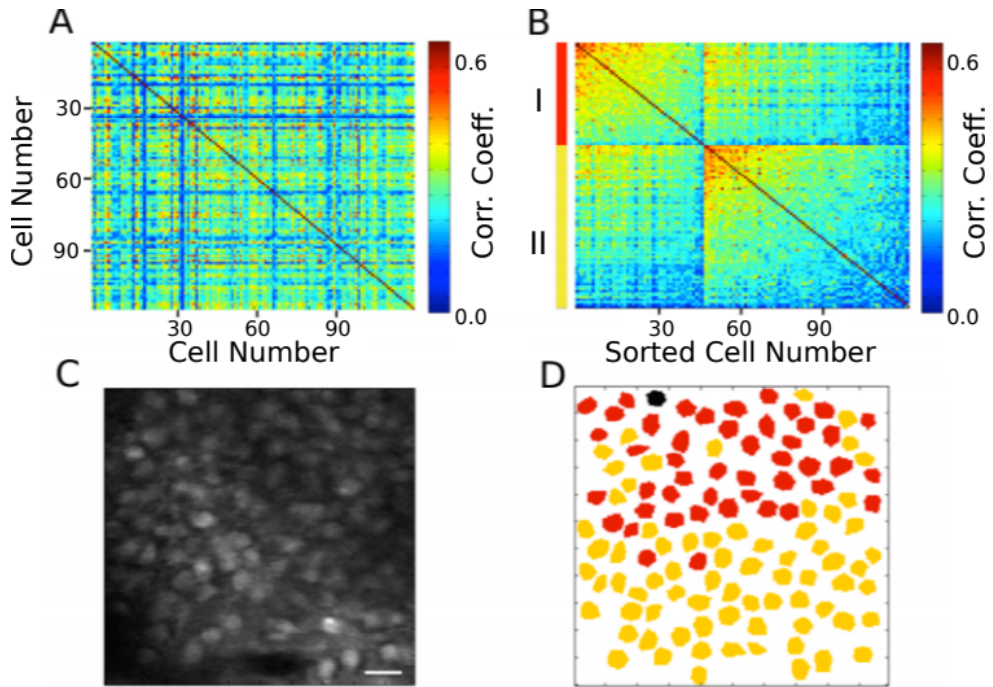


Figure 29: (A) Correlation Coefficients for cell pairs from an example two-photon recording. (B) Meta-K Means clustering with cell pairs using the heuristic that within group pairs would be more similar than between group pairs. In this example, the cells were clustered into two groups, I (red) and II (yellow). (C) Two-Photon image of the field of view of cells; same as Figure 25A. (D) Spatial organization of correlated cell pair groups during spontaneous activity (Modi et al., 2014).

2418 Stimulus evoked responses

2419

2420 We also recorded calcium activity from the same cells during
 2421 presentation of various neutral stimuli to the animals. Here are the
 2422 results of the auditory (tone) and somatosensory (whisker) stimulus
 2423 experiments.

2424

2425 A neutral auditory tone at 5000 Hz (for 1 sec) was presented to the
2426 animals N= 6 animals; 25 trials). We observed no clear signs of cell
2427 activity modulation by neutral tones. Below, we show an example
2428 animal with trial-averaged calcium traces as dF/F (%), across all
2429 recorded cells with a 1 sec tone presentation (Figure 30A). We also
2430 presented animals to whisker stimulation by playing a 1s long air-puff
2431 (5 LPM) to the ipsilateral (left) whisker (N = 5 animals; 25 trials). In this
2432 case, we observed whisker-stimulation based cell activity modulation.
2433 Below, we show the trial-averaged calcium traces as dF/F (%) of the
2434 same example animal as above, presented with a 1 sec whisker-puff
2435 (Figure 30B).

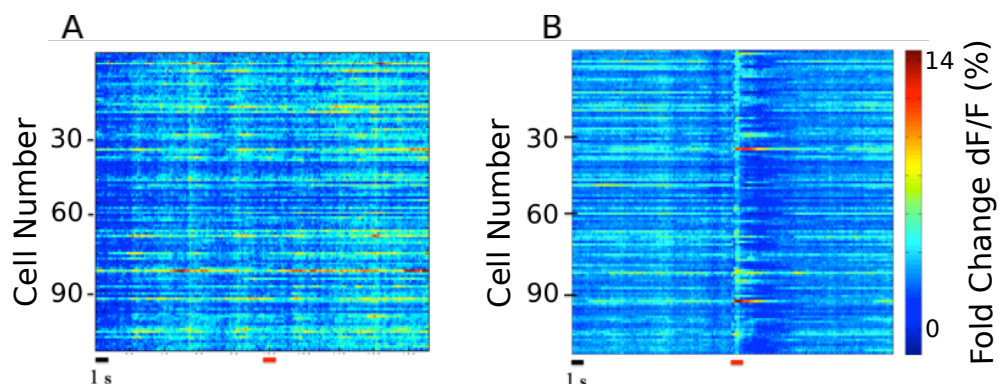


Figure 30: (A) Trial-averaged (25 trials) calcium activity from ~100 CA1 cells in trials where a 5000 Hz tone was presented (red bar). (B) Trial-averaged (18 trials) calcium activity from the same cells in trials where a 5 LPM air-puff to the ipsilateral whiskers was presented (red bar).

2437 **Spatial organization of activity correlated cells post whisker-puff**
2438 **stimulation**
2439
2440 We attempted the same clustering analysis using Meta-K-Means on
2441 the activity profiles of all the cells post presentation of the whisker-puff

2442 till the end of the trial, across all trials. These functionally correlated
2443 cell pair groups were found distributed across the imaging plane with
2444 no clear sign of spatial clustering (Figure 31).
2445 Comparing Figure 29D and Figure 31C, we observe that the whisker-
2446 puff stimulation results in a change in the spatial map of correlated
2447 activity, in the same network of cells.

2448

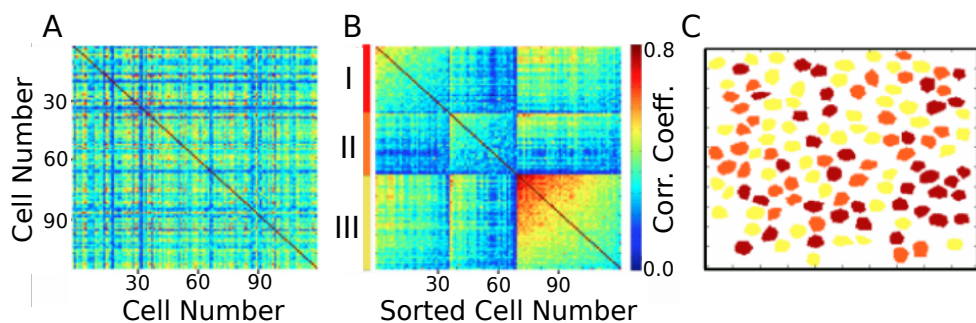


Figure 31: (A) Correlation Coefficients for cell pairs from post whisker-puff stimulation periods. (B) Meta-K Means clustering with cell pairs using the heuristic that within group pairs would be more similar than between group pairs. In this example, the cells were clustered into three groups I (red), II (orange), and III (yellow). (D) No clear spatial organization of correlated cell pair groups post whisker stimulation

2450 As a control, we shuffled the trial time points for each cell
2451 pseudorandomly, to artificially break activity correlations.
2452 When we attempted the Meta-K-Means clustering on this
2453 surrogate dataset, we did not observe functional clustering
2454 (Figure 32).

2455

2456

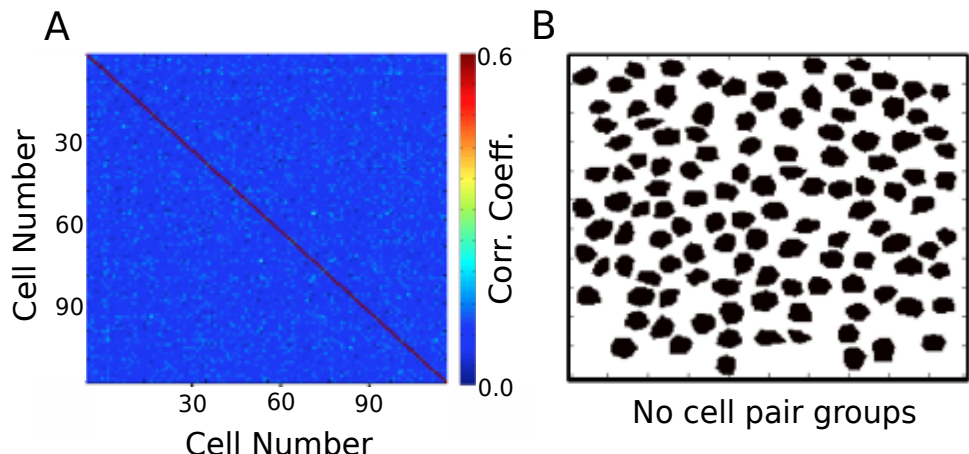


Figure 32: (A) Correlation Coefficients for cell pairs from a trial-shuffle control dataset (B) Meta-K Means clustering revealed that there were no cell pair groups identified.

2458 **Chronic imaging now possible for weeks with the same**
 2459 **mouse**
 2460
 2461 The need for multi-day tracking was mandated for recordings through
 2462 behavioural training, since the animals typically only learn Trace Eye-
 2463 Blink Conditioning (TEC; Chapter 2) over the course of 3-7 days
 2464 (Siegel et al., 2015). A different experiment design would have been to
 2465 train animals and then perform the hippocampal preparation to record
 2466 CA1 neural activity while the animal(s) exhibit learnt Conditioned
 2467 Responses (CRs). However, we argued against this experimental
 2468 design, on account of the following.
 2469 1. The actual cellular and network mechanisms that allow for the
 2470 animal to learn the behavioural task would be very difficult to study
 2471 given that the learning period would have passed.

2472 2. The success rate of the hippocampal preparation is typically very
2473 low (estimated at ~33-50% based on the last 200 attempts), given
2474 potential sources of failures such as tissue decay, bleeding into the
2475 imaging window from damaged parts of the hippocampus, implant
2476 instability especially with stressed or unsettled experiment animals,
2477 and photobleaching from the 2-P excitation LASER over multiple
2478 imaging sessions. TEC is typically learnt by >50% animals (Modi et al.,
2479 2014; Siegel et al., 2015). We had argued for exposing the
2480 hippocampus for imaging before behavioural training since any
2481 successful preparations could then be subjected to the relatively more
2482 consistent behavioural training.

2483 3. Having the preparation performed before training minimizes the
2484 number of times the animal would be subjected to surgery (to just the
2485 once), improving chances of animal health through the experiment.

2486
2487 Next, we discuss some preliminary results from the chronic imaging
2488 datasets. A non-overlapping set of results that feature in “Chapter 4 -
2489 Analysis” of this thesis, have been skipped here for brevity.
2490

2491 **Preliminary analysis to identify time cells**

2492
2493 The analysis algorithm pertaining only to the results presented here in
2494 “Chapter 3 - Imaging”, was adapted from William Mau’s Temporal
2495 Information method (Mau et al., 2018; Chapter 4 - “Analysis”). This
2496 version of the algorithm is expected to be subject to some degree of
2497 Type I (false positives) and Type II (false negative) errors.
2498 Subsequently, the algorithm was developed to the extent of the

2499 Python/C++ implementation featured in “Chapter 4 – Analysis”, with
2500 much superior prediction performance.
2501

2502 1. We applied a filter to select for cells that had activity in >25% of
2503 trials (irrespective of tuning)

2504 2. We then develop Peri-stimulus Time Histograms (PSTH), using
2505 Area Under the Curve for a binsize of 3 frames, centering the “0
2506 ms” to the onset of the Conditioned Stimulus for visualization.

2507 3. Next, we estimate Temporal Information (TI), using

2508
$$TI = 1/\lambda * \sum_j \lambda_j \log_2 (\lambda_j / \lambda) P_j$$

2509 where,

2510 λ : Average Transient rate for each cell

2511 λ_j : Average transient rate for each cell in bin “j”

2512 P_j : Probability that the mouse was in time bin “j”

2513 For every trial, we also random shuffled the frame points to develop a
2514 random activity model (1000 times) and ensure that $\lambda > \lambda_{rand}$ in more
2515 than 99% of the models. Filtering for cells active in >25% trials with a λ
2516 $> \lambda_{rand}$ in >99% shuffles along with the estimation of TI, provided us a
2517 handle on reliability.

2518

2519 **Time Cells**

2520

2521 During the experience of temporally organized events or stimuli, in this
2522 case post training to Trace Eye-Blink Conditioning, a rough contingent
2523 of ~20% of the total cells recorded, were observed to showcase time-
2524 locked calcium activity mapping the Blue LED or Conditioned Stimulus
2525 (CS) to the air-puff or Unconditioned Stimulus (US). These cells were
2526 classified as time cells. Here are some example time cells (Figure 33).

2527

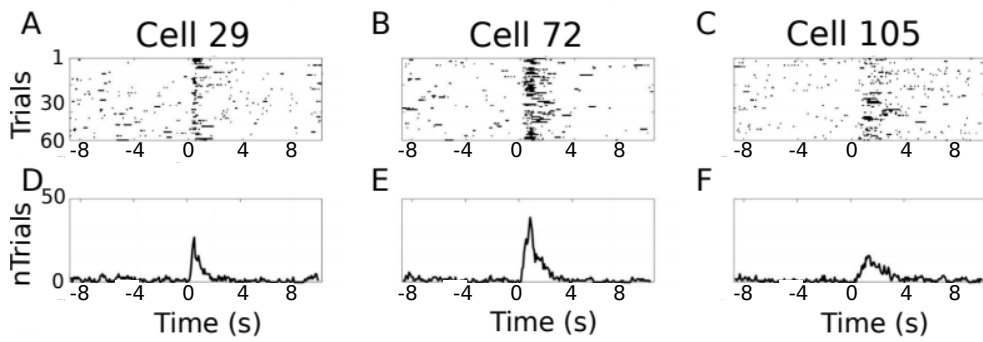


Figure 33: Example Time Cells visualized as event raster plots (A, B, C), along with the trial-summed activity profiles (D, E, F) suggesting ~50% hit trials, for cells 29 and 72 from Session 1 (session type 5) with mouse M26, and slightly lower reliability (~25% hit trials) from cell 105.

2529 **Other Cells**

2530

2531 On the other hand, most cells did not clear our analysis algorithm
 2532 checkpoints and were classified as other cells. Here are some example
 2533 Other Cells (Figure 34) from the same session with mouse M26
 2534 (Session 1; session type 5).

2535

2536

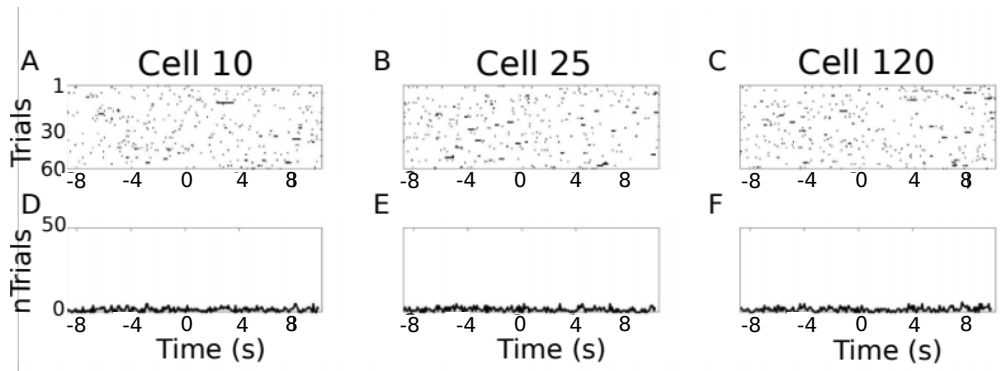


Figure 34: Example Other Cells visualized as event raster plots (A, B, C), along with the trial-summed activity profiles (D, E, F) for cells 10, 25, and 120 from Session 1 (session type 5) with mouse M26.

2538 Considering only the classified time cells, we sorted cells based on the
2539 time of the peak of the trial-average activity and a spatiotemporal
2540 sequence was visualized (Figure 35; also see “Chapter 4 - Analysis
2541 Figure 7H”).

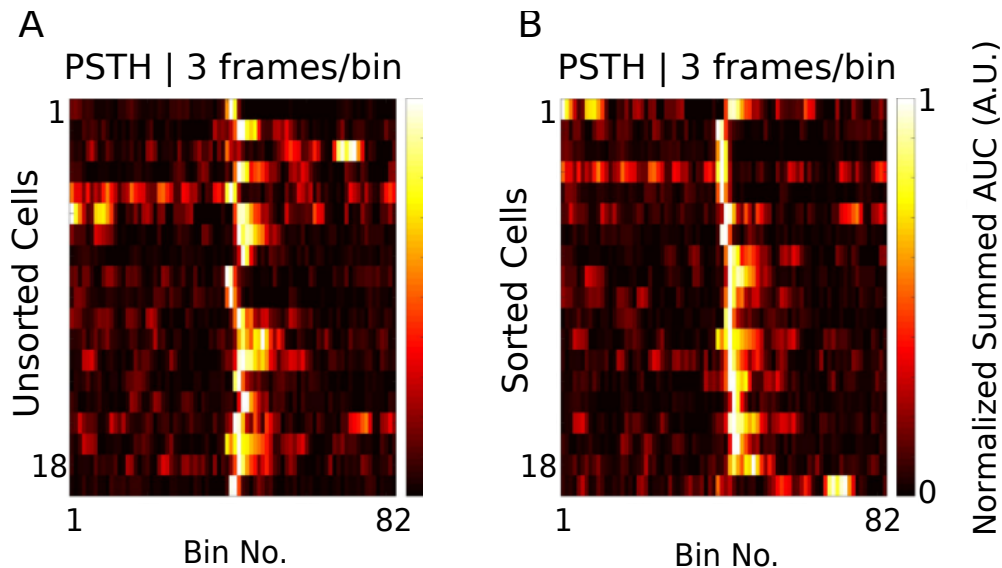


Figure 35: Event Time Histograms or tuning curves for Identified Time-Locked Cells with trial-summed peaks in session 4 of training (session type 5) with mouse M26. (A) Unsorted list of Time cells. (B) Peak-sorted list of the same cells. Here, 1 bin = 3 frames = ~210 ms (sampling rate 14.5 Hz without binning; ~5 Hz with binning). As per the (legacy) session type 5 protocol, the CS (50 ms Blue LED flash) was presented in frame bin 39, followed by a stimulus-free trace interval during frame bins 40 and 41, and then the US (50 ms airpuff to ipsilateral eye) was presented in frame bin 42.

2543 We did not observe any obvious trend in the temporal information of
 2544 time cells with peak times. For the same cells (as in Figure 35), we
 2545 now look at the actual Temporal Information estimates plotted against
 2546 sorted time cells (Figure 36) .

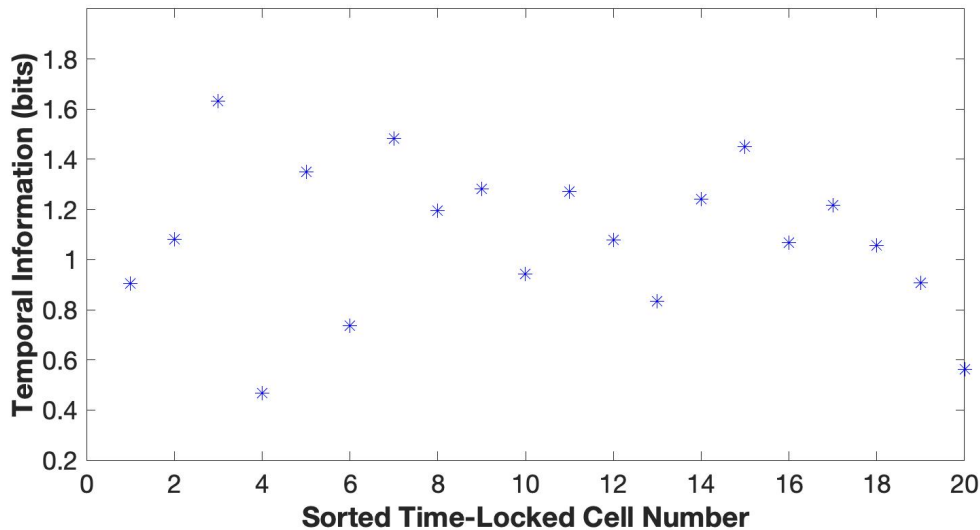


Figure 36: Temporal Information (bits) vs Sorted time cell number from the analytically identified Time Cells in Session 4 (session type 5) with mouse M26. No clear trend was observed.

2548 **Tuning, re-tuning, and de-tuning of time cells across
2549 sessions**

2550

2551 A crucial advantage of the chronic preparation was that many
2552 anatomically aligned and classified cells (as cell ROIs), could be
2553 recorded from over several days and sessions, to look for possible
2554 changes in calcium activity profiles across sessions in the same set of
2555 cells.

2556

2557 We noticed some evidence for an expansion of the set of identified
2558 time cells with sessions, up to a reliable pool of ~20% time cells.

2559 Altogether, from the pool of chronically aligned cells (across sessions),

2560 there was an increase from 7.7% to 23.1% of time cells. Considering
2561 the full cohort cells (irrespective of tracking across multiple training
2562 sessions) the increase was from 7.2% to 21.1% time cells. Here are
2563 the classified time cells between two independent recording sessions,
2564 early in training (Figure 37).
2565

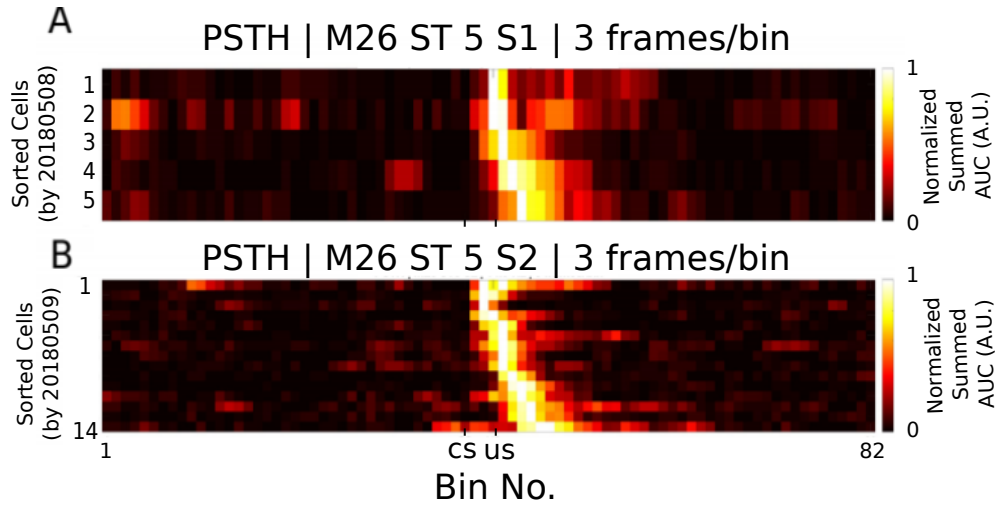


Figure 37: More time cells observed to attain tuning as training sessions. Event Time Histograms of the identified set of time cells between A) Sessions 1 and (B) Session 2, with mouse M26 (session type 5).

2567 The same may also be visualized as trial-averaged calcium activity
2568 profiles for all recorded cells across independent recording sessions
2569 (Figure 38).
2570

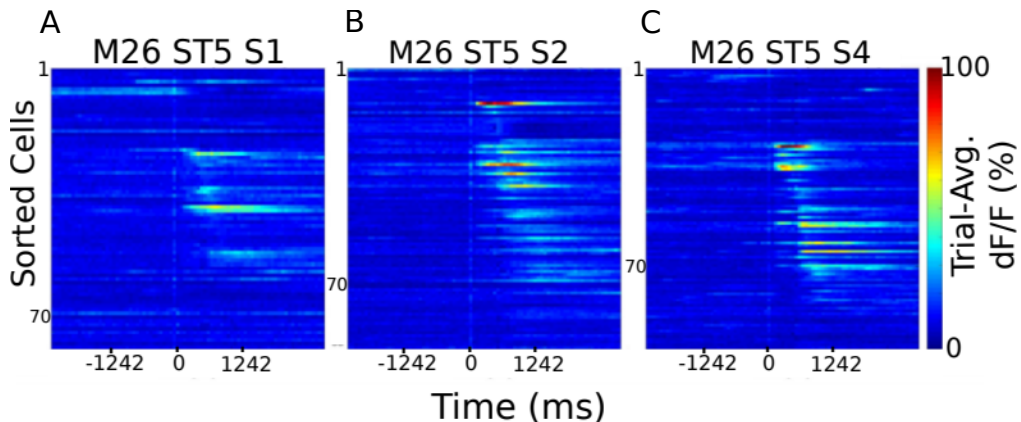


Figure 38: Sorted Time Cells form Sequences that develop with learning. Trial-Averaged calcium activity traces for all recorded cells across A) Session 1, B) Session 2, and C) Session 4, with mouse M26 (sessiontype 5). Time 0 ms was aligned to the CS. The CS + Trace + US interval lasted from 0-600 ms, here.

2572 Chronically tracked time cells that showed reliable tuning across
 2573 sessions were then compared to look for any shifts in the peak tuning
 2574 bin. We observed examples of cells that maintained their tuning across
 2575 pairs of sessions (Figure 39).

2576

2577

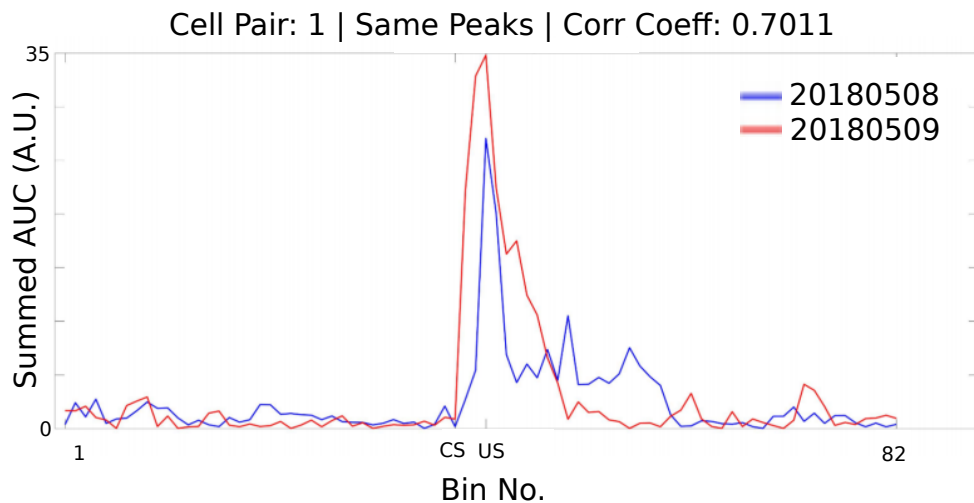


Figure 39: Same/similar tuning across session 1 and session 2 for this example time cell. Blue Event Time Histograms represent the tuning curve for the cell for session 1 (date: 20180508) and Red represent the same but for session 2 (date: 20180509). Pearson's correlation coefficient between the two session pairs was 0.7011.

2579 Here are examples wherein the tuning curve peaks shift to earlier time
 2580 points, across sessions (Figure 40) for Mouse M26, session type 5,
 2581 session 1 vs 2.
 2582

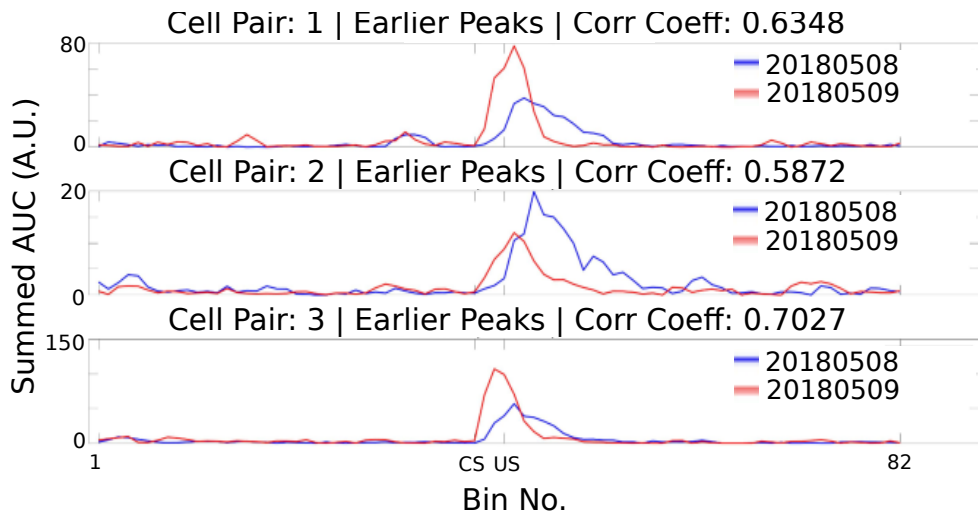


Figure 40: Three example chronically tracked cell pairs with tuning peaks arriving earlier with training sessions (rows). Blue Event Time Histograms represent the tuning curve for any cell for session 1 (date: 20180508) and Red represent the same but for session 2 (date: 20180509). Pearson's correlation coefficient between the session pairs was 0.6.348, 0.5872 and 0.7027 for A) cell pair 1, B) cell pair 2, and C) cell pair3, respectively.

2584 Here is an example of a cell showcasing de-tuning for the CS-US
 2585 interval, across sessions (Figure 41), potentially with a new, delayed
 2586 peak almost 100 frames later.
 2587

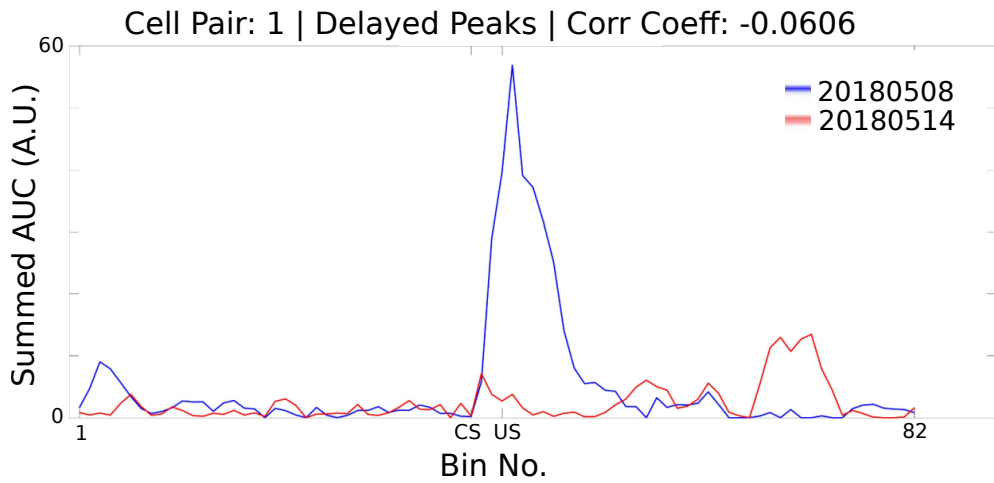


Figure 41: Example chronically tracked cell pair with de-tuning between session 1 and 4. Blue Event Time Histograms represent the tuning curve for the example cell for session 1 (date: 20180508) and Red represent the same but for session 4 (date: 20180514). Pearson's correlation coefficient between the two curves was -0.0606.

2589 A full summary of the correlation based peak timing analysis for
 2590 chronically identified time cells with mouse M26 is shown (Figure 42).
 2591 Across all same cell pairs, there was positive correlation (>0.2) in 71%
 2592 of Time Cells. Also a comparison of the tuning curve peaks between
 2593 the same time cell pairs revealed that a majority of the re-tuned peaks
 2594 occurred earlier in time, going across sessions (71%), with an equal
 2595 proportion of cells without much re-tuning (14%) or de-tuning to later
 2596 time points (14%).

2597

2598

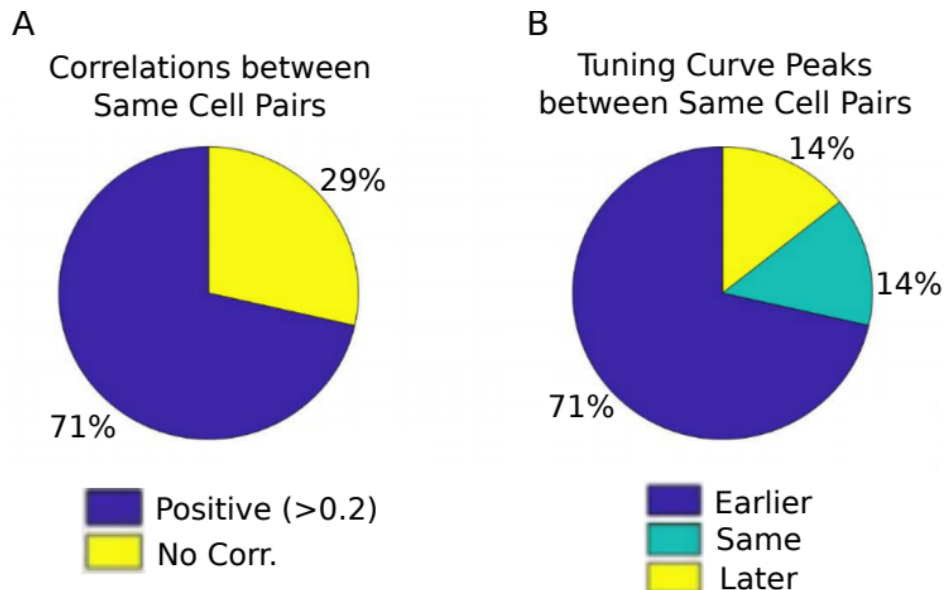


Figure 42: Comparing chronically tracked time cells across sessions for all matched cell pairs by (A) Correlation Analysis, and (B) Timing of peaks.

2600 A summary of the key preliminary results observed using real
 2601 physiology data is as follows.
 2602 1. Time cell tuning curve peaks typically began only after the
 2603 presentation of the CS.
 2604 2. The width of the tuning curve peaks for time cells increased with
 2605 tuning to later frame bins. This was consistent with the recordings
 2606 presented in literature under physiological conditions (B. Kraus et al.,
 2607 2013; MacDonald et al., 2011, 2013; Mau et al., 2018; Modi et al.,
 2608 2014; Pastalkova et al., 2008).
 2609 3. Pairwise time cell tuning curves for different time cells may have
 2610 some overlap in timing, but peaks were observed in all frame bins
 2611 between the CS and the US. This particular observation is confounded
 2612 by the short number of Trace period frames recorded and the
 2613 requirement to consider 3 recording frames to every bin (Mau et al.,

2614 2018), decreasing the effective sampling rate even further (14.5 Hz
2615 without binning, to ~5 Hz with binning). However, the observation is still
2616 consistent with previous literature (B. Kraus et al., 2013; B. J. Kraus et
2617 al., 2015; MacDonald et al., 2011, 2013; Mau et al., 2018; Modi et al.,
2618 2014; Pastalkova et al., 2008).

2619 4. A surprisingly large number of time cells could be identified with
2620 tuning peaks for frame bins occurring after the termination of the US.

2621 5. Considering all chronically tracked cells, the classified and sorted
2622 time cells formed sequences that were dynamic across learning
2623 sessions. Many time cells developed tuning curves with sessions while
2624 some time cells lost their tuning.

2625 6. For the majority of time cells, re-tuning occurred with initial tuning
2626 to the timing of the US in earlier sessions, followed by a shift to earlier
2627 time points for the tuning peak, as training progressed through
2628 sessions.

2629

2630 Future directions to be explored in the lab include studying the
2631 reliability of a larger pool of chronically tracked cells with switches in
2632 the inter-stimulus interval (ISI) between the CS and the US as well as
2633 with a larger palette of different stimuli testing out a battery of
2634 Conditioned Stimuli (CS1, CS2, etc.) and Unconditioned Stimuli (US1,
2635 US2, etc.). The goal is to understand how well the internal neural
2636 spatiotemporal CA1 sequence maps to the external behavioural
2637 protocol parameters, *in vivo*.

2638 **Bibliography**

2639 Abe, R., Sakaguchi, T., Matsumoto, N., Matsuki, N., & Ikegaya, Y.
2640 (2014). Sound-induced hyperpolarization of hippocampal neurons.

- 2641 *Neuroreport*, 25(13), 1013–1017.
2642 <https://doi.org/10.1097/WNR.0000000000000206>
- 2643 Andersen, P., Morris, R., Amaral, D., Bliss, T., & O'Keefe, J. (Eds.).
2644 (2006). *The Hippocampus Book*. Oxford University Press.
2645 <https://doi.org/10.1093/acprof:oso/9780195100273.001.0001>
- 2646 Attardo, A., Fitzgerald, J. E., & Schnitzer, M. J. (2015). Impermanence
2647 of dendritic spines in live adult CA1 hippocampus. *Nature*,
2648 523(7562), 592–596. <https://doi.org/10.1038/nature14467>
- 2649 Bellistri, E., Aguilar, J., Brotons-Mas, J. R., Foffani, G., & de la Prida, L.
2650 M. (2013). Basic properties of somatosensory-evoked responses
2651 in the dorsal hippocampus of the rat. *The Journal of Physiology*,
2652 591(10), 2667–2686. <https://doi.org/10.1113/jphysiol.2013.251892>
- 2653 Dhawale, A. K. (2013). *Temporal and spatial features of sensory*
2654 *coding in the olfactory bulb and hippocampus*. Tata Institute of
2655 Fundamental Research.
- 2656 Dombeck, D. A., Harvey, C. D., Tian, L., Looger, L. L., & Tank, D. W.
2657 (2010). Functional imaging of hippocampal place cells at cellular
2658 resolution during virtual navigation. *Nature Neuroscience*, 13(11),
2659 1433–1440. <https://doi.org/10.1038/nn.2648>
- 2660 Fanselow, M. S., & Dong, H.-W. (2010). Are the dorsal and ventral
2661 hippocampus functionally distinct structures? *Neuron*, 65(1), 7–19.
2662 <https://doi.org/10.1016/j.neuron.2009.11.031>
- 2663 Harvey, C. D., Collman, F., Dombeck, D. A., & Tank, D. W. (2009).
2664 Intracellular dynamics of hippocampal place cells during virtual
2665 navigation. *Nature*, 461(7266), 941–946.
2666 <https://doi.org/10.1038/nature08499>
- 2667 Hjorth-Simonsen, A., & Jeune, B. (1972). Origin and termination of the
2668 hippocampal perforant path in the rat studied by silver
2669 impregnation. *The Journal of Comparative Neurology*, 144(2),
2670 215–232. <https://doi.org/10.1002/cne.901440206>
- 2671 Itskov, P. M., Vinnik, E., & Diamond, M. E. (2011). Hippocampal
2672 representation of touch-guided behavior in rats: persistent and

- 2673 independent traces of stimulus and reward location. *PLoS One*,
2674 6(1), e16462. <https://doi.org/10.1371/journal.pone.0016462>
- 2675 Kaifosh, P., Lovett-Barron, M., Turi, G. F., Reardon, T. R., & Losonczy,
2676 A. (2013). Septo-hippocampal GABAergic signaling across
2677 multiple modalities in awake mice. *Nature Neuroscience*, 16(9),
2678 1182–1184. <https://doi.org/10.1038/nn.3482>
- 2679 Kamondi, A. (1998). *Theta Oscillations in Somata and Dendrites of*
2680 *Hippocampal Pyramidal Cells In Vivo: Activity-Dependent Phase-*
2681 *Precession of Action Potentials*. 261(March), 244–261.
- 2682 Kraus, B. J., Brandon, M. P., Robinson, R. J., Connerney, M. A.,
2683 Hasselmo, M. E., & Eichenbaum, H. (2015). During Running in
2684 Place, Grid Cells Integrate Elapsed Time and Distance Run.
2685 *Neuron*, 88(3), 578–589.
2686 <https://doi.org/10.1016/j.neuron.2015.09.031>
- 2687 Kraus, B., Robinson, R., White, J., Eichenbaum, H., & Hasselmo, M.
2688 (2013). Hippocampal “Time Cells”: Time versus Path Integration.
2689 *Neuron*, 78(6), 1090–1101.
2690 <https://doi.org/10.1016/j.neuron.2013.04.015>
- 2691 Lovett-Barron, M., Kaifosh, P., Kheirbek, M. A., Danielson, N.,
2692 Zaremba, J. D., Reardon, T. R., Turi, G. F., Hen, R., Zemelman,
2693 B. V., & Losonczy, A. (2014). Dendritic inhibition in the
2694 hippocampus supports fear learning. *Science (New York, N.Y.)*,
2695 343(6173), 857–863. <https://doi.org/10.1126/science.1247485>
- 2696 MacDonald, C. J., Carrow, S., Place, R., & Eichenbaum, H. (2013).
2697 Distinct hippocampal time cell sequences represent odor
2698 memories in immobilized rats. *The Journal of Neuroscience : The*
2699 *Official Journal of the Society for Neuroscience*, 33(36), 14607–
2700 14616. <https://doi.org/10.1523/JNEUROSCI.1537-13.2013>
- 2701 MacDonald, C. J., Lepage, K. Q., Eden, U. T., & Eichenbaum, H.
2702 (2011). Hippocampal “time cells” bridge the gap in memory for
2703 discontiguous events. *Neuron*, 71(4), 737–749.
2704 <https://doi.org/10.1016/j.neuron.2011.07.012>

- 2705 Mau, W., Sullivan, D. W., Kinsky, N. R., Hasselmo, M. E., Howard, M.
2706 W., & Eichenbaum, H. (2018). The Same Hippocampal CA1
2707 Population Simultaneously Codes Temporal Information over
2708 Multiple Timescales. *Current Biology*, 28(10), 1499-1508.e4.
2709 <https://doi.org/10.1016/j.cub.2018.03.051>
- 2710 McHugh, T. J., Jones, M. W., Quinn, J. J., Balthasar, N., Coppari, R.,
2711 Elmquist, J. K., Lowell, B. B., Fanselow, M. S., Wilson, M. A., &
2712 Tonegawa, S. (2007). Dentate gyrus NMDA receptors mediate
2713 rapid pattern separation in the hippocampal network. *Science*
2714 (*New York, N.Y.*), 317(5834), 94–99.
2715 <https://doi.org/10.1126/science.1140263>
- 2716 Min, E., Ban, S., Wang, Y., Bae, S. C., Popescu, G., Best-Popescu, C.,
2717 & Jung, W. (2017). Measurement of multispectral scattering
2718 properties in mouse brain tissue. *Biomedical Optics Express*, 8(3),
2719 1763–1770. <https://doi.org/10.1364/BOE.8.001763>
- 2720 Mizrahi, A. (2004). High-Resolution In Vivo Imaging of Hippocampal
2721 Dendrites and Spines. *Journal of Neuroscience*, 24(13), 3147–
2722 3151. <https://doi.org/10.1523/JNEUROSCI.5218-03.2004>
- 2723 Modi, M. N., Dhawale, A. K., & Bhalla, U. S. (2014). CA1 cell activity
2724 sequences emerge after reorganization of network correlation
2725 structure during associative learning. *eLife*, 3, e01982–e01982.
2726 <https://doi.org/10.7554/eLife.01982>
- 2727 Moser, M.-B., & Moser, E. I. (1998). Distributed encoding and retrieval
2728 of spatial memory in the hippocampus. In *The Journal of*
2729 *Neuroscience* (Vol. 18, pp. 7535–7542). Society for Neuroscience.
- 2730 Nakashiba, T., Young, J. Z., McHugh, T. J., Buhl, D. L., & Tonegawa,
2731 S. (2008). Transgenic inhibition of synaptic transmission reveals
2732 role of CA3 output in hippocampal learning. *Science* (*New York,*
2733 *N.Y.*), 319(5867), 1260–1264.
2734 <https://doi.org/10.1126/science.1151120>
- 2735 Pachitariu, M., Stringer, C., Dipoppa, M., Schröder, S., Rossi, L. F.,
2736 Dalgleish, H., Carandini, M., & Harris, K. D. (2017). Suite2p:

- 2737 beyond 10,000 neurons with standard two-photon microscopy.
2738 *BioRxiv*, 61507. <https://doi.org/10.1101/061507>
- 2739 Pastalkova, E., Itskov, V., Amarasingham, A., & Buzsaki, G. (2008).
2740 Internally Generated Cell Assembly Sequences in the Rat
2741 Hippocampus. *Science*, 321(5894), 1322–1327.
2742 <https://doi.org/10.1126/science.1159775>
- 2743 Peron, S. P., Freeman, J., Iyer, V., Guo, C., & Svoboda, K. (2015). A
2744 Cellular Resolution Map of Barrel Cortex Activity during Tactile
2745 Behavior. *Neuron*, 86(3), 783–799.
2746 <https://doi.org/10.1016/j.neuron.2015.03.027>
- 2747 Poort, J., Khan, A. G., Pachitariu, M., Nemri, A., Orsolic, I., Krupic, J.,
2748 Bauza, M., Sahani, M., Keller, G. B., Mrsic-Flogel, T. D., & Hofer,
2749 S. B. (2015). Learning Enhances Sensory and Multiple Non-
2750 sensory Representations in Primary Visual Cortex. *Neuron*, 86(6),
2751 1478–1490. <https://doi.org/10.1016/j.neuron.2015.05.037>
- 2752 Sheffield, M. E. J., & Dombeck, D. A. (2014). Calcium transient
2753 prevalence across the dendritic arbour predicts place field
2754 properties. *Nature*, 517(7533), 200–204.
2755 <https://doi.org/10.1038/nature13871>
- 2756 Siegel, J. J., Taylor, W., Gray, R., Kalmbach, B., Zemelman, B. V.,
2757 Desai, N. S., Johnston, D., & Chitwood, R. A. (2015). Trace
2758 Eyeblink Conditioning in Mice Is Dependent upon the Dorsal
2759 Medial Prefrontal Cortex, Cerebellum, and Amygdala: Behavioral
2760 Characterization and Functional Circuitry. *ENeuro*, 2(4),
2761 ENEURO.0051-14.2015. <https://doi.org/10.1523/ENEURO.0051-14.2015>
- 2763 Sofroniew, N. J., Flickinger, D., King, J., & Svoboda, K. (2016). A large
2764 field of view two-photon mesoscope with subcellular resolution for
2765 in vivo imaging. *eLife*, 5(JUN2016), 1–20.
2766 <https://doi.org/10.7554/eLife.14472>
- 2767 Stosiek, C., Garaschuk, O., Holthoff, K., & Konnerth, A. (2003). In vivo
2768 two-photon calcium imaging of neuronal networks. *Proceedings of
2769 the National Academy of Sciences of the United States of*

- 2770 *America*, 100(12), 7319–7324.
2771 <https://doi.org/10.1073/pnas.1232232100>
- 2772 Suh, J., Rivest, A. J., Nakashiba, T., Tominaga, T., & Tonegawa, S.
2773 (2011). Entorhinal cortex layer III input to the hippocampus is
2774 crucial for temporal association memory. *Science (New York,*
2775 *N.Y.*), 334(6061), 1415–1420.
2776 <https://doi.org/10.1126/science.1210125>
- 2777 Vinogradova, O. S. (2001). Hippocampus as comparator: Role of the
2778 two input and two output systems of the hippocampus in selection
2779 and registration of information. *Hippocampus*, 11(5), 578–598.
2780 <https://doi.org/https://doi.org/10.1002/hipo.1073>

2781 **Chapter 4 – Analysis**

2782

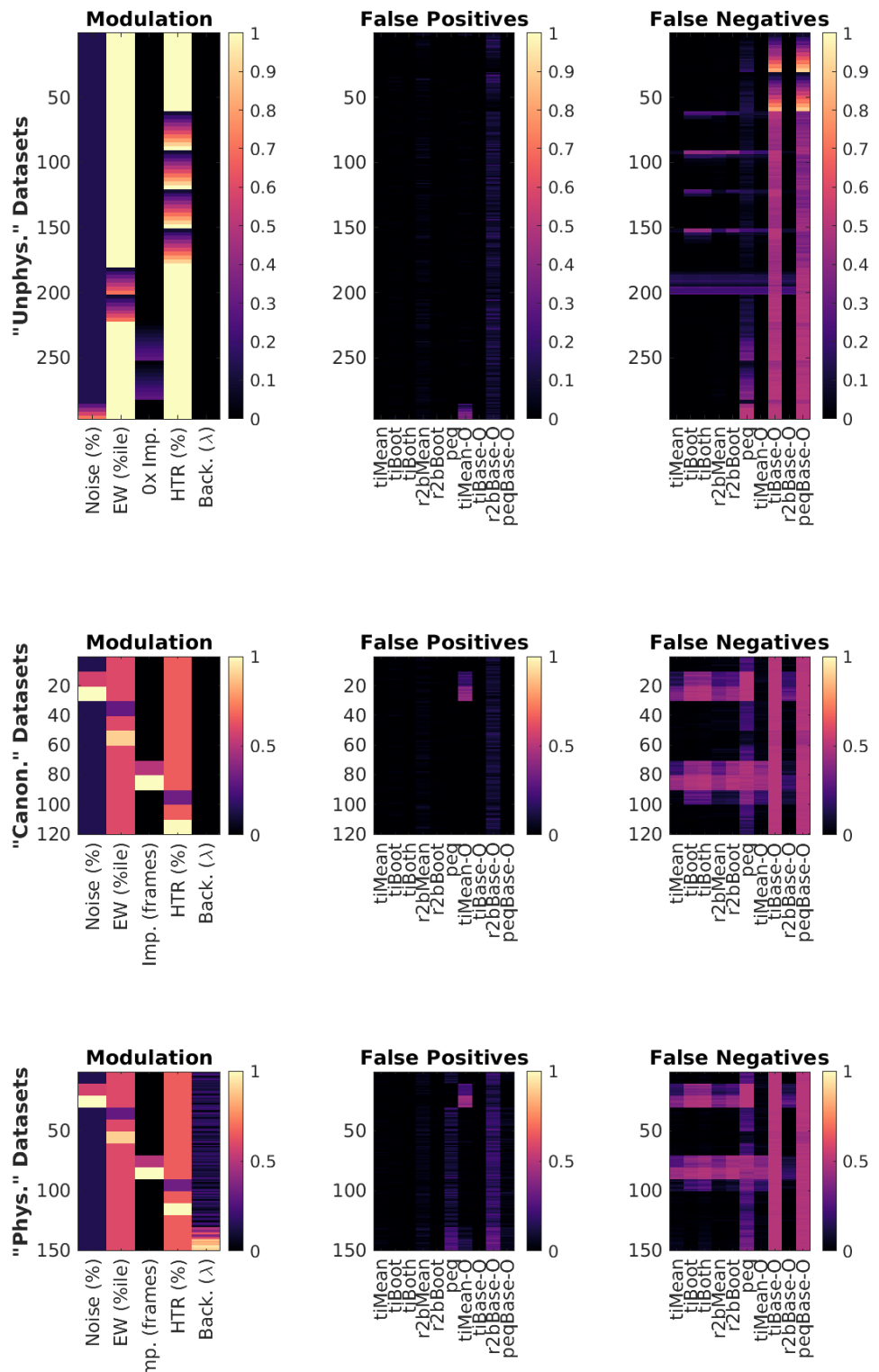
2783

2784 Our efforts to identify the best use cases for the various implemented
2785 time cell analysis algorithms on the basis of a testbed of user-defined,
2786 categorically labeled synthetic data with known ground truth (Project
2787 III), have been consolidated into a publication. The early access
2788 version of our paper (along with supplementary figures) has been
2789 attached.

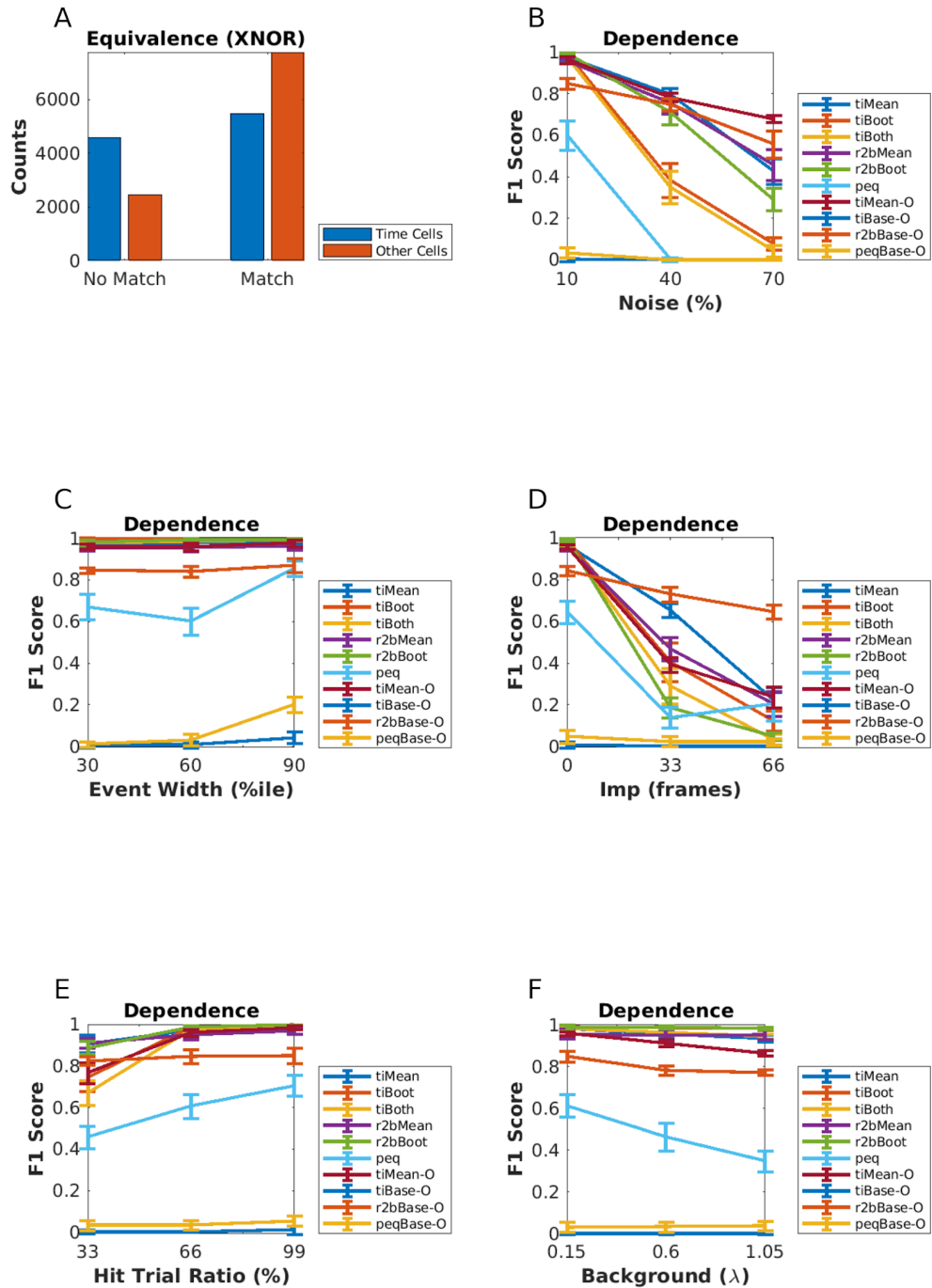
2790 **Extended Data Figures (Supplementary)**

2791

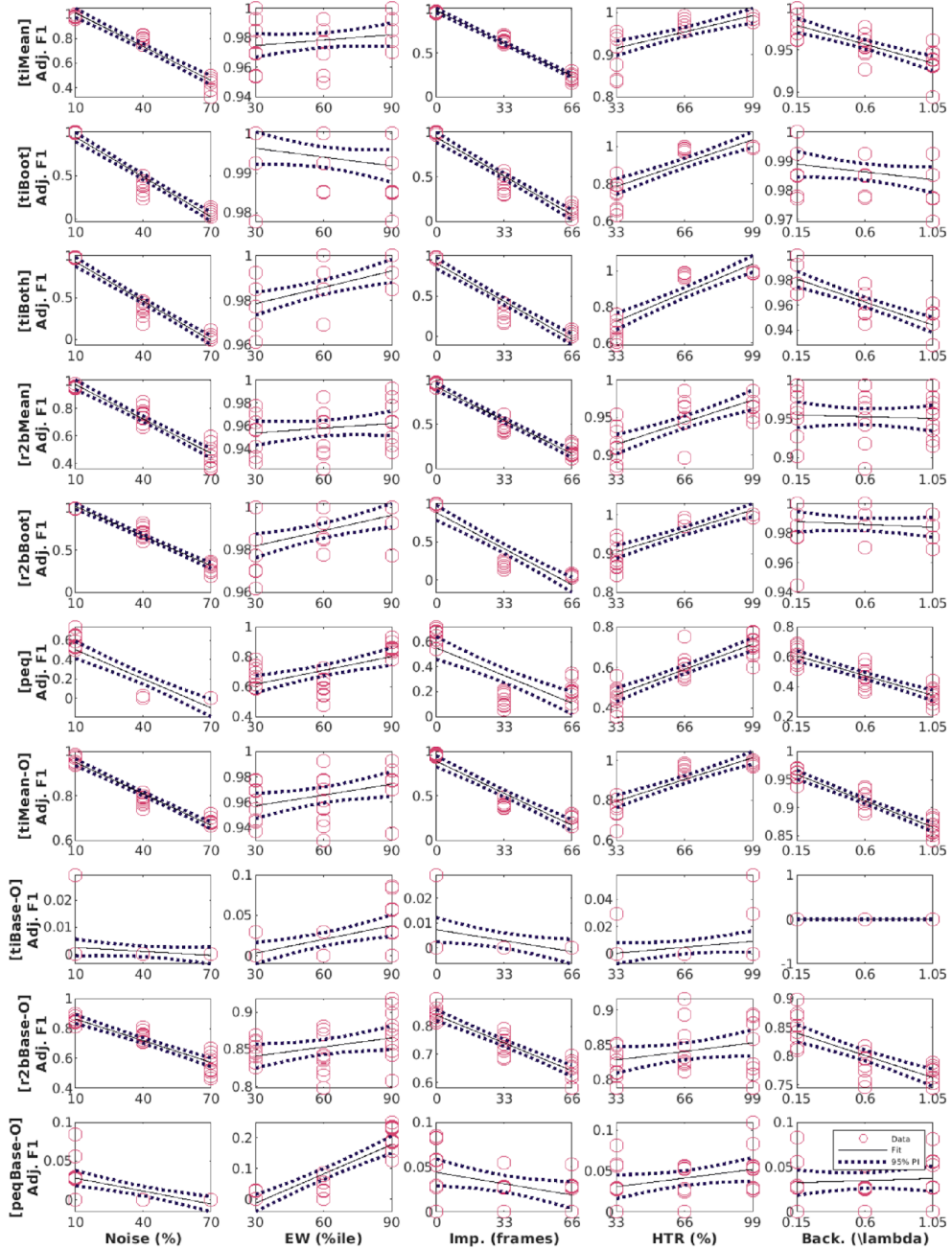
2792 **Figure 1-1.** Modulation profile along with the False Positive and False
2793 Negative rates per dataset, for important parameters configured in each of
2794 the 567 synthetic datasets generated. A-C: “Unphysiological Regime”, D-F:
2795 “Canonical Regime”, G-I: “Physiological Regime”.



2797 **Figure 6-1.** A: Equivalence by XNOR matching the prediction lists from the
2798 top six detection algorithms (Blue: Time Cells; Red: Other Cells). B-F:
2799 Dependence of the predictive performance (F1 Score) on the various
2800 important synthetic dataset configuration parameters, B: Noise (%), C: Event
2801 Width (%ile), D: Imprecision (frames), E: Hit Trial Ratio (%), and F:
2802 Background Activity (λ).



2804 Figure 6-2: Linear Regression fits for all algorithm parameter dependence
2805 curves with data points (red circles), best fit line (black), and the 95%
2806 prediction interval (PI; dotted black lines). The columns represent the
2807 physiology regime modulation parameter (out of the 5 main parameters
2808 tested), and the rows represent the various implemented algorithms for time
2809 cell detection.



2811 **Chapter 5 - Discussion**

2812 **The study of hippocampal CA1 sequences**

2813

2814 The standardized protocols described in the thesis are expected to aid
2815 in future experiments studying hippocampal CA1 sequences. Our
2816 simultaneous 2-photon calcium imaging recordings and behavioural
2817 training provided us the platform to study neural activity from ~100-150
2818 cells/animal at behaviourally relevant timescales (~70 ms per frame).

2819

2820 We standardized a multi-day Trace Eye-Blink Conditioning ("Chapter 2
2821 - Behaviour") training system for mice based on previous literature
2822 (Modi et al., 2014; Siegel et al., 2015) and could demonstrate several
2823 types of behavioural adaptations that experimental animals could learn
2824 under a variety of experiment conditions and modulations. Notably,

2825 1. The animals typically learnt the tasks quickly, within 1-2 weeks of
2826 training.

2827 2. Modulating the inter-stimulus interval (ISI) between the CS and
2828 US results affected the expression of the conditioned response (CR).

2829 3. A wide palette of stimuli may now be incorporated into existing
2830 protocols as either of the presented stimuli

2831

2832 Simultaneous large-scale recordings have been fundamental to the
2833 discovery of long spatiotemporal activity patterns with several
2834 participant CA1 neurons (Davidson et al., 2009; Foster, 2017).

2835 Electrical recordings provide many orders of magnitude better temporal
2836 resolution, not to mention being a direct readout of action potentials.

2837 However at the time of the design of the thesis, imaging based
2838 approaches could yield more recorded neurons per experiment animal.
2839 We standardized 2-photon fluorescence based chronic imaging of
2840 hippocampal CA1 neurons to allow calcium imaging based recording of
2841 the spatiotemporal sequences across multiple days ("Chapter 3 -
2842 Imaging"). This gave us the ability to
2843 1. Record neurophysiology over a large population of neurons
2844 (~100), in conjunction with temporally relevant behavioural contexts
2845 and modulations, albeit at ~100 ms temporal resolution.
2846 2. Chronically track cells across various behaviour sessions without
2847 ambiguity.
2848 3. Allow for scalability in the per animal yield of recording neurons with
2849 the use of faster and modern 2-photon microscope hardware utilizing
2850 Resonant Scanning instead of Galvo-Scanning, as well as multi-
2851 channel imaging.
2852
2853 We could identify time cells with the ability to retain, de-tune, or even
2854 re-tune, over the course of multiple sessions. Given no change in the
2855 behaviour protocol variables, it is unlikely we would have found such
2856 adaptations without scaling up the yield of cells or improving our
2857 temporal resolution while recording each individual session. Since the
2858 behaviour task is typically learnt to ~70-80% performance levels over
2859 the course of multiple sessions, our methodology gives us the ability to
2860 look into learning mechanisms utilized by the CA1 in the interim.
2861 Production quality datasets were quickly obtained by colleagues in the
2862 lab, following the protocols standardized and described here.
2863

2866 37), with subsequent sessions. Early in training, the timing of tuning
2867 peaks would typically occur near the time of the Unconditioned
2868 Stimulus (US; air-puff to eye). Our experiments presenting stimuli to
2869 naive animals (in accordance with Dhawale, 2013) suggested that
2870 somatosensory stimuli may be able to modulate CA1 responses, while
2871 many neutral stimuli may not (Chapter 3 – “Imaging”, Figure 29),
2872 without training. These results do allow for speculation on how initially
2873 neutral Conditioned Stimuli (CS; Light LED pulse) could develop
2874 behavioural valence for the animal, viz., the selective suppression of
2875 Response Inhibition to the previously neutral CS. An as yet unknown
2876 fraction of time cells may initially be triggered by the Unconditioned
2877 Stimulus (US; air-puff), but over the course of multiple training
2878 sessions, shift tuning fields to respond to the CS at the level of the CA1
2879 network. However, many more datasets would be required to firmly
2880 establish any mechanistic insight into the phenomenon.
2881

2882 **Mapping sequences to abstract
2883 variables**

2884
2885 Visual cues are typically considered important to place cell activity and
2886 tuning. The specific requirement of vision, however, was tested in a
2887 study published in 2015. Experimenters switched off the lights as their
2888 animals navigated a maze. The animals were provided only olfactory
2889 cues at specific locations in the maze, yet place cell activity and tuning
2890 could be recorded. This suggested that the hippocampus could use
2891 non-visuospatial resources to generate spatial representations, when
2892 vision was compromised (Zhang & Manahan-Vaughan, 2015).

2893
2894 In a sound manipulation task (SMT) rats changed the frequency of
2895 auditory tones in their environment, by self-initiated joystick control,
2896 ramping logarithmic sweeps of frequency space. The rate of change in
2897 frequency could be manipulated either by the animal or
2898 pseudorandomly by the experimenter. This study describes neural
2899 activity recorded from the medial entorhinal cortex (MEC) as well as
2900 the hippocampal CA1 with sub-populations that were found tuned to
2901 specific frequency “landmarks” during the auditory sequence (Aronov
2902 et al., 2017). The CA1 were, thus, argued to be capable of tuning to
2903 abstract variables and were designed to map out sequences of
2904 events/stimuli in their own spatiotemporal patterns of activity.
2905
2906 The ubiquity of neural sequences in a wide variety of systems has
2907 been discussed previously (Bhalla, 2019; Conen & Desrochers, 2022;
2908 S. Zhou et al., 2020) and over a century of research has discovered
2909 remarkable physiological features that may be used to identify neurons
2910 that participate in these sequences. However, research is still required
2911 to carefully dissect out the contribution that each participant neuron
2912 has to behaviour, an important goal in neuroscience (Ranck, 1973,
2913 1975).
2914
2915 The use of user-configurable, categorically labeled synthetic calcium
2916 activity profiles allowed us to probe and compare a range of different
2917 time cell detection algorithms, identifying strategies to best classify
2918 time cells. We were able to identify Temporal Information as a strong
2919 contender for the choice of algorithm for such classification (“Chapter 4
2920 - Analysis”; Ananthamurthy & Bhalla, 2023). The algorithms developed
2921 along the way were tested within the time scales of ~100 ms, that

2922 correspond to Replay Sequences or other behaviour timescale
2923 sequences. We expect the analysis routines to be useful in a variety of
2924 different experiments that could potentially help describe the neural
2925 code in more detail.

2926 **Does the brain create or predict?**

2927
2928 Predictive coding has been considered as a way for the brain to
2929 ultimately use external sensory information to minimize prediction
2930 errors during tasks (Doya et al., 2007; Rao & Ballard, 1999). One of
2931 the core ideas of Bayesian approaches to neurophysiology and
2932 behaviour is that the brain could be modeled as a prediction machine
2933 that is constantly modeling the change of variables. These variables
2934 may be external or internal yet salient concepts to any experimental
2935 animal, arguably expressed in neurophysiology as the dynamics of
2936 engrams. The ability of the mammalian hippocampus to bind both
2937 information streams to create new, more elaborate engrams, is likely
2938 crucial to the learning of new concepts behaviourally (N. J. Cohen &
2939 Eichenbaum, 1993; Eichenbaum, 2017).

2940
2941 Attentional states have been shown to have a bidirectional relationship
2942 with the expression of memory and learning (Chun & Johnson, 2011;
2943 Hutchinson & Turk-Browne, 2012; Uncapher et al., 2011). Specifically,
2944 Trace Eye-Blink Conditioning (TEC) performance has been suggested
2945 to be positively correlated with attention (Manns et al., 2000). The
2946 question of the effect of attentional states on the dynamics of the
2947 associated engram motivated an important milestone for the Thesis,

2948 *viz.*, to combine stable, adaptable behaviour studies with large-scale
2949 neurophysiology.
2950
2951 We were able to train head-fixed mice to TEC and confirm adaptable
2952 conditioned responses to task variables. We were also able to
2953 simultaneous record from ~100 hippocampal CA1 cell bodies as the
2954 animals acquired top behavioural performance. We observed in our
2955 preliminary results that many identified time cells showcased the ability
2956 to tune to different time points across sessions or days, as has been
2957 previously reported (Mau et al., 2018). This standardization of
2958 simultaneous behaviour and imaging ensured that colleagues from our
2959 lab were able to generate production quality data, quickly.
2960
2961 Several more high quality recordings and behaviour modulations would
2962 be required to conclusively describe time cells physiology and engram
2963 dynamics, at least at the level of a sub-population of hippocampal CA1.
2964 However, progress has been made to suggest the best time cell
2965 detection algorithm(s) based on their sensitivity to different recording
2966 parameters (Ananthamurthy & Bhalla, 2023). We hope that the Thesis
2967 is of aid to future research on the neural mechanisms of Learning and
2968 Memory by the nervous system.
2969

2970 **Bibliography**

2971 Ananthamurthy, K. G., & Bhalla, U. S. (2023). Synthetic Data Resource
2972 and Benchmarks for Time Cell Analysis and Detection Algorithms.
2973 *ENeuro*, ENEURO.0007-22.2023.
2974 <https://doi.org/10.1523/ENEURO.0007-22.2023>

- 2975 Aronov, D., Nevers, R., & Tank, D. W. (2017). Mapping of a non-spatial
2976 dimension by the hippocampal-entorhinal circuit. *Nature*,
2977 543(7647), 719–722. <https://doi.org/10.1038/nature21692>
- 2978 Bhalla, U. S. (2019). Dendrites, deep learning, and sequences in the
2979 hippocampus. *Hippocampus*, 29(3), 239–251.
2980 <https://doi.org/https://doi.org/10.1002/hipo.22806>
- 2981 Chun, M. M., & Johnson, M. K. (2011). Memory: enduring traces of
2982 perceptual and reflective attention. *Neuron*, 72(4), 520–535.
2983 <https://doi.org/10.1016/j.neuron.2011.10.026>
- 2984 Cohen, N. J., & Eichenbaum, H. (1993). *Memory, amnesia, and the*
2985 *hippocampal system*.
- 2986 Conen, K. E., & Desrochers, T. M. (2022). *The Neural Basis of*
2987 *Behavioral Sequences in Cortical and Subcortical Circuits*. Oxford
2988 University Press.
2989 <https://doi.org/10.1093/acrefore/9780190264086.013.421>
- 2990 Davidson, T. J., Kloosterman, F., & Wilson, M. A. (2009). Hippocampal
2991 replay of extended experience. *Neuron*, 63(4), 497–507.
2992 <https://doi.org/10.1016/j.neuron.2009.07.027>
- 2993 Dhawale, A. K. (2013). *Temporal and spatial features of sensory*
2994 *coding in the olfactory bulb and hippocampus*. Tata Institute of
2995 Fundamental Research.
- 2996 Doya, K., Ishii, S., Pouget, A., & Rao, R. P. N. (2007). Bayesian brain:
2997 Probabilistic approaches to neural coding. In K. Doya, S. Ishii, A.
2998 Pouget, & R. P. N. Rao (Eds.), *Bayesian brain: Probabilistic*
2999 *approaches to neural coding*. MIT Press.
- 3000 Eichenbaum, H. (2017). On the Integration of Space, Time, and
3001 Memory. *Neuron*, 95(5), 1007–1018.
3002 <https://doi.org/10.1016/j.neuron.2017.06.036>
- 3003 Foster, D. J. (2017). Replay Comes of Age. *Annual Review of*
3004 *Neuroscience*, 40, 581–602. <https://doi.org/10.1146/annurev-neuro-072116-031538>

- 3006 Hutchinson, J. B., & Turk-Browne, N. B. (2012). Memory-guided
3007 attention: control from multiple memory systems. *Trends in*
3008 *Cognitive Sciences*, 16(12), 576–579.
3009 <https://doi.org/10.1016/j.tics.2012.10.003>
- 3010 Manns, J. R., Clark, R. E., & Squire, L. R. (2000). Parallel acquisition
3011 of awareness and trace eyeblink classical conditioning. *Learning*
3012 & *Memory (Cold Spring Harbor, N.Y.)*, 7(5), 267–272.
3013 <https://doi.org/10.1101/lm.33400>
- 3014 Mau, W., Sullivan, D. W., Kinsky, N. R., Hasselmo, M. E., Howard, M.
3015 W., & Eichenbaum, H. (2018). The Same Hippocampal CA1
3016 Population Simultaneously Codes Temporal Information over
3017 Multiple Timescales. *Current Biology*, 28(10), 1499-1508.e4.
3018 <https://doi.org/10.1016/j.cub.2018.03.051>
- 3019 Modi, M. N., Dhawale, A. K., & Bhalla, U. S. (2014). CA1 cell activity
3020 sequences emerge after reorganization of network correlation
3021 structure during associative learning. *eLife*, 3, e01982–e01982.
3022 <https://doi.org/10.7554/eLife.01982>
- 3023 Ranck, J. B. (1973). Studies on single neurons in dorsal hippocampal
3024 formation and septum in unrestrained rats: Part I. Behavioral
3025 correlates and firing repertoires. *Experimental Neurology*, 41(2),
3026 462–531. [https://doi.org/https://doi.org/10.1016/0014-4886\(73\)90290-2](https://doi.org/https://doi.org/10.1016/0014-4886(73)90290-2)
- 3027
- 3028 Ranck, J. B. (1975). *Behavioral Correlates and Firing Repertoires of
3029 Neurons in the Dorsal Hippocampal Formation and Septum of
3030 Unrestrained Rats BT - The Hippocampus: Volume 2:
3031 Neurophysiology and Behavior* (R. L. Isaacson & K. H. Pribram
3032 (Eds.); pp. 207–244). Springer US. https://doi.org/10.1007/978-1-4684-2979-4_7
- 3033
- 3034 Rao, R. P. N., & Ballard, D. H. (1999). Predictive coding in the visual
3035 cortex: a functional interpretation of some extra-classical
3036 receptive-field effects. *Nature Neuroscience*, 2(1), 79–87.
3037 <https://doi.org/10.1038/4580>

- 3038 Siegel, J. J., Taylor, W., Gray, R., Kalmbach, B., Zemelman, B. V.,
3039 Desai, N. S., Johnston, D., & Chitwood, R. A. (2015). Trace
3040 Eyeblink Conditioning in Mice Is Dependent upon the Dorsal
3041 Medial Prefrontal Cortex, Cerebellum, and Amygdala: Behavioral
3042 Characterization and Functional Circuitry. *ENeuro*, 2(4),
3043 ENEURO.0051-14.2015. <https://doi.org/10.1523/ENEURO.0051-14.2015>
- 3045 Uncapher, M. R., Hutchinson, J. B., & Wagner, A. D. (2011).
3046 Dissociable effects of top-down and bottom-up attention during
3047 episodic encoding. *The Journal of Neuroscience : The Official
3048 Journal of the Society for Neuroscience*, 31(35), 12613–12628.
3049 <https://doi.org/10.1523/JNEUROSCI.0152-11.2011>
- 3050 Zhang, S., & Manahan-Vaughan, D. (2015). Spatial olfactory learning
3051 contributes to place field formation in the hippocampus. *Cerebral
3052 Cortex (New York, N.Y. : 1991)*, 25(2), 423–432.
3053 <https://doi.org/10.1093/cercor/bht239>
- 3054 Zhou, S., Masmanidis, S. C., & Buonomano, D. V. (2020). Neural
3055 Sequences as an Optimal Dynamical Regime for the Readout of
3056 Time. *Neuron*, 108(4), 651-658.e5.
3057 <https://doi.org/https://doi.org/10.1016/j.neuron.2020.08.020>

3058 All Bibliography

- 3059
- 3060 Abe, R., Sakaguchi, T., Matsumoto, N., Matsuki, N., & Ikegaya, Y.
3061 (2014). Sound-induced hyperpolarization of hippocampal neurons.
3062 *Neuroreport*, 25(13), 1013–1017.
3063 <https://doi.org/10.1097/WNR.0000000000000206>
- 3064 Abeles, M. (1982). *Local Cortical Circuits: An Electrophysiological Study*. Springer-Verlag. <https://books.google.co.in/books?id=s25lwwEACAAJ>
- 3065
- 3066
- 3067 Abeles, M. (1991). *Corticonics: Neural Circuits of the Cerebral Cortex*.
3068 Cambridge University Press. <https://doi.org/DOI:10.1017/CBO9780511574566>
- 3069
- 3070 Abeles, M. (2004). Time Is Precious. *Science*, 304(5670), 523–524.
3071 <https://doi.org/10.1126/science.1097725>
- 3072 Abeles, M. (2009). *Synfire Chains* (L. R. B. T.-E. of N. Squire (Ed.); pp.
3073 829–832). Academic Press.
3074 <https://doi.org/https://doi.org/10.1016/B978-008045046-9.01437-6>
- 3075 Abeles, M., Hayon, G., & Lehmann, D. (2004). Modeling
3076 compositionality by dynamic binding of synfire chains. *Journal of
3077 Computational Neuroscience*, 17(2), 179–201.
3078 <https://doi.org/10.1023/B:JCNS.0000037682.18051.5f>
- 3079 Ananthamurthy, K. G., & Bhalla, U. S. (2023). Synthetic Data Resource
3080 and Benchmarks for Time Cell Analysis and Detection Algorithms.
3081 *ENeuro*, ENEURO.0007-22.2023.
3082 <https://doi.org/10.1523/ENEURO.0007-22.2023>
- 3083 Andermann, M. L., Gilfoy, N. B., Goldey, G. J., Sachdev, R. N. S.,
3084 Wölfel, M., McCormick, D. A., Reid, R. C., & Levene, M. J. (2013).
3085 Chronic Cellular Imaging of Entire Cortical Columns in Awake
3086 Mice Using Microprisms. *Neuron*, 80(4), 900–913.
3087 <https://doi.org/10.1016/j.neuron.2013.07.052>

- 3088 Andersen, P., Morris, R., Amaral, D., Bliss, T., & O'Keefe, J. (Eds.).
3089 (2006). *The Hippocampus Book*. Oxford University Press.
3090 <https://doi.org/10.1093/acprof:oso/9780195100273.001.0001>
- 3091 Andersen, R. A., Snyder, L. H., Li, C.-S., & Stricanne, B. (1993).
3092 Coordinate transformations in the representation of spatial
3093 information. *Current Opinion in Neurobiology*, 3(2), 171–176.
3094 [https://doi.org/https://doi.org/10.1016/0959-4388\(93\)90206-E](https://doi.org/https://doi.org/10.1016/0959-4388(93)90206-E)
- 3095 Aronov, D., Nevers, R., & Tank, D. W. (2017). Mapping of a non-spatial
3096 dimension by the hippocampal-entorhinal circuit. *Nature*,
3097 543(7647), 719–722. <https://doi.org/10.1038/nature21692>
- 3098 Attardo, A., Fitzgerald, J. E., & Schnitzer, M. J. (2015). Impermanence
3099 of dendritic spines in live adult CA1 hippocampus. *Nature*,
3100 523(7562), 592–596. <https://doi.org/10.1038/nature14467>
- 3101 Barreto, R. P. J., Messerschmidt, B., & Schnitzer, M. J. (2009). In vivo
3102 fluorescence imaging with high-resolution microlenses. *Nature
Methods*, 6(7), 511–512. <https://doi.org/10.1038/nmeth.1339>
- 3104 Barreto, R. P. J., & Schnitzer, M. J. (2012). In vivo optical
3105 microendoscopy for imaging cells lying deep within live tissue.
3106 *Cold Spring Harbor Protocols*, 2012(10), 1029–1034.
3107 <https://doi.org/10.1101/pdb.top071464>
- 3108 Bellistri, E., Aguilar, J., Brotons-Mas, J. R., Foffani, G., & de la Prida, L.
3109 M. (2013). Basic properties of somatosensory-evoked responses
3110 in the dorsal hippocampus of the rat. *The Journal of Physiology*,
3111 591(10), 2667–2686. <https://doi.org/10.1113/jphysiol.2013.251892>
- 3112 Bhalla, U. S. (2019). Dendrites, deep learning, and sequences in the
3113 hippocampus. *Hippocampus*, 29(3), 239–251.
3114 <https://doi.org/https://doi.org/10.1002/hipo.22806>
- 3115 Bienenstock, E. (1995). A model of neocortex. *Network: Computation
3116 in Neural Systems*, 6(2), 179–224. https://doi.org/10.1088/0954-898X_6_2_004

- 3118 Bjerknes, T. L., Moser, E. I., & Moser, M.-B. (2014). Representation of
3119 Geometric Borders in the Developing Rat. *Neuron*, 82(1), 71–78.
3120 <https://doi.org/10.1016/j.neuron.2014.02.014>
- 3121 Brown, G. D. (1998). Nonassociative learning processes affecting
3122 swimming probability in the seashell Tritonia diomedea:
3123 habituation, sensitization and inhibition. *Behavioural Brain
3124 Research*, 95(2), 151–165.
3125 [https://doi.org/https://doi.org/10.1016/S0166-4328\(98\)00072-2](https://doi.org/https://doi.org/10.1016/S0166-4328(98)00072-2)
- 3126 Buzsáki, G., & Llinás, R. (2017). Space and time in the brain. *Science
3127 (New York, N.Y.)*, 358(6362), 482–485.
3128 <https://doi.org/10.1126/science.aan8869>
- 3129 Cai, D. J., Aharoni, D., Shuman, T., Shobe, J., Biane, J., Song, W.,
3130 Wei, B., Veshkini, M., La-Vu, M., Lou, J., Flores, S. E., Kim, I.,
3131 Sano, Y., Zhou, M., Baumgaertel, K., Lavi, A., Kamata, M.,
3132 Tuszyński, M., Mayford, M., ... Silva, A. J. (2016). A shared neural
3133 ensemble links distinct contextual memories encoded close in
3134 time. *Nature*, 534(7605), 115–118.
3135 <https://doi.org/10.1038/nature17955>
- 3136 Caporale, N., & Dan, Y. (2008). Spike timing-dependent plasticity: a
3137 Hebbian learning rule. *Annual Review of Neuroscience*, 31, 25–
3138 46. <https://doi.org/10.1146/annurev.neuro.31.060407.125639>
- 3139 Carew, T. J., Castellucci, V. F., & Kandel, E. R. (1971). An Analysis of
3140 Dishabituation and Sensitization of The Gill-Withdrawal Reflex In
3141 Aplysia. *International Journal of Neuroscience*, 2(2), 79–98.
3142 <https://doi.org/10.3109/00207457109146995>
- 3143 Chen, T.-W., Wardill, T. J., Sun, Y., Pulver, S. R., Renninger, S. L.,
3144 Baohan, A., Schreiter, E. R., Kerr, R. A., Orger, M. B., Jayaraman,
3145 V., Looger, L. L., Svoboda, K., & Kim, D. S. (2013). Ultrasensitive
3146 fluorescent proteins for imaging neuronal activity. *Nature*,
3147 499(7458), 295–300. <https://doi.org/10.1038/nature12354>
- 3148 Chun, M. M., & Johnson, M. K. (2011). Memory: enduring traces of
3149 perceptual and reflective attention. *Neuron*, 72(4), 520–535.
3150 <https://doi.org/10.1016/j.neuron.2011.10.026>

- 3151 Cohen, M. R., & Kohn, A. (2011). Measuring and interpreting neuronal
3152 correlations. *Nature Neuroscience*, 14(7), 811–819.
3153 <https://doi.org/10.1038/nn.2842>
- 3154 Cohen, N. J., & Eichenbaum, H. (1993). *Memory, amnesia, and the*
3155 *hippocampal system.*
- 3156 Conen, K. E., & Desrochers, T. M. (2022). *The Neural Basis of*
3157 *Behavioral Sequences in Cortical and Subcortical Circuits*. Oxford
3158 University Press.
3159 <https://doi.org/10.1093/acrefore/9780190264086.013.421>
- 3160 Csicsvari, J., O'Neill, J., Allen, K., & Senior, T. (2007). Place-selective
3161 firing contributes to the reverse-order reactivation of CA1
3162 pyramidal cells during sharp waves in open-field exploration. *The*
3163 *European Journal of Neuroscience*, 26(3), 704–716.
3164 <https://doi.org/10.1111/j.1460-9568.2007.05684.x>
- 3165 Davidson, T. J., Kloosterman, F., & Wilson, M. A. (2009). Hippocampal
3166 replay of extended experience. *Neuron*, 63(4), 497–507.
3167 <https://doi.org/10.1016/j.neuron.2009.07.027>
- 3168 Denk, W., Strickler, J. H., & Webb, W. W. (1990). Two-photon laser
3169 scanning fluorescence microscopy. *Science (New York, N.Y.)*,
3170 248(4951), 73–76. <https://doi.org/10.1126/science.2321027>
- 3171 Deshmukh, S. S., & Bhalla, U. S. (2003). Representation of odor
3172 habituation and timing in the hippocampus. *The Journal of*
3173 *Neuroscience : The Official Journal of the Society for*
3174 *Neuroscience*, 23(5), 1903–1915.
3175 <https://doi.org/10.1523/JNEUROSCI.23-05-01903.2003>
- 3176 Dhawale, A. K. (2013). *Temporal and spatial features of sensory*
3177 *coding in the olfactory bulb and hippocampus*. Tata Institute of
3178 Fundamental Research.
- 3179 Dhawale, A. K., Poddar, R., Wolff, S. B. E., Normand, V. A.,
3180 Kopelowitz, E., & Ölveczky, B. P. (2017). Automated long-term
3181 recording and analysis of neural activity in behaving animals.
3182 *eLife*, 6, e27702. <https://doi.org/10.7554/eLife.27702>

- 3183 Diba, K., & Buzsáki, G. (2007). Forward and reverse hippocampal
3184 place-cell sequences during ripples. *Nature Neuroscience*, 10(10),
3185 1241–1242. <https://doi.org/10.1038/nn1961>
- 3186 Dickinson, A., Nicholas, D. J., & Mackintosh, N. J. (1983). A re-
3187 examination of one-trial blocking in conditioned suppression. *The
3188 Quarterly Journal of Experimental Psychology B: Comparative
3189 and Physiological Psychology*, 35, 67–79.
3190 <https://doi.org/10.1080/14640748308400914>
- 3191 Dombeck, D. A., Graziano, M. S., & Tank, D. W. (2009). Functional
3192 clustering of neurons in motor cortex determined by cellular
3193 resolution imaging in awake behaving mice. *The Journal of
3194 Neuroscience : The Official Journal of the Society for
3195 Neuroscience*, 29(44), 13751–13760.
3196 <https://doi.org/10.1523/JNEUROSCI.2985-09.2009>
- 3197 Dombeck, D. A., Harvey, C. D., Tian, L., Looger, L. L., & Tank, D. W.
3198 (2010). Functional imaging of hippocampal place cells at cellular
3199 resolution during virtual navigation. *Nature Neuroscience*, 13(11),
3200 1433–1440. <https://doi.org/10.1038/nn.2648>
- 3201 Doya, K., Ishii, S., Pouget, A., & Rao, R. P. N. (2007). Bayesian brain:
3202 Probabilistic approaches to neural coding. In K. Doya, S. Ishii, A.
3203 Pouget, & R. P. N. Rao (Eds.), *Bayesian brain: Probabilistic
3204 approaches to neural coding*. MIT Press.
- 3205 Dragoi, G., & Buzsáki, G. (2006). Temporal encoding of place
3206 sequences by hippocampal cell assemblies. *Neuron*, 50(1), 145–
3207 157. <https://doi.org/10.1016/j.neuron.2006.02.023>
- 3208 Dragoi, G., Carpi, D., Recce, M., Csicsvari, J., & Buzsáki, G. (1999).
3209 Interactions between hippocampus and medial septum during
3210 sharp waves and theta oscillation in the behaving rat. *The Journal
3211 of Neuroscience : The Official Journal of the Society for
3212 Neuroscience*, 19(14), 6191–6199.
3213 <http://www.ncbi.nlm.nih.gov/pubmed/10407055>

- 3214 Dragoi, G., & Tonegawa, S. (2011). Preplay of future place cell
3215 sequences by hippocampal cellular assemblies. *Nature*,
3216 469(7330), 397–401. <https://doi.org/10.1038/nature09633>
- 3217 Dragoi, G., & Tonegawa, S. (2013). Distinct preplay of multiple novel
3218 spatial experiences in the rat. *Proceedings of the National
3219 Academy of Sciences of the United States of America*, 110(22),
3220 9100–9105. <https://doi.org/10.1073/pnas.1306031110>
- 3221 Eichenbaum, H. (2004). Hippocampus: Cognitive processes and
3222 neural representations that underlie declarative memory. *Neuron*,
3223 44(1), 109–120. <https://doi.org/10.1016/j.neuron.2004.08.028>
- 3224 Eichenbaum, H. (2017). On the Integration of Space, Time, and
3225 Memory. *Neuron*, 95(5), 1007–1018.
3226 <https://doi.org/10.1016/j.neuron.2017.06.036>
- 3227 Fanselow, M. S., & Dong, H.-W. (2010). Are the dorsal and ventral
3228 hippocampus functionally distinct structures? *Neuron*, 65(1), 7–19.
3229 <https://doi.org/10.1016/j.neuron.2009.11.031>
- 3230 Fassihi, A., Akrami, A., Pulecchi, F., Schönfelder, V., & Diamond, M. E.
3231 (2017). Transformation of Perception from Sensory to Motor
3232 Cortex. *Current Biology : CB*, 27(11), 1585-1596.e6.
3233 <https://doi.org/10.1016/j.cub.2017.05.011>
- 3234 Ferbinteanu, J., & Shapiro, M. L. (2003). Prospective and retrospective
3235 memory coding in the hippocampus. *Neuron*, 40(6), 1227–1239.
3236 [https://doi.org/10.1016/s0896-6273\(03\)00752-9](https://doi.org/10.1016/s0896-6273(03)00752-9)
- 3237 Ferbinteanu, J., Shirvalkar, P., & Shapiro, M. L. (2011). Memory
3238 Modulates Journey-Dependent Coding in the Rat Hippocampus.
3239 *The Journal of Neuroscience*, 31(25), 9135 LP – 9146.
3240 <https://doi.org/10.1523/JNEUROSCI.1241-11.2011>
- 3241 Foster, D. J. (2017). Replay Comes of Age. *Annual Review of
3242 Neuroscience*, 40, 581–602. <https://doi.org/10.1146/annurev-neuro-072116-031538>

- 3244 Foster, D. J., & Wilson, M. A. (2006). Reverse replay of behavioural
3245 sequences in hippocampal place cells during the awake state.
3246 *Nature*, 440(7084), 680–683. <https://doi.org/10.1038/nature04587>
- 3247 Foster, D. J., & Wilson, M. A. (2007). Hippocampal theta sequences.
3248 *Hippocampus*, 17(11), 1093–1099.
3249 <https://doi.org/10.1002/hipo.20345>
- 3250 Francis, M., Qian, X., Charbel, C., Ledoux, J., Parker, J. C., & Taylor,
3251 M. S. (2012). Automated region of interest analysis of dynamic
3252 Ca²⁺ signals in image sequences. *American Journal of*
3253 *Physiology. Cell Physiology*, 303(3), C236-43.
3254 <https://doi.org/10.1152/ajpcell.00016.2012>
- 3255 Frank, L. M., Brown, E. N., & Wilson, M. (2000). Trajectory encoding in
3256 the hippocampus and entorhinal cortex. *Neuron*, 27(1), 169–178.
3257 [https://doi.org/10.1016/s0896-6273\(00\)00018-0](https://doi.org/10.1016/s0896-6273(00)00018-0)
- 3258 Fyhn, M., Molden, S., Witter, M. P., Moser, E. I., & Moser, M.-B.
3259 (2004). Spatial representation in the entorhinal cortex. *Science*
3260 (*New York, N.Y.*), 305(5688), 1258–1264.
3261 <https://doi.org/10.1126/science.1099901>
- 3262 Giovannucci, A., Badura, A., Deverett, B., Najafi, F., Pereira, T. D.,
3263 Gao, Z., Ozden, I., Kloth, A. D., Pnevmatikakis, E., Paninski, L.,
3264 De Zeeuw, C. I., Medina, J. F., & Wang, S. S.-H. (2017).
3265 Cerebellar granule cells acquire a widespread predictive feedback
3266 signal during motor learning. *Nature Neuroscience*, 20(5), 727–
3267 734. <https://doi.org/10.1038/nn.4531>
- 3268 Grün, S. (2009). Data-Driven Significance Estimation for Precise Spike
3269 Correlation. *Journal of Neurophysiology*, 101(3), 1126–1140.
3270 <https://doi.org/10.1152/jn.00093.2008>
- 3271 Guo, Z. V., Hires, S. A., Li, N., O'Connor, D. H., Komiyama, T., Ophir,
3272 E., Huber, D., Bonardi, C., Morandell, K., Gutnisky, D., Peron, S.,
3273 Xu, N., Cox, J., & Svoboda, K. (2014). Procedures for Behavioral
3274 Experiments in Head-Fixed Mice. *PLOS ONE*, 9(2), e88678.
3275 <https://doi.org/10.1371/journal.pone.0088678>

- 3276 Gupta, A. S., van der Meer, M. A. A., Touretzky, D. S., & Redish, A. D.
3277 (2010). Hippocampal Replay Is Not a Simple Function of
3278 Experience. *Neuron*, 65(5), 695–705.
3279 <https://doi.org/https://doi.org/10.1016/j.neuron.2010.01.034>
- 3280 Hafting, T., Fyhn, M., Molden, S., Moser, M.-B., & Moser, E. I. (2005).
3281 Microstructure of a spatial map in the entorhinal cortex. *Nature*,
3282 436(7052), 801–806. <https://doi.org/10.1038/nature03721>
- 3283 Han, J.-H., Kushner, S. A., Yiu, A. P., Hsiang, H.-L. L., Buch, T.,
3284 Waisman, A., Bontempi, B., Neve, R. L., Frankland, P. W., &
3285 Josselyn, S. A. (2009). Selective erasure of a fear memory.
3286 *Science (New York, N.Y.)*, 323(5920), 1492–1496.
3287 <https://doi.org/10.1126/science.1164139>
- 3288 Harvey, C. D., Collman, F., Dombeck, D. A., & Tank, D. W. (2009).
3289 Intracellular dynamics of hippocampal place cells during virtual
3290 navigation. *Nature*, 461(7266), 941–946.
3291 <https://doi.org/10.1038/nature08499>
- 3292 Hebb, D. O. (1949). The organization of behavior; a
3293 neuropsychological theory. In *The organization of behavior; a*
3294 *neuropsychological theory*. Wiley.
- 3295 Helmchen, F., & Denk, W. (2005). *Deep tissue two-photon microscopy*.
3296 2(12), 9. <https://doi.org/10.1038/nmeth818>
- 3297 Heys, J. G., Rangarajan, K. V., & Dombeck, D. A. (2014). The
3298 Functional Micro-organization of Grid Cells Revealed by Cellular-
3299 Resolution Imaging. *Neuron*, 84(5), 1079–1090.
3300 <https://doi.org/10.1016/j.neuron.2014.10.048>
- 3301 Hjorth-Simonsen, A., & Jeune, B. (1972). Origin and termination of the
3302 hippocampal perforant path in the rat studied by silver
3303 impregnation. *The Journal of Comparative Neurology*, 144(2),
3304 215–232. <https://doi.org/10.1002/cne.901440206>
- 3305 Hubel, D. H., & Wiesel, T. N. (1962). Receptive fields, binocular
3306 interaction and functional architecture in the cat's visual cortex.
3307 *The Journal of Physiology*, 160(1), 106–154.
3308 <https://doi.org/10.1113/jphysiol.1962.sp006837>

- 3309 Hutchinson, J. B., & Turk-Browne, N. B. (2012). Memory-guided
3310 attention: control from multiple memory systems. *Trends in*
3311 *Cognitive Sciences*, 16(12), 576–579.
3312 <https://doi.org/10.1016/j.tics.2012.10.003>
- 3313 Ikegaya, Y., Aaron, G., Cossart, R., Aronov, D., Lampl, I., Ferster, D.,
3314 & Yuste, R. (2004). Synfire chains and cortical songs: temporal
3315 modules of cortical activity. *Science (New York, N.Y.)*, 304(5670),
3316 559–564. <https://doi.org/10.1126/science.1093173>
- 3317 Itskov, P. M., Vinnik, E., & Diamond, M. E. (2011). Hippocampal
3318 representation of touch-guided behavior in rats: persistent and
3319 independent traces of stimulus and reward location. *PloS One*,
3320 6(1), e16462. <https://doi.org/10.1371/journal.pone.0016462>
- 3321 Itskov, V., Pastalkova, E., Mizuseki, K., Buzsaki, G., & Harris, K. D.
3322 (2008). Theta-mediated dynamics of spatial information in
3323 hippocampus. *The Journal of Neuroscience : The Official Journal*
3324 *of the Society for Neuroscience*, 28(23), 5959–5964.
3325 <https://doi.org/10.1523/JNEUROSCI.5262-07.2008>
- 3326 Jadhav, S. P., Kemere, C., German, P. W., & Frank, L. M. (2012).
3327 Awake hippocampal sharp-wave ripples support spatial memory.
3328 *Science (New York, N.Y.)*, 336(6087), 1454–1458.
3329 <https://doi.org/10.1126/science.1217230>
- 3330 Jaramillo, S., & Zador, A. M. (2014). Mice and rats achieve similar
3331 levels of performance in an adaptive decision-making task . In
3332 *Frontiers in Systems Neuroscience* (Vol. 8).
3333 <https://www.frontiersin.org/articles/10.3389/fnsys.2014.00173>
- 3334 Josselyn, S. A., & Tonegawa, S. (2020). Memory engrams: Recalling
3335 the past and imagining the future. *Science (New York, N.Y.)*,
3336 367(6473). <https://doi.org/10.1126/science.aaw4325>
- 3337 Jun, J. J., Steinmetz, N. A., Siegle, J. H., Denman, D. J., Bauza, M.,
3338 Barbarits, B., Lee, A. K., Anastassiou, C. A., Andrei, A., Aydin, Ç.,
3339 Barbic, M., Blanche, T. J., Bonin, V., Couto, J., Dutta, B., Gratiy,
3340 S. L., Gutnisky, D. A., Häusser, M., Karsh, B., ... Harris, T. D.
3341 (2017). Fully integrated silicon probes for high-density recording of

- 3342 neural activity. *Nature*, 551(7679), 232–236.
3343 <https://doi.org/10.1038/nature24636>
- 3344 Kaifosh, P., Lovett-Barron, M., Turi, G. F., Reardon, T. R., & Losonczy,
3345 A. (2013). Septo-hippocampal GABAergic signaling across
3346 multiple modalities in awake mice. *Nature Neuroscience*, 16(9),
3347 1182–1184. <https://doi.org/10.1038/nn.3482>
- 3348 Kalmbach, B. E., Davis, T., Ohyama, T., Riusech, F., Nores, W. L., &
3349 Mauk, M. D. (2010). Cerebellar Cortex Contributions to the
3350 Expression and Timing of Conditioned Eyelid Responses. *Journal*
3351 *of Neurophysiology*, 103(4), 2039–2049.
3352 <https://doi.org/10.1152/jn.00033.2010>
- 3353 Kalmbach, B. E., Ohyama, T., & Mauk, M. D. (2010). Temporal
3354 Patterns of Inputs to Cerebellum Necessary and Sufficient for
3355 Trace Eyelid Conditioning. *Journal of Neurophysiology*, 104(2),
3356 627–640. <https://doi.org/10.1152/jn.00169.2010>
- 3357 Kamondi, A. (1998). *Theta Oscillations in Somata and Dendrites of*
3358 *Hippocampal Pyramidal Cells In Vivo: Activity-Dependent Phase-*
3359 *Precession of Action Potentials*. 261(March), 244–261.
- 3360 Khan, A. G., Parthasarathy, K., & Bhalla, U. S. (2010). Odor
3361 representations in the mammalian olfactory bulb. *Wiley*
3362 *Interdisciplinary Reviews. Systems Biology and Medicine*, 2(5),
3363 603–611. <https://doi.org/10.1002/wsbm.85>
- 3364 Kraus, B. J., Brandon, M. P., Robinson, R. J., Connerney, M. A.,
3365 Hasselmo, M. E., & Eichenbaum, H. (2015). During Running in
3366 Place, Grid Cells Integrate Elapsed Time and Distance Run.
3367 *Neuron*, 88(3), 578–589.
3368 <https://doi.org/10.1016/j.neuron.2015.09.031>
- 3369 Kraus, B., Robinson, R., White, J., Eichenbaum, H., & Hasselmo, M.
3370 (2013). Hippocampal “Time Cells”: Time versus Path Integration.
3371 *Neuron*, 78(6), 1090–1101.
3372 <https://doi.org/10.1016/j.neuron.2013.04.015>

- 3373 Kropff, E., Carmichael, J. E., Moser, M.-B., & Moser, E. I. (2015).
3374 Speed cells in the medial entorhinal cortex. *Nature*, 523(7561),
3375 419–424. <https://doi.org/10.1038/nature14622>
- 3376 Krupa, D., & Thompson, R. (2003). Inhibiting the Expression of a
3377 Classically Conditioned Behavior Prevents Its Extinction. *The
3378 Journal of Neuroscience : The Official Journal of the Society for
3379 Neuroscience*, 23, 10577–10584.
3380 <https://doi.org/10.1523/JNEUROSCI.23-33-10577.2003>
- 3381 Lever, C., Burton, S., Jeewajee, A., O'Keefe, J., & Burgess, N.
3382 (2009). Boundary Vector Cells in the Subiculum of the
3383 Hippocampal Formation. *The Journal of Neuroscience*, 29(31),
3384 9771 LP – 9777. <https://doi.org/10.1523/JNEUROSCI.1319-09.2009>
- 3386 Lovett-Barron, M., Kaifosh, P., Kheirbek, M. A., Danielson, N.,
3387 Zaremba, J. D., Reardon, T. R., Turi, G. F., Hen, R., Zemelman,
3388 B. V., & Losonczy, A. (2014). Dendritic inhibition in the
3389 hippocampus supports fear learning. *Science (New York, N.Y.)*,
3390 343(6173), 857–863. <https://doi.org/10.1126/science.1247485>
- 3391 Luo, L., Callaway, E. M., & Svoboda, K. (2018). Genetic Dissection of
3392 Neural Circuits: A Decade of Progress. *Neuron*, 98(2), 256–281.
3393 <https://doi.org/https://doi.org/10.1016/j.neuron.2018.03.040>
- 3394 MacDonald, C. J., Carrow, S., Place, R., & Eichenbaum, H. (2013).
3395 Distinct hippocampal time cell sequences represent odor
3396 memories in immobilized rats. *The Journal of Neuroscience : The
3397 Official Journal of the Society for Neuroscience*, 33(36), 14607–
3398 14616. <https://doi.org/10.1523/JNEUROSCI.1537-13.2013>
- 3399 MacDonald, C. J., Lepage, K. Q., Eden, U. T., & Eichenbaum, H.
3400 (2011). Hippocampal “time cells” bridge the gap in memory for
3401 discontiguous events. *Neuron*, 71(4), 737–749.
3402 <https://doi.org/10.1016/j.neuron.2011.07.012>
- 3403 Manns, J. R., Clark, R. E., & Squire, L. R. (2000). Parallel acquisition
3404 of awareness and trace eyeblink classical conditioning. *Learning*

- 3405 & Memory (*Cold Spring Harbor, N.Y.*), 7(5), 267–272.
3406 <https://doi.org/10.1101/lm.33400>
- 3407 Maruyama, R., Maeda, K., Moroda, H., Kato, I., Inoue, M., Miyakawa,
3408 H., & Aonishi, T. (2014). Detecting cells using non-negative matrix
3409 factorization on calcium imaging data. *Neural Networks : The
3410 Official Journal of the International Neural Network Society*, 55,
3411 11–19. <https://doi.org/10.1016/j.neunet.2014.03.007>
- 3412 Mau, W., Sullivan, D. W., Kinsky, N. R., Hasselmo, M. E., Howard, M.
3413 W., & Eichenbaum, H. (2018). The Same Hippocampal CA1
3414 Population Simultaneously Codes Temporal Information over
3415 Multiple Timescales. *Current Biology*, 28(10), 1499-1508.e4.
3416 <https://doi.org/10.1016/j.cub.2018.03.051>
- 3417 McHugh, T. J., Jones, M. W., Quinn, J. J., Balthasar, N., Coppari, R.,
3418 Elmquist, J. K., Lowell, B. B., Fanselow, M. S., Wilson, M. A., &
3419 Tonegawa, S. (2007). Dentate gyrus NMDA receptors mediate
3420 rapid pattern separation in the hippocampal network. *Science
(New York, N.Y.)*, 317(5834), 94–99.
3421 <https://doi.org/10.1126/science.1140263>
- 3422
- 3423 McLelland, D., & Paulsen, O. (2007). Cortical Songs Revisited: A
3424 Lesson in Statistics. *Neuron*, 53(3), 319–321.
3425 <https://doi.org/https://doi.org/10.1016/j.neuron.2007.01.020>
- 3426 McNaughton, N., & Gray, J. A. (2000). Anxiolytic action on the
3427 behavioural inhibition system implies multiple types of arousal
3428 contribute to anxiety. *Journal of Affective Disorders*, 61(3), 161–
3429 176. [https://doi.org/10.1016/s0165-0327\(00\)00344-x](https://doi.org/10.1016/s0165-0327(00)00344-x)
- 3430 Medina, J. F., Garcia, K. S., Nores, W. L., Taylor, N. M., & Mauk, M. D.
3431 (2000). Timing mechanisms in the cerebellum: testing predictions
3432 of a large-scale computer simulation. *The Journal of
3433 Neuroscience : The Official Journal of the Society for
3434 Neuroscience*, 20(14), 5516–5525.
3435 <https://doi.org/10.1523/JNEUROSCI.20-14-05516.2000>
- 3436 Meeks, J. P., Arnson, H. A., & Holy, T. E. (2010). Representation and
3437 transformation of sensory information in the mouse accessory

- 3438 olfactory system. *Nature Neuroscience*, 13(6), 723–730.
3439 <https://doi.org/10.1038/nn.2546>
- 3440 Miller, A. M. P., Jacob, A. D., Ramsaran, A. I., De Snoo, M. L.,
3441 Josselyn, S. A., & Frankland, P. W. (2023). Emergence of a
3442 predictive model in the hippocampus. *Neuron*.
3443 <https://doi.org/10.1016/j.neuron.2023.03.011>
- 3444 Min, E., Ban, S., Wang, Y., Bae, S. C., Popescu, G., Best-Popescu, C.,
3445 & Jung, W. (2017). Measurement of multispectral scattering
3446 properties in mouse brain tissue. *Biomedical Optics Express*, 8(3),
3447 1763–1770. <https://doi.org/10.1364/BOE.8.001763>
- 3448 Mizrahi, A. (2004). High-Resolution In Vivo Imaging of Hippocampal
3449 Dendrites and Spines. *Journal of Neuroscience*, 24(13), 3147–
3450 3151. <https://doi.org/10.1523/JNEUROSCI.5218-03.2004>
- 3451 Modi, M. N., Dhawale, A. K., & Bhalla, U. S. (2014). CA1 cell activity
3452 sequences emerge after reorganization of network correlation
3453 structure during associative learning. *eLife*, 3, e01982–e01982.
3454 <https://doi.org/10.7554/eLife.01982>
- 3455 Mokeichev, A., Okun, M., Barak, O., Katz, Y., Ben-Shahar, O., &
3456 Lampl, I. (2007). Stochastic Emergence of Repeating Cortical
3457 Motifs in Spontaneous Membrane Potential Fluctuations In Vivo.
3458 *Neuron*, 53, 413–425.
3459 <https://doi.org/10.1016/j.neuron.2007.01.017>
- 3460 Mollinedo-Gajate, I., Song, C., & Knöpfel, T. (2021). Genetically
3461 Encoded Voltage Indicators. *Advances in Experimental Medicine
3462 and Biology*, 1293, 209–224. https://doi.org/10.1007/978-981-15-8763-4_12
- 3464 Morris, R. G. M., Garrud, P., Rawlins, J. N. P., & O'Keefe, J. (1982).
3465 Place navigation impaired in rats with hippocampal lesions.
3466 *Nature*, 297(5868), 681–683. <https://doi.org/10.1038/297681a0>
- 3467 Moser, M.-B., & Moser, E. I. (1998). Distributed encoding and retrieval
3468 of spatial memory in the hippocampus. In *The Journal of
3469 Neuroscience* (Vol. 18, pp. 7535–7542). Society for Neuroscience.

- 3470 Moyer, J. R., Deyo, R. A., & Disterhoft, J. F. (1990). Hippocampectomy
3471 disrupts trace eye-blink conditioning in rabbits. *Behavioral*
3472 *Neuroscience*, 104(2)(Apr 1990), 243–252.
3473 <https://doi.org/10.1037/0735-7044.104.2.243>
- 3474 Mukamel, E. A., Nimmerjahn, A., & Schnitzer, M. J. (2009). Automated
3475 analysis of cellular signals from large-scale calcium imaging data.
3476 *Neuron*, 63(6), 747–760.
3477 <https://doi.org/10.1016/j.neuron.2009.08.009>
- 3478 Muller, R. U., & Kubie, J. L. (1989). The firing of hippocampal place
3479 cells predicts the future position of freely moving rats. *The*
3480 *Journal of Neuroscience : The Official Journal of the Society for*
3481 *Neuroscience*, 9(12), 4101–4110.
3482 <https://doi.org/10.1523/JNEUROSCI.09-12-04101.1989>
- 3483 Murray, T. A., & Levene, M. J. (2012). Singlet gradient index lens for
3484 deep in vivo multiphoton microscopy. *Journal of Biomedical*
3485 *Optics*, 17(2), 021106. <https://doi.org/10.1117/1.JBO.17.2.021106>
- 3486 Nakashiba, T., Young, J. Z., McHugh, T. J., Buhl, D. L., & Tonegawa,
3487 S. (2008). Transgenic inhibition of synaptic transmission reveals
3488 role of CA3 output in hippocampal learning. *Science (New York,*
3489 *N.Y.*), 319(5867), 1260–1264.
3490 <https://doi.org/10.1126/science.1151120>
- 3491 O'Keefe, J., & Burgess, N. (1996). Geometric determinants of the
3492 place fields of hippocampal neurons. *Nature*, 381(6581), 425–428.
3493 <https://doi.org/10.1038/381425a0>
- 3494 O'Keefe, J., & Dostrovsky, J. (1971). The hippocampus as a spatial
3495 map. Preliminary evidence from unit activity in the freely-moving
3496 rat. *Brain Research*, 34(1), 171–175. [https://doi.org/10.1016/0006-8993\(71\)90358-1](https://doi.org/10.1016/0006-8993(71)90358-1)
- 3498 O'Keefe, J., & Nadel, L. (1978). The Hippocampus as a Cognitive Map.
3499 In *Philosophical Studies* (Vol. 27).
3500 <https://doi.org/10.5840/philstudies19802725>

- 3503 *Hippocampus*, 3(3), 317–330.
3504 <https://doi.org/10.1002/hipo.450030307>
- 3505 Ohya, T., Nores, W. L., Murphy, M., & Mauk, M. D. (2003). What
3506 the cerebellum computes. *Trends in Neurosciences*, 26(4), 222–
3507 227. [https://doi.org/10.1016/S0166-2236\(03\)00054-7](https://doi.org/10.1016/S0166-2236(03)00054-7)
- 3508 Ozden, I., Lee, H. M., Sullivan, M. R., & Wang, S. S.-H. (2008).
3509 Identification and Clustering of Event Patterns From In Vivo
3510 Multiphoton Optical Recordings of Neuronal Ensembles. *Journal*
3511 *of Neurophysiology*, 100(1), 495–503.
3512 <https://doi.org/10.1152/jn.01310.2007>
- 3513 Pachitariu, M., Stringer, C., Dipoppa, M., Schröder, S., Rossi, L. F.,
3514 Dalgleish, H., Carandini, M., & Harris, K. D. (2017). Suite2p:
3515 beyond 10,000 neurons with standard two-photon microscopy.
3516 *BioRxiv*, 61507. <https://doi.org/10.1101/061507>
- 3517 Paredes, R. M., Etzler, J. C., Watts, L. T., Zheng, W., & Lechleiter, J.
3518 D. (2008). Chemical calcium indicators. *Methods (San Diego,*
3519 *Calif.)*, 46(3), 143–151.
3520 <https://doi.org/10.1016/j.ymeth.2008.09.025>
- 3521 Pastalkova, E., Itskov, V., Amarasingham, A., & Buzsaki, G. (2008).
3522 Internally Generated Cell Assembly Sequences in the Rat
3523 Hippocampus. *Science*, 321(5894), 1322–1327.
3524 <https://doi.org/10.1126/science.1159775>
- 3525 Pavlov, I. P. (1927). Conditioned reflexes: an investigation of the
3526 physiological activity of the cerebral cortex. In *Conditioned*
3527 *reflexes: an investigation of the physiological activity of the*
3528 *cerebral cortex*. Oxford Univ. Press.
- 3529 Peron, S. P., Freeman, J., Iyer, V., Guo, C., & Svoboda, K. (2015). A
3530 Cellular Resolution Map of Barrel Cortex Activity during Tactile
3531 Behavior. *Neuron*, 86(3), 783–799.
3532 <https://doi.org/10.1016/j.neuron.2015.03.027>
- 3533 Petersen, C. C. H. (2019). Sensorimotor processing in the rodent
3534 barrel cortex. *Nature Reviews. Neuroscience*, 20(9), 533–546.
3535 <https://doi.org/10.1038/s41583-019-0200-y>

- 3536 Pfeiffer, B. E., & Foster, D. J. (2013). Hippocampal place-cell
3537 sequences depict future paths to remembered goals. *Nature*,
3538 497(7447), 74–79. <https://doi.org/10.1038/nature12112>
- 3539 Pfeiffer, B. E., & Foster, D. J. (2015). Autoassociative dynamics in the
3540 generation of sequences of hippocampal place cells. *Science*,
3541 349(6244), 180–183. <https://doi.org/10.1126/science.aaa9633>
- 3542 Pnevmatikakis, E. A., Soudry, D., Gao, Y., Machado, T. A., Merel, J.,
3543 Pfau, D., Reardon, T., Mu, Y., Lacefield, C., Yang, W., Ahrens, M.,
3544 Bruno, R., Jessell, T. M., Peterka, D. S., Yuste, R., & Paninski, L.
3545 (2016). Simultaneous Denoising, Deconvolution, and Demixing of
3546 Calcium Imaging Data. *Neuron*, 89(2), 285–299.
3547 <https://doi.org/https://doi.org/10.1016/j.neuron.2015.11.037>
- 3548 Poort, J., Khan, A. G., Pachitariu, M., Nemri, A., Orsolic, I., Krupic, J.,
3549 Bauza, M., Sahani, M., Keller, G. B., Mrsic-Flogel, T. D., & Hofer,
3550 S. B. (2015). Learning Enhances Sensory and Multiple Non-
3551 sensory Representations in Primary Visual Cortex. *Neuron*, 86(6),
3552 1478–1490. <https://doi.org/10.1016/j.neuron.2015.05.037>
- 3553 Ranck, J. B. (1973). Studies on single neurons in dorsal hippocampal
3554 formation and septum in unrestrained rats: Part I. Behavioral
3555 correlates and firing repertoires. *Experimental Neurology*, 41(2),
3556 462–531. [https://doi.org/https://doi.org/10.1016/0014-4886\(73\)90290-2](https://doi.org/https://doi.org/10.1016/0014-4886(73)90290-2)
- 3558 Ranck, J. B. (1975). *Behavioral Correlates and Firing Repertoires of
3559 Neurons in the Dorsal Hippocampal Formation and Septum of
3560 Unrestrained Rats BT - The Hippocampus: Volume 2:
3561 Neurophysiology and Behavior* (R. L. Isaacson & K. H. Pribram
3562 (Eds.); pp. 207–244). Springer US. https://doi.org/10.1007/978-1-4684-2979-4_7
- 3564 Rao, R. P. N., & Ballard, D. H. (1999). Predictive coding in the visual
3565 cortex: a functional interpretation of some extra-classical
3566 receptive-field effects. *Nature Neuroscience*, 2(1), 79–87.
3567 <https://doi.org/10.1038/4580>

- 3568 Reyes, A. D. (2003). Synchrony-dependent propagation of firing rate in
3569 iteratively constructed networks in vitro. *Nature Neuroscience*,
3570 6(6), 593–599. <https://doi.org/10.1038/nn1056>
- 3571 Rogerson, T., Cai, D. J., Frank, A., Sano, Y., Shobe, J., Lopez-Aranda,
3572 M. F., & Silva, A. J. (2014). Synaptic tagging during memory
3573 allocation. *Nature Reviews Neuroscience*, 15(3), 157–169.
3574 <https://doi.org/10.1038/nrn3667>
- 3575 Savelli, F., Yoganarasimha, D., & Knierim, J. J. (2008). Influence of
3576 boundary removal on the spatial representations of the medial
3577 entorhinal cortex. *Hippocampus*, 18(12), 1270–1282.
3578 <https://doi.org/10.1002/hipo.20511>
- 3579 Schreurs, B. G. (1989). Classical conditioning of model systems: A
3580 behavioral review. *Psychobiology*, 17(2), 145–155.
3581 <https://doi.org/10.3758/BF03337830>
- 3582 Scoville, W. B., & Milner, B. (1957). Loss of recent memory after
3583 bilateral hippocampal lesions. In *Journal of Neurology,*
3584 *Neurosurgery & Psychiatry* (Vol. 20, pp. 11–21). BMJ Publishing
3585 Group. <https://doi.org/10.1136/jnnp.20.1.11>
- 3586 Sheffield, M. E. J., & Dombeck, D. A. (2014). Calcium transient
3587 prevalence across the dendritic arbour predicts place field
3588 properties. *Nature*, 517(7533), 200–204.
3589 <https://doi.org/10.1038/nature13871>
- 3590 Siegel, J. J., & Mauk, M. D. (2013). Persistent Activity in Prefrontal
3591 Cortex during Trace Eyelid Conditioning: Dissociating Responses
3592 That Reflect Cerebellar Output from Those That Do Not. *The*
3593 *Journal of Neuroscience*, 33(38), 15272 LP – 15284.
3594 <https://doi.org/10.1523/JNEUROSCI.1238-13.2013>
- 3595 Siegel, J. J., Taylor, W., Gray, R., Kalmbach, B., Zemelman, B. V.,
3596 Desai, N. S., Johnston, D., & Chitwood, R. A. (2015). Trace
3597 Eyeblink Conditioning in Mice Is Dependent upon the Dorsal
3598 Medial Prefrontal Cortex, Cerebellum, and Amygdala: Behavioral
3599 Characterization and Functional Circuitry. *ENeuro*, 2(4),

- 3600 ENEURO.0051-14.2015. <https://doi.org/10.1523/ENEURO.0051-14.2015>
- 3602 Skaggs, W., McNaughton, B., Gothard, K., & Markus, E. (1996). An
3603 Information-Theoretic Approach to Deciphering the Hippocampal
3604 Code. *Neural Inf. Process Syst.*, 5.
- 3605 Sofroniew, N. J., Flickinger, D., King, J., & Svoboda, K. (2016). A large
3606 field of view two-photon mesoscope with subcellular resolution for
3607 in vivo imaging. *eLife*, 5(JUN2016), 1–20.
3608 <https://doi.org/10.7554/eLife.14472>
- 3609 Solstad, T., Boccara, C. N., Kropff, E., Moser, M.-B., & Moser, E. I.
3610 (2008). Representation of Geometric Borders in the Entorhinal
3611 Cortex. *Science*, 322(5909), 1865–1868.
3612 <https://doi.org/10.1126/science.1166466>
- 3613 Souza, B. C., Pavão, R., Belchior, H., & Tort, A. B. L. (2018). On
3614 Information Metrics for Spatial Coding. *Neuroscience*, 375, 62–73.
3615 <https://doi.org/10.1016/j.neuroscience.2018.01.066>
- 3616 Stosiek, C., Garaschuk, O., Holthoff, K., & Konnerth, A. (2003). In vivo
3617 two-photon calcium imaging of neuronal networks. *Proceedings of
3618 the National Academy of Sciences of the United States of
3619 America*, 100(12), 7319–7324.
3620 <https://doi.org/10.1073/pnas.1232232100>
- 3621 Suh, J., Rivest, A. J., Nakashiba, T., Tominaga, T., & Tonegawa, S.
3622 (2011). Entorhinal cortex layer III input to the hippocampus is
3623 crucial for temporal association memory. *Science (New York,
3624 N.Y.)*, 334(6061), 1415–1420.
3625 <https://doi.org/10.1126/science.1210125>
- 3626 Taube, J. S., Muller, R. U., & Ranck, J. B. J. (1990). Head-direction
3627 cells recorded from the postsubiculum in freely moving rats. I.
3628 Description and quantitative analysis. *The Journal of
3629 Neuroscience : The Official Journal of the Society for
3630 Neuroscience*, 10(2), 420–435.
3631 <https://doi.org/10.1523/JNEUROSCI.10-02-00420.1990>

- 3632 Uncapher, M. R., Hutchinson, J. B., & Wagner, A. D. (2011).
3633 Dissociable effects of top-down and bottom-up attention during
3634 episodic encoding. *The Journal of Neuroscience : The Official
3635 Journal of the Society for Neuroscience*, 31(35), 12613–12628.
3636 <https://doi.org/10.1523/JNEUROSCI.0152-11.2011>
- 3637 Valero, M., Cid, E., Averkin, R. G., Aguilar, J., Sanchez-Aguilera, A.,
3638 Viney, T. J., Gomez-Dominguez, D., Bellistri, E., & de la Prida, L.
3639 M. (2015). Determinants of different deep and superficial CA1
3640 pyramidal cell dynamics during sharp-wave ripples. *Nature
3641 Neuroscience*. <https://doi.org/10.1038/nn.4074>
- 3642 Velasco, M. G. M., & Levene, M. J. (2014). In vivo two-photon
3643 microscopy of the hippocampus using glass plugs. *Biomedical
3644 Optics Express*, 5(6), 1700–1708.
3645 <https://doi.org/10.1364/BOE.5.001700>
- 3646 Vinogradova, O. S. (2001). Hippocampus as comparator: Role of the
3647 two input and two output systems of the hippocampus in selection
3648 and registration of information. *Hippocampus*, 11(5), 578–598.
3649 <https://doi.org/https://doi.org/10.1002/hipo.1073>
- 3650 Voelcker, B., Pancholi, R., & Peron, S. (2022). Transformation of
3651 primary sensory cortical representations from layer 4 to layer 2.
3652 *Nature Communications*, 13(1), 5484.
3653 <https://doi.org/10.1038/s41467-022-33249-1>
- 3654 Wood, E. R., Dudchenko, P. A., Robitsek, R. J., & Eichenbaum, H.
3655 (2000). Hippocampal Neurons Encode Information about Different
3656 Types of Memory Episodes Occurring in the Same Location.
3657 *Neuron*, 27(3), 623–633.
3658 [https://doi.org/https://doi.org/10.1016/S0896-6273\(00\)00071-4](https://doi.org/https://doi.org/10.1016/S0896-6273(00)00071-4)
- 3659 Yiu, A. P., Mercaldo, V., Yan, C., Richards, B., Rashid, A. J., Hsiang,
3660 H.-L. L., Pressey, J., Mahadevan, V., Tran, M. M., Kushner, S. A.,
3661 Woodin, M. A., Frankland, P. W., & Josselyn, S. A. (2014).
3662 Neurons are recruited to a memory trace based on relative
3663 neuronal excitability immediately before training. *Neuron*, 83(3),
3664 722–735. <https://doi.org/10.1016/j.neuron.2014.07.017>

- 3665 Zhang, S., & Manahan-Vaughan, D. (2015). Spatial olfactory learning
3666 contributes to place field formation in the hippocampus. *Cerebral*
3667 *Cortex (New York, N.Y. : 1991)*, 25(2), 423–432.
3668 <https://doi.org/10.1093/cercor/bht239>
- 3669 Zhou, S., Masmanidis, S. C., & Buonomano, D. V. (2020). Neural
3670 Sequences as an Optimal Dynamical Regime for the Readout of
3671 Time. *Neuron*, 108(4), 651-658.e5.
3672 <https://doi.org/https://doi.org/10.1016/j.neuron.2020.08.020>
- 3673 Zhou, Y., Won, J., Karlsson, M. G., Zhou, M., Rogerson, T., Balaji, J.,
3674 Neve, R., Poirazi, P., & Silva, A. J. (2009). CREB regulates
3675 excitability and the allocation of memory to subsets of neurons in
3676 the amygdala. *Nature Neuroscience*, 12(11), 1438–1443.
3677 <https://doi.org/10.1038/nn.2405>
- 3678 Ziv, Y., Burns, L. D., Cocker, E. D., Hamel, E. O., Ghosh, K. K., Kitch,
3679 L. J., El Gamal, A., & Schnitzer, M. J. (2013). Long-term dynamics
3680 of CA1 hippocampal place codes. *Nature Neuroscience*, 16(3),
3681 264–266. <https://doi.org/10.1038/nn.3329>

Novel Tools and Methods

Synthetic Data Resource and Benchmarks for Time Cell Analysis and Detection Algorithms

Kambadur G. Ananthamurthy and Upinder S. Bhalla

<https://doi.org/10.1523/ENEURO.0007-22.2023>

National Centre for Biological Sciences - Tata Institute of Fundamental Research, Bellary Road, Bengaluru - 560065, Karnataka, India

Abstract

Hippocampal CA1 cells take part in reliable, time-locked activity sequences in tasks that involve an association between temporally separated stimuli, in a manner that tiles the interval between the stimuli. Such cells have been termed time cells. Here, we adopt a first-principles approach to comparing diverse analysis and detection algorithms for identifying time cells. We generated synthetic activity datasets using calcium signals recorded *in vivo* from the mouse hippocampus using two-photon (2-P) imaging, as template response waveforms. We assigned known, ground truth values to perturbations applied to perfect activity signals, including noise, calcium event width, timing imprecision, hit trial ratio and background (untuned) activity. We tested a range of published and new algorithms and their variants on this dataset. We find that most algorithms correctly classify over 80% of cells, but have different balances between true and false positives, and different sensitivity to the five categories of perturbation. Reassuringly, most methods are reasonably robust to perturbations, including background activity, and show good concordance in classification of time cells. The same algorithms were also used to analyze and identify time cells in experimental physiology datasets recorded *in vivo* and most show good concordance.

Significance Statement

Numerous approaches have been developed to analyze time cells and neuronal activity sequences, but it is not clear whether their classifications match, nor how sensitive they are to various sources of data variability. We provide two main contributions to address this: (1) a resource to generate ground truth labeled synthetic two-photon (2-P) calcium activity data with defined distributions for confounds such as noise and background activity, and (2) a survey of several methods for analyzing time cell data using our synthetic data as ground truth. As a further resource, we provide a library of efficient C++ implementations of several algorithms with a Python interface. The synthetic dataset and its generation code are useful for profiling future methods, testing analysis toolchains, and as input to computational and experimental models of sequence detection.

Introduction

The mammalian hippocampus is important for the formation of several kinds of memory, one of which is the association between stimuli occurring separately in time. Time cells were originally described using tuning curves from single-unit recordings of cellular activity when rats ran on a running wheel in between behavioral decisions (Pastalkova et al., 2008). These cells exhibited time tuning of the order of seconds. Several further studies have shown that small populations of hippocampal CA1 cells

fire in time-locked sequences, “bridging” the time gap between stimulus and response in temporal delay tasks lasting several seconds (Pastalkova et al., 2008; MacDonald et al., 2011, 2013; Kraus et al., 2013). Cellular calcium imaging studies have also been used to report time cells, albeit at slower sampling rate (Modi et al., 2014; Mau et al., 2018). For example, similar interval tiling properties of hippocampal CA1 neurons were observed on much shorter, 500 ms timescales in a Trace Eyeblink Conditioning (TEC) task (Modi et al., 2014). Spontaneous sequential activity

Received January 2, 2022; accepted February 9, 2023; First published February 23, 2023.

The authors declare no competing financial interests.

Author contributions: K.G.A. and U.S.B. designed research; K.G.A. performed research; K.G.A. and U.S.B. analyzed data; K.G.A. and U.S.B. wrote the paper.

has also been reported in free-running animals (Villette et al., 2015). Such cells with a well-defined temporal firing field are commonly termed time cells (MacDonald et al., 2011; Eichenbaum, 2017). However, there is a wide diversity of methods used to detect and characterize time cells, and it is not clear how consistent these methods are in classifying cells as time cells. It is also unclear how sensitive each method may be to a range of physiological sources of variability and noise. A consistent set of benchmarks of classification performance is necessary to draw accurate and comparable conclusions from real physiology data across different methods and different laboratories. Our approach in the current study is not prescriptive, but pragmatic: we ask how existing methods work when we already know exactly which cells are time cells, and we determine how well each method deals with imperfect data.

The major approaches used to identifying time cells are tuning curves (peristimulus time histograms), temporal information (TI), principal component analysis with time offset, support vector machines, and bootstrap analysis of activity peaks. Several studies have used a temporal delay task lasting several seconds, in which a rat runs on a treadmill during the delay period. A temporal information metric (Mau et al., 2018) has been used to find individual time cells in such tasks. A distinct task involves monitoring recurrent sequences of activity during free-running treadmill recordings. Such datasets have been analyzed using offset principal component analysis (Kaifosh et al., 2013; Villette et al., 2015; Malvache et al., 2016), to first denoise two-photon (2-P) data, establish correlation coefficients, and detect hippocampal CA1 sequences. Time cells have also been reported for much shorter duration tasks (~500 ms) such as hippocampus-dependent trace conditioning (Tseng et al., 2004; Modi et al., 2014). Time cells in these 2-P datasets were identified using yet another method, in which bootstrapping was used to determine whether peak activity at a given time was different from chance. This method was termed ratio of ridge/background (Modi et al., 2014). Yet other methods have utilized support vector machines to categorize time cells (Ahmed et al., 2020). Additionally, while the applicability of a variety of algorithms for place cell detection has been previously compared (Souza et al., 2018), we have

K.G.A. and the experiments received support from the Department of Biotechnology Grant BT/PR12255/MED/122/8/2016 (to U.S.B.). National Centre for Biological Sciences-Tata Institute of Fundamental Research (NCBS-TIFR) provided resources for analysis equipment and support to U.S.B. through intramural funds supported by the Department of Atomic Energy, Government of India, Project Identification No. TRI 4006.

Acknowledgments: We thank Daniel Dombeck for help with the chronic preparation for physiological 2-P calcium recording of hippocampal CA1 cells and William Mau for his Temporal Information calculation code. We also thank Vinu Varghese and Bhanu Priya Somashekhar for helpful comments on this manuscript.

Correspondence should be addressed to Upinder S. Bhalla at bhalla@ncbs.res.in.

<https://doi.org/10.1523/ENEURO.0007-22.2023>

Copyright © 2023 Ananthamurthy and Bhalla

This is an open-access article distributed under the terms of the Creative Commons Attribution 4.0 International license, which permits unrestricted use, distribution and reproduction in any medium provided that the original work is properly attributed.

focused on methods which are fully automatable and which scale well to large datasets, specifically comparing algorithms to detect time cells.

Time cell detection is closely related to sequence detection, which has been fraught with statistical challenges. For example, detection of synfire chains has been the subject of some debate (Ikegaya et al., 2004; Lee and Wilson, 2004; Mokeichev et al., 2007; Schrader et al., 2008). Time cell detection is usually easier, in that in most experiments there is a well-defined initiating stimulus and a known delay or trace phase (however, see Villette et al., 2015). For any cell identified as a time cell, it is desirable to define a score to measure quality or reliability along with decodable time. Hence it is also valuable to be able to compare the score of a time cell across recordings and even between groups, using well defined, analog measures. Each algorithm currently used in the literature implements a different scoring method and it is as yet unclear whether comparable results would be observed with other metrics.

In the current study, we compare these diverse methods by estimating their performance on synthetic test datasets where we controlled all features of the data, including the identity and timing of each time cell. The development of a synthetic dataset serves two purposes. First, it facilitates principled comparison of different methods, since the ground truth is known. Second, it facilitates an analysis over many dimensions of input variance, corresponding to very different experimental and neural circuit contexts. Richness in variety of input data allows for better sampling of the performance of the analyses under many potential conditions. We have explored variance along the key dimensions of noise, timing imprecision, signal widths, frequency of occurrence, as well as several others. To strengthen the applicability of this synthetic data resource to real data, our generated output uses sampled experimental data.

Our experimental data, synthetic dataset, and code base are intended to be a resource for algorithm testing and optimization.

Materials and Methods

Animals, chronic implants, and behavioral training

All animal procedures were performed in accordance with the National Centre for 114 Biological Sciences Institutional Animal Ethics Committee (project ID NCBS115 IAE-2016/20(M)), in accordance with the guidelines of the Government of India (Animal Facility CPCSEA registration number 109/1999/CPCSEA) and equivalent guidelines of the Society for Neuroscience.

To chronically monitor the activity of the same population of hippocampal CA1 cells, we implanted two- to four-month-old male and female GCaMP6f mice [Tg(Thy1-GCaMP6f)GP5.17Dkim JAX stock #025393] with an optical window and head-bar using a protocol adapted from previously published methods (Dombeck et al., 2010). Briefly, anesthesia was induced with 2–3% isoflurane in a chamber, and subsequently maintained (breathing rate of ~1 Hz) with 1–2% isoflurane, directly to the mouse's nose using an inverted pipette tip. Surgery was performed on a

temperature-controlled table, maintained at 36.5°C, while the anaesthetized animal was cheek-clamped. After a haircut, a ~5 cm piece of scalp was cut open to reveal the skull. A ~3 mm circular craniotomy was then performed at a position 2 mm caudal and ~1.5 mm lateral to bregma, on the left hemisphere. After gently tearing off the dura, the underlying cortex was carefully aspirated till the corpus callosum (CC) layer, clearing out any blood using repeated washes of cortex buffer (Modi et al., 2014). A small thickness of corpus callosum fibers were then carefully aspirated till horizontal CC fibers were sparse but visible. The cortex buffer was then carefully suctioned out to dry the exposure till tacky. The exposure was then quickly sealed using a thin layer of Kwik-Sil and a coverslip attached to the bottom of a 3 mm steel cannula. This preparation left the CA1 cell body layer ~200 μm below the most exposed tissue. Finally, an imaging head-bar was surgically implanted and fixed to the scalp, using dental cement and skull screws, before the animal was brought out of anesthesia.

The animals were allowed to recover for 1–5 d after implantation, with a further 3–4 d of habituation to the rig. Following this simultaneous behavioral training and 2-P *in vivo* imaging was conducted.

Trace Eyeblink Conditioning (TEC)

We standardized a multi-session Trace Eyeblink Conditioning (TEC) paradigm to train head-fixed mice, based on previous literature (Siegel et al., 2015). TEC involves an association between a previously neutral conditioned stimulus (CS) with an eyeblink inducing unconditioned stimulus (US), across an intervening, stimulus-free, trace interval. Training involved 60 trials per session, one session a day, for approximately two weeks. The CS was a 50 ms blue LED flash while the US was a 50 ms air-puff to the left eye. The stimulus-free trace interval was 250–750 ms long, depending on the session. Additionally, a pseudorandom 10% of the trials were CS-only probe trials (no US) to test for learning. All behavior routines were controlled by programmed Arduinos. Eyeblinks were measured for every trial, by video camera (Point Gray Chameleon3 1.3 MP Monochrome USB3.0) based detection.

The conditioned response (CR) is observed as a preemptive blink before the US is delivered, in animals that learn the task. The analysis of the behavioral data was performed using custom written MATLAB scripts. In brief, each frame for every trial was:

1. Cropped to get the eye;
2. Binarized to get the pixels defining just the eye, and finally;
3. Given an FEC score from 0 to 1 (see below).

Every trial was then scored as a hit or miss, using the result of a two-sample Kolmogorov-Smirnov test between the FEC during the trace and pre-CS period (1% significance). The performance of an animal for a session was then established as the percentage of hit trials/total trials.

Definitions:

FEC: The fraction of eye-closed is estimated by counting the pixels defining the eye in every image of a time series, normalized by the maximum number of pixels defining the eye, in that session. Thus, every frame was given an analog score from 0 to 1, where,

- 0: fully opened eye
- 1: fully closed eye

CR: The conditioned response is the eye-closing transition during the trace period.

UR: The unconditioned response is the eye-closing transition when the US is delivered.

Performance: Percentage of hit trials/total trials. This allowed us to observe how the animals perform during and across sessions.

Two-photon imaging

We used a custom-built two photon laser-scanning microscope (Modi et al., 2014) to record calcium activity from 100–150 hippocampal CA1 cell bodies *in vivo*, at cellular resolution. We performed galvo-scans through the imaging window, over a field of view of ~100 × 100 μm², at 14.5 Hz, during TEC (Fig. 1A). An Arduino microcontroller was used to control the behavior routines, and it additionally sent a TTL trigger to initiate the imaging trials. The behavior and imaging were conducted simultaneously to record calcium activity when the animal was learning the task.

Time-series fluorescence data for various cells was extracted using Suite2P (Pachitariu et al., 2017). All further analysis and code development was done on MATLAB R2017b and batch analysis runs were performed on MATLAB R2021a. The average of the fluorescence values for cell specific pixels is then converted into the fold change relative to the baseline (dF/F₀; F₀ as 10th percentile), for every marked cell, in every trial (Fig. 1B). These dF/F traces were used for the rest of the analysis.

Curating a library of calcium events

For all synthetic data experiments, we used one good quality 2-P recording session's worth of data from one animal. We mapped our imaging dataset into a matrix of dF/F values for all cells, trials, and frames. We then identified calcium events as signal deviations that were above a threshold (mean ± 2*SD) for more than four consecutive frames (frame rate: 14.5 Hz or ~70 ms per frame). Once identified, we curated a library for each event by a cell, and saved the respective start indices and widths. Using this library, we generated synthetic data by inserting experimental calcium events into the time series for each simulated cell. This approach just uses a time series of signal bins and amplitudes, hence is signal-agnostic and could be applied to other imaging and recording modalities. In the interests of data integrity, our synthetic datasets were watermarked to be distinguishable from real physiology datasets.

Generating synthetic data

Synthetic data were generated using a custom-written MATLAB function script “generateSyntheticData()” in the provided code repository. We preallocated and set up a 3-D matrix of zeros (as cells, trials, frames), and added

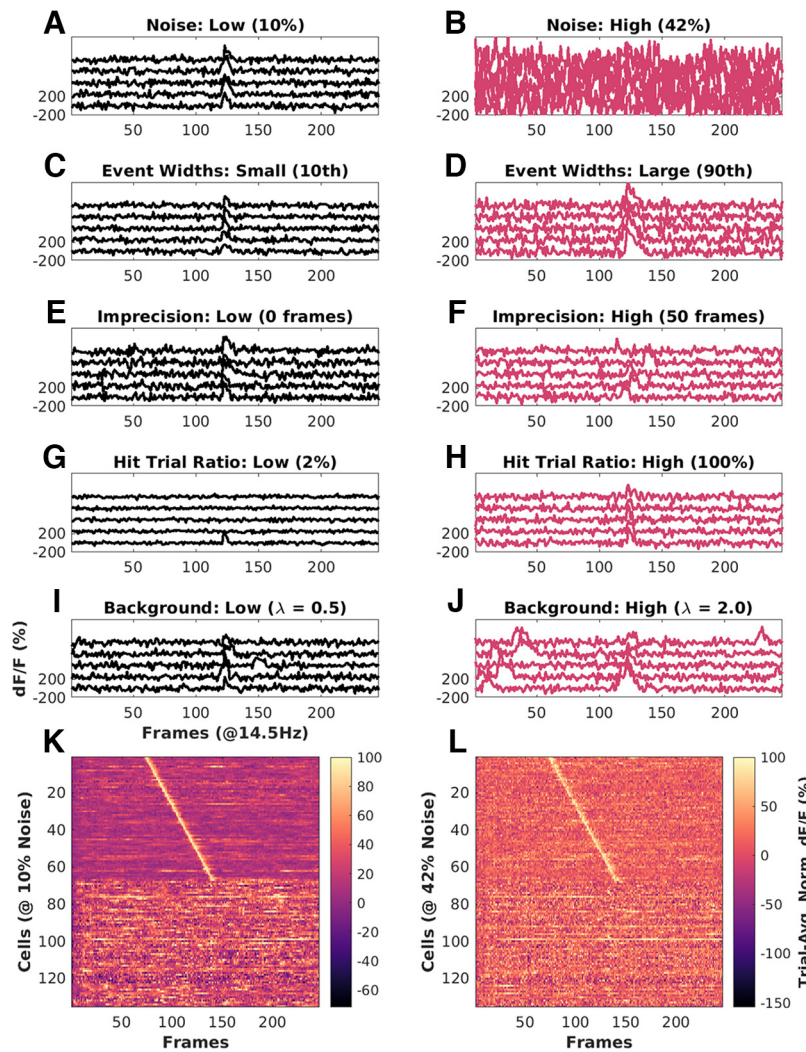


Figure 1. Key features of synthetic datasets. Left, Black panels, Low range of features. Right, Red panels, High range of features. **A**, Noise = 10%. **B**, Noise = 42%. **C**, Event width: 10th percentile ± 1 SD. **D**, Event width 90th percentile ± 1 SD. **E**, Imprecision at 0 frames FWHM. **F**, Imprecision at 50 frames FWHM. **G**, Hit trial ratio from 0% to 2%. **H**, Hit trial ratio from 0% to 100%. **I**, **J**, Background activity with the number of background spikes per background sampled from a Poisson distribution for with mean (λ), for **I**: $\lambda = 0.5$ (low), and **J**: $\lambda = 2.0$ (high). **K**, **L**, Trial-averaged Calcium traces from example synthetic datasets of 135 neurons, displayed as heatmap sorted by time of peak Ca signal. **K**, Baseline physiology synthetic data trial-average with 10% noise (low) and high background activity ($\lambda = 2$ to 3 events/trial). **L**, Same as **K** with 42% noise (high) and comparable background activity ($\lambda = 2$ to 3 events/trial). In both cases, 50% of the cells (top 67) are time cells and the remainder are not. Extended Data Figure 1-1 describes the most important parameters modulated for datasets in each of the three parameter regimes, “Unphysiological,” “Canonical,” and “Physiological,” along with the false positives and false negatives, for each of the 10 implemented algorithms.

calcium events sampled from the Calcium Event Library at frames (time) determined by the synthesis algorithm. The input parameters to this algorithm included timing, noise, imprecision, event width selection, hit trial ratio, background activity, and several others. We aimed to cover the most likely conditions to affect timing and other experiment design properties. In more detail, we generated synthetic datasets using the following control parameters:

- Time cell percent

Value: Number between 0 and 100. This sets the number of cells that are assigned tuned calcium activity as a

percentage of total cells, and controls the number of positive and negative class cells in the dataset.

- Cell order

Value: ‘basic’ or ‘random.’ In ‘basic’ mode, time cells are indexed lower than other cells. In ‘random’ mode, the indices of time cells and other cells are randomly selected. This should have no impact on algorithm detection but is useful for visualization.

- Max hit trial percent

Value: Number between 0 and 100. This sets the maximum possible fraction of total trials, during which a Time Cell will exhibit tuned calcium activity.

- Hit trial percent assignment

Value: ‘fixed’ or ‘random.’ In ‘fixed’ mode, the number of hit trials is set as defined by max hit trial percent. In ‘random’ mode, the number of hit trials is calculated by randomly picking a value from a range ($\frac{1}{2} \times \text{max hit trials}$, max hit trials).

- Trial order

Value: ‘basic’ or ‘random.’ In ‘basic’ mode, the hit trials are indexed lower than miss trials. In ‘random’ mode, the indices of hit and miss trials are randomly selected. Specific patterns of hit and miss trials for a session have not been reported in physiology, so this feature is not implemented.

- Event width

Value: {0–100 percentile value, Integer N}. For each cell, this defines the selection of events based on width in frames. The percentile value is estimated from the histogram of all event widths. The variance of this selection is set by “N,” which adds N^*SD to the selection. All synthetic cells exhibit a range of different calcium events. This is considered an important parameter.

- Event amplification factor

Value: Number from 0 to $+\infty$. This allows additional control to multiplicatively amplify any chosen calcium event, before incorporation. Our library was curated from physiologically recorded signals. The default value is 1.

- Event timing

Value: ‘sequential’ or ‘random.’ In ‘sequential’ mode, the time of peak calcium activity is reflected by the indexing of the time cells. In ‘random’ mode, the time of peak calcium activity is randomly dispersed over the trial frame points.

- Start frame

Value: Number from 0 to total number of frames. This sets the timing of the first cell in a time cell sequence.

- End frame

Value: Number from 0 to total number of frames. This sets the timing of the last cell in a time cell sequence.

- Imprecision full width at half max (FWHM)

Value: Number from 0 to total number of frames. This sets the lower and upper bounds for the difference in timing of calcium activity across trial pairs for a time cell. We use this parameter to model trial to trial variability and is considered an important parameter to test.

- Imprecision type

Value: ‘none,’ ‘uniform,’ or ‘normal.’ In ‘uniform’ and ‘normal’ modes, the trial pair Imprecision is picked from a normal and uniform distribution, respectively. In ‘none’ mode, the trial pair Imprecision defaults to 0.

- Noise

Value: ‘Gaussian’ or ‘none.’ In ‘Gaussian’ mode, the noise is sampled as a time-series vector with points from

a Gaussian distribution. In ‘none’ mode, the noise percent defaults to 0.

- Noise percent

Value: Number from 0 to 100. This allows scaling for any sample noise point, based on the max signal value for any cell.

- Add background spikes for time cells

Value: Boolean 0 or 1. This switch controls the incorporation of background (untuned) activity for putative time cells.

- Add background spikes for other cells

Value: Boolean 0 or 1. This switch controls the incorporation of background (untuned) activity for other (nontime) cells.

- Background distribution mean

Value: Number from 0 to $+\infty$. This sets the mean (λ) of the Poisson distribution to sample from when selecting how many background events to add per trial, for any given cell.

Implementation of a reference quality measure, Q

In order to compare the readouts from the various time-cell detection methods, we implemented a reference measure of quality (Q) of synthetic time cells that used the known inputs to the generation algorithm.

Based on preliminary analysis, we selected following five parameters as the most likely to affect the behavior and detection of time cells:

1. Noise
2. Event width
3. Imprecision
4. Hit trial ratio
5. Background activity

Accordingly, we were able to calculate a reference quality measure, using the following equation:

$$\text{RefQ} = \text{HTR} \times \exp - \{\alpha \times \text{MNP}/100 \times \text{EAF} + \beta \times \text{std. dev. EW}/\text{meanEW} + \gamma \times \text{std. dev. Imp}/\text{Stim Win}\}, \quad (1)$$

where HTR: hit trial ratio

MNP: max noise percent (%)

EAF: event amplification factor

EW: event widths (frames)

Imp: imprecision (frames)

Stim Win: stimulus window (frames)

α : 1

β : 1

γ : 10

The values of α , β , and γ , were set to have comparable effects of each of the terms inside the exponent. This reference Q was useful for debugging code and was the basis for a further metric for time cell classification discussed below. A representative synthetic activity trace for ‘low’ and ‘high’ values of each of these five parameters is shown in Figure 1.

All modulations for the datasets in this study along with the estimates for false positives and false negatives, across all algorithms are shown in Extended Data Figure 1-1.

Separate analysis modules were developed for three categories of analysis

We implemented three analysis modules: *ti*, *r2b*, and *peq*, shorthand for temporal information, ridge-to-background, and parametric equations. The *ti* module implements three algorithms from Mau et al. (2018). The *r2b* module implements two algorithms from Modi et al. (2014). The *peq* module computes estimates for noise, hit trial ratio, event width and imprecision, and estimates a Q score as above. All three methods were implemented in C++ with a PyBind11 interface to Python. This combination is fast and efficient in memory use, and also has the ease-of-use of Python. Thanks to the native MATLAB interface to Python, all three methods can also be called from MATLAB.

Synthetic datasets generated and analyzed in batch mode

We generated datasets pertaining to parameter sensitivity analysis by modulating one of the four main parameters and setting the others to noninterference levels. In this manner, we devised 99 cases to study in which one of the main parameters was varied. Note that in these cases the resultant activity was in an unphysiological regime because other sources of variation were kept to low levels so as not to interfere with the parameter of interest. With three randomized shuffles, we generated 297 unique datasets.

We wanted to use more realistic datasets, where we would modulate one of the four parameters while keeping the others to ranges typical of physiological data. We devised 12 canonical cases. With 10 randomized shuffles each, we generated 120 additional unique datasets in the canonical regime. Finally, we devised 12 physiological regime cases, identical to those in the canonical regime, with the addition of background (untuned) activity. This yielded another 150 datasets, with randomization.

Altogether, we had 567 unique datasets for our tests, each with 135 cells (total: 76,545 cells), 60 trials, and 246 frames/trial. Except when the percent time cells were modulated, all datasets featured 50% time cells.

We next implemented an analysis pipeline to run all the datasets through the time cell detection algorithms, yielding scores and predictions for each case. Finally, all the scores and predictions were collated for comparison and benchmarks as shown in the schematic (Fig. 2).

Metrics for time cell classification performance

Recall is inversely proportional to the number of false negatives (Type II error) and is the fraction of true positive class predictions over all positive class ground labels.

$$\text{Recall} = \text{TPR}/(\text{TPR} + \text{FNR}) \quad (2)$$

Precision is inversely proportional to the number of false positives (Type I error) and is the fraction of true positive class predictions over all positive class predictions.

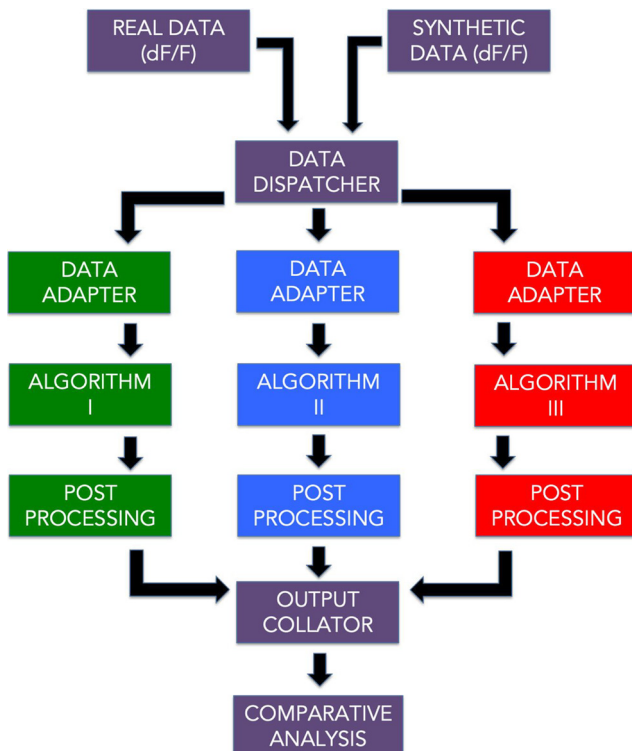


Figure 2. A schematic representation of the analysis pipeline. Physiology data as well as synthetic data were analyzed by 10 different implemented algorithms and the output was collated for comparative benchmarks.

$$\text{Precision} = \text{TPR}/(\text{TPR} + \text{FPR}). \quad (3)$$

F1 Score is the harmonic mean of recall and precision.

$$\text{F1 Score} = 2 * \text{Precision} * \text{Recall}/(\text{Precision} + \text{Recall}), \quad (4)$$

where

TPR: true positive rate

FNR: false negative rate

FPR: false positive rate

Here are the definitions for predictive/classification performance evaluation (Table 1).

Here are the important functions provided in the code base (Table 2).

Here are the MATLAB scripts running the comparative analysis and figure generation (Table 3).

Code and resource availability

The code/software described in the paper is freely available online at <https://github.com/BhallaLab/TimeCellAnalysis>. The code is available as Extended Data 1.

Results

We developed a pipeline (Fig. 2) with 10 different algorithm implementations for time cell detection, which involve scoring and then classifying cells.

Here, we describe the implementation of each of the methods.

Table 1: Definitions for predictive/classification performance evaluation

Ground truth	Prediction/classification	Remark
0/false/other cell	0/false	True negative (TN)
0/false/other cell	1/true	False positive (FP)
1/true/time cell	0/false	False negative (FN)
1/true/time cell	1/true	True positive (TP)

For each detection algorithm, the classification results were compared with known ground truth values to get the total number of true positive (TP), true negative (TN), false positive (FP), and false negative (FN) cases.

Time cell scoring methods and classification

Temporal information: *tiBoot*, *tiMean*, *tiBoth*, *tiMean-O*, *tiBase-O* (Mau et al., 2018)

Here, we used the algorithm from Mau et al. (2018) as follows. There was an initial criterion of cells to have activity in at least 25% of trials. Their activity was summed into event time histograms with a bin size of three frames. The temporal information (TI) was estimated using Equation 5,

$$TI = 1 \times \lambda j \times \log_2 \lambda j \times P_j, \quad (5)$$

where, λ is the average transient rate for each cell;

λj is the average transient rate for each cell in bin “j”; P_j is the probability that the mouse was in time bin “j.”

Bootstrapping was used to determine whether each cell had a TI greater than chance. We circularly randomized the frame points to develop a random activity model (1000 iterations) and classified cells as time cells if $\lambda > \lambda_{rand}$ in >99% of the models for at least two consecutive bins. We implemented the activity filter from Mau et al. (2018); by considering the trial-averaged peak of the calcium traces for each of the cells, and testing for significance using bootstrapping (*tiMean*). A logical AND operation between the prediction lists for *tiBoot* and *tiMean*, provided us with the full Mau et al., 2018 Temporal Information based detection algorithm (*tiBoth*).

Additionally, we used Otsu’s threshold (Otsu, 1979) on the temporal information scores as well as the trial-averaged peaks to get *tiBase-O* and *tiMean-O* using the MATLAB function “graythresh()” (<https://in.mathworks.com/help/images/ref/graythresh.html>). The purpose of adding the Otsu’s threshold-based classification step was to study how well the scores could be classified with a fast thresholding method, rather than the computationally expensive bootstrap.

Table 2: List of important functions provided in the code base

Name	Description	Command line	Location	Language
synthesis Demo.m	Command line demo, output to file: “synthData-demo.mat”. Generates a synthetic 2-P time cell dataset file	\$ cd TimeCellAnalysis/rho-matlab/demos && matlab -nodisplay -nosplash -r “synthesisDemo; quit”	rho-matlab/demos	MATLAB
ti_demo.py	Command-line demo, output to console.	\$ python TcPy(ti_demo.py sampleData/sample_synth_data.mat	TcPy	Python interface and C++ numerics
r2b_demo.py	Command-line demo, output to console. Runs Ridge-to-Background analysis from Modi et al. (2014). Reports R2B Mean and R2B Bootstrap classifications	\$ python TcPy(r2b_demo.py sampleData/sample_synth_data.mat	TcPy	Python interface and C++ numerics
peq_demo.py	Command-line demo, output to console. Runs parametric equation analysis from current study. Reports PEQ threshold classification, and estimates for noise, event width, imprecision, and hit trial ratio for dataset	\$ python TcPy(peq_demo.py sampleData/sample_synth_data.mat	TcPy	Python interface and C++ numerics
ground_truth_check.py	Command-line demo, output to console. Uses synthetic data files to assess accuracy of classification by the various Mau and Modi algorithms	\$ python TcPy/ground-truth_check.py sampleData/sample_synth_data.mat	TcPy	Python interface and C++ numerics
Benchmark.py	Command-line demo, output to console. Simple time and memory benchmarks for the Mau, Modi, or PEQ algorithms	\$ python TcPy/run_batch_analysis.py sampleData/sample_synth_data.mat	TcPy	Python interface and C++ numerics
run_batch_analysis.py	Command-line production script, output to CSV files. Runs a batch analysis using all methods on a data file. Generates .csv files for TI, R2B, PEQ, and ground truth classifications	\$ python TcPy(ti_demo.py sampleData/sample_synth_data.mat	TcPy	Python interface and C++ numerics
pyBindMap.py	Provides an interface for MATLAB programmers, to the python/C__ fuctions using two wrapper functions: runTlAnalysis and runR2Banalysis	Utility function, not run from command line	TcPy	Python
dodFbF.m	Utility function to convert experimental raw 2p calcium activity data from Suite2P to df/F form.	Utility function, not run from command line	rho-matlab/CustomFunctions	MATLAB

All these functions should be run from the cloned repository, TimeCellAnalysis.

Table 3: List of paper figure generating scripts

Name	Description	Command line
paperFigures	Plots all figures estimating algorithm performance for synthetic data analysis (paper Figs. 1, 4–6, and 8)	\$ matlab -r "paperFiguresSynth"
Synth.m		
paperFigures	Plots all figures estimating algorithm performance for real physiology data analysis (paper Fig. 7)	\$ matlab -r "paperFiguresReal"
Real.m		
paperFigures	For diagnostics; plots figures estimating algorithm performance over all the regimes (unphysiological, canonical, and physiologic)	\$ cd .. /src && matlab -r "paperFiguresSplits"
Splits.m		

All these functions should be run from the cloned repository, TimeCellAnalysis/p-matlab/paperFigures.

Ratio of ridge/background, *r2bMean*, *r2bBoot*, *r2bBase-O* (Modi et al., 2014)

Here, we re-implemented the algorithm from Modi et al., 2014. The time of peak response for each cell was identified in averaged, nonoverlapping trials' worth of $\Delta F/F$ traces, in the CS-onset to US-onset period, or as specified. The rest of the trials were averaged and the summed area under the time of peak was estimated. The ridge was then defined to be a 200 ms window centered at the peak. Next, we calculated the summed area in the ridge window as well as the background (non-ridge frames) to get the ridge to background ratio. As a control condition, these traces were given random time-offsets and then averaged. An independent time of peak was identified for each random-offset, averaged trace and ridge to background ratio calculated for it. This bootstrapping was repeated 1000 times for each cell's data and averaged. The reliability score was then calculated individually, for each cell, as the ratio of the ridge to background ratio for aligned traces to the mean of that of the random-offset traces (*r2bMean*).

We also studied the significance of each cell's raw *r2b* values by comparing them to each of the *r2b* values of the randomized datasets, thresholding significance at the 99th percentile (*r2bBoot*). Finally, the raw *r2b* values were also thresholding using Otsu's Thresholding (*r2bBase-O*; Otsu 1979).

Parametric equations, *peqBase* and *peqBase-O* (in-house)

We developed this method to score cells in a manner similar to the reference quality, which uses the known ground truth of the input parameters given to the generator functions for the synthetic dataset. Rather than using the known inputs, this method computes the corresponding parameters read out or estimated from the dataset, whether synthetic or real. It is applicable to labeled or unlabeled datasets. It is defined as:

$$Q = \text{HTR} \times \exp - \{\alpha \times N/S + \beta \times \text{std. dev. EW} / \text{mean EW} + \gamma \times \text{std. dev. Imp/Stim Win}\}, \quad (6)$$

where HTR: hit trial ratio

N/S: estimated noise/signal

EW: read out event widths (frames)

Imp: estimated imprecision (frames)

Stim Wind: stimulus window (frames)

$\alpha: 10$

$\beta: 1$

$\gamma: 10$

While $10 \times \alpha$ was required, β , and γ , were inspired by the same used for reference Q. Classification was then performed using Bootstrapping (as described above) as well as Otsu's threshold.

All of these implemented algorithms can handle unlabeled (real) or ground truth labeled (synthetic) data.

A schematic to describe the steps involved in each algorithm is shown (Fig. 3). We were then able to run all our synthetically generated datasets through each of the 10 implemented algorithms and perform comparative benchmarks.

Good predictive power in time cell quality scores despite different distributions

We ran each of the analysis methods on our synthetic datasets to assess how they scored the (known) time cells. There were four methods that provided a scoring function for time-cell classification: *tIMean*, *tIBase*, *r2bBase*, and *peqBase* (Fig. 4A–D). By inspection, these methods appeared to have distinct distributions. Below we describe how we compare the distributions using correlation analysis. In subsequent sections we describe other methods in our study that used these scores to generate a categorization through thresholding or bootstrap.

In these synthetic experiments, time cells were generated with a single calcium event per hit trial. Event insertions into the synthetic datasets were subject to noise, variable selection of event widths, trial-pair or timing imprecision, and hit trial ratio. We generated 99 unique unphysiological combinations (3 \times randomized shuffles) 12 unique canonical regime combinations (10 \times randomized shuffles), as well as 15 unique physiological regime combinations featuring background activity (10 \times randomized shuffles). In all, we performed our comparative analysis studies using 567 datasets, each with 135 cells, 60 trials/session, and 246 frames/trial at 14.5 Hz). We found that only *tIMean* and *tIBase* had a correlation coefficient of ~ 0.6 , whereas other pairs were correlated below 0.4 (Fig. 4E).

Generalized linear regression (GLM) models were generated to look for the ideal thresholding value for the best classification predictions by each method. We used the MATLAB implementation of GLMs (*fitglm*); <https://in.mathworks.com/help/stats/fitglm.html>). This is a linear model assuming a binomial distribution of categories (0 or 1, i.e., other cell or time cell; Collett, 2002). We obtained good predictive power for the four methods that provided a scoring function for time-cell classification. We generated Receiver Operating Characteristic (ROC) curves by going over the full range of thresholds for the range of scores for each method

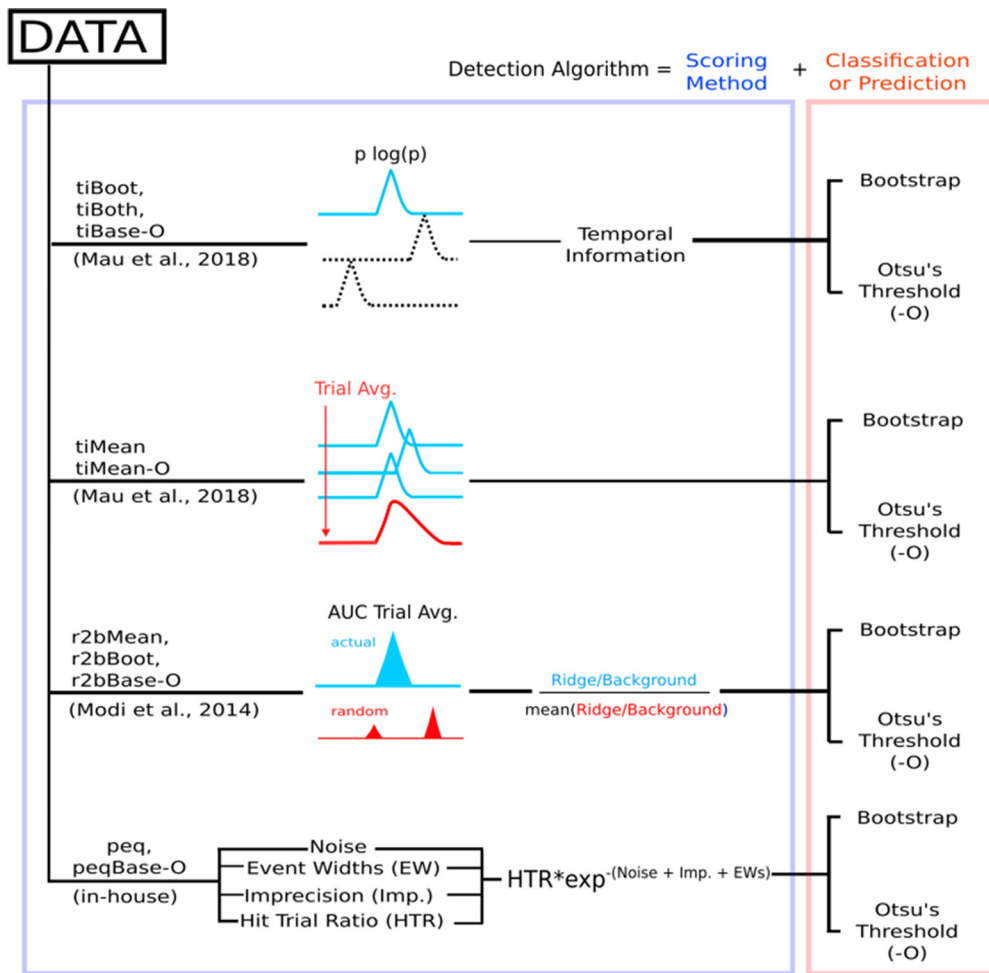


Figure 3. Schematic representation of the implemented algorithms, involving four different scoring methods followed by a classification step (bootstrapping or Otsu's automatic threshold) to have 10 complete time cell detection algorithms.

(ROC curves; Fig. 4F). We found that each distribution of scores had good predictive power, since ideal thresholds could be found to maximize TPR/FPR in all cases. We used the *tiBoth* categorization to distinguish time cells (Fig. 4G) from other cells (Fig. 4H), and plotted trial-averaged calcium traces to visually assess quality of classification as seen from raw data. Overall, each of our methods had distinct distributions of their base scores, but all had good predictive power for classification. The outcome of the classification steps is described in the next sections.

All algorithms exhibit near perfect precision with good recall

Next, we used the scores to classify the cells in our synthetic datasets, compared the predictions to ground truth, and established summaries for true and false cases. Confusion matrices were estimated to compare the predictions (classifications) for each algorithm, with reference to ground truth, and are shown (Fig. 5A,B). All methods exhibit very good precision (true positive classifications over the sum of all positive classifications), suggesting low false positive rates (Type I error; Fig. 5C). Most algorithms also generate good values for recall (true positive

classifications over ground-truth positives). We observed F1 scores (harmonic mean of recall and precision) >0.75 , all the way to 1 (perfect score), for most of the algorithms, as shown (Fig. 5C), suggesting overall usability.

We noticed moderate to strong correlation (>0.8) between the Boolean prediction lists for *tiMean*, *tiBoot*, *tiBoth*, *r2bMean*, and *r2bBoot* (Fig. 5D), but only weak to moderate correlation (<0.6) between the other pairs of predictions. The *tiMean-O* method does slightly better (correlation ~ 0.7 with the first five methods).

Algorithms differ in memory use and speed

Hardware and runtime requirements are a secondary, but practical concern when designing analysis of large datasets, and are specially relevant for experiment designs that require online analysis. We therefore looked at how memory use and runtime scaled on a per dataset basis when considering 67 or 135 cells per dataset ($2\times$).

We ran the memory usage and runtime experiments on a gaming laptop (Lenovo Ideapad 3 Gaming) with a 6 core AMD Ryzen 5 4600H, 16 GB DDR4 RAM (3200 MHz) running MATLAB R2021a on Ubuntu 20.04. Note, however, that we have implemented all the time cell algorithms in

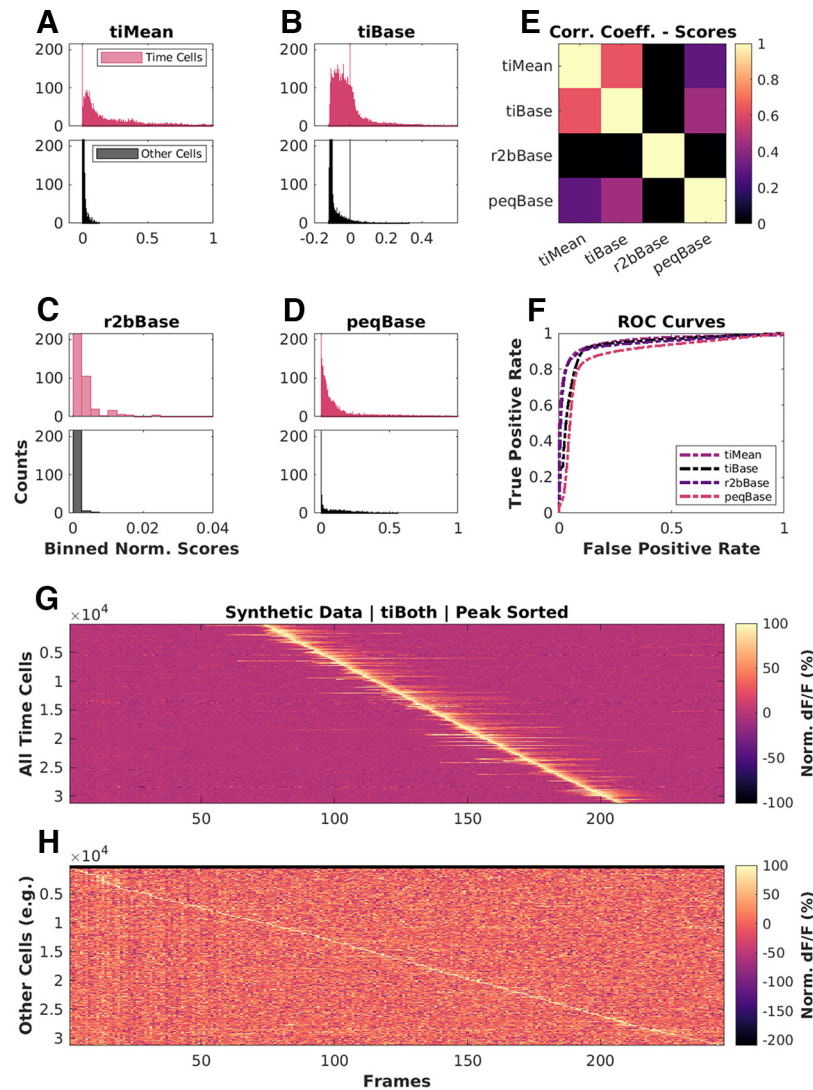


Figure 4. Base scores for different methods differ in their distributions but all have good predictive power. Scores for top (blue): time cells; bottom (red): other cells, across **A**, **tiMean**; **B**, **tiBase**; **C**, **r2bBase**; **D**, **peqBase**. **E**, Pairwise correlation coefficients between the distributions of analog scores (pooling time cells and other cells) by each of the four scoring methods. **F**, Receiver-operator characteristic (ROC) curves after generalized linear regression using the respective distributions of scores and comparisons with known ground truth. **G**, **H**, Trial-averaged calcium activity traces for cells classified as **G**, time cells; **H**, other cells.

serial and these do not use the additional cores. We found that most algorithms ran to completion requiring \sim 15 MB/dataset at a rate of \sim 1–4 s/dataset (135 cells/dataset). With 67 cells/dataset, the memory requirement and runtimes are approximately halved, suggesting that computational costs in memory and time were roughly linear with dataset size. We note that the analysis algorithms work independently for each cell. Thus, in principle, the analysis could be run in an embarrassingly parallel manner and should scale well on multicore architectures.

The synthesis of the main benchmarking datasets ($N=567$ datasets or 76,545 total cells) required a more powerful analysis machine, running a 6 core AMD Ryzen 5 3600, 32GB of DDR4 RAM, running MATLAB R2021a on Ubuntu 20.04. Dataset batches up to \sim 30 datasets ($N=40,500$ cells), however, could be easily handled by a less powerful laptop. The memory usage and runtime for

135 cells per dataset were accordingly, \sim 30 MB/dataset requiring \sim 1 s to complete. Thus, the methods scale readily to handle large datasets on modern hardware.

Physiologic range tests show sensitivity to noise but not to other features of the dataset

We next set out to see how these methods would work in estimated physiological ranges of signal confounds. Given our categorical labels on the synthetic data, we were able to split the datasets to look for the effects of the five main parameters: noise, event widths, imprecision, hit trial ratio, and background activity. We first computed the baseline physiology readouts keeping noise to 10%, event widths to the 60th percentile (± 1 SD), imprecision to 0 frames, hit trial ratios to a range of 33–66%, and background activity to 0.9–1.2 events/trial for time cells

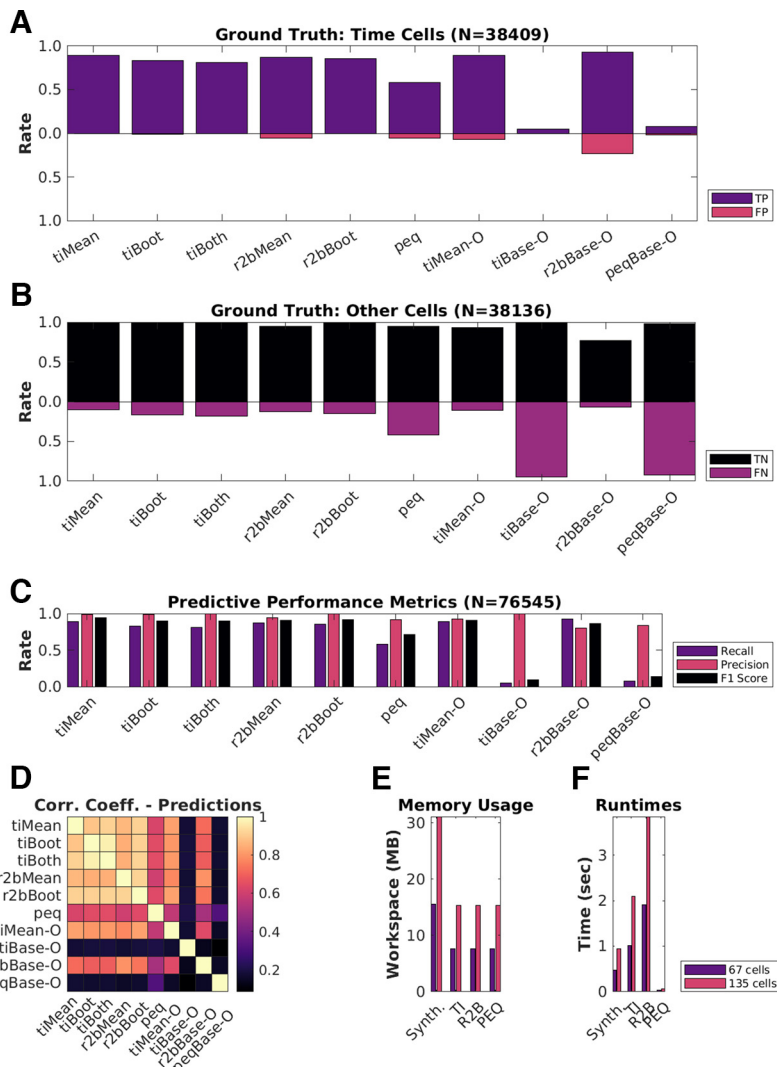


Figure 5. Good predictive performance by all algorithms. **A, B**, Classification performance of each of the 10 implemented detection algorithms. **A**, True positives (TP; purple), false positives (FP; red). **B**, True negatives (TN; black), false negatives (FN; purple). **C**, Predictive performance metrics [Recall = TP/(TP + FN), Precision = TP/(TP + FP), and F1 Score = Harmonic mean of Recall and Precision] to consolidate the confusion matrices. **D**, Pairwise correlation coefficients between the Boolean prediction lists by each of the 10 detection algorithms. Note that the first six methods correlate strongly. **E**, Average memory usage per dataset by the implemented algorithms on datasets with either 67 cells (purple) or 135 cells (red). **F**, Average runtimes per dataset by the implemented algorithms on datasets with either 67 cells (purple) or 135 cells (red).

(~50% of all synthetically generated cells, $N=50$ baseline datasets, 135 cells/dataset, 60 trials/dataset). Next, we established dependency slopes for each of the algorithms, based on their predictions ($N=10$ randomized shuffles for each case; Fig. 6B–F; Extended Data Figs. 6-1, 6-2).

Most methods exhibited a negative dependence of noise (range: 10% to 70%) on prediction F1 score (Fig. 6B). Although many methods are designed with some form of denoising strategy (trial-averaging, etc.), as expected all algorithms ran into classification difficulties at higher Noise levels. This reinforces the value of relatively high signal-to-noise recordings.

The relative insensitivity to event widths (Fig. 6C) is potentially useful for calcium imaging datasets where events may be slow, and in cases where slower tuning curves are

expected. However, this criterion may need to be stringent for analyses that need to precisely identify fine differences in cell responses.

We observed that most algorithms were insensitive to how frequently time cells were active across trials in a session (HTR). This is possibly the reason for the potential confusion among physiologists with regard to how many time cells were expected in a recorded dataset.

We found that the first six algorithms (*tiMean*, *tiBoot*, *tiBoth*, *r2bMean*, *r2bBoot*, and *peq*) gave equivalent predictions in ~66% of cases (Extended Data Fig. 6-1A). Next, we considered the various prediction lists across these top six algorithms and looked for consensus in time cell predictions from the most lenient threshold (“ ≥ 1 ” algorithm), incrementally through the most stringent threshold (“ $=10$ ” algorithms). We thus established a

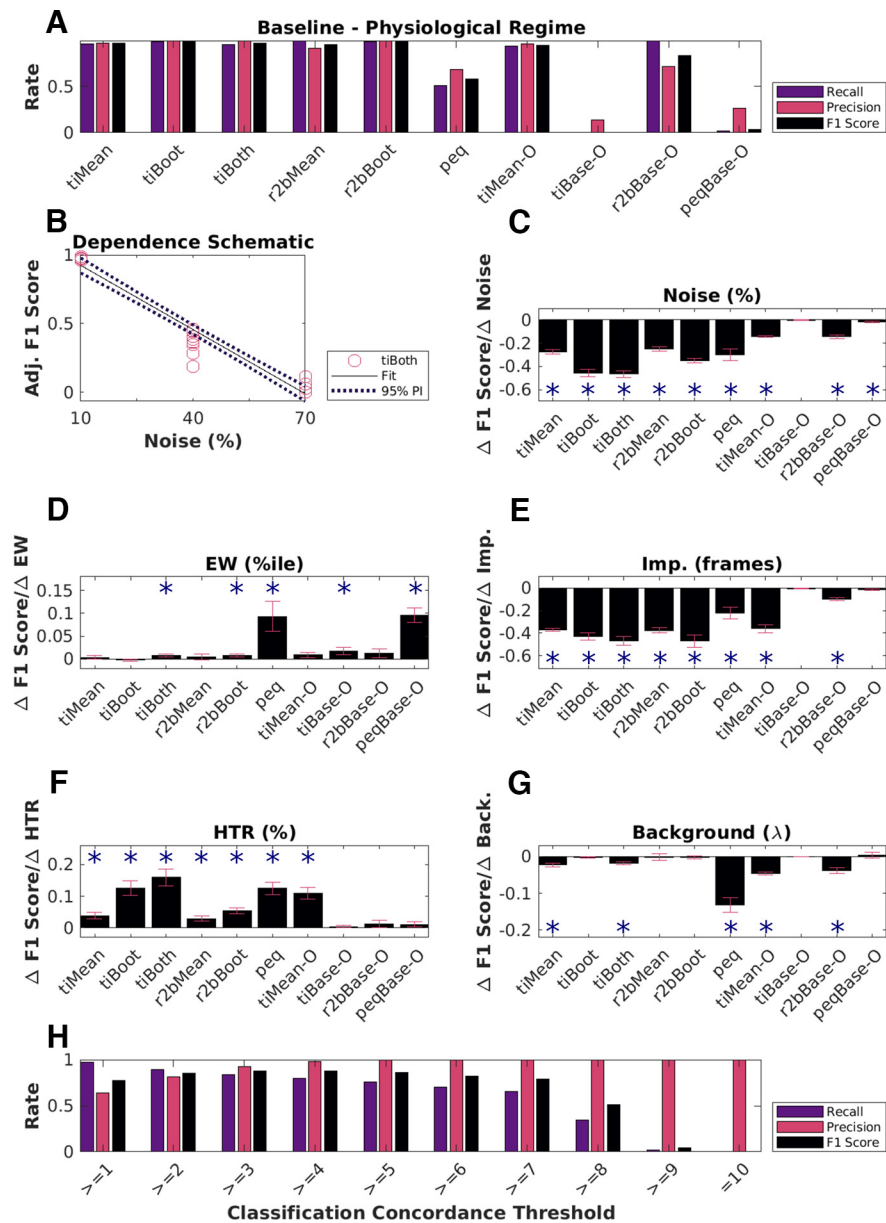


Figure 6. Physiological sensitivity analysis and concordance. **A**, Classification performance scores for all algorithms with the baseline physiology synthetic datasets ($N=6750$ cells). The first five methods perform well. Peq does poorly by all measures when confronted with physiology-range activity variability. Otsu's threshold method for score classification also does not work well for any method under physiological conditions. **B**, Dependence of F1 score on noise as a schematic. This has an overall negative slope (dashed line) which was used for panel **C**, TI-both. A similar calculation was performed for each method. Panels **C–G**, Parameters were systematically modulated one at a time with respect to baseline and the impact on classification score for each algorithm was estimated by computing the slope, using repeats over 10 datasets each with an independent random seed. Significant dependence on the perturbing parameter was determined by testing whether the slope differed from 0 at $p < 0.01$, indicated by asterisks using the MATLAB function `coeffTest()`. Plotted here are bar graphs with mean and error as RMSE normalized by the square root of N ($N=10$ datasets). **C**, Dependence on noise %. **D**, Dependence on event width percentiles. **E**, Dependence on imprecision frames. **F**, Dependence on hit trial ratio (HTR; %). **G**, Background activity (Poisson distribution mean, λ). **H**, Classification performance using concordance for a range of classification thresholds. Extended Data Figure 6-1 describes the three-point line plot dependency curves for the F1 score for each of the implemented algorithms against each of the five main parameters modulated, as the mean of $N=10$ datasets for each case, with error bars as SD. Extended Data Figure 6-2 showcases the linear regression fits for the same, with 95% prediction intervals (PIs), used to estimate the slopes of the various dependency curves.

Concordance based metric for time cell classification. We tested the predictive power of this Concordance based metric, which considers time cells based on consensus among the predictions from all the 10 implemented algorithms.

We identified differences in the classification performance, across the full range of concordance thresholds (Fig. 6H). With lower threshold values (“ $>=4$ ” and below), we notice a slight drop in the Precision, indicating an

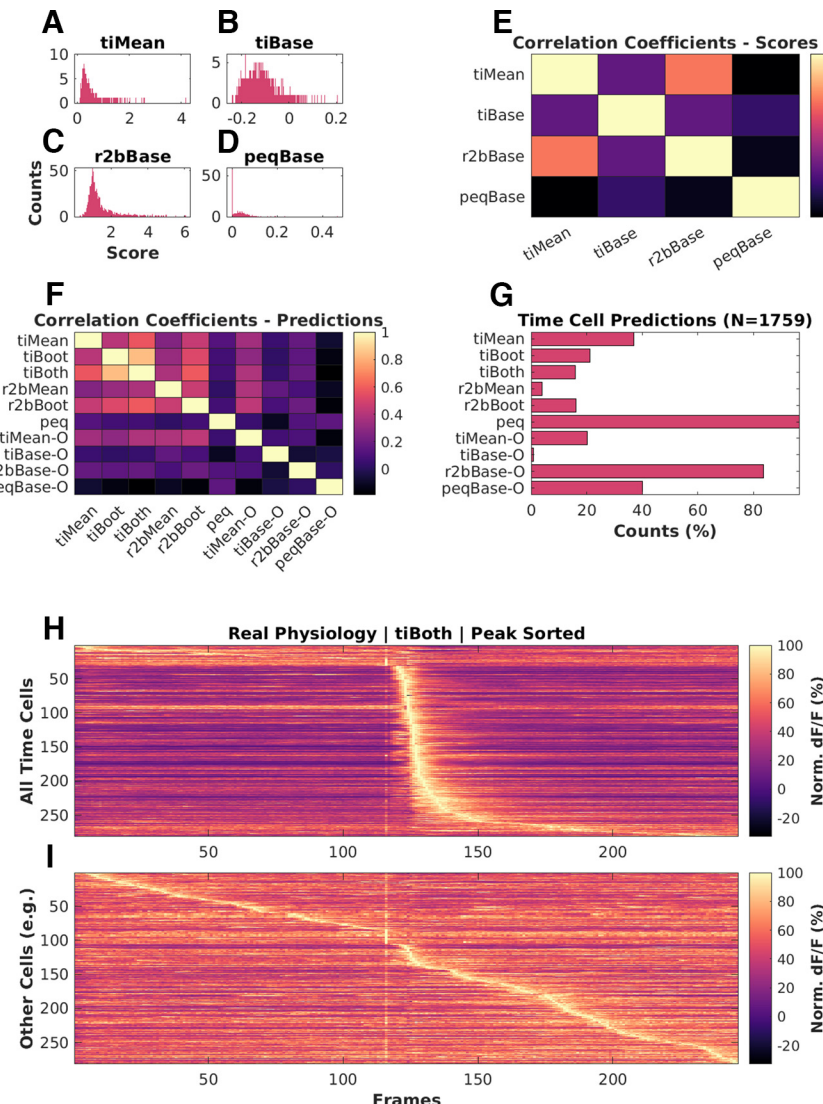


Figure 7. Analysis of experimental 2-P recordings of Ca^{2+} signals. **A–D**, Histograms of scores for physiologically recorded *in vivo* calcium activity from hippocampal CA1 cells (total $N = 1759$), by (A) tiMean, (B) tiBase, (C) r2bBase, and (D) peqBase. **E**, Pairwise correlation coefficients between the distributions of analog scores by the four scoring methods. **F**, Pairwise correlation coefficients between the Boolean prediction lists by the 10 detection algorithms. **G**, Numbers of positive class (time cell) predictions by each of the detection algorithms. **H, I**, Trial-averaged calcium activity traces for (**H**) time cells and (**I**) other cells. LED conditioned stimulus (CS) is presented at frame number 116, as seen by the bright band of the stimulus artifact. Most cells classified as time cells are active just after the stimulus. There is a characteristic broadening of the activity peak for classified time cells at longer intervals after the stimulus. Some of the cells at the top of panel **H** may be false positives because their tuning curve is very wide or because of picking up the stimulus transient. Similarly, some of the cells in the middle of panel **I** may be false negatives because of stringent cutoffs, although they appear to be responsive to the stimulus.

increase in false positive rate (Type I error). On the other hand, with increasing threshold values it is the Recall that drops, suggesting a higher false negative rate (Type II error). We find that a concordance threshold of “ $>=4$ ” achieves the best recall, precision, and F1 scores, for time cell prediction (Fig. 6F). The utility of this approach is subject to the availability of resources to apply multiple algorithms to each dataset.

Time cells identified in real physiology recordings

We used the 10 different implemented algorithms on *in vivo* 2-P calcium recordings ($N = 13$ datasets, namely,

1759 isolated cells from three animals across chronically recorded datasets), to compare time cell classification between the algorithms. As we observed for the synthetic data, experimental 2-P Ca traces also yielded different base scores from the four different methods (Fig. 7A–D). Again, consistent with the synthetic data, the pairwise correlation was weak to moderate (Fig. 7E). When we consider the boolean prediction lists (Fig. 7F), we observed moderate pairwise correlation between tiMean, tiBoot, tiBoth, r2bMean, and r2bBoot (>0.5), and low or weak correlation between the other pairs (<0.5). This was consistent with observations for the synthetic data but the correlations were overall slightly

weaker. The total number of time cells predicted were also different across the implemented algorithms (Fig. 7G). Algorithms such as *r2bBase-O* and *peq*, which had more false positives (Fig. 5B) also had more cells classified as time cells. The converse was not true. *r2bMean*, which had moderate false negatives as well as false positives on the synthetic dataset, classified very few of the experimental set as time cells. The trial-averaged activity of the detected time cells (Fig. 7H; including false positives) and other cells (Fig. 7I), based on the predictions by *tiBoth*, are shown. The experimentally recorded time cells exhibited a characteristic widening of tuning curves (Pastalkova et al., 2008; MacDonald et al., 2011, 2013; Kraus et al., 2013; Mau et al., 2018) with tuning to later time points (Fig. 7H).

Overall, four of the algorithms from the literature seemed consistent in their classifications as well as having reasonable numbers of classified time cells. These were the three algorithms from Mau et al. (2018; *tiMean*, *tiBoot*, and *tiBoth*), and the *r2bBoot* method derived from Modi et al. (2014). This is broadly in agreement with their performance on the synthetic datasets.

Discussion

We have developed a full pipeline for comparing time cell detection algorithms. This starts with synthetic datasets for benchmarking, in which we program in the ground truth of cell identity and timed activity, and a range of perturbations characteristic of experiments. These include noise, event widths, trial-pair timing imprecision, hit trial ratio, and background activity. This resource is, in itself, a key outcome of the current study, and though it is designed for 2-P calcium imaging data it can be extended to rate-averaged single-unit recordings. We built a pipeline for running and comparing the outcome from five methods derived from two previous studies, and one from the current work. These algorithms were applied to synthetic and experimental datasets and compared against each other and, where possible, against ground truth. We observed that most algorithms perform well and substantially agree in their time cell classification, but there were different degrees of sensitivity to different forms of signal variability, notably noise and imprecision.

The value of synthetic data in experimental science

Synthetic neural activity datasets are valuable in at least two main ways: evaluating algorithms for detection of important activity features, and for delivering stimuli to *in vitro* and simulated neurons, so as to provide a more physiological context in which to study input-output properties (Abbasi et al., 2020). While we have deployed our synthetic dataset for the specific purpose of comparing time cell detection algorithms, we suggest that it could also be useful for evaluating sequence analysis algorithms (Ikegaya et al., 2004; Foster and Wilson, 2006; Villette et al., 2015). Beyond the domain of neuronal data analysis, such synthetic datasets act as a test-bed for critique and development of analysis algorithms meant for deployment on real-world or typical use case data. They have been used previously to benchmark unsupervised outlier detection

(Steinbuss and Bohm, 2020), explainable machine learning (Liu et al., 2021), intrusion detection systems (Iannucci et al., 2017), 3D reconstruction algorithms (Koch et al., 2021), among several others. We report the first use of synthetic data pertaining to cellular physiology in the context of identifying time cells from network recordings. Moreover, our experiments study important operational differences across several previously published and new detection algorithms.

Our dataset may also be valuable for the second use case, stimulus delivery. There is a growing body of work on network detection of sequences (Ikegaya et al., 2004; Foster and Wilson, 2006; Csicsvari et al., 2007; Jadhav et al., 2012; Villette et al., 2015; Malvache et al., 2016) or even single-neuron sequence selectivity (Branco et al., 2010; Bhalla, 2017). More realistic input activity patterns with a range of physiological perturbations may be useful probes for such experimental and theoretical studies. Further, experimenter-defined neural activity inputs through optogenetic stimulation has already begun to use more complex temporal patterns than static or periodic illumination (Schrader et al., 2008; Dhawale et al., 2010; Bhatia et al., 2021). Our approaches to synthetic sequential neuronal activity generation may be useful to add more physiological dimensions to the sequential activity employed in such studies.

Further dimensions of time cell modulation

Our experiments allowed us to probe for parametric dependence systematically across published and new algorithms. We observed little or no dependence of the predictive performance (F1 score) of the various algorithms to event widths, hit trial ratios, and background activity. We did observe the F1 scores for most algorithms to be negatively dependent on noise and imprecision. On the one hand, this is a useful outcome in that different methods yield similar time-cell classification. It is a limitation, however, if the network uses such response features for coding, since it means that these methods are insensitive to relevant response changes. Further potential coding dimensions were not explored. Thus, several potential behavioral correlates of tuned cells (Ranck, 1973), could not be studied in our experiments. Such correlates include but are not limited to measurements of spatial navigation (O'Keefe and Dostrovsky, 1971; O'Keefe and Nadel, 1978; Wilson and McNaughton, 1993) and decision-making (Foster and Wilson, 2006; Csicsvari et al., 2007; Diba and Buzsáki, 2007; Davidson et al., 2009; Karlsson and Frank, 2009; Gupta et al., 2010; MacDonald et al., 2013; Villette et al., 2015), as well as navigation across tone frequencies (Aronov and Tank, 2014). While each of these further inputs would be interesting to incorporate into synthetic datasets, this requires that the time cell generation algorithm itself incorporate some form of simulation of the neural context. This is beyond the scope of the current study.

A specific limitation of our dataset is that it assumes that time is encoded by individual neurons. This leaves out population encoding schemes in which no one cell responds with the level of precision or consistency that would clear the criteria we use. For example, many of the same studies that use the methods tested here also use

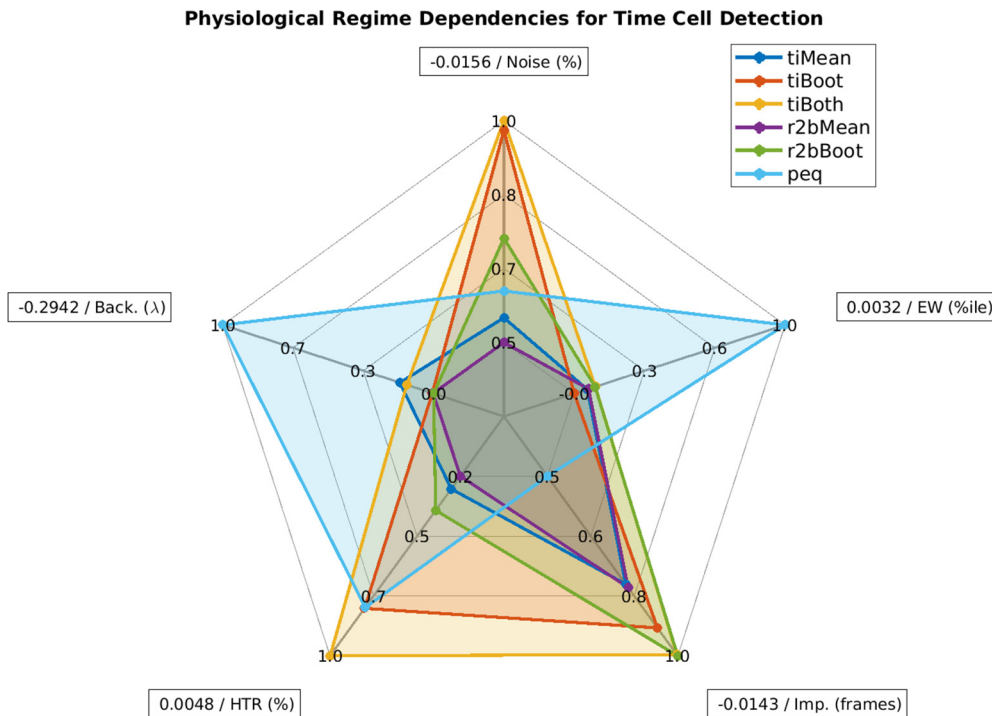


Figure 8. Spider plot summary. Relative sensitivity of the six best detection algorithms (*tiMean*, *tiBoot*, *tiBoth*, *r2bMean*, *r2bBoth*, and *peq*) to the five main parameters for data variability, noise (%), event widths (%ile), imprecision (frames), hit trial ratio (%), and background activity (λ). A perfect algorithm would have very small values (i.e., low sensitivity) for each of the parameters and, thus, occupy only the smallest pentagon in the middle. Note that even the maximal absolute value of sensitivity for most parameters (outer perimeter) is quite small, indicated in boxes at the points of the spider plot.

neural network decoders to report time (Mau et al., 2018). Such decoders might detect time encoding without time cells. A similar situation of individual versus network coding appears for the closely related problem of sequence representation. Place cell replay sequences have been shown to be modulated by the prevalence of location specific aversive (Wu et al., 2017) as well as appetitive stimuli (Bhattarai et al., 2020). Such physiological findings have been the subject of theoretical models of behavior planning (Foster, 2017; Mattar and Daw, 2018), and have been reported to improve performance on multiple Atari games by artificial neural networks (Mnih et al., 2015) featuring salience detection and experience mapping. We suggest that synthetic data for such higher-order encoding schemes might be a useful tool, and could draw on the approaches in the current study.

Comparative analysis benchmarks and concordance

A particularly challenging time cell classification problem is when the same cells may play different timing roles, such as forward and reverse replay. This is made more difficult because of the relative rarity of forward replay sequences over the more typical reverse replay (Diba and Buzsáki, 2007; Foster, 2017). Preplay is also a topic of some debate (Dragoi and Tonegawa, 2013; Foster, 2017). At least one possible problem in such debates is the degree of consistency between time cell or sequence classifiers. Our pipeline allows for (1) error correction in case of nonconcordant classifications, (2) suggest candidate algorithms

with a dependence on dataset features like event widths, imprecision, and hit trial ratio, as well as (3) the possibility to expand the detection regime in more realistic physiological datasets using concordance.

Which algorithms to use?

We did not set out to rank algorithms, but our analysis does yield suggestions for possible use domains based on sensitivity to experimental perturbations (Fig. 8). In cases where runtime and compute resource use is a concern, we recommend using the temporal information method with Bootstrap along with the activity filter (*tiBoth*). Combinations of *tiBoth* with *r2bBoth* may be useful where there are rare and potentially multimodally tuned time cells (Pastalkova et al., 2008; Villette et al., 2015), either to combine their classification for stringent time cell identification, or to pool their classified cells. While it is tempting to use Otsu's threshold as a very fast alternative to bootstrapping, we found that none of the Otsu variants of these methods did a good job of classification. Ultimately, five of our algorithms *tiMean*, *tiBoot*, *tiBoth*, *r2bMean*, and *r2bBoth*: all based on either Mau et al. (2018) or Modi et al. (2014), have very good Precision, and classify with very few false positives (low Type I error). Many methods are susceptible to classification errors if the dataset has high noise.

Here we also implemented the parametric equation (*peq*) algorithm. It is not very good for time cell classification per se, as it is prone to false positives and is susceptible to noise and low hit trial ratios. However, it generates useful

additional estimates of the four key parameters of real data, namely, noise, hit trial ratio, event width and imprecision. This is useful for a first-pass characterization of the properties of the dataset.

Sequence detection in large-scale recordings and scaling of analysis runs

The discovery of replay over the past two decades, has benefitted from the technological advances made in increasing the cellular yield of network recordings and has been reviewed previously (Foster, 2017). Further advances such as with the large scale recordings of $\sim 10^3$ single units by electrical recording using Neuropixels (Jun et al., 2017), fast volumetric fluorescence scanning with up to $\sim 10^4$ cells using resonant electro-optic imaging (Poort et al., 2015; Pachitariu et al., 2017; Bowman and Kasevich, 2021), $\sim 10^3$ mesoscopes (Sofroniew et al., 2016), as well as advances in automated cell region of interest (ROI) detection, denoising, and neuropil subtraction (Pachitariu et al., 2017; Pnevmatikakis et al., 2016) only increase the scale and size of datasets, likely leading to longer analysis runtimes. In addition to our recommendations above for the temporal information/boot method for scalable time-cell analysis, our C++/Python implementations may also be useful in further optimizing these methods. Our implementations allow for relatively fast analysis of the same datasets with multiple algorithms.

References

- Abbasi S, Maran S, Jaeger D (2020) A general method to generate artificial spike train populations matching recorded neurons. *J Comput Neurosci* 48:47–63.
- Ahmed MS, Priestley JB, Castro A, Stefanini F, Solis Canales AS, Balough EM, Lavoie E, Mazzucato L, Fusi S, Losonczy A (2020) Hippocampal network reorganization underlies the formation of a temporal association memory. *Neuron* 107:283–291.e6.
- Aronov D, Tank DW (2014) Engagement of neural circuits underlying 2D spatial navigation in a rodent virtual reality system. *Neuron* 84:442–456.
- Bhalla US (2017) Synaptic input sequence discrimination on behavioral timescales mediated by reaction-diffusion chemistry in dendrites. *Elife* 6:e25827.
- Bhatia A, Moza S, Bhalla US (2021) Patterned optogenetic stimulation using a DMD projector. *Methods Mol Biol* 2191:173–188.
- Bhattarai B, Lee JW, Jung MW (2020) Distinct effects of reward and navigation history on hippocampal forward and reverse replays. *Proc Natl Acad Sci U S A* 117:689–697.
- Bowman AJ, Kasevich MA (2021) Resonant electro-optic imaging for microscopy at nanosecond resolution. *ACS Nano* 15:16043–16054.
- Branco T, Clark BA, Häusser M (2010) Dendritic discrimination of temporal input sequences in cortical neurons. *Science* 329:1671–1675.
- Collett D (2002) Modeling binary data. London: Chapman and Hall.
- Csicsvari J, O'Neill J, Allen K, Senior T (2007) Place-selective firing contributes to the reverse-order reactivation of CA1 pyramidal cells during sharp waves in open-field exploration. *Eur J Neurosci* 26:704–716.
- Davidson TJ, Kloosterman F, Wilson MA (2009) Hippocampal replay of extended experience. *Neuron* 63:497–507.
- Dhawale AK, Hagiwara A, Bhalla US, Murthy VN, Albeau DF (2010) Non-redundant odor coding by sister mitral cells revealed by light addressable glomeruli in the mouse. *Nat Neurosci* 13:1404–1412.
- Diba K, Buzsáki G (2007) Forward and reverse hippocampal place-cell sequences during ripples. *Nat Neurosci* 10:1241–1242.
- Dombeck DA, Harvey CD, Tian L, Looger LL, Tank DW (2010) Functional imaging of hippocampal place cells at cellular resolution during virtual navigation. *Nat Neurosci* 13:1433–1440.
- Dragoi G, Tonegawa S (2013) Distinct preplay of multiple novel spatial experiences in the rat. *Proc Natl Acad Sci U S A* 110:9100–9105.
- Eichenbaum H (2017) On the integration of space, time, and memory. *Neuron* 95:1007–1018.
- Foster DJ (2017) Replay comes of age. *Annu Rev Neurosci* 40:581–602.
- Foster DJ, Wilson MA (2006) Reverse replay of behavioural sequences in hippocampal place cells during the awake state. *Nature* 440:680–683.
- Gupta AS, van der Meer MAA, Touretzky DS, Redish AD (2010) Hippocampal replay is not a simple function of experience. *Neuron* 65:695–705.
- Iannucci S, Kholidy HA, Ghimire AD, Jia R, Abdelwahed S, Banicescu I (2017) A comparison of graph-based synthetic data generators for benchmarking next-generation intrusion detection systems. 2017 IEEE International Conference on Cluster Computing (CLUSTER), Honolulu, HI, pp. 278–289, <https://doi.org/10.1109/CLUSTER.2017.54>.
- Ikegaya Y, Aaron G, Cossart R, Aronov D, Lampl I, Ferster D, Yuste R (2004) Synfire chains and cortical songs: temporal modules of cortical activity. *Science* 304:559–564.
- Jadhav SP, Kemere C, German PW, Frank LM (2012) Awake hippocampal sharp-wave ripples support spatial memory. *Science* 336:1454–1458.
- Jun JJ, et al. (2017) Fully integrated silicon probes for high-density recording of neural activity. *Nature* 551:232–236.
- Kaifosh P, Lovett-Barron M, Turi GF, Reardon TR, Losonczy A (2013) Septo-hippocampal GABAergic signaling across multiple modalities in awake mice. *Nat Neurosci* 16:1182–1184.
- Karlsson MP, Frank LM (2009) Awake replay of remote experiences in the hippocampus. *Nat Neurosci* 12:913–918.
- Koch S, Worcel M, Silva C, Alexa M (2021) Hardware Design and Accurate Simulation of Structured-Light Scanning for Benchmarking of 3D Reconstruction Algorithms (Vol. 2021). Proceedings of the Neural Information Processing Systems Track on Datasets and Benchmarks 1 (NeurIPS Datasets and Benchmarks 2021). Retrieved from <https://openreview.net/forum?id=bNL5VfTe3p>.
- Kraus B, Robinson R, White J, Eichenbaum H, Hasselmo M (2013) Hippocampal “time cells”: time versus path integration. *Neuron* 78:1090–1101.
- Lee AK, Wilson MA (2004) A combinatorial method for analyzing sequential firing patterns involving an arbitrary number of neurons based on relative time order. *J Neurophysiol* 92:2555–2573.
- Liu Y, Khandagale S, White C, Neiswanger W (2021) Synthetic benchmarks for scientific research in explainable machine learning. <https://github.com/abacusai/xai-bench>.
- MacDonald CJ, Lepage KQ, Eden UT, Eichenbaum H (2011) Hippocampal “time cells” bridge the gap in memory for discontinuous events. *Neuron* 71:737–749.
- MacDonald CJ, Carrow S, Place R, Eichenbaum H (2013) Distinct hippocampal time cell sequences represent odor memories in immobilized rats. *J Neurosci* 33:14607–14616.
- Malvache A, Reichinnek S, Villette V, Haimerl C (2016) Awake hippocampal reactivations project onto orthogonal neuronal assemblies. *353:1280–1283*.
- Mattar MG, Daw ND (2018) Prioritized memory access explains planning and hippocampal replay. *Nat Neurosci* 21:1609–1617.
- Mau W, Sullivan DW, Kinsky NR, Hasselmo ME, Howard MW, Eichenbaum H (2018) The same hippocampal CA1 population simultaneously codes temporal information over multiple time-scales. *Curr Biol* 28:1499–1508.e4.
- Mnih V, Kavukcuoglu K, Silver D, Rusu AA, Veness J, Bellemare MG, Graves A, Riedmiller M, Fidjeland AK, Ostrovski G, Petersen S, Beattie C, Sadik A, Antonoglou I, King H, Kumaran D, Wierstra D,

- Legg S, Hassabis D (2015) Human-level control through deep reinforcement learning. *Nature* 518:529–533.
- Modi MN, Dhawale AK, Bhalla US (2014) CA1 cell activity sequences emerge after reorganization of network correlation structure during associative learning. *Elife* 3:e01982.
- Mokeichev A, Okun M, Barak O, Katz Y, Ben-Shahar O, Lampl I (2007) Stochastic emergence of repeating cortical motifs in spontaneous membrane potential fluctuations in vivo. *Neuron* 53:413–425.
- O'Keefe J, Dostrovsky J (1971) The hippocampus as a spatial map. Preliminary evidence from unit activity in the freely-moving rat. *Brain Res* 34:171–175.
- O'Keefe J, Nadel L (1978) The hippocampus as a cognitive map. Oxford: Clarendon Press.
- Otsu N (1979) A threshold selection method from gray level histograms. *IEEE Trans Syst Man Cyber* 9:62–66.
- Pachitariu M, Stringer C, Dipoppa M, Schröder S, Rossi LF (2017) Suite2p: beyond 10,000 neurons with standard two-photon microscopy. *BioRxiv* 061507. <https://doi.org/https://doi.org/10.1101/061507>.
- Pastalkova E, Itskov V, Amarasingham A, Buzsáki G (2008) Internally generated cell assembly sequences in the rat hippocampus. *Science* 321:1322–1327.
- Pnevmatikakis EA, Soudry D, Gao Y, Machado TA, Merel J, Pfau D, Reardon T, Mu Y, Lacefield C, Yang W, Ahrens M, Bruno R, Jessell TM, Peterka DS, Yuste R, Paninski L (2016) Simultaneous denoising, deconvolution, and demixing of calcium imaging data. *Neuron* 89:285–299.
- Poort J, Khan AG, Pachitariu M, Nemri A, Orsolic I, Krupic J, Bauza M, Sahani M, Keller GB, Mrsic-Flogel TD, Hofer SB (2015) Learning enhances sensory and multiple non-sensory representations in primary visual cortex. *Neuron* 86:1478–1490.
- Ranck JB, J (1973) Studies on single neurons in dorsal hippocampal formation and septum in unrestrained rats. I. Behavioral correlates and firing repertoires. *Exp Neurol* 41:461–531.
- Schrader S, Grün S, Diesmann M, Gerstein GL (2008) Detecting synfire chain activity using massively parallel spike train recording. *J Neurophysiol* 100:2165–2176.
- Siegel JJ, Taylor W, Gray R, Kalmbach B, Zemelman BV, Desai NS, Johnston D, Chitwood RA (2015) Trace eyeblink conditioning in mice is dependent upon the dorsal medial prefrontal cortex, cerebellum, and amygdala: behavioral characterization and functional circuitry. *eNeuro* 2:ENEURO.0051-14.2015.
- Sofroniew NJ, Flickinger D, King J, Svoboda K (2016) A large field of view two-photon mesoscope with subcellular resolution for in vivo imaging. *Elife* 5:e14472.
- Souza BC, Pavão R, Belchior H, Tort ABL (2018) On information metrics for spatial coding. *Neuroscience* 375:62–73.
- Steinbuss G, Bohm K (2020) Generating artificial outliers in the absence of genuine ones—a survey. *arXiv*. <https://doi.org/10.48550/arXiv.2006.03646>.
- Tseng W, Guan R, Disterhoft JF, Weiss C (2004) Trace eyeblink conditioning is hippocampally dependent in mice. *Hippocampus* 14:58–65.
- Villette V, Malvache A, Tressard T, Dupuy N, Cossart R (2015) Internally recurring hippocampal sequences as a population template of spatiotemporal information. *Neuron* 88:357–366.
- Wilson MA, McNaughton BL (1993) Dynamics of the hippocampal ensemble code for space. *Science* 261:1055–1058.
- Wu CT, Haggerty D, Kemere C, Ji D (2017) Hippocampal awake replay in fear memory retrieval. *Nat Neurosci* 20:571–580.